

Holocene environmental change at the southern Cape coast of South Africa

Coastal lake sediment records from
Eilandvlei and Groenvlei



seit 1558

Dissertation

(kumulativ)

zur Erlangung des akademischen Grades
Dr. rer. nat. (doctor rerum naturalium)

vorgelegt dem Rat der Chemisch-Geowissenschaftlichen Fakultät der
Friedrich-Schiller-Universität Jena

von **Michael Wündsch (M.Sc.)**

geboren am 15.12.1984 in Erfurt

Gutachter:

1. Prof. Dr. Roland Mäusbacher, Friedrich-Schiller-Universität Jena
2. PD Dr. Torsten Haberzettl, Friedrich-Schiller-Universität Jena
3. Prof. Dr. Antje Schwalb, Technische Universität Braunschweig

Datum der Verteidigung: 08.08.2017

Table of contents

Acknowledgements	II
Manuscript overview	III
Abstract	1
Kurzfassung	4
Chapter 1 - Introduction	8
1.1 Major climate factors and climate change in South Africa	9
1.2 Reconstructions of Holocene climate change in South Africa	10
1.3 The framework of the RAIN project	13
1.4 Regional setting and study site – The Wilderness embayment	14
1.5 Thesis outline	16
1.6 References	17
Chapter 2 - Sea level and climate change at the southern Cape coast, South Africa, during the past 4.2 kyr	22
Chapter 3 - The impact of changing reservoir effects on the ¹⁴C chronology of a Holocene sediment record from South Africa	36
Chapter 4 - Holocene environmental change along the southern Cape coast of South Africa – Insights from the Eilandvlei sediment record spanning the last 8.9 kyr	50
Chapter 5 - Synthesis	83
5.1 Synthesis and discussion	84
5.2 Driving forces of Holocene climate change at the southern Cape coast	86
5.3 Conclusions	88
5.4 Implications for future climate change at the southern Cape coast	88
5.5 Outlook	89
5.6 References	90
Statement of authorship (Selbstständigkeitserklärung)	94

Acknowledgements

I would like to thank my supervisors PD Dr. Torsten Haberzettl and Prof. Dr. Roland Mäusbacher who gave me the chance to take up the position within this research project. Beyond that, I am indebted to many people who contributed to make the completion of this thesis possible. Therefore, I do not want to name all the names here, as the likelihood to forget somebody is very high. Nevertheless, I thank all colleagues, technicians, lab staff, student helpers and secretaries of the departments of Physical Geography and Soil Science at the Institute of Geography, Friedrich Schiller University Jena. Moreover, I thank all my co-authors and colleagues from other institutions, especially from the Department of Environmental and Geographical Science (University of Cape Town), the Center for Marine Environmental Sciences (University of Bremen) and the Institute of Geosciences (Friedrich Schiller University Jena). I would like to acknowledge the German Federal Ministry of Education and Research (BMBF) for funding the research project “Regional Archives for Integrated iNvestigations”, wherein this thesis is embedded. Finally, I am deeply grateful to my parents who supported me throughout my life as well as to my friends and my girlfriend.

Manuscript overview

**Manuscripts as part of the PhD-thesis; statement of own contributions to the manuscripts;
rights and permissions for the reuse of publications**

(Manuskripte als Teil der kumulativen Dissertation; Erklärung zu den Eigenanteilen
an Publikationen; Rechte zur Wiederverwendung von
Publikationen/Zweitpublikationsrechte)

Für alle in dieser kumulativen Dissertation verwendeten Manuskripte liegen die notwendigen Genehmigungen der Verlage
(„Reprint permissions“) für die Zweitpublikation vor.

- [1] **Wündsich, M.**, Haberzettl, T., Kirsten, K.L., Kasper, T., Zabel, M., Dietze, E., Baade, J., Daut, G., Meschner, S., Meadows, M.E., Mäusbacher, R. (2016): Sea level and climate change at the southern Cape coast, South Africa, during the past 4.2 kyr. *Palaeogeography, Palaeoclimatology, Palaeoecology* 446, 295-307.

Authors	Concept of the research approach	Analyses design	Data collection	Data analysis and interpretation	Writing the manuscript	Suggested publication-equivalent
Wündsich	X	X	X	X	X	1.0
Haberzettl	X	X	X	X		n.a.
Kirsten			X	X		n.a.
Kasper			X	X		n.a.
Zabel	X		X			n.a.
Dietze			X	X		n.a.
Baade	X					n.a.
Daut	X					n.a.
Meschner			X			n.a.
Meadows	X					n.a.
Mäusbacher	X					n.a.

License:

Licensed Content Publisher: Elsevier

License Number: 4046521017976

License Date: February 12, 2017

- [2] **Wündsch, M.**, Haberzettl, T., Meadows, M.E., Kirsten, K.L., Kasper, T., Baade, J., Daut, G., Stoner, J.S., Mäusbacher, R. (2016): The impact of changing reservoir effects on the ^{14}C chronology of a Holocene sediment record from South Africa. *Quaternary Geochronology* 36, 148-160.

Authors	Concept of the research approach	Analyses design	Data collection	Data analysis and interpretation	Writing the manuscript	Suggested publication-equivalent
Wündsch	X	X	X	X	X	1.0
Haberzettl	X	X	X	X		n.a.
Meadows	X		X			n.a.
Kirsten				X		n.a.
Kasper				X		n.a.
Baade	X					n.a.
Daut	X					n.a.
Stoner			X			n.a.
Mäusbacher	X					n.a.

License:

Licensed Content Publisher: Elsevier

License Number: 4046531068249

License Date: February 12, 2017

- [3] **Wündsich, M.**, Haberzettl, T., Cawthra, H.C., Kirsten, K.L., Quick, L.J., Zabel, M., Frenzel, P., Baade, J., Daut, G., Kasper, T., Meadows, M.E., Mäusbacher, R. (subm.): Holocene environmental change along the southern Cape coast of South Africa – Insights from the Eilandvlei sediment record spanning the last 8.9 kyr.

Submitted to: Quaternary Science Reviews
 Date of Submission: 21.05.2017
 Manuscript ID: JQSR_2017_288

Authors	Concept of the research approach	Analyses design	Data collection	Data analysis and interpretation	Writing the manuscript	Suggested publication-equivalent
Wündsich	X	X	X	X	X	1.0
Haberzettl	X	X	X	X		n.a.
Cawthra			X	X		n.a.
Kirsten			X	X		n.a.
Quick			X	X		n.a.
Zabel	X		X			n.a.
Frenzel	X		X	X		n.a.
Baade	X		X	X		n.a.
Daut	X					n.a.
Kasper			X			n.a.
Meadows	X					n.a.
Mäusbacher	X					n.a.

License:

Licensed Content Publisher: n.a.

License Number: n.a.

License Date: n.a.

Die Co-Autoren der in dieser kumulativen Dissertation verwendeten Manuskripte sind sowohl über die Nutzung als auch über die oben angegebenen Eigenanteile informiert und stimmen dem zu.

Die Anteile des Promovenden als (Co-)Autor an den Publikationen und Zweitpublikationsrechte bei einer kumulativen Dissertation sind in der Anlage aufgeführt.

Name des Promovenden

Datum

Ort

Unterschrift

Ich bin mit der Abfassung der Dissertation als publikationsbasiert, d.h. kumulativ, einverstanden und bestätige die vorstehenden Angaben. Eine entsprechend begründete Befürwortung mit Angabe des wissenschaftlichen Anteils des Doktoranden / der Doktorandin an den verwendeten Publikationen werde ich parallel an den Rat der Fakultät der Chemisch-Geowissenschaftlichen Fakultät richten.

Name Erstbetreuer(in)

Datum

Ort

Unterschrift

Name Zweitbetreuer(in)

Datum

Ort

Unterschrift

Abstract

The modern climate of South Africa is determined by complex interactions of different oceanic and atmospheric circulation systems as well as the topography of the country. Large parts of South Africa receive precipitation mainly during austral summer (SRZ: summer rainfall zone). Such rainfall is mostly of tropical origin resulting from seasonal migrations of the Intertropical Convergence Zone and influenced by the warm Agulhas Current east of the country. Within a narrow belt along the southwestern part of South Africa, especially in the area around Cape Town, rainfall occurs mainly during winter when the southern westerlies are displaced equatorwards (WRZ: winter rainfall zone). The northern part of the WRZ is relatively arid which is i.a., due to the influence of the cold Benguela Current west of the sub-continent. The intermediary area between the WRZ and SRZ is characterized by a low seasonality with rainfall throughout the year (YRZ: year-round rainfall zone).

The southern Cape coast is part of the YRZ and belongs to the most humid regions within South Africa, although the range of annual rainfall totals is relatively high. Recent climatological studies aimed to quantify the contributions of different large-scale weather systems to the annual rainfall totals and found that the main portions of rainfall are brought by circulation systems that originate from the southern westerly wind belt. Furthermore, these works suggest an association between annual rainfall totals at the southern Cape coast and the Antarctic Oscillation (also known as the Southern Annular Mode) as well as the El Niño-Southern Oscillation (ENSO).

Like many other countries, South Africa is affected by modern climate change. Towards the end of this century, the IPCC (Intergovernmental Panel on Climate Change) predicts a substantial decrease in the mean evaporation and rainfall totals for southern Africa. Within the arid regions, this would lead to shorter rainfall seasons and extended droughts. In contrast, more extreme rainfall events and a generally higher weather unpredictability is expected for the more humid areas. In order to improve the prediction of future climate change, a fundamental understanding of the long-term climate dynamics during the Holocene is of particular importance. For that reason, the investigation of suitable Holocene geoarchives is essential.

Due to the geological evolution of South Africa, the occurrence of natural lakes or marshes is relatively scarce. Hence, the availability of terrestrial geoarchives for Holocene palaeoclimatological reconstructions is very limited. Moreover, the arid conditions and pronounced rainfall seasonality in large parts of the country were not favourable for the preservation of existing geoarchives whose quality was often reduced by desiccation and erosion events. Many Holocene records therefore contain hiatuses which inhibits continuous climate reconstructions. For that reason, many palaeoenvironmental reconstructions from South Africa are based on other geoarchives, such as marine sediments, speleothems or accumulated excretions of rock hyraxes (*Procapra capensis*). While recent studies from the SRZ and WRZ distinctly extended the knowledge about Holocene climate change and its triggers,

the available and partly contradicting data from the YRZ have thus far not led to a coherent understanding for this region.

The aim of this thesis is to improve the understanding of Holocene climate and environmental changes in the YRZ. For that purpose, several sediment cores were recovered from two coastal lakes (Eilandvlei and Groenvlei) at the southern Cape coast of South Africa, which is part of the YRZ.

Eilandvlei and Groenvlei are located within the Wilderness embayment about 20 km apart from each other. While Groenvlei has only a very small catchment, no river inflow and no surface connection to the Indian Ocean, Eilandvlei is fed with freshwater by two rivers and connected to the ocean via an estuary. From Groenvlei a 1.21 m sediment core was retrieved. A profile of 30.5 m length was compiled based on several sediment cores from Eilandvlei, thus representing a unique geoarchive for southern Africa. For the recovered cores, age-depth models were established using different dating methods to allow a chronological control of environmental changes. Sedimentological, geochemical and biological proxy data sets were gained for these records reflecting distinct environmental changes during the Holocene. The data provide information not only on climatic variations but also on the evolution of the present coastal lake system via different stages of connectivity to the ocean due to sea level changes.

For the sediment core from Groenvlei an age-depth model was established based on ^{14}C and ^{210}Pb dating revealing a basal age of about 4210 cal BP. The period between 2710 and 1210 cal BP is represented by only a few centimetre-thick sediments which probably indicates a hiatus in the record. The deposited sediments are mainly composed of autochthonous carbonates. A marked change in the carbonate mineralogy was identified by geochemical and mineralogical analyses. While from 4210 to 2710 cal BP, aragonite and dolomite were the main deposited carbonate phases, the period between 1210 cal BP and the present was dominated by the formation of calcite. It is concluded that the salinity of the lake water in Groenvlei was distinctly higher from 4210 to 2710 cal BP than at present. This points to an increased impact of marine water on the lake which was probably associated with a higher sea level during that time as well as with a lower precipitation/evaporation ratio and thus, drier conditions. In contrast, the period between 1210 cal BP and the present was characterized by a decreased marine influence as well as generally more humid conditions. Additionally, multiple event layers were identified which were probably deposited due to extreme rainfall events.

For the 30.5 m sediment core from Eilandvlei, a ^{14}C based age-depth model was established, where special emphasis was placed on the calibration of the conventional ^{14}C ages. These were partly obtained from samples which probably contain high amounts of marine, ^{14}C -depleted carbon which can lead to overestimations of the calibrated ^{14}C ages. Therefore, the regional marine reservoir effect and its past variations were determined and considered for the age calibration. This approach provided a reliable chronology for this exceptional and continuous geoarchive covering the past 8920 cal BP. For the topmost 1.5 m of the record (\cong past millennium), the established chronology was corroborated by palaeomagnetic secular variation stratigraphy.

In order to reconstruct environmental and climate change since 8920 cal BP, a multi-proxy data set was produced including geochemical, biological and sedimentological data. In addition, a seismic survey was conducted on Eilandvlei to get information on the sediment thickness and structure within the lake basin. The data clearly indicate that the region was subjected to marked climate and sea level changes. The rapid sea level rise during the early Holocene (8920-7870 cal BP) caused the flooding of a palaeovalley that probably formed during the Pleistocene and in which the present Eilandvlei is located. During the mid-Holocene, the sea level rose up to 3 m above its present height, which presumably caused the inundation of the entire Wilderness embayment by sea water (7870-4670 cal BP). Subsequently, the sea level dropped and a lagoon system developed that was more separated from the Ocean (4670-1240 cal BP). Finally, the present coastal lake system formed (1240 cal BP-present) which is connected to the ocean via estuaries. The palaeoclimatic data suggest that the periods from 7870 to 6440 cal BP and 3000 cal BP to the present were characterized by increased precipitation, whereas reduced rainfall occurred from 8920 to 7870 cal BP and 6440 to 3000 cal BP. Similar to the results obtained from Groenvlei, three extreme rainfall events could also be reconstructed from the Eilandvlei record (at 2070 $^{+190}/_{-160}$, 1410 $^{+120}/_{-120}$ and 1250 $^{+130}/_{-160}$ cal BP). The results obtained from both lake sediment records are generally in good agreement corroborating the reconstructed environmental conditions for the region.

The produced data sets are finally compared to available Holocene proxy data from other studies. The comparison suggests that changes in different climate factors caused rainfall variations at the southern Cape coast: for example, the data from the Eilandvlei and Groenvlei cores show similarities with reconstructed sea surface temperatures at the Southern Ocean, which in turn are probably linked to the Antarctic sea ice extent, the position of the mid-latitude westerlies and hence the Southern Annular Mode. Changes in ENSO as well as the seasonal insolation also seemed to influence climatic conditions at the southern Cape coast. Based on these comparisons, it is hypothesized that increased (reduced) rainfall at the southern Cape coast is generally associated with poleward contractions (equatorward expansions) of the Antarctic sea ice extent and the southern westerlies as well as with an enhanced (diminished) ENSO climate mode.

According to the future climate change predictions of the IPCC, the Antarctic sea ice extent and the southern westerly wind belt will be displaced further polewards until the end of this century. Moreover, a global mean sea level rise of up to 1 m is prognosticated. If both the predictions of the IPCC and the hypotheses constructed in this thesis are true, the southern Cape coast will experience not only higher annual rainfall totals and more frequent extreme rainfall events, but also a flooding of low-lying areas like the Wilderness embayment, due to rising sea levels. Such changes would cause severe socio-economic and -cultural consequences (e.g., flooding and destruction of settlements and infrastructure).

Kurzfassung

Das Klima Südafrikas ist sowohl durch das komplexe Zusammenspiel verschiedener ozeanischer und atmosphärischer Zirkulationssysteme als auch die Topographie des Landes geprägt. Der überwiegende Landesteil erhält seine Niederschläge vor allem während der südhemisphärischen Sommermonate (SRZ: Sommerregenzone). Diese Regenfälle sind meist tropischen Ursprungs und resultieren vor allem aus der saisonalen Verschiebung der Innertropischen Konvergenzzone sowie dem Einfluss des warmen Agulhasstroms im Osten des Landes. In einem schmalen Streifen im Südwesten Südafrikas fallen die Niederschläge überwiegend im Winter, wenn die Westwindzone nach Norden verlagert ist und insbesondere die Region um Kapstadt mit Regen versorgt (WRZ: Winterregenzone). Der nördliche Teil der WRZ ist jedoch zunehmend arider, was u.a. auch auf den Einfluss des kalten Benguelastroms im Westen Südafrikas zurückzuführen ist. Zwischen der WRZ und SRZ befindet sich ein Übergangsbereich, der durch eine geringe Saisonalität und ganzjährige Regenfälle gekennzeichnet ist (YRZ: ganzjährige Regenzone).

Obwohl die Spannweite der Jahresniederschlagssummen relativ groß ist, zählt die Südküste, die Teil der YRZ ist, im langjährigen Mittel zu den humidesten Regionen Südafrikas. Jüngere klimatologische Studien quantifizieren die Anteile verschiedener Großwetterlagen am Jahresgesamtniederschlag in dieser Region und fanden heraus, dass der überwiegende Teil des Regens aus Zirkulationssystemen stammt, die ihren Ursprung im Gebiet der südhemisphärischen Westwindzone haben. Darüber hinaus legen diese Arbeiten einen Zusammenhang zwischen den Jahresniederschlagsmengen an der südafrikanischen Südküste und der Antarktischen Oszillation (Southern Annular Mode) sowie dem Klimaphänomen ENSO (El Niño-Southern Oscillation) nahe.

Wie viele andere Länder ist auch Südafrika vom modernen Klimawandel betroffen. Zum Ende dieses Jahrhunderts prognostiziert der Weltklimarat IPCC (Intergovernmental Panel on Climate Change) für das südliche Afrika einen erheblichen Rückgang der durchschnittlichen Verdunstung und Niederschlagsmengen. Dies würde insbesondere in den ariden Gebieten des Landes zu verkürzten Regenzeiten und häufigeren Dürreperioden führen. In den feuchteren Landesteilen hingegen ist ein gehäuftes Auftreten von extremen Starkniederschlagsereignissen und eine generell ungenauere Vorhersagbarkeit des Wetters zu erwarten. Um zukünftige Klimavariationen besser prognostizieren zu können, ist ein grundlegendes Verständnis der langfristigen Klimadynamik während des Holozäns und damit die Untersuchung holozäner Geoarchive von enormer Bedeutung.

Aufgrund der geologischen Entwicklung Südafrikas ist das Vorkommen natürlicher Depressionen, wie z.B. Seen oder Sümpfe und damit die Anzahl verfügbarer terrestrischer Geoarchive zur Paläoumweltrekonstruktion äußerst limitiert. Zudem wurde die Erhaltung vieler Archive aufgrund des ariden Klimas, der ausgeprägten Niederschlags-saisonalität und den damit einhergehenden Austrocknungs- und Erosionsereignissen deutlich vermindert. Viele holozäne Sedimentsequenzen weisen daher Schichtlücken auf, was eine kontinuierliche Klimarekonstruktion erschwert. Deshalb basieren viele Umweltrekonstruktionen für

Südafrika auf anderen Geoarchiven, wie z.B. marinen Sedimenten, Stalagmiten oder den akkumulierten Ausscheidungen von Klippschliefern (*Procavia capensis*). Während neuere Studien aus der SRZ und WRZ den Wissensstand über holozäne Klimaschwankungen und deren Ursachen deutlich erweitern konnten, reichen die bisher vorhandenen und teilweise widersprüchlichen Arbeiten aus der YRZ bei weitem noch nicht aus um ein grundlegendes Verständnis zu entwickeln.

Das Ziel der vorliegenden Arbeit ist es den Kenntnisstand über holozäne Klima- und Umweltveränderungen in der YRZ zu erweitern. Aus diesem Grund wurden im Oktober 2013 mehrere Sedimentbohrkerne aus zwei Küstenseen (Eilandvlei und Groenvlei) an der südafrikanischen Südküste entnommen.

Die Küstenseen Eilandvlei und Groenvlei liegen etwa 20 km voneinander entfernt in der Wilderness-Region. Während der Groenvlei oberirdisch nur ein sehr kleines Einzugsgebiet, keine Zuflüsse und auch keine Verbindung zum Indischen Ozean besitzt, wird der Eilandvlei von zwei Flüssen mit Süßwasser gespeist und ist über ein Ästuarsystem mit dem Ozean verbunden. Aus dem Groenvlei konnte ein 1,21 m langer Bohrkern gewonnen werden; aus dem Eilandvlei wurden mehrere Bohrkern zu einem 30,5 m langen Sedimentprofil zusammengesetzt, was ein bisher einmaliges Geoarchiv für ganz Südafrika darstellt. Für die gewonnenen Sedimentbohrkerne wurden mithilfe verschiedener Datierungsverfahren Alters-Tiefen-Modelle erstellt um die erhobenen Umweltparameter zeitlich möglichst genau einordnen zu können. Darüber hinaus wurden für diese Archive u.a. sedimentologische, geochemische und biologische Datensätze generiert, die deutliche Umweltveränderungen während des Holozäns widerspiegeln. Neben paläoklimatischen Veränderungen lässt sich aus den Daten auch die Entwicklung der heutigen Küstenseen rekonstruieren, die aufgrund von Meeresspiegelschwankungen durch mehrere Phasen unterschiedlicher Konnektivität zum Indischen Ozean gekennzeichnet ist.

Für den Sedimentbohrkern aus dem Groenvlei wurde basierend auf ^{14}C - und ^{210}Pb -Datierungen ein Alters-Tiefen-Modell erstellt, das ein Basisalter von etwa 4210 cal BP aufweist. Der Zeitraum von 2710 bis 1210 cal BP wird durch nur wenige Zentimeter Sediment repräsentiert, was wahrscheinlich auf eine Schichtlücke hinweist. Die abgelagerten Sedimente bestehen überwiegend aus autochthonen Carbonaten. Mithilfe von mineralogischen und geochemischen Untersuchungen konnte ein markanter Wechsel in der Carbonatmineralogie der Sedimente nachgewiesen werden. Während von 4210 bis 2710 cal BP überwiegend Aragonit und Dolomit abgelagert wurden, bildete sich zwischen 1210 cal BP und der Gegenwart hauptsächlich Calcit. Dies legt nahe, dass die Salinität des Seewassers im Groenvlei zwischen 4210 und 2710 cal BP meist deutlich höher als heute war, was vermutlich mit dem größeren Einfluss von Salzwasser aufgrund eines höheren Meeresspiegels zusammenhängt. Außerdem deutet dies auf ein deutlich niedrigeres Verhältnis von Niederschlag zu Evaporation und damit generell trockenere Bedingungen als heute hin. Im Gegensatz dazu war der Zeitraum von 1210 cal BP bis zur Gegenwart durch einen geringeren marinen Einfluss und generell feuchtere Bedingungen geprägt. Darüber hinaus konnten mehrere Event-Lagen

im Sediment identifiziert werden, die wahrscheinlich als Folge von Starkniederschlagsereignissen abgelagert wurden.

Für den 30,5 m Sedimentbohrkern aus dem Eilandvlei wurde zunächst ein auf ^{14}C -Datierungen basierendes Alters-Tiefen-Modell erstellt. Der Fokus lag hierbei insbesondere auf der Kalibration der konventionellen ^{14}C -Alter, da diese zum Teil an Proben ermittelt wurden, die wahrscheinlich überwiegend marinen, ^{14}C -abgereicherten Kohlenstoff enthalten, der zur Überschätzung der kalibrierten ^{14}C -Alter führen kann. Aus diesem Grund wurden der lokale marine Reservoir-Effekt und dessen zeitliche Variationen ermittelt und bei der Kalibration berücksichtigt. Damit konnte eine robuste Chronologie für dieses einzigartige und kontinuierliche Geoarchiv erstellt werden, das wertvolle Informationen über Umweltveränderungen seit ca. 8920 cal BP enthält. Die ^{14}C -Chronologie wurde außerdem für die obersten 1,5 m des Kerns (\cong ca. letztes Jahrtausend) mithilfe von paläomagnetischen Säkularvariationen verifiziert.

Um Klima- und Umweltveränderungen seit 8920 cal BP zu rekonstruieren, wurde ein Multi-Parameter-Datensatz für den Sedimentbohrkern generiert, der u.a. auf geochemischen, biologischen und sedimentologischen Analysen basiert. Darüber hinaus wurden mehrere seismische Messungen auf dem Eilandvlei durchgeführt, die Aufschluss über die Sedimentmächtigkeit und -struktur im Becken des Sees geben. Die Interpretation der Daten zeigt, dass die Küstenregion sowohl durch Meeresspiegel- als auch Klimaschwankungen geprägt wurde. So führte der relativ schnelle Meeresspiegelanstieg im frühen Holozän (8920-7870 cal BP) dazu, dass ein wahrscheinlich bereits im Pleistozän angelegtes Tal, in dem sich der heutige Eilandvlei befindet, geflutet wurde. Im mittleren Holozän (7870-4670 cal BP) stieg der Meeresspiegel bis zu 3 m über sein heutiges Niveau an, sodass vermutlich die gesamte Wilderness-Region von Meerwasser überflutet war. Anschließend sank der Meeresspiegel, sodass sich zunächst ein stärker vom Ozean abgetrenntes Lagunensystem (4670-1240 cal BP) und letztlich die heutigen Küstenseen im späten Holozän (1240 cal BP-Gegenwart) entwickelten, die über Ästuare mit dem Indischen Ozean verbunden sind. Die gewonnenen Paläoklimaindikatoren deuten darauf hin, dass zwischen 7870 und 6440 cal BP sowie von 3000 cal BP bis zur Gegenwart relativ hohe und von 8920 bis 7870 cal BP und 6440 bis 3000 cal BP relativ niedrige Niederschlagsmengen an der südafrikanischen Südküste fielen. Außerdem konnten, ähnlich wie für den Groenvlei, drei Starkniederschlagsereignisse (um 2070 $^{+190/-160}$, 1410 $^{+120/-120}$ und 1250 $^{+130/-160}$ cal BP) rekonstruiert werden. Die Ergebnisse vom Eilandvlei und Groenvlei zeigen gute Übereinstimmungen und untermauern somit die für die Region rekonstruierten Umweltbedingungen.

Die gewonnenen Daten wurden schließlich mit den Ergebnissen anderer paläoklimatischer Studien verglichen. Hierbei zeigte sich, dass Schwankungen genau jener Klimafaktoren vermutlich eine wichtige Rolle spielten, die auch gegenwärtig für Regenfälle an der südafrikanischen Südküste verantwortlich sind. So zeigen die Daten aus dem Eilandvlei und Groenvlei Übereinstimmungen mit rekonstruierten Meeresoberflächentemperaturen im Südlichen Ozean, die wahrscheinlich wiederum mit der Ausdehnung des antarktischen Meereises sowie der Lage der Westwindzone und damit auch der Antarktischen

Oszillation in Zusammenhang stehen. Des Weiteren scheinen u.a. auch Variationen in der Ausprägung des Klimaphänomens ENSO sowie Änderungen der solaren Insolation eine Rolle zu spielen. Aus den verglichenen Daten wurde die Hypothese abgeleitet, dass feuchte (trockene) Bedingungen an der südafrikanischen Südküste generell mit einer polwärtigen (äquatorwärtigen) Verlagerung des antarktischen Meereises und der südhemisphärischen Westwindzone einhergehen sowie mit einem ausgeprägten (abgeschwächten) ENSO-Klimamodus.

Laut einer vom IPCC erstellten Prognose werden sich im Zuge des modernen Klimawandels nicht nur die antarktische Meereisbedeckung und die Westwindzone bis zum Ende dieses Jahrhunderts noch weiter polwärts verlagern, sondern auch der mittlere globale Meeresspiegel bis zu einem Meter ansteigen. Sollten sich sowohl die Prognosen des IPCC als auch die in dieser Arbeit aufgestellten Hypothesen bewahrheiten, dann wird für das Gebiet der südafrikanischen Südküste nicht nur mit höheren Jahresniederschlagsmengen und häufigeren Starkniederschlagsereignissen zu rechnen sein, sondern aufgrund des steigenden Meeresspiegels auch mit der zunehmenden Überflutung tief gelegener Landesteile wie der Wilderness-Region. Solche klimatischen Veränderungen könnten drastische sozioökonomische und -kulturelle Auswirkungen haben (z.B. Überflutung und Zerstörung von Siedlungsgebieten und Infrastruktur).

Chapter 1

Introduction

Author: Michael Wündsch

1.1 Major climate factors and climate change in South Africa

The climate of South Africa is determined by different major atmospheric and oceanic circulation systems (Fig. 1-1). The main part of the country, including most of the interior as well as the east coast, receives the majority of rainfall from tropical easterlies during austral summer. This area is referred to as the summer rainfall zone (SRZ) (Scott and Lee-Thorp, 2004). In contrast, the southwestern part of South Africa is affected by the mid-latitude westerly wind belt migrating equatorwards during austral winter and bringing rainfall to the area, which is designated as winter rainfall zone (WRZ) (Chase and Meadows, 2007). In between, there is an intermediary area that is influenced by the interaction of both tropical and temperate circulation systems. This region receives rainfall throughout the year and is therefore referred to as the year-round rainfall zone (YRZ) (Engelbrecht et al., 2015).

Rainfall amounts and distribution across South Africa are further related to the topography of the country with its elevated interior as well as to the two major oceanic circulation systems, the Benguela and Agulhas Currents (Lutjeharms et al., 2001). At the east coast of South Africa, the Agulhas Current carries warm water masses southwestwards along the continental shelf. At the west coast, the Benguela Current flows northwards representing an important upwelling system of ascending nutrient-rich and cold Antarctic waters significantly contributing to the semi-arid conditions along the northwestern part of the country (Jury et al., 1990; Lutjeharms et al., 2001).

Southern Africa represents a highly sensitive region to modern climate change as the afore-mentioned climate factors are vulnerable to variations, which may cause changes in rainfall amounts, distribution and seasonality at the sub-continent. Future scenarios published by the Intergovernmental Panel on Climate Change (IPCC) predict rising temperatures as well as a substantial mean decrease in evaporation and rainfall for southern Africa (Collins et al., 2013). Such changes in the rainfall regime would amplify droughts especially in the semi-arid regions in the northwestern part of South Africa and lead to shorter rainfall seasons, an increased frequency of extreme rainfall events as well as a generally much greater weather unpredictability in the more humid parts of the country (DEA, 2013; Thomas et al., 2007; Ziervogel et al., 2014). Moreover, climate change would drastically affect coastal areas due to rising sea levels (Brundrit and Cartwright, 2012; Mather, 2007). Changes in the water availability would have severe impacts not only on the natural ecology and biodiversity but also on the water access for farmers in agriculture as well as the population. Therefore, scientists and governmental institutions started to develop various strategies for the adaptation to modern climate change (e.g., Bryan et al., 2009; DEA, 2013; Thomas et al., 2007; Ziervogel et al., 2014).

In order to improve the prediction of and adaptation to future climate change, it is of particular importance to develop a better understanding of the mechanisms driving long-term climate change in South Africa. On glacial-interglacial timescales, palaeoclimatic studies suggest a clear relationship between climate variations and changes in the earth's orbital parameters as well as in the volume of the high-latitude ice sheets (Partridge et al., 1997; Scott et al., 2003). However, it is not well understood yet if and how these factors affected climate

variability on decadal to millennial timescales throughout the Holocene. Therefore, further work on Holocene climate variability is urgently required.

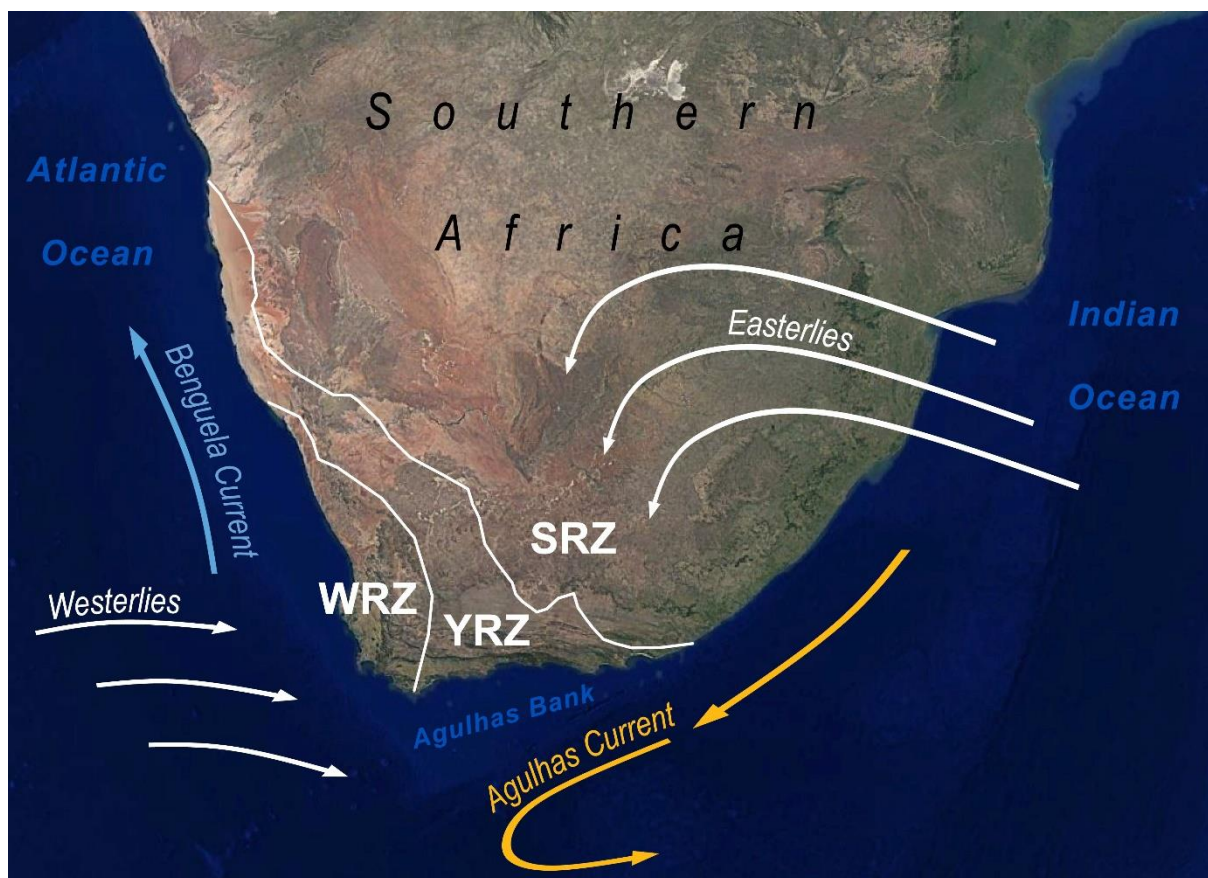


Fig. 1-1: Map of southern Africa (Google earth image) with its different rainfall zones (WRZ: winter rainfall zone, SRZ: summer rainfall zone, YRZ: year-round rainfall zone) and major atmospheric and oceanic circulation systems.

1.2 Reconstructions of Holocene climate change in South Africa

The reconstruction of Holocene climate change in South Africa is a challenging task. Due to the geological evolution of the country, natural depressions containing lakes are relatively scarce and hence the availability of suitable and high-resolution Holocene geoarchives is limited (Scott and Lee-Thorp, 2004). Moreover, the pronounced seasonality prevailing in large parts of the country repeatedly led to desiccation and erosion events which have diminished the quality of many existing terrestrial sediment sequences (Chase and Meadows, 2007; Scott and Lee-Thorp, 2004). As a result, many existing sediment records are either discontinuous or confined to certain periods of the Holocene (Baxter and Meadows, 1999; Stager et al., 2012, 2013). Due to dating uncertainties and low sampling intervals some investigated archives only provide a low temporal resolution (Finch and Hill, 2008; Meadows and Baxter, 2001; Scott et al., 2012; Stager et al., 2013). Another type of geoarchives that have been increasingly explored in South Africa during the last decades, are urinary and faecal accumulations of rock hyraxes (*Procavia capensis*), forming stratified middens that allow conclusions about feeding habits and moisture availability (Chase et al., 2012, 2013; Scott and Woodborne, 2007). A few data sets are available from speleothem records which were interpreted to reflect temperature and hydrological changes (Holmgren et al., 2003; Lee-Thorp et al., 2001; Talma and Vogel, 1992).

Coastal wetlands, such as lagoons and coastal lakes, provide another opportunity for palaeoenvironmental reconstructions as they can contain well-preserved and continuous sediment deposits. However, potential climate signals in these archives are often superimposed by past sea level changes associated with local geomorphological alterations (Baxter and Meadows, 1999; Carr et al., 2015; Compton, 2001; Meadows and Baxter, 2001).

Due to the afore-mentioned difficulties and the spatial heterogeneity of the nature and direction of reconstructed local climate trends, a comprehensive understanding of the larger-scale mechanisms and driving forces of Holocene climate change in southern Africa is thus far absent (Burrough and Thomas, 2013; Chase and Meadows, 2007). The scarcity of palaeoclimatic proxy data moreover limits the testing of hypotheses inferred from conceptual climate models (Valsecchi et al., 2013). Nevertheless, various climate factors have been discussed in conjunction with available Holocene palaeoclimatic proxy data from southern Africa, such as variations in the solar insolation (Chase et al., 2009; Chevalier and Chase, 2015; Zhao et al., 2016), the position and strength of the mid-latitude westerlies (Chase and Meadows, 2007; Stager et al., 2012) and the Intertropical Convergence Zone (Burrough and Thomas, 2013; Scott et al., 2012) as well as the varying influences of the Agulhas and Benguela Current (Chase et al., 2010; Scott et al., 2012). Within the last few years, several recent studies have been published contributing new palaeoclimatic evidence and increasing the spatial coverage of Holocene proxy data from South Africa (Chase et al., 2013, 2015a, 2015b; Chevalier and Chase, 2015; Hahn et al., 2016; Zhao et al., 2016). Especially for the WRZ and SRZ, existing data sets have been synthesized and linked to changing climate factors (Chevalier and Chase, 2015; Zhao et al., 2016). A clear trend from drier conditions in the early Holocene towards wetter conditions in the late Holocene was reconstructed for the northern part of the SRZ and linked to an increasing regional summer insolation (Chevalier and Chase, 2015). In contrast, Holocene precipitation changes in the WRZ were attributed to changes in the position of the mid-latitude westerlies (Zhao et al., 2016).

The available palaeoclimatic data from the YRZ is difficult to reconcile and has consequently not led to a coherent understanding of Holocene climatic variability and its driving mechanisms for this region (Chase et al., 2013; Cohen and Tyson, 1995; Martin, 1959, 1968; Quick et al., 2015, 2016; Talma and Vogel, 1992). Pollen and diatom assemblages were investigated in coastal fen sediments from a wetland near Groenvlei, a coastal lake located at the southern Cape coast (YRZ; Fig. 1-2) (Martin, 1959, 1968). The data mainly reflect ecological changes due to Holocene sea level variations, but also point to changes in the vegetation cover on the surrounding dunes and hence changes in sand transport and moisture availability. However, only two ^{14}C ages were determined, providing just a vague age control for these sediments which are assumed to represent the last ~8 kyr (Martin, 1959, 1968).

Another pollen record spanning the last ~140 kyr is available from a sediment core from Vankervelsvlei, a wetland situated about 3 km inland from Groenvlei (Fig. 1-2) (Quick et al., 2016). The record reflects regional vegetation changes during the Pleistocene, but does not allow any conclusions about climatic variations within the Holocene, which is represented only by two samples.

Sediment cores from the coastal lake Eilandvlei (Fig. 1-2) were investigated by Reinwarth et al. (2013) and Kirsten (2014). The former study applied geochemical and sedimentological analyses on a short core which covers only the past ~0.7 kyr. The data possibly reflect increased runoff and rainfall since the Little Ice Age from 550 cal BP onwards although the signal is superimposed by enhanced anthropogenic impact in the catchment since the 19th century (Reinwarth et al., 2013). The latter examined the diatom assemblages in a sediment core spanning the last ~4 kyr and focussed particularly on the coastal lake evolution in relation to varying marine influences. In contrast to the former study, a declining percentage of freshwater species from 500 cal BP onwards points to decreasing freshwater inputs since the Little Ice Age (Kirsten, 2014).

Geochemical proxies were obtained from a marine sediment core (GeoB18308-1) recovered ~4 km off the Gouritz River mouth (Fig. 1-2) (Hahn et al., 2016). This record spans the last ~4.8 kyr and was interpreted to reflect arid climatic conditions from 4880 to 1150 cal BP and from the Little Ice Age onwards (after 600 cal BP) as well as humid conditions in the Gouritz River catchment during the Medieval Climate Anomaly (1150-650 cal BP) (Hahn et al., 2016).

Holocene sea surface temperatures (SSTs) of the Agulhas Bank were reconstructed based on $\delta^{18}\text{O}$ data obtained from marine mollusc shells deposited at Nelson Bay Cave (Fig. 1-2) (Cohen and Tyson, 1995). However, the significance of this record is limited as the reconstructed SST data contain very high uncertainties, are very fragmentary especially for the late Holocene and are presented based on conventional radiocarbon ages. Nevertheless, the data indicate that higher SSTs than at present prevailed at the Agulhas Bank around 6000 BP (Cohen and Tyson, 1995).

Based on $\delta^{13}\text{C}$ and $\delta^{18}\text{O}$ data obtained from a stalagmite record from the Cango Caves (Fig. 1-2), a Holocene temperature reconstruction of the past ~5 kyr is available for the YRZ (Talma and Vogel, 1992). The data suggest that between 5000 and 2500 cal BP, temperatures were approximately 1-2 °C lower than at present and distinctly increased thereafter. The authors hypothesized that the period from 5000 to 2500 cal BP was characterized by a winter rainfall seasonality, whereas between 2500 cal BP and the present, the modern year-round rainfall pattern established (Talma and Vogel, 1992).

Two hyrax midden records were analysed from Seweweekspoort (YRZ), located in the Swartberg Mountains (Fig. 1-2). The obtained $\delta^{15}\text{N}$ data were interpreted to reflect changes in moisture availability during the past ~8 kyr (Chase et al., 2013). However, the reliability of the two published records is questionable as they do not show consistent variations over time. Moreover, additional midden records from this site are currently being investigated whereby the published data will become obsolete in its present form (Chase pers. comm.).

A multi-proxy approach was applied on a sediment core retrieved from a wetland near Still Bay (Fig. 1-2) (Quick et al., 2015). The record spans the last ~16 kyr and suggests a relatively humid early (11000-7000 cal BP) and late Holocene (2200 cal BP-present) as well as more arid conditions during the mid-Holocene (7000-3300 cal BP) (Quick et al., 2015).

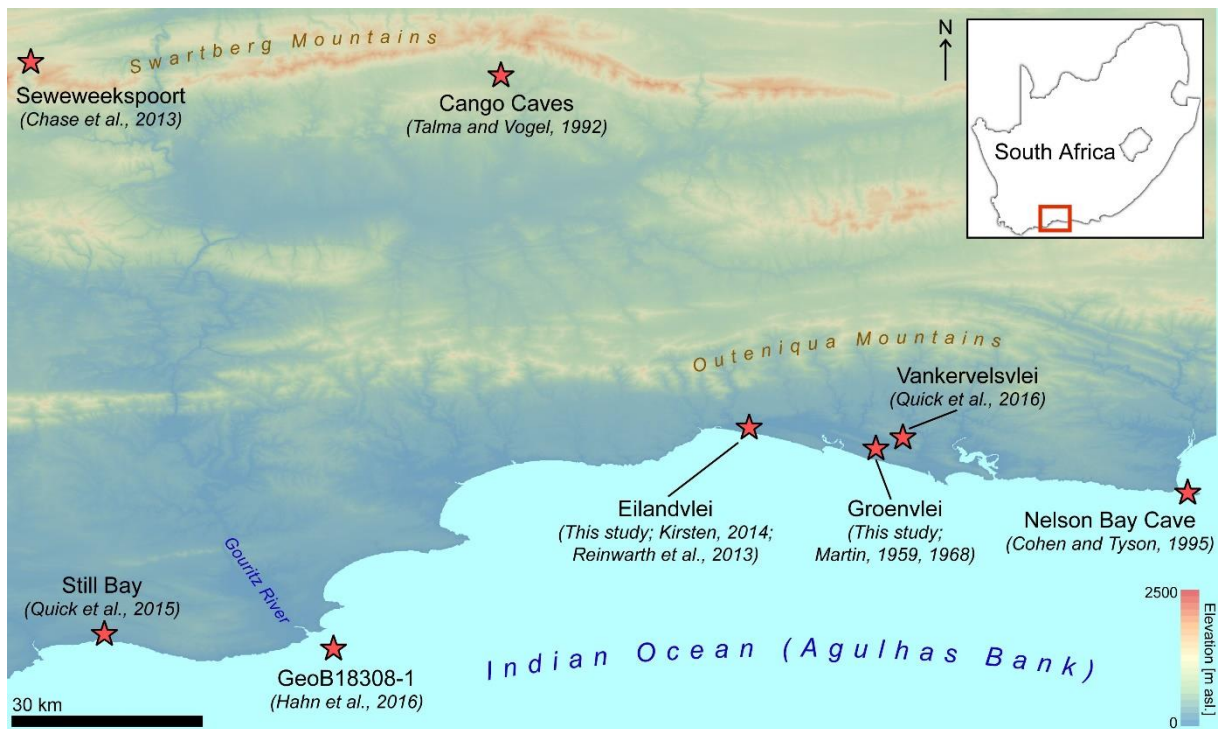


Fig. 1-2: Map of the southern Cape coast of South Africa showing locations of available geoarchives (red stars) from the year-round rainfall zone (YRZ). The location of this map section within South Africa is shown in the upper right corner.

1.3 The framework of the RAIN project

This PhD thesis is part of the collaborative project RAIN (Regional Archives for Integrated iNvestigations; Fig. 1-3) that is embedded in the international research programme SPACES (Science Partnership for the Assessment of Complex Earth System Dynamics) and funded by the German Federal Ministry of Education and Research (BMBF) (Haberzettl et al., 2014). The main objective of the project, which started in July 2013, is to contribute new knowledge about Holocene palaeoclimate dynamics in southern Africa. In particular, RAIN aims to gain a better understanding of the interactions between atmospheric and oceanic circulation systems both driving climate change at the sub-continent. Therefore, proxy data sets from terrestrial and marine geoarchives from all three rainfall zones are investigated and interpreted in conjunction.



Fig. 1-3: Logo of the collaborative research project RAIN (Regional Archives for Integrated iNvestigations) funded by the German Federal Ministry of Education and Research (BMBF).

RAIN is subdivided in four scientific sub-projects and one for education and capacity building. Within the scientific sub-projects a variety of interdisciplinary approaches are applied (e.g., geochronology, stable isotope analyses, organic and inorganic geochemistry, mineralogy, micropalaeontology) (Haberzettl et al., 2014). The presented thesis is part of RAIN

sub-project 1 ('Lacustrine sediments: high-resolution paleoenvironmental archives') and focuses on sediment cores from the YRZ which were recovered from the coastal lakes Groenvlei and Eilandvlei, located within the Wilderness embayment at the southern Cape coast of South Africa (Fig. 1-4).

1.4 Regional setting and study site – The Wilderness embayment

The southern Cape coast is part of the YRZ and characterized by an almost uniform annual rainfall distribution with each month contributing $\geq 5\%$ to the annual rainfall totals (1979-2011) (Engelbrecht et al., 2015). The Wilderness area is relatively humid as shown by the three closest weather stations which recorded yearly rainfall totals ranging between 375 and 1474 mm (mean: 800 mm; 1993-2016) (SAWS, 2017). Complex interactions of tropical moisture-bearing systems with the mid-latitude westerlies produce different weather systems causing rainfall along the southern Cape coast (Tyson, 1986). Ridging anticyclones and cut-off lows represent the main synoptic-scale weather systems bringing rainfall from the mid-latitude westerlies. Tropical-temperate trough cloud bands create rainfall of tropical origin (Engelbrecht et al., 2015; Favre et al., 2013). Cut-off lows can cause extreme rainfall events leading to destructive floods in the area (Engelbrecht et al., 2015; Rouault et al., 2002; Weldon and Reason, 2014). It was found that the frequency of cut-off lows seems to be linked to the El Niño-Southern Oscillation (ENSO) indicating an increased number of cut-off lows during La Niña events (Engelbrecht and Landman, 2016; Favre et al., 2013; Weldon and Reason, 2014). Moreover, the rainfall variability in South Africa is likely associated with the Southern Annular Mode (SAM) which reflects the atmospheric zonal mean pressure gradient between the mid-latitudes ($\sim 40^\circ\text{S}$) and Antarctica ($\sim 65^\circ\text{S}$) (Marshall, 2003; Thompson and Wallace, 2000). During the positive (negative) state of the SAM, this gradient is enhanced (diminished) and rainfall occurs more (less) frequently along the southern Cape coast (Engelbrecht and Landman, 2016; Reason and Rouault, 2005). Rainfall distribution is moreover influenced by the local topography that induces orographic rainfall as well as by the SSTs off South Africa, especially at the Agulhas Current region (Engelbrecht and Landman, 2016; Engelbrecht et al., 2015; Rouault et al., 2002; Singleton and Reason, 2006).

The Wilderness embayment is situated at the southern Cape coast (Fig. 1-4) and most likely formed after multiple transgressive-regressive cycles during the Pleistocene (Bateman et al., 2011; Birch et al., 1978; Cawthra et al., 2014; Hart, 1995; Martin, 1962). To the south, the lakes are separated from the Indian Ocean by Pleistocene aeolianites which are partly covered by unconsolidated Holocene sands (Bateman et al., 2011; Illenberger, 1996). To the north, the embayment is bordered by an up to 200 m high coastal platform composed of granitic and metasedimentary bedrocks (Browning and Macey, 2015; Ferré and Améglio, 2000; Frimmel and Van Achterbergh, 1995), which are partly covered by Pleistocene sands (Marker and Holmes, 2002). The coastal platform was tectonically lifted during the Neogene (Partridge, 1997), but within the Quaternary the southern Cape coast is considered as tectonically stable (Cawthra et al., 2014). Several southward flowing rivers created deeply incised valleys crossing the coastal platform and entering the coastal lakes (Fig. 1-4). The upper catchments

and springs of these rivers are located within the up to 1500 m high Outeniqua Mountains to the north, which are mainly composed of quartzites, quartzitic sandstones and shales (Balfour and Bond, 1993; Booth, 2011).

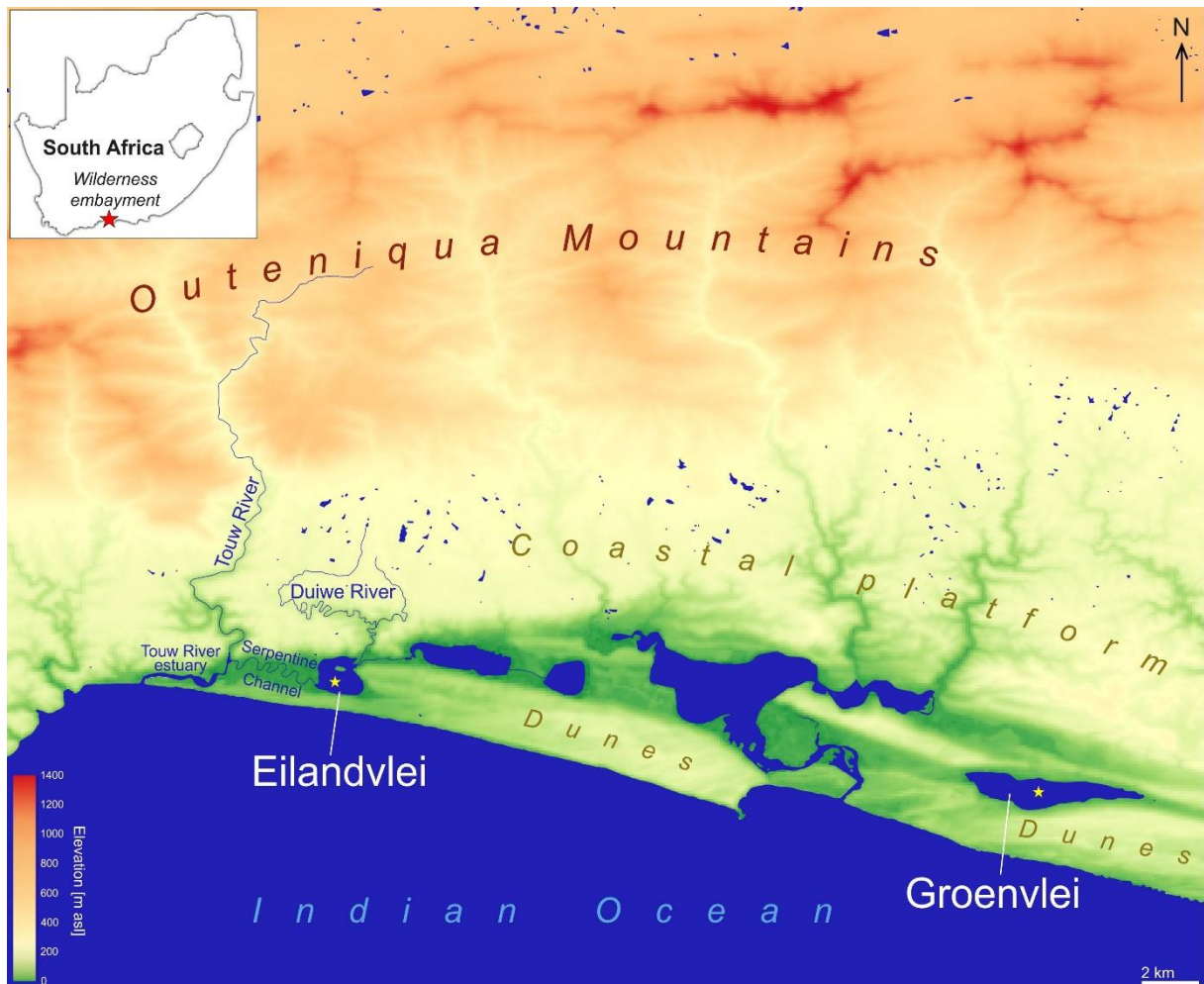


Fig. 1-4: The Wilderness embayment including the coastal lakes Eilandvlei and Groenvlei. The coring positions at both lakes are indicated as yellow stars. The location of the Wilderness embayment within South Africa is shown as red star in the upper left corner.

The terrestrial vegetation around the lakes is composed of various species of the Fynbos Biome which is particularly prevalent on the dunes. Moreover, several species of the Southern Afrotemperate Forest mainly occur in the river valleys (Mucina and Rutherford, 2006; Quick et al., 2016). Semi-aquatic, emergent plants cover the floodplains around the lakes and aquatic, submerged plants and algae represent major proportions of biomass within the lakes (Allanson and Whitfield, 1983; Howard-Williams, 1980; Russell, 2003).

Eilandvlei is the westernmost coastal lake within the Wilderness embayment. It is connected to the Indian Ocean via the Serpentine Channel and the Touw River estuary (Fig. 1-4). A temporarily forming sandbar blocks the Touw River estuary mouth and hence the surface connection of Eilandvlei to the Indian Ocean. When the estuary mouth is open, seawater can enter the Touw River estuary and the coastal lakes. When the estuary mouth is closed, freshwater discharge from the Touw River mixes with brackish water of the estuary and may cause the backflow via the Serpentine Channel into Eilandvlei. The Duiwe River

enters Eilandvlei from the northeast. To the east, Eilandvlei is connected to the adjacent coastal lake Langvlei via a narrow channel. In contrast, Groenvlei represents the easternmost coastal lake within the Wilderness embayment and has no surface connection to the Indian Ocean, no river inflow and a very small aboveground catchment. Thus, the lake is mainly fed by direct rainfall and to a lesser degree by ground water discharge from the north (Parsons, 2014).

1.5 Thesis outline

The main goal of this PhD thesis is to generate and interpret new proxy data from the southern Cape coast in order to improve the understanding of Holocene climate dynamics and its drivers in the YRZ. For that purpose, sediment cores from the coastal lakes Groenvlei and Eilandvlei (Fig. 1-5) are investigated. Past geomorphological changes of the present estuarine/coastal lake system due to Holocene sea level changes are inferred from the interpreted proxy data. Palaeoclimatic long-term changes as well as short-term events in the lake catchment are reconstructed and discussed in the context of varying large-scale climate factors. Special emphasis is placed on age determination, calibration and the establishment of robust age-depth models for these sediment cores to allow a reliable geochronological control of the discussed proxy data.

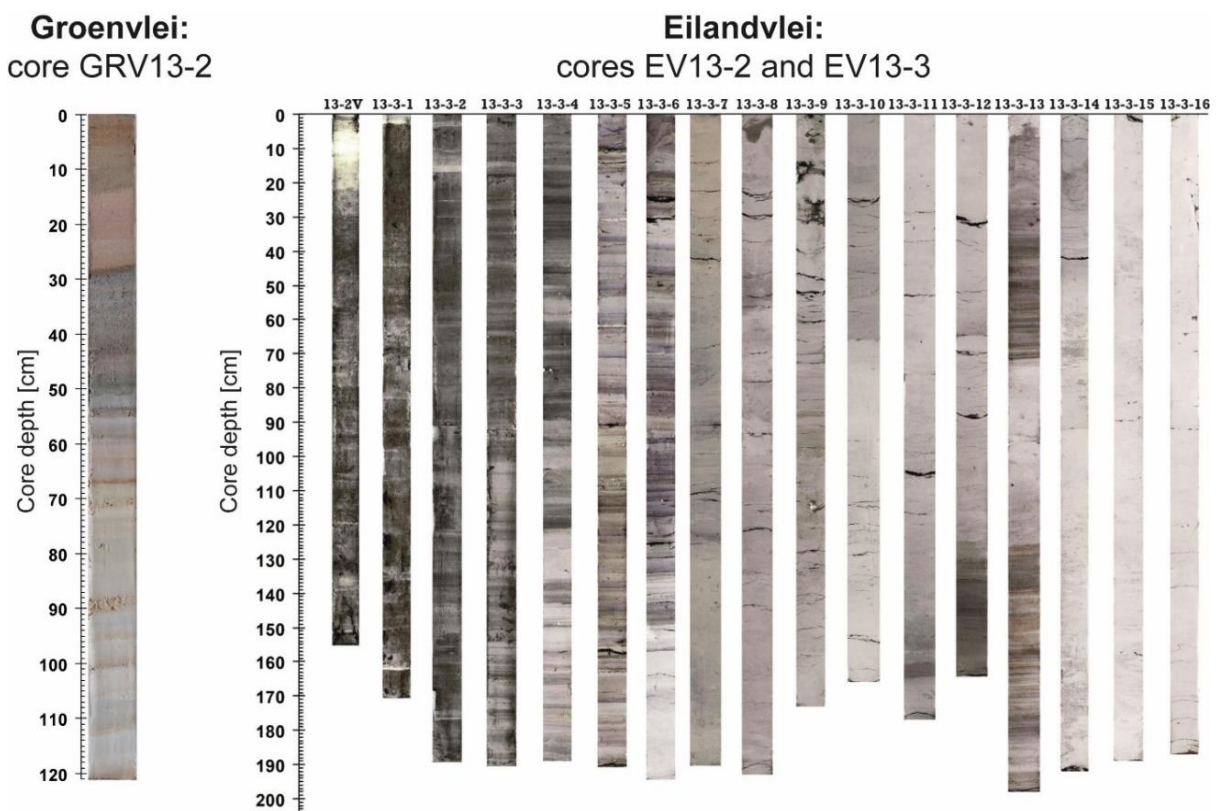


Fig. 1-5: Investigated sediment cores in this thesis; left: image of core GRV13-2 from Groenvlei; right: contrast-enhanced images of several core sections (EV13-2 and EV13-3) from Eilandvlei.

Firstly, proxy data derived from the Groenvlei sediment short core (1.21 m; Fig. 1-5) are presented and discussed as well as an age-depth model dating back to 4210 cal BP. The applied methods include grain size analyses as well as geochemical and mineralogical

investigations with a special focus on the carbonate sedimentology. The interpreted data are mainly discussed in terms of environmental changes in and around Groenvlei, which are linked to regional sea level and climate variations (**chapter 2**).

Secondly, a 30.5 m profile is compiled based on three sediment cores recovered from Eilandvlei (Fig. 1-5). A robust chronology for this exceptional geoarchive is established to provide a solid basis for palaeoenvironmental reconstructions. The age-depth model is based on 24 ¹⁴C-dated samples of different material. Past changes in the regional marine reservoir effect are reconstructed and considered during the calibration of conventional radiocarbon ages. The established chronology reveals a basal age of 8920 cal BP and is corroborated by palaeomagnetic secular variation stratigraphy for the topmost part of the record (**chapter 3**).

Thirdly, a multi-proxy data set (including geochemical, mineralogical, grain size, seismic, foraminifera and diatom data) is gained from the Eilandvlei sediment core to infer environmental changes in the area. The Holocene evolution of the Wilderness embayment towards the present estuarine/coastal lake system is reconstructed. Distinct phases of connectivity to the ocean due to sea level changes are traced back as well as local variations in the fluvial sediment supply associated with precipitation changes. The palaeorainfall proxies are further compared to regional and remote proxy data. Variations in regional and hemispheric climate factors are discussed as possible drivers of climate change at the southern Cape coast (**chapter 4**).

Finally, the results obtained within this thesis are synthesized with those from previous studies from the YRZ to draw a comprehensive picture of Holocene environmental change in this region. The outcome is further discussed in the context of transregional palaeoclimatic changes in the southern hemisphere as well as for the perception of recent and future climate change in South Africa. Additionally, unresolved questions are discussed which may represent opportunities for future research (**chapter 5**).

1.6 References

- Allanson, B.R., Whitfield, A.K., 1983. The Limnology of the Touw River floodplain. South African Scientific Programmes, Report No 79, Pretoria, South Africa.
- Balfour, D., Bond, W., 1993. Factors limiting climber distribution and abundance in a southern African forest. *Journal of Ecology*, 93-100.
- Bateman, M.D., Carr, A.S., Dunajko, A.C., Holmes, P.J., Roberts, D.L., McLaren, S.J., Bryant, R.G., Marker, M.E., Murray-Wallace, C.V., 2011. The evolution of coastal barrier systems: a case study of the Middle-Late Pleistocene Wilderness barriers, South Africa. *Quaternary Science Reviews* 30, 63-81.
- Baxter, A.J., Meadows, M.E., 1999. Evidence for Holocene sea level change at Verlorenvlei, Western Cape, South Africa. *Quaternary International* 56, 65-79.
- Birch, G., Du Plessis, A., Willis, J., 1978. Offshore and onland geological and geophysical investigations in the Wilderness Lakes region. *Transactions of the Geological Society of South Africa* 81, 339-352.
- Booth, P., 2011. Stratigraphic, structural and tectonic enigmas associated with the Cape Fold Belt: challenges for future research. *South African Journal of Geology* 114, 235-248.
- Browning, C., Macey, P., 2015. Lithostratigraphy of the George Pluton Units (Cape Granite Suite), South Africa. *South African Journal of Geology* 118, 323-330.
- Brundrit, G., Cartwright, A., 2012. Understanding the risks to Cape Town of inundation from the sea. In: Cartwright, A., Parnell, S., Oelofse, G., Ward, S. (Eds.). *Climate Change at the City Scale: Impacts, Mitigation and Adaptation in Cape Town*. Routledge, New York, USA, 21-37.

- Bryan, E., Deressa, T.T., Gbetibouo, G.A., Ringler, C., 2009. Adaptation to climate change in Ethiopia and South Africa: options and constraints. *Environmental Science & Policy* 12, 413-426.
- Burrough, S., Thomas, D., 2013. Central southern Africa at the time of the African Humid Period: a new analysis of Holocene palaeoenvironmental and palaeoclimate data. *Quaternary Science Reviews* 80, 29-46.
- Carr, A.S., Boom, A., Chase, B.M., Meadows, M.E., Grimes, H.L., 2015. Holocene sea level and environmental change on the west coast of South Africa: evidence from plant biomarkers, stable isotopes and pollen. *Journal of Paleolimnology* 53, 415-432.
- Cawthra, H.C., Bateman, M.D., Carr, A.S., Compton, J.S., Holmes, P.J., 2014. Understanding Late Quaternary change at the land–ocean interface: a synthesis of the evolution of the Wilderness coastline, South Africa. *Quaternary Science Reviews* 99, 210-223.
- Chase, B.M., Boom, A., Carr, A.S., Carré, M., Chevalier, M., Meadows, M.E., Pedro, J.B., Stager, J.C., Reimer, P.J., 2015a. Evolving southwest African response to abrupt deglacial North Atlantic climate change events. *Quaternary Science Reviews* 121, 132-136.
- Chase, B.M., Boom, A., Carr, A.S., Meadows, M.E., Reimer, P.J., 2013. Holocene climate change in southernmost South Africa: rock hyrax middens record shifts in the southern westerlies. *Quaternary Science Reviews* 82, 199-205.
- Chase, B.M., Lim, S., Chevalier, M., Boom, A., Carr, A.S., Meadows, M.E., Reimer, P.J., 2015b. Influence of tropical easterlies in southern Africa's winter rainfall zone during the Holocene. *Quaternary Science Reviews* 107, 138-148.
- Chase, B.M., Meadows, M.E., 2007. Late Quaternary dynamics of southern Africa's winter rainfall zone. *Earth-Science Reviews* 84, 103-138.
- Chase, B.M., Meadows, M.E., Scott, L., Thomas, D., Marais, E., Sealy, J., Reimer, P., 2009. A record of rapid Holocene climate change preserved in hyrax middens from southwestern Africa. *Geology* 37, 703-706.
- Chase, B.M., Scott, L., Meadows, M.E., Gil-Romera, G., Boom, A., Carr, A.S., Reimer, P.J., Truc, L., Valsecchi, V., Quick, L.J., 2012. Rock hyrax middens: a palaeoenvironmental archive for southern African drylands. *Quaternary Science Reviews* 56, 107-125.
- Chevalier, M., Chase, B.M., 2015. Southeast African records reveal a coherent shift from high-to low-latitude forcing mechanisms along the east African margin across last glacial–interglacial transition. *Quaternary Science Reviews* 125, 117-130.
- Cohen, A., Tyson, P.D., 1995. Sea-surface temperature fluctuations during the Holocene off the south coast of Africa: implications for terrestrial climate and rainfall. *The Holocene* 5, 304-312.
- Collins, M., Knutti, R., Arblaster, J., Dufresne, J.-L., Fichefet, T., Friedlingstein, P., Gao, X., Gutowski, W.J., Johns, T., Krinner, G., Shongwe, M., Tebaldi, C., Weaver, A.J., Wehner, M., 2013. Long-term Climate Change: Projections, Commitments and Irreversibility. In: Stocker, T.F., Qin, D., Plattner, G.-K., Tignor, M., Allen, S.K., Boschung, J., Nauels, A., Xia, Y., Bex, V., Midgley, P.M. (Eds.). *Climate Change 2013: The Physical Science Basis. Contribution of Working Group I to the Fifth Assessment Report of the Intergovernmental Panel on Climate Change*. Cambridge University Press, Cambridge, United Kingdom and New York, NY, USA.
- Compton, J.S., 2001. Holocene sea-level fluctuations inferred from the evolution of depositional environments of the southern Langebaan Lagoon salt marsh, South Africa. *The Holocene* 11, 395-405.
- DEA (Department of Environmental Affairs), 2013. Long-Term Adaptation Scenarios for South Africa. Report No. 7 for the long-term adaptation scenarios flagship research program (LTAS). Department of Environmental Affairs, Pretoria, South Africa.
- Engelbrecht, C.J., Landman, W.A., 2016. Interannual variability of seasonal rainfall over the Cape south coast of South Africa and synoptic type association. *Climate Dynamics* 47, 295-313.
- Engelbrecht, C.J., Landman, W.A., Engelbrecht, F.A., Malherbe, J., 2015. A synoptic decomposition of rainfall over the Cape south coast of South Africa. *Climate Dynamics* 44, 2589-2607.
- Favre, A., Hewitson, B., Lennard, C., Cerezo-Mota, R., Tadross, M., 2013. Cut-off lows in the South Africa region and their contribution to precipitation. *Climate Dynamics* 41, 2331-2351.
- Ferré, E., Améglio, L., 2000. Preserved magnetic fabrics vs. annealed microstructures in the syntectonic recrystallised George granite, South Africa. *Journal of Structural Geology* 22, 1199-1219.

- Finch, J.M., Hill, T.R., 2008. A late quaternary pollen sequence from Mfabeni Peatland, South Africa: reconstructing forest history in Maputaland. *Quaternary Research* 70, 442-450.
- Frimmel, H., Van Achterbergh, E., 1995. Metamorphism of calc-silicate and associated rocks in the Pan-African Kaaimans Group, Saldania Belt, South Africa. *Mineralogy and Petrology* 53, 75-102.
- Haberzettl, T., Baade, J., Compton, J., Daut, G., Dupont, L., Finch, J., Frenzel, P., Green, A., Hahn, A., Hebbeln, D., Helmschrot, J., Humphries, M., Kasper, T., Kirsten, K.L., Mäusbacher, R., Meadows, M.E., Meschner, S., Quick, L.J., Schefuß, E., Wüdsch, M., Zabel, M., 2014. Paleoenvironmental investigations using a combination of terrestrial and marine sediments from South Africa - The RAIN (Regional Archives for Integrated iNvestigations) approach. *Zentralblatt für Geologie und Paläontologie, Teil I, Heft 1*, 55-73.
- Hahn, A., Schefuß, E., Andò, S., Cawthra, H.C., Frenzel, P., Kugel, M., Meschner, S., Mollenhauer, G., Zabel, M., 2016. Linking catchment hydrology and ocean circulation in Late Holocene southernmost Africa. *Climate of the Past Discussions*. doi:10.5194/cp-2016-100.
- Hart, R.C., 1995. South African coastal lakes. In: Cowan, G.I., (Ed.). *Wetlands of South Africa*. Pretoria: Department of Environmental Affairs and Tourism, 103-130.
- Holmgren, K., Lee-Thorp, J.A., Cooper, G.R., Lundblad, K., Partridge, T.C., Scott, L., Sithaldeen, R., Talma, A.S., Tyson, P.D., 2003. Persistent millennial-scale climatic variability over the past 25,000 years in Southern Africa. *Quaternary Science Reviews* 22, 2311-2326.
- Howard-Williams, C., 1980. Aquatic macrophyte communities of the Wilderness lakes: community structure and associated environmental conditions. *Journal of the Limnological Society of Southern Africa* 6, 85-92.
- Illenberger, W.K., 1996. The geomorphologic evolution of the Wilderness dune cordons, South Africa. *Quaternary International* 33, 11-20.
- Jury, M., MacArthur, C., Brundrit, G., 1990. Pulsing of the Benguela upwelling region: large-scale atmospheric controls. *South African Journal of Marine Science* 9, 27-41.
- Kirsten, K., 2014. Late Holocene diatom community responses to climate variability along the southern Cape coastal plain, South Africa. PhD Thesis. University of Cape Town, Cape Town, South Africa.
- Lee-Thorp, J., Holmgren, K., Lauritzen, S.E., Linge, H., Moberg, A., Partridge, T.C., Stevenson, C., Tyson, P., 2001. Rapid climate shifts in the southern African interior throughout the mid to late Holocene. *Geophysical Research Letters* 28, 4507-4510.
- Lutjeharms, J., Monteiro, P., Tyson, P., Obura, D., 2001. The oceans around southern Africa and regional effects of global change: START Regional Syntheses. *South African Journal of Science* 97, 119-130.
- Marker, M.E., Holmes, P.J., 2002. The distribution and environmental implications of coversand deposits in the Southern Cape, South Africa. *South African Journal of Geology* 105, 135-146.
- Marshall, G.J., 2003. Trends in the Southern Annular Mode from observations and reanalyses. *Journal of Climate* 16, 4134-4143.
- Martin, A.R.H., 1959. The stratigraphy and history of Groenvlei, a South African coastal fen. *Australian Journal of Botany* 7, 142-167.
- Martin, A.R.H., 1962. Evidence relating to the Quarternary history of the Wilderness lakes. *Transactions of the Geological Society of South Africa* 65, 19-42.
- Martin, A.R.H., 1968. Pollen analysis of Groenvlei lake sediments, Knysna (South Africa). *Review of Palaeobotany and Palynology* 7, 107-144.
- Mather, A., 2007. Linear and nonlinear sea-level changes at Durban, South Africa. *South African Journal of Science* 103, 509-512.
- Meadows, M.E., Baxter, A.J., 2001. Holocene vegetation history and palaeoenvironments at Klaarfontein Springs, Western Cape, South Africa. *The Holocene* 11, 699-706.
- Mucina, L., Rutherford, M.C., 2006. *The vegetation of South Africa, Lesotho and Swaziland*. South African National Biodiversity Institute, Pretoria.
- Parsons, R.P., 2014. Quantifying the role of groundwater in sustaining Groenvlei, a shallow lake in the southern Cape region of South Africa. PhD Thesis. University of the Free State, Bloemfontein, South Africa.

- Partridge, T.C., 1997. Cainozoic environmental change in southern Africa, with special emphasis on the last 200 000 years. *Progress in Physical Geography* 21, 3-22.
- Partridge, T.C., DeMenocal, P., Lorentz, S., Paiker, M., Vogel, J., 1997. Orbital forcing of climate over South Africa: a 200,000-year rainfall record from the Pretoria Saltpan. *Quaternary Science Reviews* 16, 1125-1133.
- Quick, L.J., Carr, A.S., Meadows, M.E., Boom, A., Bateman, M.D., Roberts, D.L., Reimer, P.J., Chase, B.M., 2015. A late Pleistocene–Holocene multi-proxy record of palaeoenvironmental change from Still Bay, southern Cape Coast, South Africa. *Journal of Quaternary Science* 30, 870-885.
- Quick, L.J., Meadows, M.E., Bateman, M.D., Kirsten, K.L., Mäusbacher, R., Haberzettl, T., Chase, B.M., 2016. Vegetation and climate dynamics during the last glacial period in the fynbos-afrotemperate forest ecotone, southern Cape, South Africa. *Quaternary International* 404, Part B, 136-149.
- Reason, C., Rouault, M., 2005. Links between the Antarctic Oscillation and winter rainfall over western South Africa. *Geophysical Research Letters* 32, L07705, doi:10.1029/2005GL022419.
- Reinwarth, B., Franz, S., Baade, J., Haberzettl, T., Kasper, T., Daut, G., Helmschrot, J., Kirsten, K.L., Quick, L.J., Meadows, M.E., 2013. A 700-year record on the effects of climate and human impact on the southern Cape coast inferred from lake sediments of Eilandvlei, Wilderness Embayment, South Africa. *Geografiska Annaler: Series A, Physical Geography* 95, 345-360.
- Rouault, M., White, S., Reason, C., Lutjeharms, J., Jobard, I., 2002. Ocean–atmosphere interaction in the Agulhas Current region and a South African extreme weather event. *Weather and Forecasting* 17, 655-669.
- Russell, I., 2003. Changes in the distribution of emergent aquatic plants in a brackish South African estuarine-lake system. *African Journal of Aquatic Science* 28, 103-122.
- SAWS (South African Weather Service), 2017. Rainfall data from the weather stations 0012661 7 (George WO), 0014123 3 (Knysna), and 0028776 9 (George Witfontein). South African Weather Service, Pretoria, South Africa.
- Scott, L., Holmgren, K., Talma, A.S., Woodborne, S., Vogel, J.C., 2003. Age interpretation of the Wonderkrater spring sediments and vegetation change in the Savanna Biome, Limpopo province, South Africa: research letter. *South African Journal of Science* 99, 484-488.
- Scott, L., Lee-Thorp, J.A., 2004. Holocene climatic trends and rhythms in southern Africa. In: Battarbee, R.W., Gasse, F., Stickley, C.E. (Eds.). *Past Climate variability through Europe and Africa*. Springer, Dordrecht, The Netherlands, 69-91.
- Scott, L., Neumann, F.H., Brook, G.A., Bousman, C.B., Norström, E., Metwally, A., 2012. Terrestrial fossil-pollen evidence of climate change during the last 26 thousand years in Southern Africa. *Quaternary Science Reviews* 32, 100-118.
- Scott, L., Woodborne, S., 2007. Vegetation history inferred from pollen in Late Quaternary faecal deposits (hyraceum) in the Cape winter-rain region and its bearing on past climates in South Africa. *Quaternary Science Reviews* 26, 941-953.
- Singleton, A., Reason, C., 2006. Numerical simulations of a severe rainfall event over the Eastern Cape coast of South Africa: sensitivity to sea surface temperature and topography. *Tellus* 58A, 355-367.
- Stager, J.C., Mayewski, P.A., White, J., Chase, B.M., Neumann, F.H., Meadows, M.E., King, C.D., Dixon, D.A., 2012. Precipitation variability in the winter rainfall zone of South Africa during the last 1400 yr linked to the austral westerlies. *Climate of the Past* 8, 877-887.
- Stager, J.C., Ryves, D.B., King, C., Madson, J., Hazzard, M., Neumann, F.H., Maud, R., 2013. Late Holocene precipitation variability in the summer rainfall region of South Africa. *Quaternary Science Reviews* 67, 105-120.
- Talma, A., Vogel, J.C., 1992. Late Quaternary paleotemperatures derived from a speleothem from Cango caves, Cape province, South Africa. *Quaternary Research* 37, 203-213.
- Thomas, D.S., Twyman, C., Osbahr, H., Hewitson, B., 2007. Adaptation to climate change and variability: farmer responses to intra-seasonal precipitation trends in South Africa. *Climatic Change* 83, 301-322.
- Thompson, D.W., Wallace, J.M., 2000. Annular modes in the extratropical circulation. Part I: Month-to-month variability. *Journal of Climate* 13, 1000-1016.
- Tyson, P.D., 1986. *Climatic change and variability in southern Africa*. Oxford University Press, Cape Town, South Africa.

- Valsecchi, V., Chase, B.M., Slingsby, J.A., Carr, A.S., Quick, L.J., Meadows, M.E., Cheddadi, R., Reimer, P.J., 2013. A high resolution 15,600-year pollen and microcharcoal record from the Cederberg Mountains, South Africa. *Palaeogeography, Palaeoclimatology, Palaeoecology* 387, 6-16.
- Weldon, D., Reason, C., 2014. Variability of rainfall characteristics over the South Coast region of South Africa. *Theoretical and applied climatology* 115, 177-185.
- Zhao, X., Dupont, L., Schefuß, E., Meadows, M.E., Hahn, A., Wefer, G., 2016. Holocene vegetation and climate variability in the winter and summer rainfall zones of South Africa. *The Holocene* 26, 843-857.
- Ziervogel, G., New, M., Archer van Garderen, E., Midgley, G., Taylor, A., Hamann, R., Stuart-Hill, S., Myers, J., Warburton, M., 2014. Climate change impacts and adaptation in South Africa. *WIREs Climate Change* 5, 605-620.

Sea level and climate change at the southern Cape coast, South Africa, during the past 4.2 kyr

Authors: Michael Wündsch, Torsten Haberzettl, Kelly L. Kirsten, Thomas Kasper, Matthias Zabel, Elisabeth Dietze, Jussi Baade, Gerhard Daut, Stephanie Meschner, Michael E. Meadows, Roland Mäusbacher

Published in:
Palaeogeography, Palaeoclimatology, Palaeoecology 446 (2016), 295-307

Keywords: Palaeoclimate, Sea level change, Holocene, South Africa, Lacustrine sediments, Carbonate sedimentology



Sea level and climate change at the southern Cape coast, South Africa, during the past 4.2 kyr



Michael Wündsch^{a,*}, Torsten Haberzettl^a, Kelly L. Kirsten^b, Thomas Kasper^a, Matthias Zabel^c, Elisabeth Dietze^d, Jussi Baade^a, Gerhard Daut^a, Stephanie Meschner^e, Michael E. Meadows^b, Roland Mäusbacher^a

^a Institute of Geography, Friedrich Schiller University Jena, Löbdergraben 32, 07743 Jena, Germany

^b Department of Environmental and Geographical Science, University of Cape Town, South Lane, Upper Campus, 7701 Rondebosch, South Africa

^c MARUM, Center for Marine Environmental Sciences, University of Bremen, Leobenerstraße, 28359, Bremen, Germany

^d GFZ, German Research Centre for Geosciences, Helmholtz Centre Potsdam, Telegrafenberg, 14473 Potsdam, Germany

^e Institute of Geosciences, Friedrich Schiller University Jena, Burgweg 11, 07749 Jena, Germany

ARTICLE INFO

Article history:

Received 14 August 2015

Received in revised form 10 January 2016

Accepted 13 January 2016

Available online 21 January 2016

Keywords:

Palaeoclimate

Sea level change

Holocene

South Africa

Lacustrine sediments

Carbonate sedimentology

ABSTRACT

South African coastal lake sediments provide an excellent opportunity to investigate environmental changes such as sea level and climate variability during the Holocene period. In this study we present a sediment record from the coastal lake Groenvlei located in the southern Cape region which is part of South Africa's year-round rainfall zone. In order to improve the understanding of palaeoenvironmental changes in this region, we provide a high-resolution multi-proxy data set derived from geochemical, mineralogical, isotopic and granulometric analyses. The age-depth model is based on ¹⁴C and ²¹⁰Pb dating and reveals a basal age of 4210 ⁺²⁰⁰/₋₁₂₀ cal BP. Differences in the mineralogical composition of deposited carbonates reflect changes in the past lake water chemistry, probably caused by variations in both sea level and climate. Compared to the present, mostly drier conditions and a greater marine influence due to a higher sea level are inferred for the period between 4210 and 2710 cal BP. However, the record also indicates the occurrence of short humid phases during this time, which were probably associated with heavy rainfall events. A transition layer was deposited between 2710 and 1210 cal BP, probably as a result of reworking of sediment. During this time, the lake passed through a major change finally turning into a freshwater system from at least 1210 cal BP until the present. Our data indicate that the marine influence on the lake decreased due to a lower sea level and climate became generally more humid after 1210 cal BP probably resulting in a greater lake-internal and -external bioproductivity. Based on a comparison with other palaeoenvironmental studies from South Africa, our record suggests a prevailing winter rainfall seasonality at the southern Cape coast between 4210 and 2710 cal BP and a stronger influence of summer rainfall from 1210 cal BP onwards.

© 2016 Elsevier B.V. All rights reserved.

1. Introduction

Southern Africa occupies a key position in the southern hemisphere regarding the comprehension of past dynamics and interactions of various atmospheric and oceanic circulation systems (Chase and Meadows, 2007). The subcontinent is subjected to three different rainfall zones (Fig. 1a): the summer rainfall zone (SRZ) covering the main part of the interior is affected by migrations of the Intertropical Convergence Zone and hence the tropical easterlies. Circumpolar westerlies are the main source of precipitation within the temperate winter rainfall zone (WRZ) along the west coast. The year-round rainfall zone (YRZ) represents a transition area between the SRZ and WRZ receiving both summer and winter rainfall (Chase and Meadows, 2007; Stager et al.,

2013). Moreover, the climate of southern Africa is influenced by surrounding oceans, the Atlantic Ocean in the west with its cold Benguela Current as well as the warm Agulhas Current located in the Indian Ocean south and east of the mainland (Fig. 1a) (Cohen and Tyson, 1995; Scott and Lee-Thorp, 2004). Although these major climatic driving factors are known, their past dynamics and interactions are not yet fully understood (Stager et al., 2013).

In South Africa the occurrence of basins containing Holocene deposits, such as lakes or wetlands, is relatively rare and the quality of existing geoarchives, particularly in terms of their preservation, is often reduced due to the mostly arid and seasonal climate causing desiccation and/or erosion of these deposits (Scott and Lee-Thorp, 2004; Chase and Meadows, 2007). Therefore, Holocene records suitable for palaeoenvironmental reconstructions are scarce and existing records are often of low temporal resolution (Scott and Lee-Thorp, 2004). Several Holocene records from the YRZ either provide only coarse resolution

* Corresponding author.

E-mail address: michael.wuendsch@uni-jena.de (M. Wündsch).

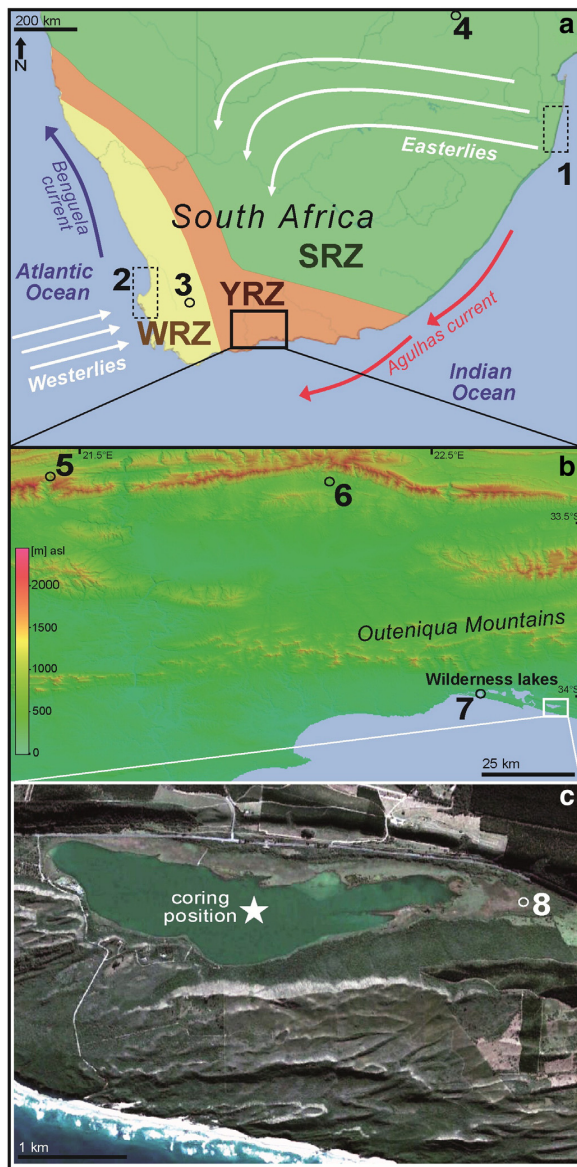


Fig. 1. Study area: a) The three rainfall zones of southern Africa (WRZ: winter rainfall zone, SRZ: summer rainfall zone, YRZ: year-round rainfall zone) as well as important oceanic and atmospheric circulation systems. b) Location of the Wilderness lakes at the southern Cape coast. c) The coring position of this study within the central part of Groenvlei (map source: Google Earth). Additionally shown are locations of several studies mentioned in the text: sea level reconstructions of 1) Neumann et al. (2010); Ramsay (1995); 2) Carr et al. (2015); Compton (2001); Baxter and Meadows (1999), and Miller et al. (1995); 3) Hyrax midden record from Katbakkies Pass (Chase et al., 2015); 4) Cold Air Cave stalagmite record (Holmgren et al., 2003); 5) Hyrax midden records from Seweweekspoort (Chase et al., 2013); 6) Congo caves stalagmite record (Talma and Vogel, 1992); 7) Eilandvlei lake sediments (Kirsten, 2014; Reinwarth et al., 2013); 8) Coring location of previous studies on the fen east of Groenvlei (Martin, 1959, 1968).

reconstructions (Carr et al., 2006), are intermittent (Cohen and Tyson, 1995), or their age models are based on very few control points (Martin, 1959, 1968; Scholtz, 1986). Further Holocene records for the YRZ are available from the Cape Fold Mountains: A $\delta^{18}\text{O}$ and $\delta^{13}\text{C}$ stalagmite record from the Congo Caves (Fig. 1b) has been interpreted as evidence for variations in temperature and rainfall seasonality leading to

changes in the vegetation composition (Talma and Vogel, 1992); two rock hyrax midden records from Seweweekspoort (Fig. 1b) provide information about Holocene hydroclimatic variability and vegetation change in the area (Chase et al., 2013).

Moreover, several studies on archives from the coastal realm are available which provide insights into sea level variations during the Holocene (Miller et al., 1995; Ramsay, 1995; Baxter and Meadows, 1999; Compton, 2001; Neumann et al., 2010; Carr et al., 2015). However, these sea level reconstructions reveal discrepancies in terms of the exact timing of transgression and regression periods. The reconstructed timing of the Holocene sea level highstand (up to 3.5 m above the present sea level) ranges in these studies between ~7000 and 3500 cal BP. After which, all records show oscillations of a few metres above and below the present sea level before reaching modern conditions.

In the present study, we focus on a lacustrine archive from the YRZ represented by the sediments from the coastal lake Groenvlei located in the Wilderness embayment (Fig. 1). Previous studies on sediments from the Wilderness area already indicated that these archives are suitable for reconstructing sea level and climatic variations (Martin, 1959, 1968; Reinwarth et al., 2013; Kirsten, 2014). Several investigations on sediment cores from the fen east of Groenvlei were conducted by Martin (1959, 1968) mainly applying palynological and diatom analyses. The main conclusions of these investigations concerning changes in the marine influence on the lake were that between ~4000 and 2000 BP, Groenvlei was in a lagoon stage and turned into a freshwater lake from ~2000 BP onwards (Martin, 1959, 1968). Regarding palaeoecological changes for the period between ~6870 and 2000 BP, Martin (1968) suggested that the vegetation spread in the area was restricted due to the instability of the dunes and hence sand movement. However, the author proposed two alternative palaeoclimatic interpretations for this period: climate was either dry and hot or wet (Martin, 1968). For the time frame from ~2000 BP onwards, a more effective moisture availability was inferred which was conducive to vegetation spread in the area (Martin, 1968). However, the palaeoenvironmental interpretations of this record are only based on two radiocarbon ages causing uncertainties in the reliability of the chronology.

The aim of this study is to contribute to a better and more comprehensive understanding of palaeoenvironmental change in this area during the Holocene. Therefore, we retrieved a new sediment core from the profundal of Groenvlei and present a more detailed and robust radiocarbon chronology for this geoarchive. A multi-proxy approach including geochemical, mineralogical, stable isotope and granulometric methods was employed. In particular, the investigations on the carbonate mineralogy of our sediment core represent a novel methodological approach for this region. We provide a high-resolution record of environmental change giving new and more detailed insights into the past lake evolution at Groenvlei linked to Holocene sea level and climatic variations in South Africa.

2. Study site

Groenvlei represents the easternmost of several coastal lakes within the Wilderness embayment located at the southern Cape, South Africa (Fig. 1). At the north and south the lake is flanked by up to 200 m a.s.l. high, coast-parallel dune cordons of Pleistocene age (Illenberger, 1996; Bateman et al., 2004, 2011). These dunes evolved into the present aeolianites mainly consisting of well-rounded quartz and bioclastic sand cemented by calcium carbonate. At the top, the aeolianites of the seaward dune cordon south of Groenvlei are covered by unconsolidated Holocene sands of variable thicknesses (Bateman et al., 2011).

Groenvlei probably started to form in times of lower sea levels during the last glacial–interglacial cycles of the Late Pleistocene (Birch et al., 1978; Martin, 1959; Cawthra et al., 2014). During the Holocene sea level rise, the depression between the dune cordons was flooded (Martin, 1959). Thereafter, a possible former surface hydrological connection

via the Swartvlei estuary to the Indian Ocean was probably blocked by sand movement (Martin, 1959). At the northern shore a roughly 200 m wide platform is located at a slightly higher elevation than the present water surface, similar to the wetland situated east of Groenvlei, suggesting a higher lake level in the past (Martin, 1968). At present, the lake is ca. 4 km long and 0.9 km wide and the surface area of the open water body is about 2.45 km². The average water depth is about 3.7 m and the water table currently ranges between 2.2 and 3.4 m a.s.l. (1980–2013; Parsons, 2014). The aboveground catchment of the lake is very small (about 9.45 km²; Watling, 1979) and consists mainly of the slopes of the dunes around the lake. Parsons (2014) estimated the subterranean area that contributes to the lake inflow to ~25 km². Since Groenvlei has no river inflow the lake is mainly fed by direct rainfall (72%; Parsons, 2014). The remaining 28% is supplied by ground water discharge, mainly from the north. The major losses of water are due to evaporation from the lake surface (62%), transpiration of the reed belt (21%) and ground water outflow to the south (17%; Parsons, 2014). Hence, the hydrological budget and the lake water chemistry are strongly dependent on the precipitation/evaporation ratio and thus local climate. The lake water is alkaline with a positive calcium carbonate precipitation potential and can be classified as NaCl type (Parsons, 2014).

The climate in the Wilderness area is characteristic of the YRZ in being temperate and mild, with rainfall throughout the year (Allanson and Whitfield, 1983; Kruger, 2004). Average daily temperatures range from a maximum of 23.8 °C in February to a minimum of 8.0 °C in August; the mean annual precipitation is about 650 mm (1981–2012) ranging between 37 mm in May and 68 mm in October (Parsons, 2014). Rainfall can be highly variable leading to droughts as well as to floods in the area. For example, the area received 275 mm precipitation within 2 days in August 2006 (Parsons, 2014). The major wind directions are east to southeast in summer and west to northwest during winter (Kruger, 2002). Up to 1500 m high Outeniqua Mountains some 20 km to the north (Fig. 1b) induce orographic precipitation in the area (Parsons, 2014). So-called 'bergwinds' can occur during winter originating from the arid and high elevation interior and bringing dry and warm air masses to the area that facilitate the occurrence of regional fires (Geldenhuys, 1994).

The vegetation in and around Groenvlei has been described in detail by Martin (1956, 1960, 1968). The lake floor is predominantly covered by *Chara* algae and *Potamogeton* communities. Closer to the littoral is a succession of partially submerged fen vegetation species. The dunes are covered and stabilised by patchy distributed woodland and fynbos heath vegetation (Martin, 1960). Soils developed on the dunes range from alkaline sands to weathered, reddish, loamy sands that are partly ferruginised (Illenberger, 1996). Several outcropping palaeosols occur at the dune slopes (Bateman et al., 2011).

3. Materials and methods

3.1. Sample recovery and dating

In October 2013, a 121 cm long sediment core was retrieved from the central part of the lake (34°1.796'S, 22°51.409'E; water depth: 5.8 m) (Fig. 1c) using a UWITEC corer (core diameter: 90 mm). In order to fingerprint potential sources of the lacustrine carbonates deposited in Groenvlei and to assess the contribution of carbonates from the dunes, five surface samples were collected from the dune cordon south of the lake (Table 1). After splitting the core was described lithologically and documented photographically. The core was continuously subsampled in 1 cm intervals using the double L-channel method (Nakagawa et al., 2012). Preliminary microscopic investigation was conducted on core subsamples at 5 cm intervals. Except for aliquots used for grain size analysis and scanning electron microscope (SEM) imaging, all subsamples were freeze-dried, ground (<40 µm) and homogenised.

Table 1
Dune samples.

Sample type	Sample ID	Coordinates [°]		CaCO ₃ [wt.%]	δ ¹⁸ O [‰]	δ ¹³ C [‰]
		S	E			
Unconsolidated sand	D1	34.04329	22.83931	28.1	0.51	0.65
Aeolianite	D2	34.04667	22.83883	49.6	-2.65	-2.76
Aeolianite	D3	34.04588	22.83598	40.6	-1.75	-2.72
Aeolianite	D4	34.04588	22.83598	41.5	-1.88	-3.38
Aeolianite	D5	34.03135	22.7966	31.6	-1.91	-2.05

The chronology for the sediment record was established based on 20 bulk samples from the topmost part of the core (from 0 to 8 cm sediment depth in 0.5 cm intervals, from 8 to 12 cm in 1 cm intervals) which were sent for ²¹⁰Pb-dating (Radiochronology Laboratory, Centre for Northern Studies, Laval University, Québec, Canada) and eight bulk sediment samples which were sent for AMS-¹⁴C-dating (Beta Analytic Inc., Miami, Florida, USA). The bulk organic sediment fraction was used for the AMS-¹⁴C-dating after applying the 'acid washes' pre-treatment of the samples. The calibration of the ¹⁴C-ages (2σ) was carried out using the SHcal13 data set (Hogg et al., 2013). The measured ²¹⁰Pb activities were converted to ages applying the CRS (constant rate of ²¹⁰Pb supply) model (Appleby, 2008; Appleby and Oldfield, 1978). Based on the calibrated ¹⁴C and ²¹⁰Pb data, the final age–depth relation was calculated using the R software package Bacon 2.2 (Fig. 2; Blaauw and Christen, 2011).

3.2. Geochemical analyses (ICP-OES and CN)

For the preparation of the ICP-OES measurements the subsamples were digested in a microwave using a treatment of modified aqua regia (1 ml deionised H₂O, 2 ml HCl 30% and 4 ml HNO₃ 30%). Subsequently, quantitative element concentrations of Al, Ca, Fe, K, Mg, Sr and Ti were measured at intervals of 1 cm using a Varian 725-ES instrument.

For the determination of total carbon (TC) and total nitrogen (TN) at an interval of 1 cm, the core samples were measured with a CNS elemental analyser (EuroEA, Eurovector). Afterwards, the samples were treated with 3% and 20% HCl at 80 °C to remove carbonates and then measured with the CNS analyser again to obtain the total organic carbon (TOC) contents. Total inorganic carbon (TIC) concentrations were subsequently calculated as the difference between TC and TOC and molar TOC/TN ratios were calculated. The calcium carbonate content of the ground and freeze-dried dune samples was determined using the Scheibler method (DIN, 1997).

3.3. Stable carbon and oxygen isotope analyses (δ¹⁸O and δ¹³C) on the carbonate fraction

The isotopic analyses on the carbonate fraction were carried out on the core samples at an interval of 1 cm as well as on the dune samples using a Thermo-Finnigan MAT251 mass spectrometer interfaced with a Kiel Device (MARUM, University of Bremen, Germany). The analytical precision (1σ) averages 0.07‰ for δ¹⁸O and 0.05‰ for δ¹³C and is based on an in-house standard (Solnhofen limestone) which was calibrated to the international NBS19 standard. All isotopic values are given relative to VPDB.

3.4. Powder X-ray diffraction (XRD) and SEM imaging

Mineralogical investigations were conducted on the dune and core samples initially at an interval of 2 cm and subsequently at 1 cm intervals in core sections which revealed major changes in the already measured and evaluated data. The samples were measured using an X-ray diffractometer (D8-Discover, Bruker AXS) equipped with a CuKα X-ray tube and a gas proportional counter (HI-STAR area detector,

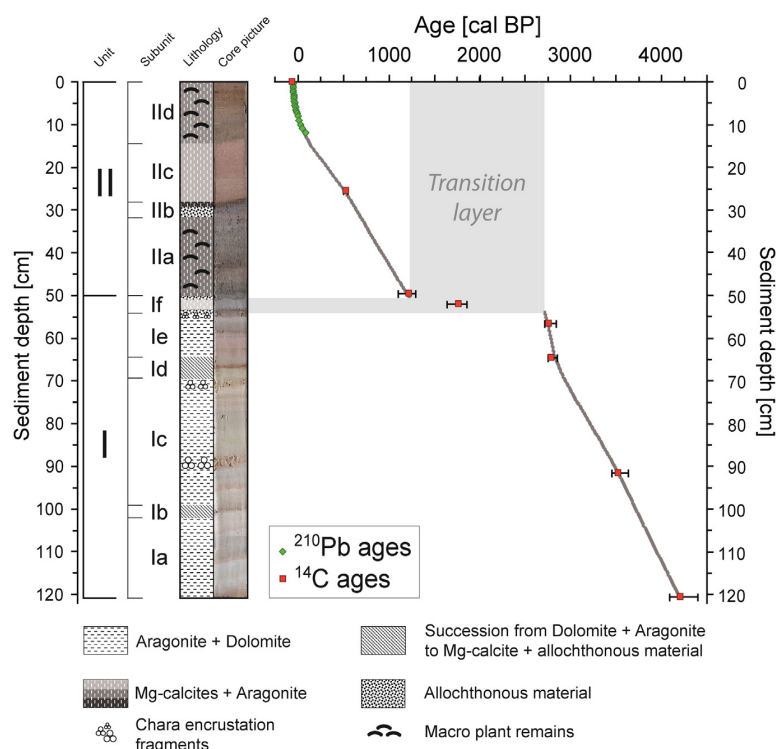


Fig. 2. Core picture and lithology with defined (sub)units (on the left) and the age–depth model based on AMS- ^{14}C and ^{210}Pb dating (on the right). Calibrated radiocarbon ages are displayed as medians with 2σ errors. The age–depth relation (grey line) was calculated using the R software package Bacon 2.2 (Blaauw and Christen, 2011). The grey bar representing unit If is interpreted as a transition layer maximally covering the period between 2710 and 1210 cal BP.

Bruker AXS). After the qualitative phase identification a semi-quantitative evaluation based on the reference intensity ratio (RIR) method (Chung, 1975; Hubbard et al., 1976) was carried out for each diffractogram using the software Match! 2.0.9. Given percentages exclusively express the relative amounts of the evaluated minerals to each other and therefore do not consider other parts of the sediment such as amorphous or organic substances. Mg contents in dolomite were roughly estimated based on the relationship between the molar Mg percentage and the interplanar lattice spacing (Goldsmith and Graf, 1958; Zhang et al., 2010). The semi-quantitative evaluation of co-occurring Mg-calcites with different Mg contents does not provide reliable results in situations where the differences in Mg content are so small that there is overlapping of closely spaced peaks, which inhibits their precise identification (Titschack et al., 2011). This proved to be the case in most samples, such that only one Mg-calcite phase was considered for the RIR method using the highest Mg-calcite main peak.

For SEM-imaging, dried samples were affixed on a sample holder and coated with a thin gold layer. Images were obtained using a Zeiss Auriga 60 scanning electron microscope equipped with an EDX detector.

3.5. Grain size analysis and end member modelling

The grain size distributions were measured at intervals of 1 cm using a Laser Diffraction Particle Size Analyser (Beckman Coulter LS 13320) utilizing the Aqueous Liquid Module. For optical modelling of light scattering the Fraunhofer diffraction theory was applied (de Boer et al., 1987). Prior to the measurement, organic matter and carbonates were eliminated with H_2O_2 (30%) and HCl (10%). A solution of $\text{Na}_4\text{P}_2\text{O}_7 \cdot 10\text{H}_2\text{O}$ (0.1 M) was added as a dispersion medium and subsequently samples were shaken for at least 2 h. The measurements were taken in

several runs until a reproducible signal was obtained. The first reproducible run was used for further statistical treatment. The grain size fractions were calculated using a modified version of Gradistat 4.2 (Blott and Pye, 2001). An end-member (EM) modelling algorithm (Dietze et al., 2012) was applied on the grain size distributions using the R software package EMMAgeo (Dietze and Dietze, 2013; <http://cran.r-project.org/web/packages/EMMAgeo/>). The EM modelling uses a combination of factor and eigenspace analysis as well as different scaling procedures whereby grain size distributions were mathematically unmixed to allow process-related interpretation of the different grain size EMs. The statistically most characteristic EMs were defined by similar-likely model runs of different EM number and weight transformation quantiles (so-called robust end-members, rEM; Dietze et al., 2012, 2014).

4. Results

Based on the core lithology, our data and their interpretations, which are shown in the following, the core was subdivided in two main units (unit I: 121–50 cm, unit II: 50–0 cm) composed of several subunits (units Ia–If and Ila–IId) (Figs. 2, 3). The slightly reddish white to grey sediments of unit I look generally different compared to the reddish brown sediments of unit II. Within both main units several distinct layers appear, characterised for example by changes in colour, macroscopic grain size and the occurrence of macro plant remains or *Chara* encrustation fragments (see Fig. 2 for further details).

The established age–depth model for the Groenvlei core (Fig. 2, Table 2) reveals a basal median age of 4210^{+200}_{-120} cal BP. The calculated age–depth relationship indicates continuous sedimentation for units Ia to Ie (121 to 54 cm; 4210 to 2710 cal BP) with an average sediment accumulation rate of 0.45 mm yr^{-1} as well as for unit II (50 to

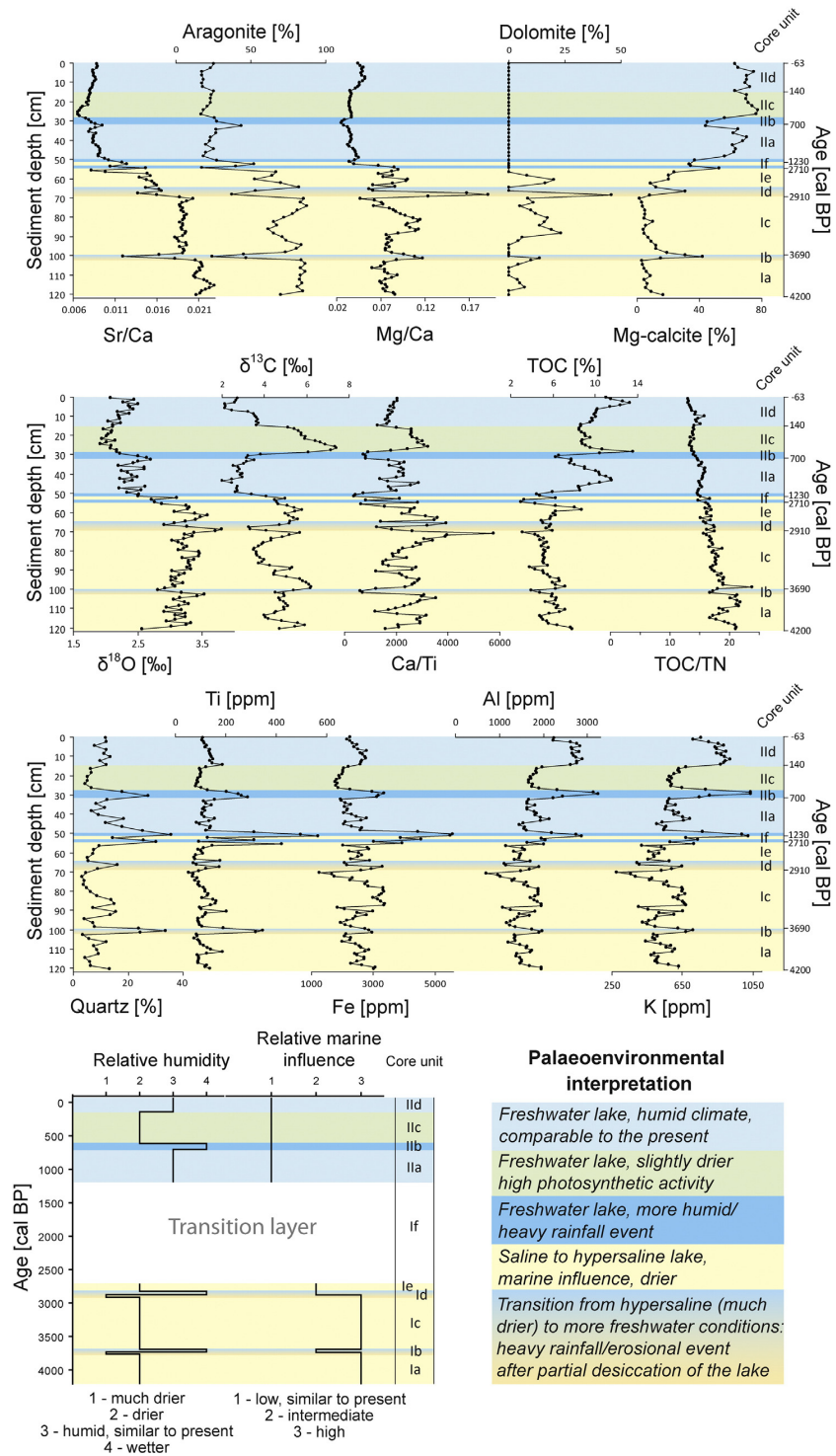


Fig. 3. Bulk geochemical data (Al, Ca/Ti, Fe, K, Mg/Ca, Sr/Ca, Ti, TOC, and TOC/TN), stable isotopes of the carbonate fraction ($\delta^{13}\text{C}$ and $\delta^{18}\text{O}$), and semi-quantitatively evaluated mineralogical data (aragonite, dolomite, Mg-calcite, quartz) plotted against sediment depth on the left and (non-equidistantly scaled) age on the right. The palaeoenvironmental interpretation of the distinct core units (bottom right) is depicted by different colours. Based on the palaeoenvironmental interpretations, indices for relative humidity and marine influence were compiled (bottom left). The relative humidity index was categorised into four classes (1: much drier than at present; 2: drier than at present; 3: humid, similar conditions to present; 4: wetter than at present) and the relative marine influence index in three classes (1: low, similar to present; 2: slightly higher than at present; 3: much higher than at present).

Table 2
AMS-¹⁴C data.

Lab-ID	Sediment depth [cm]	Conventional radiocarbon age [BP]	Median calibrated age (SHcal13) [cal BP]	2σ +	2σ -
Beta - 369,751	0	104.8 ± 0.4 pMC	-	-	-
Beta - 369,752	25.5	540 ± 30	530	30	30
Beta - 403,101	49.5	1330 ± 30	1220	70	120
Beta - 403,102	52	1870 ± 30	1770	90	130
Beta - 403,103	56.5	2670 ± 30	2760	90	40
Beta - 369,753	64.5	2720 ± 30	2780	70	40
Beta - 369,754	91.5	3350 ± 30	3530	100	80
Beta - 369,750	120.5	3860 ± 30	4210	200	120

0 cm; 1210 to -63 cal BP) with 0.39 mm yr^{-1} . However, between 54 and 50 cm (unit If) there is an offset of about 1500 years. A radiocarbon-dated sample in between (at 52 cm) provides a median age of $1770^{+90}/_{-130}$ cal BP (Fig. 2, Table 2). This sample is from a light grey, homogeneous layer which is stratigraphically bordered by two distinct sand layers below and above (54 and 50 cm). Due to these dating results in association with the lithological characteristics, this core section between 54 and 50 cm is referred to as a transition layer maximally covering the period from 2710 to 1210 cal BP (Fig. 2). However, a hiatus in this time interval cannot be ruled out. The sediment surface contains $104.8 \pm 0.4\%$ modern carbon and therefore, its age was set to -63 cal BP, the year of the core recovery.

Preliminary microscopic investigations revealed that calcareous microfossils are abundant throughout the core, predominantly represented by ostracods. Gastropods occur occasionally, but foraminifera are absent. Various diatom species were found within the topmost 30 cm of the core. Between 30 and 50 cm fewer diatoms occur which are poorly preserved. Hardly any diatoms were found in unit I.

The lacustrine sediments from Groenvlei consist mostly of different carbonates (45–77 wt.%, 62 wt.% avg.) and quartz; detected carbonate minerals in the core samples are low-Mg calcite (LMC), high-Mg calcite (HMC), aragonite and dolomite (Fig. 4a). In contrast, the dune samples reveal a mineralogical composition with quartz as dominant, LMC as the sole Mg-calcite and aragonite as a minor component (Fig. 4b, c). The XRD data reveal a major shift in the carbonate mineralogy around 50 cm sediment depth. Whilst unit I is mostly dominated by aragonite (up to 87%) and to a lesser degree by dolomite (up to 46%; Fig. 3), unit II mainly consists of Mg-calcites (up to 77%). Aragonite contents are distinctly lower in unit II fluctuating around 20% and dolomite is completely absent. Conspicuously, there are two sections within unit I revealing a similar succession of different carbonate minerals: Within the units Ib and Id aragonite contents decrease, whilst dolomite shows peaks at the bottom of these sections (at 102–101 cm and 69–68 cm) and Mg-calcites peak shortly thereafter (101–99 cm and 67–66 cm) (Fig. 3).

Since typical ordering peaks for dolomite (Vasconcelos et al., 1995) are not visible in the XRD pattern, the occurring dolomite in this core is probably poorly ordered. Moreover, the dolomite from Groenvlei is rather Ca-rich containing between ~25–40 mol% (Goldsmith and Graf, 1958) and ~30–55 mol% MgCO₃ (Zhang et al.,

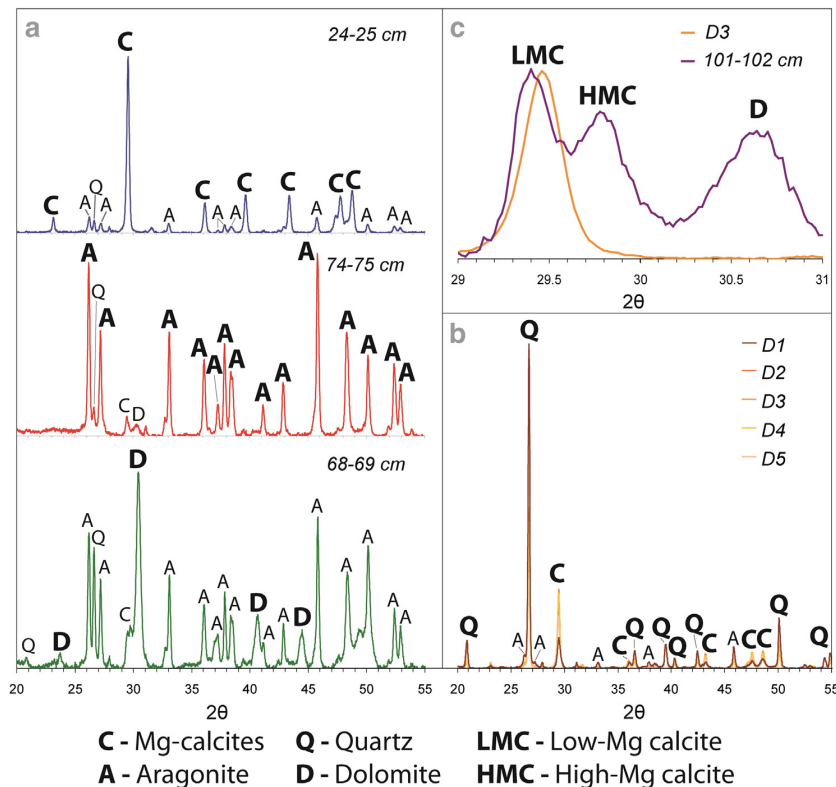


Fig. 4. a) Three typical diffractograms from different sediment depths representing the distinct carbonate minerals. Top: Sample from 24 to 25 cm core depth (unit Ilc) with Mg-calcite as major and aragonite as minor carbonate phase; centre: sample from 74 to 75 cm (unit Ic) core depth mainly composed of aragonite; bottom: sample from 68 to 69 cm (unit Id) which contains the highest dolomite percentage of the record. b) Diffractograms of the five dune samples (D1–D5) depicted one above the other. All samples reveal the same qualitative mineralogical composition containing quartz, Mg-calcite, and minor aragonite. c) Comparison of one dune sample (D3) with a typical core sample from 101 to 102 cm (unit Ib). All dune samples consist exclusively of LMC as sole Mg-calcite phase. In contrast, the core samples contain a mixture of LMC, HMC, and partly dolomite in unit I. The selected sample from 101 to 102 cm shows clearly separable peaks of HMC and LMC.

2010), depending on which empirical curve for the Mg content determination is applied.

The varying carbonate mineralogy within the Groenvlei core was also detected by SEM imaging. The typical euhedral to subhedral aragonite needles of the precipitated carbonate of the *Chara* encrustation fragments (Fig. 5a) as well as in the bulk sediment (Fig. 5c) are representative for unit I. The coalesced, rhombohedral dolomite occurs solely in unit I (Fig. 5b). Within unit II, the Mg-calcites mainly occur as small micritic, anhedral crystals (Fig. 5d). In contrast to unit I, these sediments are characterised by the abundance of biogenic silica remains, particularly of sponge spicules (Fig. 5e) and to a lesser degree from diatoms (Fig. 5f).

The $\delta^{18}\text{O}$ and $\delta^{13}\text{C}$ data of bulk sediment samples exhibit a weak correlation along the entire core ($r = 0.14$). Three different clusters of isotopic composition can be distinguished which are related to different sediment core sections (Fig. 6). Also within each of these three clusters, there is no correlation between $\delta^{18}\text{O}$ and $\delta^{13}\text{C}$. Unit I is characterised by $\delta^{18}\text{O}$ values ranging from 2.56‰ to 3.81‰ and $\delta^{13}\text{C}$ values between 3.25‰ and 6.22‰. The core units IIa, IIb and IIc show lower values for both $\delta^{18}\text{O}$ (2.04‰–2.70‰) and $\delta^{13}\text{C}$ (1.99‰–4.08‰). The third cluster is associated with unit IIc and reveals relatively low $\delta^{18}\text{O}$ (1.92‰–2.18‰) and high $\delta^{13}\text{C}$ values (5.10‰–7.35‰). For the entire record, $\delta^{18}\text{O}$ is well correlated with Sr/Ca ($r = 0.85$) and Mg/Ca ($r = 0.79$) (Fig. 3). The carbonates contained in the dune samples show isotopically much lighter $\delta^{18}\text{O}$ and $\delta^{13}\text{C}$ values compared to those of the lake sediments (Fig. 6).

The sediment organic matter ranges between approximately 5 and 23 wt.% (12 wt.% avg.) across the core. TOC concentrations reveal low values in unit I and high values in unit II. The TOC/TN ratios show a slightly decreasing trend across the core with values ranging between 13 and 24 (Fig. 3).

The allochthonous sediment fraction is roughly calculated (total sample [100 wt.%] minus estimated CaCO_3 [wt.%] minus estimated organic matter [wt.%]) as lying between 10 and 40 wt.% (25 wt.% avg.) within the core. The clastic material consists mainly of quartz and to a

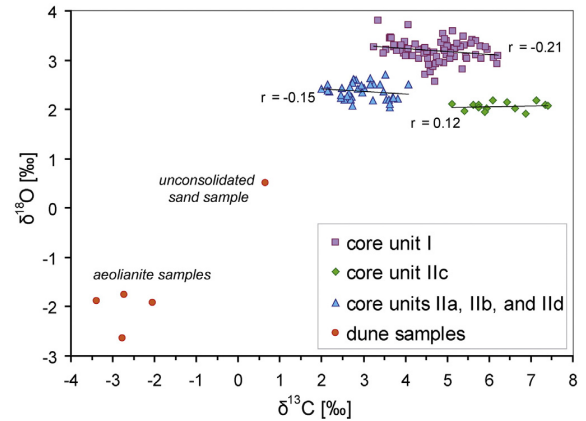


Fig. 6. Carbonate $\delta^{13}\text{C}$ plotted against $\delta^{18}\text{O}$ of the core and the dune samples. The plot reveals three distinct clusters associated with certain core units. Conspicuous is the low correlation within the three clusters as well as their parallel trend to the $\delta^{13}\text{C}$ axis. The dune samples are characterised by a lighter isotopic composition.

smaller degree of feldspars which could be detected only sporadically and in minor quantities across the core and were therefore not considered for the semi-quantitative, mineralogical analysis. The quartz data (maximum values up to 36%) reveal some marked peaks across the core together with the elements Al, Fe, K and Ti (units Ib, d, f and IIb; Fig. 3). In the units Ia, c, e and IIa these data show minor variations. In unit IIc the data are consistently low and shift to a distinctly elevated level at unit IIc. In contrast, the Ca/Ti ratios show an inverse pattern to the aforementioned parameters along the core.

The grain size analysis revealed that the majority of the allochthonous sediment fraction is composed of silts across the entire record. Sand contents are generally higher in unit I than unit II, whereas clay

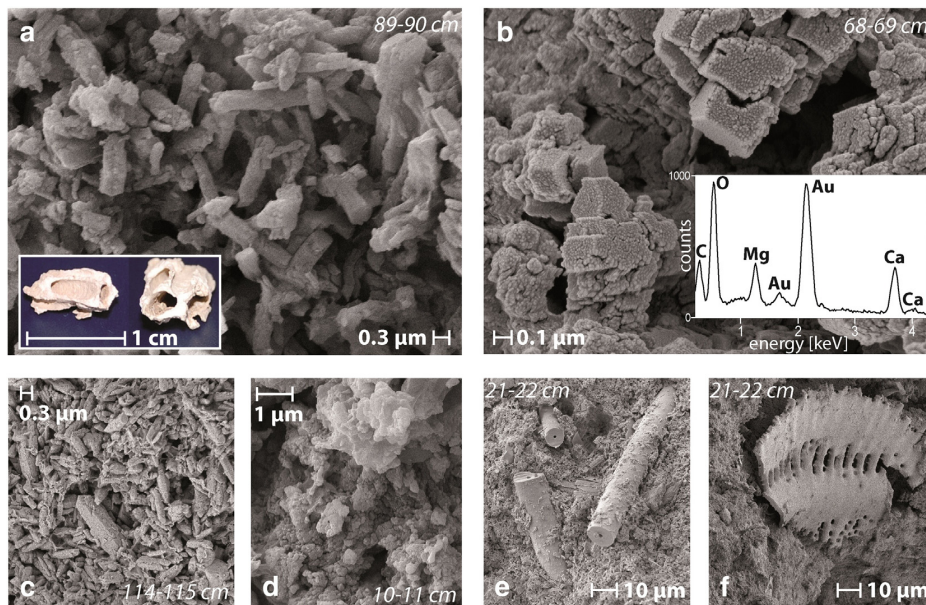


Fig. 5. Scanning electron microscope (SEM) images of selected samples from different sediment depths. a) The *Chara* encrustation fragments (sample from 89 to 90 cm core depth, unit Ic; inset) are composed of typical euhedral to subhedral aragonite needles as well as c) the bulk sediment in unit Ia (sample from 114 to 115 cm). b) Coalesced rhombohedral dolomite crystals from 68 to 69 cm sediment depth (unit Id). In addition, an energy dispersive X-ray (EDX) spectrum with peaks for Ca and Mg confirming the presence of dolomite is shown. The Au peaks merely originate from the coating necessary for the measurement. d) Micritic, anhedral Mg-calcite crystals typical for the sediments in unit II (sample from 10 to 11 cm core depth, unit IIc). Unit II generally contains distinctly more biogenic silica remains like e) sponge spicules and f) diatom fragments (both pictures from a sample in 21–22 cm sediment depth, unit IIc).

contents are consistently low (Fig. 7a). The grain size end-member modelling provided five uncorrelated, robust end-members (rEM) (Fig. 7c). Their mean model explains 81.4% of the total variance within the multimodal grain size distributions. A medium to coarse sandy, bimodal rEM1 with maximum EM loadings at 400–500 μm and 180–250 μm explains 6.6% of the total EM variance; the fine to medium sandy rEM2 explains 31.7% and has its mode at \sim 80–100 μm . Medium to coarse silty rEM3, medium silty rEM4 and fine to medium silty rEM5 have modes at \sim 25–50 μm , \sim 20–25 μm and at \sim 8–20 μm explaining 7.7%, 32.4% and 21.6%, respectively. The two rEMs with the highest explained variances are rEM2 and rEM4. Whilst rEM2 is prevalent in unit I, rEM4 is dominant in unit II (Fig. 7b). rEM1 is only sporadically present across the record and its highest scores appear mostly together with peaks in the geochemical and mineralogical parameters which are indicative for allochthonous input (quartz, Ti, Fe, Al, K). rEM3 and rEM5 reveal fluctuating scores across the entire core.

5. Discussion

5.1. Implications for the origin of the lacustrine carbonates

Lacustrine carbonates have a variety of origins and their deposition typically occurs as a function of several different mechanisms and pathways. Hence, the following processes should be considered: (1) the detrital input of allochthonous carbonates from the lake catchment by erosion and transport as solid phase; (2) the deposition of calcareous remains produced by organisms which occur sporadically in lake sediments in general; (3) the inorganic precipitation from the water column caused either by biogenic (photosynthetic activity of aquatic plants and algae like *Chara*) or physicochemical factors (e.g., temperature effect on the CO_2 solubility, concentration effects due to evaporation, mixing of different waters); and (4) the diagenetic alteration of deposited carbonates and their transformation in secondary mineral phases (Kelts and Hsü, 1978; Kelts and Talbot, 1990).

The mineralogical and isotopic differences of the lake sediment compared to the dune samples indicate clearly that detrital carbonates play only a minor role in the Groenvlei record and that the lacustrine carbonates predominantly formed within the lake. As the analysed dune samples contain no dolomite, the lacustrine dolomite at Groenvlei is very likely of primary origin formed within the lake water or of secondary, diagenetic origin formed within the sediments from a precursor (Last, 1990). Despite the abundance of carbonates in the lake catchment, their detrital input is probably negligible because of the high infiltration capacity of the dune cordons and thereby the rarity of surface runoff which only occurs during exceptional heavy rainfall events (Parsons, 2014). Nevertheless, the dune material possibly represents an indirect

source for the formation of lacustrine carbonates, since Ca^{2+} and CO_3^{2-} ions are partially dissolved by rainfall and transported in solution into the lake via groundwater. Although calcareous, microfaunal remains (e.g., from ostracods) do occur in the sediments, several facts (e.g., the presence of several layers consisting of *Chara* encrustation fragments, the recent supersaturation of the lake water with respect to calcite (Parsons, 2014) and the sensitivity of the water table to evapotranspiration) indicate that most of the lacustrine carbonates at Groenvlei were chemically or biogenically precipitated from the water column.

5.2. Geochemistry and mineralogy of the lacustrine carbonate fraction

The semi-quantitative mineralogical data are confirmed by the quantitatively measured geochemical data. The aragonite contents show a similar pattern across the core as the Sr/Ca ratio (Fig. 3), probably due to the fact that aragonite is able to incorporate Sr^{2+} preferentially into the crystal lattice compared to calcite (Veizer, 1983). Dolomite contents reveal a similar pattern as the Mg/Ca ratio in unit I. In unit II, dolomite is absent and the Mg/Ca ratio, which shows distinctively lower values than in unit I, is determined mainly by the presence of Mg-calcites and their Mg content.

The Mg/Ca ratio of the lake water determines which carbonate mineral precipitates from the water column. LMC is mainly precipitated at Mg/Ca mass ratios <2 , whereas HMC and aragonite become dominant at higher Mg/Ca ratios >2 due to the inhibiting effect of Mg^{2+} on the calcite crystal growth (Müller et al., 1972; Folk, 1974). The formation of dolomite is a longstanding, controversially debated issue in sedimentary geology which is still not completely understood and is often referred to as the “dolomite problem” (e.g., Machel and Mountjoy, 1986; Hardie, 1987; Vasconcelos and McKenzie, 1997; Land, 1998; Tucker and Wright, 2009; Zhang et al., 2012). Various factors favouring the formation of dolomite have been discussed, such as high Mg/Ca ratios (mostly >10) and high alkalinities (Morrow, 1982; Machel and Mountjoy, 1986; Last, 1990). Moreover, it has been found that microbial activity, in particular sulphate reducing bacteria, probably play a crucial role (Vasconcelos et al., 1995; Vasconcelos and McKenzie, 1997; Sánchez-Román et al., 2009; Zhang et al., 2012). Although seawater is supersaturated with respect to dolomite, this mineral usually does not form under normal marine conditions (Last, 1990; Tucker and Wright, 2009). Hypersaline supratidal and subtidal environments as well as seawater/fresh water mixing zones are amongst those environments conducive to the formation of dolomite (Machel and Mountjoy, 1986). Over 95% of the global occurrences of Quaternary lacustrine dolomite were deposited in saline lakes or at least during a saline to hypersaline phase of a lake (Last, 1990).

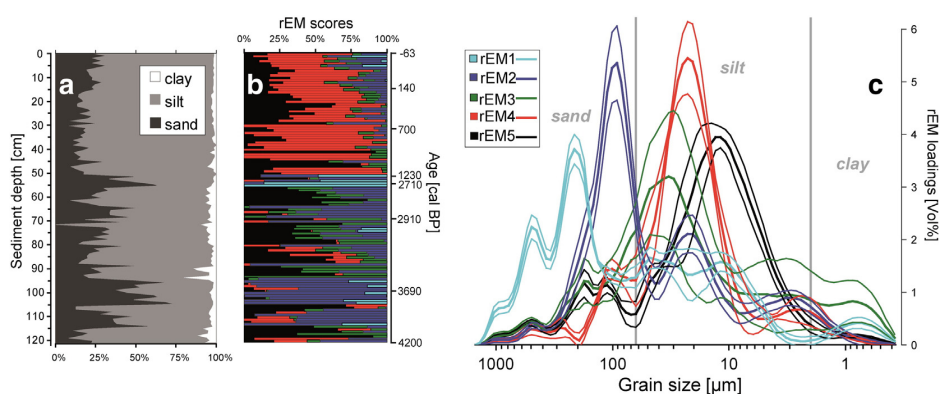


Fig. 7. Grain size data: a) Sand, silt and clay contents plotted against sediment depth and age as well as the distributions of the five robust end-members c) mean and standard deviations of rEM-loadings (scaled to be interpretable as grain size distributions) and b) rEM-scores (relative contribution of each rEM to the samples).

We hypothesise that the varying carbonate mineralogy in the Groenvlei record can be interpreted in a similar way as it was done for the Coorong lagoon system in South Australia (von der Borch, 1965, 1976) which has a comparable environmental setting to Groenvlei. At Coorong, the changing carbonate mineralogy mainly reflects two important processes: (1) the decreasing connectivity of the ocean to certain parts of the lagoon which became progressively isolated as a result of the late Holocene sea level decline; and (2) the greater influence of dry phases leading to more frequent seasonal desiccation of these separated parts of the lagoon that developed into ephemeral lakes (von der Borch, 1965, 1976). Whilst those parts of the lagoon which still have a connection to the sea are characterised by carbonates mainly composed of aragonite, the more disconnected and frequently desiccating parts predominantly produce dolomite (von der Borch, 1965, 1976). Applied to the Groenvlei record we conclude that unit I, dominated by aragonite, reflects a period when the lake was connected to the ocean, probably not by an aboveground connection (given the absence of foraminifera), but rather due to marine groundwater intrusions resulting from a slightly higher sea level and hence different hydraulic gradients between Groenvlei and the sea. The Indian Ocean represents the most likely source for Mg^{2+} which is required to produce aragonite and dolomite. Furthermore, seawater is also a source for SO_4^{2-} and the dolomite formation in Groenvlei was possibly supported by sulphate reducing bacteria whose activity typically leads to an increase in pH (Wright, 1999), which would be a plausible explanation for the poor preservation of biogenic silica remains within unit I. Those parts within unit I which show elevated dolomite contents are interpreted as dry periods leading to the evaporative modification of the marine-derived water to hypersaline conditions conducive to the formation of dolomite. At the Australian Coorong, the carbonates of the partly separated areas of the lagoon, which still have a connection to the main lagoon and hence to the ocean, contain between 0% and 25% dolomite, whereas the carbonates of the fully separated parts of the lagoon entirely consist of dolomite (von der Borch, 1976). By comparison, the maximum dolomite content of the Groenvlei record is 46%, measured only for one sample, whilst all the other samples containing dolomite reveal concentrations of less than 25%. Therefore, Groenvlei probably was influenced by the intrusion of seawater and presumably never desiccated entirely during times of dolomite formation. Those parts of the Groenvlei record which are dominated by Mg-calcites (especially unit II), in contrast, probably represent periods of a decreased marine influence and/or more humid conditions resulting in lower lake water salinities and Mg/Ca ratios.

5.3. Stable oxygen and carbon isotopes ($\delta^{18}O$ and $\delta^{13}C$) of the lacustrine carbonate fraction

The absence of correlation between $\delta^{18}O$ and $\delta^{13}C$ and the parallel trend of the $\delta^{18}O$ data to the $\delta^{13}C$ axis (Fig. 6) indicate that Groenvlei was a hydrologically open system (Talbot, 1990) during the entire period covered by our record. This means that Groenvlei was probably characterised by short residence times of its lake water and thus by relatively rapid throughflow (Talbot, 1990). Since any aboveground in- and outflows are absent, this throughflow can only occur via groundwater aquifers. The good correlation of $\delta^{18}O$ with Mg/Ca and Sr/Ca (Fig. 3) suggests that variations in $\delta^{18}O$ mainly reflect the varying mineralogical composition of the deposited carbonates and less changes in temperature or evaporative effects. Aragonite typically shows ~0.6‰ and dolomite ~3‰–4‰ isotopically heavier $\delta^{18}O$ values than calcite formed under the same conditions (Kelts and Talbot, 1990) which explains the differences in $\delta^{18}O$ between the core units I and II (Fig. 6). Variations in $\delta^{13}C$ could also be in part explained by the varying mineralogical composition since $\delta^{13}C$ and dolomite contents show an opposing trend in large parts of unit I (Fig. 3). Poorly ordered dolomite reveals 0.5‰–1‰ isotopically lighter $\delta^{13}C$ values than coexisting Mg-calcite (Botz and Von der Borch, 1984) and aragonite is ~1.8‰ isotopically

heavier than calcite (Rubinson and Clayton, 1969). However, the marked difference of $\delta^{13}C$ between the Groenvlei core units IIc and IIa, b, d (Figs. 3, 6), all of them mainly composed of Mg-calcites, cannot be explained by a varying mineralogy. Therefore, other factors have to be considered, such as changes in (1) the isotopic composition of inflowing waters, (2) the CO_2 exchange between the atmosphere and the dissolved inorganic carbon of the lake water, (3) the photosynthetic activity and respiration of aquatic plants and algae, or (4) changes in the primary bacterial processes as sulphate reduction or methanogenesis (Kelts and Talbot, 1990; Leng and Marshall, 2004).

5.4. Sediment organic matter

TOC/TN ratios are often used as indicators for the origin of organic material. Whilst algae typically show low TOC/TN ratios (from 4 to 10), vascular land plants are often characterised by higher ratios >20 (Meyers, 1994). Thus, TOC/TN ratios of the Groenvlei record suggest that the sediment organic matter represents a mixture of material of terrestrial and aquatic origin. Therefore, low TOC concentrations in unit I are interpreted to reflect both, a low input of organic matter into the lake and a low autochthonous bioproductivity of aquatic plants. In contrast, the high TOC concentrations and slightly decreasing TOC/TN ratios in unit II possibly point to an enhanced biological productivity within the lake and thus possibly to higher temperatures. Despite the slightly decreasing TOC/TN ratios in unit II indicate a greater contribution of aquatic plants/algae to the bulk organic matter, the markedly increasing TOC values may be also caused by a higher input of terrestrial organic material from the lake catchment. This hypothesis may be supported by the palynological evidence available from Martin (1968) suggesting a vegetation spread in the catchment after ~2000 BP.

5.5. Geochemistry, mineralogy and grain size analysis of the allochthonous sediment fraction

Quartz, Al, Fe, K and Ti are likely indicators of material eroded from the lake catchment (or beyond if wind is involved) and subsequently transported to and deposited within the lake. Besides the quartz sand which represents the main component of the dune material, Al, Fe and K are probably related to feldspars. Ti is mostly associated with accessory minerals like rutile or ilmenite which are resistant to post-depositional alteration (Yarincik et al., 2000; Zabel et al., 2001; Whitlock et al., 2008). Ca/Ti reflects variations in the relative proportion of the (mainly autochthonous) sediment carbonate fraction to the allochthonous, terrigenous material which was transported into the lake (Habertzell et al., 2009; Kasper et al., 2013).

Possible transport mechanisms into Groenvlei are either aeolian or fluvial. Due to the absence of rivers, the latter is probably associated with surface runoff and hence rainfall. However, as mentioned before, rainfall events must be extreme in order to generate surface runoff on the dunes and to transport allochthonous material into the lake. Aeolian transport requires threshold wind velocities and would also be favoured by a sparse vegetation cover on the dunes.

The rEMs probably reflect both fluvial and aeolian depositions. Erosion by heavy rainfall and surface runoff is indicated by medium to coarse sandy rEM1 (Dietze et al., 2014). Its score maxima occur together with peaks in other minerogenic input indicators (quartz, Ti, Fe, Al, K) and Mg-calcite (Figs. 3, 7) pointing to more humid conditions. The fine to medium sandy rEM2 (~80–100 μm) could be explained by both fluvial and aeolian transports. The interpretation as fluvial proxy might be less likely due to the high infiltration capacities of the dunes. The aeolian erosion of these relatively coarse grains, their transport by saltation and the deposition at our coring location would possibly be favoured by low lake levels and hence smaller distances between source and sink as well as by a less pronounced vegetation cover around the lake. The two end members rEM3 (~25–50 μm) and rEM4 (~20–25 μm) are possibly related to grains which were transported by aeolian

short-term suspension (Nickling, 1994). Hence, they could be reflecting the deposition of local dust (Dietze et al., 2014) mainly from the vicinity of the lake (rEM3), but possibly also from areas further beyond the small Groenvlei catchment (rEM4). The rEM5 (~8–20 µm) represents the finest grain size fraction of the Groenvlei record which is related to long-term suspension transport (Nickling, 1994; Dietze et al., 2014). Whilst rEM3 and rEM5 vary steadily across the entire record and therefore probably represent continuous background sedimentation, the marked shift from rEM2 dominating in unit I to rEM4 prevailing in unit II probably reflects a major environmental change in the area. More humid conditions in unit II could have led to an increase in the plant biomass in the catchment and hence to a lower erodibility of sandy dune material as well as possibly to an initial soil formation on the top of the dunes accompanied by weathering and thus a decrease in particle size.

5.6. Palaeoenvironmental reconstruction inferred from the Groenvlei record

The summarised palaeoenvironmental interpretation for the various core units of the Groenvlei record is displayed as indices of relative humidity and relative marine influence (Fig. 3). The majority of *unit I* (in detail the *units Ia*: 4210–3760 cal BP, *Ic*: 3690–2910 cal BP and *Ie*: 2820–2710 cal BP) is characterised by carbonates composed of aragonite and dolomite which probably suggests a greater marine influence as well as generally drier conditions resulting in lower lake levels compared to the present. Low contents of sedimentary organic matter indicate a moderate autochthonous bioproductivity within the lake as well as a low supply of allochthonous organic material. The latter is possibly due to a relatively low abundance of plant biomass in the lake catchment which is supported by the deposition of coarse allochthonous material possibly reflecting a relatively sparse vegetation cover on the dunes. Moreover, lower lake levels would have resulted in shorter distances between our coring position and the lake shore exposing more dune sands to aeolian transport and deposition at the central part of the lake. This could also explain the high sand contents (especially rEM2) in unit I. Within the *units Ib* (3760–3690 cal BP) and *Id* (2910–2820 cal BP) aragonite contents are decreased and dolomite peaks at the bases of these units indicate that the lake level was dropping further. At the top of these subunits, dolomite contents are low and Mg-calcite peaks together with the allochthonous input indicators. These sequences suggest relatively short phases of heavy rainfall events after prolonged lake level lowstands leading to (1) the erosion, fluvial transport and deposition of coarse dune material and (2) the temporary rise of the lake level associated with lower lake water Mg/Ca ratios and the precipitation of Mg-calcite. Thus, Groenvlei probably turned into a more freshwater system with lower salinities during these periods. The base of *unit If* (2710–1210 cal BP) is characterised by a distinct sand layer probably reflecting a heavy rainfall event which caused the deposition of allochthonous material from the dunes. The homogeneous carbonate layer above (1770⁺⁹⁰/₋₁₃₀ cal BP at 52 cm) contains a mixture of Mg-calcite and aragonite possibly indicating a further decreasing marine influence. This homogeneous layer is also covered by a sand layer which points to another heavy rainfall event. Viewed as a whole, this core section probably represents a period during which the lake system passed through a major change. However, the processual and chronological interpretation of this transition layer should be regarded with caution, as a time frame of 1500 years is represented only by a few centimetres of sediment (Fig. 2). Exceptional heavy rainfall events during lower lake levels could have caused reworking of already deposited sediments for example. A hiatus or a strongly reduced sediment accumulation would be other explanation attempts which, however, remain speculative.

Unit II (1210 cal BP–present) is characterised entirely by Mg-calcite as the most commonly precipitated carbonate phase. Hence, the lake turned finally into a freshwater system, as it remains today. This suggests a lower sea level and thus a reduced marine influence, but also a substantial supply of freshwater by rainfall and hence more humid conditions relative to unit I. TOC values started to increase and remain

higher than in unit I for the rest of the record. This points to an increased lake-internal bioproductivity, possibly due to higher mean temperatures and/or a greater nutrient availability. Moreover, an enhanced supply of organic matter from the catchment is indicated, which suggests the abundance of plant biomass on the dunes caused by the climatic amelioration. A possible expansion of the vegetation cover or a change in the species composition leading to increased soil formation and protection is also indicated by a shift in the grain size composition of the allochthonous material which is dominated by finer material with lower sand contents for the rest of the record. A denser vegetation cover possibly reduced the erodibility of coarser material and/or the wind energies were decreased compared to unit I. The *units IIa* (1210–700 cal BP) and *IIc* (140 cal BP–present) show slightly elevated allochthonous input suggesting that the climate was more humid compared to most parts of unit I and comparable to the present-day conditions. At *unit IIb* (700–610 cal BP) the markedly increased allochthonous input probably indicates an even wetter period than at present which possibly led to higher lake levels, an increase in the lake surface area and hence the water coverage of the platform north and east of Groenvlei. *Unit IIc* (610–140 cal BP) is the only core section characterised by Mg-calcite as the main carbonate phase and simultaneously the highest δ¹³C values of the record. Additionally, high Ca/Ti ratios and low quartz, Ti, Fe, Al and K concentrations indicate a high lake-internal carbonate production. Thus, this time period represents a unique environmental setting for the lake system. A slightly drier climate than at present is indicated for this unit possibly resulting in lower lake levels (high Ca/Ti ratios and low allochthonous input proxies) which led to higher light incidence and therefore an enhanced photosynthetic activity of the aquatic plants (high δ¹³C values).

5.7. Comparison with other local and regional records

5.7.1. Sea level

The high marine influence on Groenvlei between 4210 and 2710 cal BP, as inferred from our record, is supported by several former studies on sediments from the Wilderness embayment. Previous investigations of diatom assemblages on a sediment core from Eilandvlei (Fig. 1b) covering the past ~4000 years suggest that the lake system passed through different phases of marine influence, a 'marine phase' between ~4000 and 3450 cal BP, a 'lagoon phase' from 3450 to 2000 cal BP and a coastal lake phase from 2000 cal BP to the present (Kirsten, 2014). Studies on sediments from the fen east of Groenvlei indicate that the lake was in a 'lagoon stage' from approximately ~4000 to 2000 BP and developed into a freshwater lake thereafter (Martin, 1959, 1968). The higher marine influence during this time is probably related to an elevated sea level as it was reconstructed from several other studies in South African coastal areas, even though there are offsets in the exact reconstructed timing of the Holocene sea level highstand as well as of the transgression phases thereafter (Miller et al., 1995; Ramsay, 1995; Baxter and Meadows, 1999; Compton, 2001; Neumann et al., 2010; Carr et al., 2015; Fig. 1). In particular, the Groenvlei record shows a relatively good consistency with a sea level reconstruction from Verlorenvlei, located on the west coast of South Africa (Fig. 1a), which reveals a highstand from ~8000 to 4300 cal BP, a decreasing but still elevated sea level between ~4300 and 3300 cal BP and subsequently a lower sea level before reaching present conditions (Carr et al., 2015). Thus, the higher marine influence on Groenvlei, which lasted at least until 2710 cal BP, was probably related to the period after the Holocene sea level highstand when the sea level was dropping but still elevated relative to present.

5.7.2. Palaeoclimate

Despite the recorded short wet phases which were probably related to heavy rainfall events, the interpretation of our Groenvlei record suggests mostly drier conditions than at present between 4210 and 2710 cal BP. Palynological evidence from the fen east of Groenvlei

(Fig. 1c) point to unstable dunes in the Wilderness area and hence the restriction of forest spread due to sand movement roughly between ~6870 and 2000 BP (Martin, 1968). Bateman et al. (2011) who studied the evolution of the Wilderness dunes also identified a phase between approximately the past 3700 and 2400 years, when unconsolidated dune sand was transported and deposited – a process predominantly related to westerly wind activity in the area (Illenberger, 1996; Bateman et al., 2011). Therefore, the interpretation of our Groenvlei record may substantiate one of two alternative palaeoclimatic interpretations of Martin (1968) mentioned in the beginning, namely that the period between ~6870 and 2000 BP (as represented in our chronology: the period from 4210 to 2710 cal BP) was probably characterised by mostly drier conditions compared to the present. This, in turn, may support the hypothesis of Talma and Vogel (1992) who investigated a stalagmite from the Cango Caves (Figs. 1b, 8e) and concluded that the seasonality between 5000 and 2000 cal BP tended more towards winter rainfall. This could have resulted in drier conditions compared to the more humid, year-round rainfall pattern appearing at present. Hence, the findings inferred from our new core may support the presence of more pronounced winter rainfall seasonality in the Wilderness embayment during this time. The interpreted increase in plant biomass in the catchment of Groenvlei since 1210 cal BP as well as the establishment of the lake as a freshwater system indicates generally wetter conditions. This is supported by pollen data from the fen east of Groenvlei, which suggest a climatic amelioration with moister conditions facilitating the forest and scrub spread in the area after 2000 BP (Martin, 1968). A trend of increased humidity after 2000 cal BP is also inferred from palynological and sedimentological evidence from the Cape Agulhas Plain (Carr et al., 2006). The Cango Caves speleothem reveals a major climatic shift characterised by a marked temperature increase between 2500 and 2000 cal BP. However, Chase et al. (2013) suggested an alternative age model for this record, the consequence being that this shift would have occurred already between 5000 and 4000 cal BP. The $\delta^{15}\text{N}$ data of a hyrax midden record from Seweweekspoort (Figs. 1b, 8c) indicate a trend towards wetter conditions during the last 4500 years (Chase et al., 2013) which supports our interpretation of the Groenvlei record from generally drier conditions prior to 2710 cal BP towards a more humid climate, recorded from 1210 to 610 cal BP and 140 cal BP to the present.

A palaeoclimatic study on a stalagmite from the Cold Air Cave located in the SRZ reveals cool and dry conditions between ~6000 and 2500 years ago (Holmgren et al., 2003). Subsequently, the SRZ was probably characterised by a warm and wet climate which was interrupted by short cool periods (Fig. 8d). Zawada et al. (1996)

investigated occurrences of palaeofloods in the Orange River catchment representative for the SRZ and found no palaeoflood evidence between approximately 4120 and 1800 BP, although there were both before and thereafter; this also indicates drier climates in the SRZ around this time. The generally wetter conditions at the southern Cape coast as interpreted from our record for the past 1210 years (particularly for the periods 1210–610 cal BP and 140 cal BP–present) are therefore possibly related to more humid conditions within the SRZ. Chase et al. (2015) even concluded for a study site located in the WRZ (Katbakkies Pass, Cape Fold Mountains; Fig. 1) that it is the summer rainfall variability which primarily determines changes in humidity at that site.

During the time frame of the Little Ice Age, South Africa was characterised by a cooler climate between 650 and 100 cal BP, most probably with drier conditions in the SRZ and wetter conditions in the WRZ (Tyson and Lindesay, 1992; Stager et al., 2012). This period coincides well with unit Ilc (610–140 cal BP) of the Groenvlei record, which presumably reflects a period characterised by slightly drier conditions. This supports the conclusion that the southern Cape coast was rather more influenced by the SRZ for at least the past 1210 years.

6. Conclusions

The Groenvlei record provides insights into environmental change at the southern Cape coast during the past ~4200 years. The interpreted data indicate that a slightly higher sea level caused a marine influence on the lake from 4210 cal BP until at least 2710 cal BP. Palaeoclimatic interpretations suggest that this period was characterised by generally drier conditions than at present causing various lake level lowstands. Greater winter rainfall seasonality is associated with these drier overall conditions. However, this rather dry period was interrupted by short phases during which heavy rainfall occurred (3760–3690 cal BP and 2910–2820 cal BP). Subsequently, the ocean presumably reached its present level and Groenvlei changed from a more marine-influenced into a freshwater system between 2710 and 1210 cal BP. During the period from 1210 to 700 cal BP as well as during the last 140 years, the climate was probably wetter and comparable to the present-day conditions. Since 1210 cal BP the vegetation around the lake probably spread due to the climatic amelioration that may be linked to an enhanced influence of summer rainfall. An even wetter phase with higher lake levels than today is indicated for the time between 700 and 610 cal BP. From 610 to 140 cal BP, the period corresponding to the Little Ice Age, a higher degree of lake-internal productivity is inferred, possibly due to slightly drier conditions than at present.

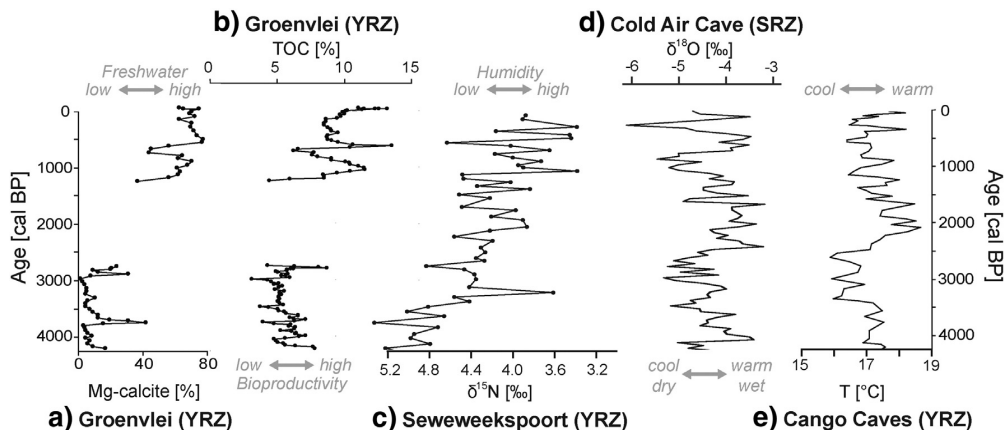


Fig. 8. Comparison of a) the Mg-calcite and b) TOC data from the Groenvlei record with proxies obtained from other studies: c) $\delta^{15}\text{N}$ from a hyrax midden record from Seweweekspoort (Chase et al., 2013); d) $\delta^{18}\text{O}$ from the Cold Air Cave stalagmite (Holmgren et al., 2003); e) temperature derived from the Cango Caves stalagmite record using the original age model as suggested by Talma and Vogel (1992).

In summary, our new high-resolution record from Groenvlei reveals valuable discoveries in terms of sea level and climate change at the southern Cape coast, especially for the periods from 4210 to 2710 cal BP and 1210 cal BP to the present. However, the exact dating of the transition of Groenvlei into a freshwater system remains uncertain. This was likely caused by a reworking of sediment due to at least two exceptional heavy rainfall events whose occurrence can currently only be roughly estimated for a time frame between 2710 and 1210 cal BP.

Acknowledgements

This study was funded by the German Federal Ministry of Education and Research (BMBF). The investigations were conducted within the collaborative project “Regional Archives for Integrated Investigations” (RAIN), which is embedded in the international research programme SPACES (Science Partnership for the Assessment of Complex Earth System Processes).

We are deeply grateful to CapeNature for the permit to conduct our fieldwork at Groenvlei, which is part of the protected Goukamma Nature Reserve. Particularly acknowledged are the helping hands of Brunhilde Dreßler, Carmen Kirchner (Friedrich Schiller University Jena) and Sabine Stahl (University of Bremen) during the laboratory work. For the use of the SEM, we thank Heidrun Garlipp for assistance and gratefully acknowledge the partial financial support of the Deutsche Forschungsgemeinschaft (DFG), grant reference INST 275/241-1 FUGG, and the Thüringer Ministerium für Bildung, Wissenschaft und Kultur (TMBWK), grant reference 62-4264 925/1/10/1/01. Elisabeth Dietze was funded by the Virtual Helmholtz Institute of Integrated Climate and Landscape Evolution Analyses (ICLEA). Moreover, we thank Jacques Labrie for providing the modified version of the Gradistat 4.2 software. Lynne J. Quick (University of Cape Town), Peter Frenzel, Holger Brand and Thomas Leser (Friedrich Schiller University Jena) are thanked for their help during the fieldwork and Peter Frenzel additionally for his valuable comments on the manuscript.

Appendix A. Supplementary data

Supplementary data to this article can be found online at <http://dx.doi.org/10.1016/j.palaeo.2016.01.027>.

References

- Allanson, B.R., Whitfield, A.K., 1983. *Limnology of the Touw River Floodplain*. Council for Scientific and Industrial Research, Pretoria.
- Appleby, P., 2008. Three decades of dating recent sediments by fallout radionuclides: a review. *The Holocene* 18, 83–93.
- Appleby, P., Oldfield, F., 1978. The calculation of lead-210 dates assuming a constant rate of supply of unsupported ^{210}Pb to the sediment. *Catena* 5, 1–8.
- Bateman, M.D., Carr, A.S., Dunajko, A.C., Holmes, P.J., Roberts, D.L., McLaren, S.J., Bryant, R.G., Marker, M.E., Murray-Wallace, C.V., 2011. The evolution of coastal barrier systems: a case study of the Middle–Late Pleistocene Wilderness barriers, South Africa. *Quat. Sci. Rev.* 30, 63–81.
- Bateman, M.D., Holmes, P.J., Carr, A.S., Horton, B.P., Jaiswal, M.K., 2004. Aeolianite and barrier dune construction spanning the last two glacial–interglacial cycles from the southern Cape coast, South Africa. *Quat. Sci. Rev.* 23, 1681–1698.
- Baxter, A.J., Meadows, M.E., 1999. Evidence for Holocene sea level change at Verlorenvlei, Western Cape, South Africa. *Quat. Int.* 56, 65–79.
- Birch, G.F., Du Plessis, A., Willis, J.P., 1978. Offshore and onland geological and geophysical investigations in the Wilderness lakes region. *Trans. Geol. Soc. S. Afr.* 81, 339–352.
- Blaauw, M., Christen, J.A., 2011. Flexible paleoclimate age–depth models using an autoregressive gamma process. *Bayesian Anal.* 6, 457–474.
- Blott, S.J., Pye, K., 2001. GRADISTAT: a grain size distribution and statistics package for the analysis of unconsolidated sediments. *Earth Surf. Process. Landf.* 26, 1237–1248.
- Botz, R.W., Von der Borch, C.C., 1984. Stable isotope study of carbonate sediments from the Coorong area, South Australia. *Sedimentology* 31, 837–849.
- Carr, A.S., Boom, A., Chase, B.M., Meadows, M.E., Grimes, H.L., 2015. Holocene sea level and environmental change on the West Coast of South Africa: evidence from plant biomarkers, stable isotopes and pollen. *J. Paleolimnol.* 53, 415–432.
- Carr, A.S., Thomas, D.S.G., Bateman, M.D., Meadows, M.E., Chase, B., 2006. Late Quaternary palaeoenvironments of the winter-rainfall zone of southern Africa: palynological and sedimentological evidence from the Agulhas Plain. *Palaeogeogr. Palaeoclimatol. Palaeoecol.* 239, 147–165.
- Cawthra, H.C., Bateman, M.D., Carr, A.S., Compton, J., Holmes, P.J., 2014. Understanding Late Quaternary change at the land–ocean interface: a synthesis of the evolution of the Wilderness coastline, South Africa. *Quat. Sci. Rev.* 99, 210–223.
- Chase, B.M., Meadows, M.E., 2007. Late Quaternary dynamics of southern Africa's winter rainfall zone. *Earth-Sci. Rev.* 84, 103–138.
- Chase, B.M., Boom, A., Carr, A.S., Meadows, M.E., Reimer, P.J., 2013. Holocene climate change in southernmost South Africa: rock hyrax middens record shifts in the southern westerlies. *Quat. Sci. Rev.* 82, 199–205.
- Chase, B.M., Lim, S., Chevalier, M., Boom, A., Carr, A.S., Meadows, M.E., Reimer, P.J., 2015. Influence of tropical easterlies in southern Africa's winter rainfall zone during the Holocene. *Quat. Sci. Rev.* 107, 138–148.
- Chung, F.H., 1975. Quantitative interpretation of X-ray diffraction patterns of mixtures. III. Simultaneous determination of a set of reference intensities. *J. Appl. Crystallogr.* 8, 17–19.
- Cohen, A.L., Tyson, P.D., 1995. Sea-surface temperature fluctuations during the Holocene off the south coast of Africa: implications for terrestrial climate and rainfall. *The Holocene* 5, 304–312.
- Compton, J.S., 2001. Holocene sea-level fluctuations inferred from the evolution of depositional environments of the southern Langebaan Lagoon salt marsh, South Africa. *The Holocene* 11, 395–405.
- de Boer, G.B., de Weerd, C., Thoenes, D., Goossens, H.W., 1987. Laser diffraction spectrometry: Fraunhofer diffraction versus Mie scattering. *Part. Part. Syst. Charact.* 4, 14–19.
- Dietze, E., Hartmann, K., Diekmann, B., Ijmker, J., Lehmkuhl, F., Opitz, S., Stauch, G., Wünnemann, B., Borchers, A., 2012. An end-member algorithm for deciphering modern detrital processes from lake sediments of Lake Donggi Cona, NE Tibetan Plateau, China. *Sediment. Geol.* 243, 169–180.
- Dietze, E., Maussion, F., Ahlborn, M., Diekmann, B., Hartmann, K., Henkel, K., Kasper, T., Locket, G., Opitz, S., 2014. Sediment transport processes across the Tibetan Plateau inferred from robust grain size end-members in lake sediments. *Clim. Past* 10, 91–106.
- Dietze, M., Dietze, E., 2013. EMMAgeo: end-member modelling algorithm and supporting functions for grain-size analysis. R package version 0.9.0. available at: <http://CRAN.R-project.org/package=EMMAgeo> (last access: 3 August 2015).
- DIN, 1997. DIN ISO 10693:1997–05. Soil Quality – Determination of Carbonate Content – Volumetric Method (ISO 10693:1995). Beuth, Berlin.
- Folk, R.L., 1974. The natural history of crystalline calcium carbonate; effect of magnesium content and salinity. *J. Sediment. Res.* 44, 40–53.
- Geldenhuis, C.J., 1994. Bergwind fires and the location pattern of forest patches in the southern Cape landscape, South Africa. *J. Biogeogr.* 21, 49–62.
- Goldsmith, J., Graf, D., 1958. Relation between lattice constants and composition of the Ca–Mg carbonates. *Am. Mineral.* 43, 84–101.
- Haberzettl, T., Anselmetti, F.S., Bowen, S.W., Fey, M., Mayr, C., Zolitschka, B., Ariztegui, D., Mauz, B., Ohlendorf, C., Kastner, S., Lücke, A., Schäbitz, F., Wille, M., 2009. Late Pleistocene dust deposition in the Patagonian steppe – extending and refining the paleoenvironmental and tephrochronological record from Laguna Portrok Aike back to 55 ka. *Quat. Sci. Rev.* 28, 2927–2939.
- Hardie, L.A., 1987. Dolomitization; a critical view of some current views. *J. Sediment. Res.* 57, 166–183.
- Hogg, A.C., Hua, Q., Blackwell, P.G., Niu, M., Buck, C.E., Guilderson, T.P., Heaton, T.J., Palmer, J.G., Reimer, P.J., Reimer, R.W., 2013. SHCal13 Southern Hemisphere Calibration, 0–50,000 Years cal BP. *Radiocarbon*.
- Holmgren, K., Lee-Thorp, J.A., Cooper, G.R.J., Lundblad, K., Partridge, T.C., Scott, L., Sithaldeen, R., Siep Talma, A., Tyson, P.D., 2003. Persistent millennial-scale climatic variability over the past 25,000 years in Southern Africa. *Quat. Sci. Rev.* 22, 2311–2326.
- Hubbard, C.R., Evans, E.H., Smith, D.K., 1976. The reference intensity ratio, I/I_0 , for computer simulated powder patterns. *J. Appl. Crystallogr.* 9, 169–174.
- Illenberger, W.K., 1996. The geomorphologic evolution of the Wilderness dune cordons, South Africa. *Quat. Int.* 33, 11–20.
- Kasper, T., Frenzel, P., Haberzettl, T., Schwarz, A., Daut, G., Meschner, S., Wang, J., Zhu, L., Mäusbacher, R., 2013. Interplay between redox conditions and hydrological changes in sediments from Lake Nam Co (Tibetan Plateau) during the past 4000 cal BP inferred from geochemical and micropaleontological analyses. *Palaeogeogr. Palaeoclimatol. Palaeoecol.* 392, 261–271.
- Kelts, K., Hsü, K.J., 1978. Freshwater carbonate sedimentation. In: Lerman, A. (Ed.), *Lakes: Chemistry, Geology, Physics*. Springer, New York, pp. 295–323.
- Kelts, K., Talbot, M., 1990. Lacustrine carbonates as geochemical archives of environmental change and biotic/abiotic interactions. In: Tilzer, M., Serruya, C. (Eds.), *Large Lakes*. Springer, Berlin Heidelberg, pp. 288–315.
- Kirsten, K.L., 2014. Late Holocene Diatom Community Responses to Climate Variability along the Southern Cape Coastal Plain, South Africa (PhD Thesis) University of Cape Town, South Africa.
- Kruger, A., 2002. Climate of South Africa: Surface Winds. South African Weather Service, Pretoria.
- Kruger, A., 2004. Climate of South Africa: Climate Regions. South African Weather Service, Pretoria.
- Land, L., 1998. Failure to precipitate dolomite at 25 °C from dilute solution despite 1000-fold oversaturation after 32 years. *Aquat. Geochem.* 4, 361–368.
- Last, W.M., 1990. Lacustrine dolomite – an overview of modern, Holocene, and Pleistocene occurrences. *Earth-Sci. Rev.* 27, 221–263.
- Leng, M.J., Marshall, J.D., 2004. Palaeoclimatic interpretation of stable isotope data from lake sediment archives. *Quat. Sci. Rev.* 23, 811–831.
- Machel, H.-G., Mountjoy, E.W., 1986. Chemistry and environments of dolomitization – a reappraisal. *Earth-Sci. Rev.* 23, 175–222.
- Martin, A.R.H., 1956. The ecology and history of Groenvlei. *S. Afr. J. Sci.* 52, 187–192.

- Martin, A.R.H., 1959. The stratigraphy and history of Groenvlei, a South African coastal fen. *Aust. J. Bot.* 7, 142–167.
- Martin, A.R.H., 1960. The ecology of Groenvlei, a South African Fen: part I. The Primary Communities. *J. Ecol.* 48, 55–71.
- Martin, A.R.H., 1968. Pollen analysis of Groenvlei Lake sediments, Knysna (South Africa). *Rev. Palaeobot. Palynol.* 7, 107–144.
- Meyers, P.A., 1994. Preservation of elemental and isotopic source identification of sedimentary organic matter. *Chem. Geol.* 114, 289–302.
- Miller, D., Yates, R., Jerardino, A., Parkington, J., 1995. Late Holocene coastal change in the southwestern Cape, South Africa. *Quat. Int.* 29, 3–10.
- Morrow, D.W., 1982. Diagenesis 1. Dolomite – part 1: the chemistry of dolomitization and dolomite precipitation. *Geosci. Can.* 9, 5–13.
- Müller, G., Irion, G., Förstner, U., 1972. Formation and diagenesis of inorganic Ca–Mg carbonates in the lacustrine environment. *Naturwissenschaften* 59, 158–164.
- Nakagawa, T., Gotanda, K., Haraguchi, T., Danhara, T., Yonenobu, H., Brauer, A., Yokoyama, Y., Tada, R., Takemura, K., Staff, R.A., 2012. SG06, a fully continuous and varved sediment core from Lake Suigetsu, Japan: stratigraphy and potential for improving the radiocarbon calibration model and understanding of late quaternary climate changes. *Quat. Sci. Rev.* 36, 164–176.
- Neumann, F.H., Scott, L., Bousman, C.B., van As, L., 2010. A Holocene sequence of vegetation change at Lake Eteza, coastal KwaZulu-Natal, South Africa. *Rev. Palaeobot. Palynol.* 162, 39–53.
- Nickling, W.G., 1994. Aeolian sediment transport and deposition. In: Pye, K. (Ed.), *Sediment Transport and Depositional Processes*. Blackwell Scientific Publications, Oxford.
- Parsons, R.P., 2014. Quantifying the Role of Groundwater in Sustaining Groenvlei, A Shallow Lake in the Southern Cape Region of South Africa (PhD Thesis) University of the Free State, Bloemfontein, South Africa.
- Ramsay, P., 1995. 9000 years of sea-level change along the southern African coastline. *Quat. Int.* 31, 71–75.
- Reinwarth, B., Franz, S., Baade, J., Haberzettl, T., Kasper, T., Daut, G., Helmschrot, J., Kirsten, K.L., Quick, L.J., Meadows, M.E., Mäusbacher, R., 2013. A 700-year record on the effects of climate and human impact on the southern Cape coast inferred from lake sediments of Eilandvlei, Wilderness embayment, South Africa. *Geogr. Ann.* 95, 345–360.
- Rubinson, M., Clayton, R.N., 1969. Carbon-13 fractionation between aragonite and calcite. *Geochim. Cosmochim. Acta* 33, 997–1002.
- Sánchez-Román, M., McKenzie, J.A., de Luca Rebello Wagener, A., Rivadeneyra, M.A., Vasconcelos, C., 2009. Presence of sulfate does not inhibit low-temperature dolomite precipitation. *Earth Planet. Sci. Lett.* 285, 131–139.
- Scholtz, A., 1986. *Palynological and Palaeobotanical Studies in the Southern Cape* (MA Thesis) University of Stellenbosch, South Africa.
- Scott, L., Lee-Thorp, J., 2004. Holocene climatic trends and rhythms in southern Africa. In: Battarbee, R., Gasse, F., Stickley, C. (Eds.), *Past Climate Variability Through Europe and Africa*. Springer, Dordrecht, pp. 69–91.
- Stager, J.C., Mayewski, P.A., White, J., Chase, B.M., Neumann, F.H., Meadows, M.E., King, C.D., Dixon, D.A., 2012. Precipitation variability in the winter rainfall zone of South Africa during the last 1400 yr linked to the austral westerlies. *Clim. Past* 8, 877–887.
- Stager, J.C., Ryves, D.B., King, C., Madson, J., Hazzard, M., Neumann, F.H., Maud, R., 2013. Late Holocene precipitation variability in the summer rainfall region of South Africa. *Quat. Sci. Rev.* 67, 105–120.
- Talbot, M.R., 1990. A review of the palaeohydrological interpretation of carbon and oxygen isotopic ratios in primary lacustrine carbonates. *Chem. Geol. Isot. Geosci. Sect.* 80, 261–279.
- Talma, A.S., Vogel, J.C., 1992. Late Quaternary paleotemperatures derived from a speleothem from Cango Caves, Cape Province, South Africa. *Quat. Res.* 37, 203–213.
- Titschack, J., Goetz-Neunhoeffer, F., Neubauer, J., 2011. Magnesium quantification in calcites [(Ca,Mg)CO₃] by Rietveld-based XRD analysis: revisiting a well-established method. *Am. Mineral.* 96, 1028–1038.
- Tucker, M.E., Wright, V.P., 2009. *Carbonate Sedimentology*. Blackwell Scientific Publications, Oxford.
- Tyson, P., Lindsay, J., 1992. The climate of the last 2000 years in southern Africa. *The Holocene* 2, 271–278.
- Vasconcelos, C., McKenzie, J.A., 1997. Microbial mediation of modern dolomite precipitation and diagenesis under anoxic conditions (Lagoa Vermelha, Rio de Janeiro, Brazil). *J. Sediment. Res.* 67, 378–390.
- Vasconcelos, C., McKenzie, J.A., Bernasconi, S., Grujic, D., Tiens, A.J., 1995. Microbial mediation as a possible mechanism for natural dolomite formation at low temperatures. *Nature* 377, 220–222.
- Veizer, J., 1983. Trace elements and isotopes in sedimentary carbonates. *Rev. Mineral. Geochem.* 11, 265–299.
- von der Borch, C.C., 1965. The distribution and preliminary geochemistry of modern carbonate sediments of the Coorong area, South Australia. *Geochim. Cosmochim. Acta* 29, 781–799.
- von der Borch, C.C., 1976. Stratigraphy and formation of Holocene dolomitic carbonate deposits of the Coorong area, South Australia. *J. Sediment. Res.* 46, 952–966.
- Watling, R.J., 1979. The distribution of trace metals in the Wilderness lakes. *Water SA* 5, 1–13.
- Whitlock, C., Dean, W., Rosenbaum, J., Stevens, L., Fritz, S., Bracht, B., Power, M., 2008. A 2650-year-long record of environmental change from northern Yellowstone National Park based on a comparison of multiple proxy data. *Quat. Int.* 188, 126–138.
- Wright, D.T., 1999. The role of sulphate-reducing bacteria and cyanobacteria in dolomite formation in distal ephemeral lakes of the Coorong region, South Australia. *Sediment. Geol.* 126, 147–157.
- Yarincik, K., Murray, R., Peterson, L., 2000. Climatically sensitive eolian and hemipelagic deposition in the Cariaco Basin, Venezuela, over the past 578,000 years: results from Al/Ti and K/Al. *Paleoceanography* 15, 210–228.
- Zabel, M., Schneider, R.R., Wagner, T., Adegbe, A.T., de Vries, U., Kolonic, S., 2001. Late Quaternary climate changes in central Africa as inferred from terrigenous input to the Niger fan. *Quat. Res.* 56, 207–217.
- Zawada, P.K., Hattingh, J., Van Bladeren, D., vir Geowetenskap, R., 1996. Paleoflood hydrological analysis of selected South African rivers. *South African Water Research Commission, Report No 509/1/96*, Pretoria.
- Zhang, F., Xu, H., Konishi, H., Kemp, J.M., Roden, E.E., Shen, Z., 2012. Dissolved sulfide-catalyzed precipitation of disordered dolomite: implications for the formation mechanism of sedimentary dolomite. *Geochim. Cosmochim. Acta* 97, 148–165.
- Zhang, F., Xu, H., Konishi, H., Roden, E.E., 2010. A relationship between d104 value and composition in the calcite-disordered dolomite solid-solution series. *Am. Mineral.* 95, 1650–1656.

Chapter 3

The impact of changing reservoir effects on the ^{14}C chronology of a Holocene sediment record from South Africa

Authors: Michael Wündsch,
Torsten Haberzettl, Michael E. Meadows, Kelly L. Kirsten,
Thomas Kasper, Jussi Baade, Gerhard Daut,
Joseph S. Stoner, Roland Mäusbacher

Published in:
Quaternary Geochronology 36 (2016), 148-160

Keywords: Coastal lake sediments, Radiocarbon dating, Marine reservoir effect, Agulhas Bank, Pre-bomb shells, Palaeomagnetic secular variations



The impact of changing reservoir effects on the ^{14}C chronology of a Holocene sediment record from South Africa



Michael Wündsche^{a,*}, Torsten Haberzettl^a, Michael E. Meadows^b, Kelly L. Kirsten^{a,b}, Thomas Kasper^a, Jussi Baade^a, Gerhard Daut^a, Joseph S. Stoner^c, Roland Mäusbacher^a

^a Physical Geography, Institute of Geography, Friedrich Schiller University Jena, Löbdergraben 32, 07743, Jena, Germany

^b Department of Environmental and Geographical Science, University of Cape Town, South Lane, Upper Campus, 7701, Rondebosch, South Africa

^c Paleomagnetic & Environmental Magnetic Research Laboratory, College of Earth, Ocean, and Atmospheric Sciences, Oregon State University, 104 CEOAS Admin Building, Corvallis, OR, 97331, USA

ARTICLE INFO

Article history:

Received 13 March 2016

Received in revised form

19 July 2016

Accepted 31 August 2016

Available online 1 September 2016

Keywords:

Coastal lake sediments

Radiocarbon dating

Marine reservoir effect

Agulhas Bank

Pre-bomb shells

Palaeomagnetic secular variations

ABSTRACT

A 30.5 m sediment core was recovered from the coastal lake Eilandvlei (EV13), which represents a unique high-resolution record of environmental change for southern Africa. For the establishment of a robust chronology, special emphasis was placed on the calibration of radiocarbon (^{14}C) ages obtained from the dating of different material. However, the reliability of ^{14}C ages can be problematic since coastal lakes interact with different source pools providing ^{14}C -depleted ("old") carbon thus causing reservoir effects. The origin of old carbon affecting the EV13 samples was most likely sourced from the Indian Ocean. Two pre-bomb marine molluscan shells were therefore analysed to determine the regional marine reservoir offset (ΔR), with obtained ΔR values of 134 ± 38 and 161 ± 38 ^{14}C yrs providing the first available data for the south coast of South Africa. However, the application of the resulting average $\Delta\text{R}_{\text{mean}} = 148 \pm 27$ ^{14}C yrs for the calibration of the entire EV13 record underestimates the variable reservoir effects throughout the Holocene. These were possibly caused by past changes in the connectivity between the present lake system and the ocean as well as a varying degree of upwelling in this area. To solve this problem, three sample pairs (each consisting of wood fragments and bulk organic sediment from the same core depth) were dated to calculate the variable past reservoir effects. This approach provided a median basal age of 8920^{+200}_{-250} cal BP. Palaeomagnetic secular variation stratigraphy was used to corroborate the chronology for the topmost 1.5 m of the record (past millennium), thus providing the first Holocene sediment based inclination and declination data from South Africa.

© 2016 Elsevier B.V. All rights reserved.

1. Introduction

Due to the geological evolution of southern Africa, the occurrence of depressions containing Holocene deposits, such as lakes or marshes, is relatively scarce. Moreover, the generally arid climate with pronounced seasonality is not conducive to the preservation of such geoarchives. Hence, the opportunity to gain suitable proxy data from Holocene sediments for palaeoenvironmental reconstructions is limited (Chase and Meadows, 2007; Haberzettl et al., 2014; Scott and Lee-Thorp, 2004). Notwithstanding, several coastal archives have provided some inferences of changing environmental conditions during the Holocene (e.g., Carr et al., 2015;

Compton, 2001; Neumann et al., 2010), but often these records are either of coarse resolution (Finch and Hill, 2008; Meadows and Baxter, 2001), discontinuous (Baxter and Meadows, 1999; Wündsche et al., 2016) or confined to specific periods of the Holocene (Reinwarth et al., 2013; Stager et al., 2012, 2013).

In the present study, we retrieved a 30.5 m sediment core from the lake Eilandvlei (EV13) located within the Wilderness embayment on the southern Cape coast (Fig. 1). Regarding the recovered length and preservation, this core represents a unique discovery for southern Africa. A prospective multi-proxy approach may give detailed insights into Holocene sea level and climate changes in this area. Therefore, it is of particular importance to establish a reliable chronology for this exceptional record allowing its comparison with results from other studies.

Radiocarbon (^{14}C) dating represents a well-established and widely used method in palaeosciences in determining chronologies

* Corresponding author.

E-mail address: michael.wuendsch@uni-jena.de (M. Wündsche).

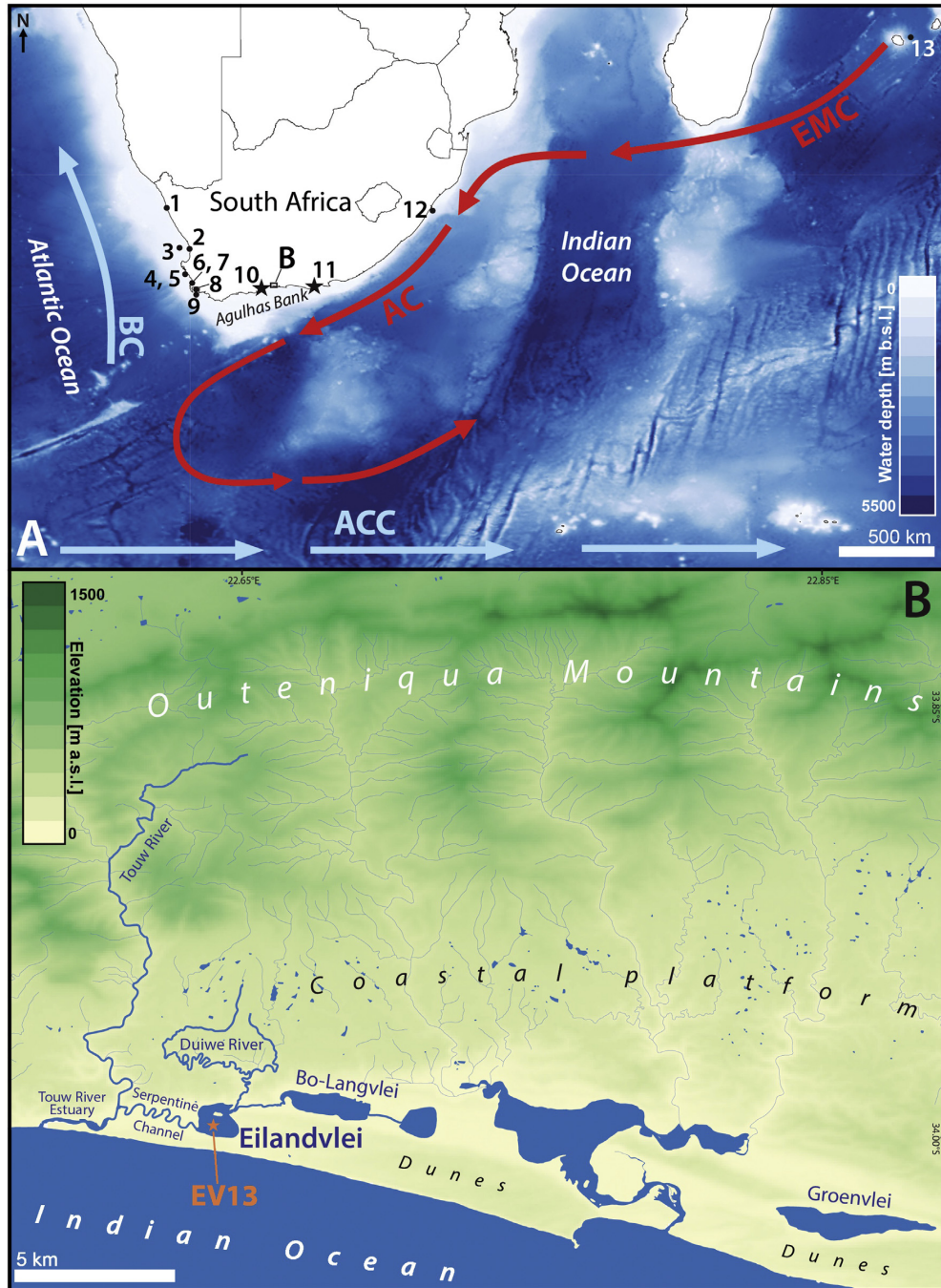


Fig. 1. Study area: **A**) Southern Africa and surrounding oceanic circulation systems (**BC**: Benguela Current, **AC**: Agulhas Current, **EMC**: East Madagascar Current, **ACC**: Antarctic Circumpolar Current); Sampling locations of the two pre-bomb shells used in this study are shown as black stars (10: Mossel Bay, 11: Jeffreys Bay); Locations of available ΔR values obtained from other studies are shown as black dots (1–8: Dewar et al. (2012); 9, 12, 13: Southon et al. (2002)); **B**) Coastal lakes within the Wilderness embayment along the southern Cape coast of South Africa. The EV13 core site is depicted as orange star. (For interpretation of the references to colour in this figure legend, the reader is referred to the web version of this article.)

for the past ~50 kyrs. To obtain precise ages it is essential to consider the possible influences of ^{14}C -depleted (“old”) carbon contained in the measured samples thus exhibiting reservoir

effects. Various natural reservoirs storing old carbon can affect coastal environments. Possible sources from the interior can be ancient soil organic matter or a geological setting characterized by

the presence of carbonates (Little, 1993); in addition, the adjacent sea provides a major pool of old carbon. ^{14}C ages of marine samples are calibrated by means of the current Marine13 calibration curve (Reimer et al., 2013), which is based on an ocean-atmosphere box diffusion model (Oeschger et al., 1975; Stuiver and Braziunas, 1993) for the period from 0 to 10500 cal BP. The differences between ^{14}C concentrations in the surface ocean waters relative to the atmosphere produce a globally averaged offset of 405 ± 22 ^{14}C yrs (Hughen et al., 2004), which is referred to as the global marine reservoir effect (R). Regionally, the marine reservoir effect can vary from that of the global model, for instance due to upwelling of ^{14}C -depleted deep ocean water providing reservoir ages that average around 1500 ^{14}C yrs during the past 9000 yrs (Stuiver et al., 1986). This local deviation from the global mean is defined as the regional marine reservoir effect (ΔR) (Stuiver and Braziunas, 1993; Stuiver et al., 1986).

For a number of regions around the globe ΔR values have been determined and are available in the marine reservoir database (<http://calib.qub.ac.uk/marine/>). The most widely used methods to estimate ΔR values are based on ^{14}C measurements of 1) shells collected alive at a known time before AD 1950 (pre-bomb), 2) sample pairs of marine (mostly shells) and terrestrial (e.g., wood or charcoal) materials which are assumed to share dates of death of the respective organisms and deposition and 3) samples which are stratigraphically related to onshore and offshore tephra layers that act as isochrones (Ascough et al., 2004, 2005; Petchey et al., 2008; Reimer et al., 2002; Russell et al., 2011).

Many studies using sediment cores apply a constant ΔR value for the reservoir correction of their whole records (e.g., Farmer et al., 2005; Roberts et al., 2011). However, to establish chronologies for marine or marine-influenced geoarchives, it is important to consider that ΔR can vary not only spatially but also temporally which has a significant impact on the accuracy of age determinations (Sarnthein et al., 2015). To take this into account other studies have applied variable ΔR values for their records (Enkin et al., 2013; Philippsen et al., 2013; Roberts et al., 2011; Sabatier et al., 2010; Schimmelmann et al., 2006).

For the east and west coast of South Africa, several ΔR values have been estimated derived from pre-bomb shells of known age (Dewar et al., 2012; Southon et al., 2002) (Fig. 1A). Additionally, a couple of past ΔR values for the late Quaternary have been reconstructed for the west coast based on the ^{14}C measurements of marine/terrestrial sample pairs from archaeological sites (Dewar et al., 2012).

In this contribution, we present two new ΔR values derived from pre-bomb shells representing the first published data for the south coast of South Africa. However, the main goal of this study is to establish a reliable ^{14}C chronology for the EV13 sediment core. Therefore, we test and compare two approaches to correct the marine reservoir effects affecting our core site throughout the Holocene: firstly, we apply the mean ΔR value derived from the pre-bomb shells for the reservoir correction of the marine-influenced samples of the entire record; secondly, we estimate and use variable past ΔR values inferred from three sample pairs consisting of different material. Additionally, we compare palaeomagnetic secular variation data for the upper part of the record to geomagnetic field models and archaeomagnetic data in order to independently substantiate the ^{14}C chronology similar to previous studies on lacustrine systems (Ahlborn et al., 2015; Haberzettl, 2015; Haberzettl et al., 2015; Kasper et al., 2012).

1.1. Regional setting

The marine environment off southern Africa is affected by the warm Agulhas Current along its east and south coast and the cold

Benguela Current along its west coast (Fig. 1A). These currents wield significant influences on the marine ecosystems as well as the climatic conditions experienced over the continent. East of South Africa, the Agulhas Current runs southwestwards relatively parallel to the continental shelf. Along the south coast the shelf broadens forming the so-called Agulhas Bank, which borders our area of investigation (Fig. 1A). Hence, the current moves further offshore and then retroflects back toward the Indian Ocean several hundred kilometres south of Cape Agulhas (Fig. 1A); this is caused by shear interactions with the Antarctic Circumpolar Current (ACC) (Feng et al., 2013; Lutjeharms et al., 2001). The Benguela Current flows northwards along the west coast of South Africa representing an important upwelling system of ascending nutrient-rich and cold Antarctic waters (Jury and Brundrit, 1992; Jury et al., 1990). The Agulhas Bank can be affected by both cold water masses from the Benguela Current (Schalke, 1973) as well as through the advection of warm surface plumes onto the bank from the Agulhas Current (Schumann et al., 1982). Although not being a major upwelling region such as the Benguela system, wind-induced coastal upwelling can also occur at the south coast of South Africa (Schumann et al., 1982; Walker, 1986).

Eilandvlei is one of several brackish, coastal lakes within the Wilderness embayment located at the southern Cape coast bordering the Agulhas Bank (Fig. 1). The embayment probably started to develop during the Pleistocene (Birch et al., 1978; Hart, 1995; Martin, 1962). To the north, it is bounded by an up to 200 m high coastal platform (Marker and Holmes, 2002) which had been deeply incised by rivers like the Duiwe and Touw River (Fig. 1B). The bedrocks in this area are composed of granites of the Woodville pluton (Browning and Macey, 2015; Ferré and Améglio, 2000) as well as metasedimentary rocks of the Kaaimans Group (Frimmel and Van Achterbergh, 1995). Further to the north, the upper catchments of these rivers are located within the Outeniqua Mountains which mainly consist of quartzites, quartzitic sandstones and shales of the Table Mountain Group (Balfour and Bond, 1993; Booth, 2011). To the south, the embayment is separated from the Indian Ocean (Agulhas Bank) by dune cordons composed of aeolianites cemented by calcium carbonate (Bateman et al., 2011; Illenberger, 1996). Due to sea level changes during the Holocene and thus varying degrees of exchanges with the ocean, the embayment passed through different environmental phases (Kirsten, 2014; Martin, 1959, 1968). In the following, these periods are referred to as the 'marine embayment', the 'lagoon system' and the 'estuarine/lacustrine system' (Figs. 2 and 3).

Eilandvlei is presently connected to the Indian Ocean via the Serpentine Channel and the Touw River estuary to the west (Fig. 1B). Temporarily, the formation of a sandbar at the mouth of the Touw River estuary blocks this connection to the ocean. When the estuary mouth is open, tidal influences, especially during spring tides, may cause the inflow of saline water into the lake via the Serpentine Channel. Marine ground water intrusions and sea spray may provide minor inputs of seawater into the lake. Freshwater enters Eilandvlei from the Duiwe River to the northeast and intermittently from the Touw River via the Serpentine Channel. The lake is further connected, via a narrow channel, to Bo-Langvlei to the east. The lake water salinity is highly variable ranging between 2 and 12 g kg⁻¹ (1991–2010) (Russell, 2013). The river waters are acidic and consequently characterized by low alkalinities; the mean pH values (1991–1997) are 5.4 for the Touw River and 6.5 for Duiwe River (Russell, 1999). For the Touw River the median alkalinity between 1969 and 2015 was 5 mg l⁻¹ (DWS, 2015). In contrast, the lake water of Eilandvlei is characterized by alkaline pH values with a median of 8.1 and a median alkalinity of 110 mg l⁻¹ (1998–1999) (DWS, 2015). Seawater in comparison has a typical pH range of 7.6–8.4 and alkalinities of 100–110 mg l⁻¹ (Oikawa et al., 2003).

Thus, the lake water chemistry of Eilandvlei, with respect to pH and alkalinity, is less influenced by the inflowing rivers, but rather by the intrusion of seawater as well as by the photosynthetic activity of aquatic plants and algae (Russell, 1999).

The terrestrial vegetation within the Eilandvlei catchment is comprised of various species of the fynbos biome as well as by the Southern Afrotropical Forest which is patchily distributed particularly in the river valleys (Mucina and Rutherford, 2006; Quick et al., 2016). The littoral zone around Eilandvlei and the floodplains of the Serpentine Channel as well as the channel to Bo-Langvlei, are mainly covered by semi-aquatic, emergent plants (Howard-Williams, 1980; Russell, 2003). Regarding their produced biomasses (between 1978 and 1979), these communities are predominantly composed of *Phragmites australis* (131.4 t yr⁻¹), *Scirpus littoralis* (32.1 t yr⁻¹) and *Typha latifolia* (20.0 t yr⁻¹) (Howard-Williams, 1980). Moreover, the aquatic, submerged plants and algae contribute a major proportion to the produced biomass within the lake. These species are dominated by *Potamogeton pectinatus* (231.2 t yr⁻¹), Characeae (*Chara globularis*, *Lamprothamnium papulosum*; 1.0 t yr⁻¹) and *Ruppia cirrhosa* (0.7 t yr⁻¹) (Allanson and Whitfield, 1983; Howard-Williams, 1980). However, the species composition of the vegetation is variable over time, for example, there was a dramatic change in the abundance of Characeae which densely covered the lake floor before 1978/79 and declined distinctly thereafter (Howard-Williams, 1980; Russell, 2003).

1.2. Consideration of distinct carbon reservoirs at Eilandvlei

Sediments are mostly composed of several distinct fractions of organic and inorganic material containing various carbon-bearing compounds. A generalized schematic of known and assumed carbon pools and their interactions in Eilandvlei is shown in Fig. 2. Terrigenous inputs of carbonates from the interior into Eilandvlei are likely of minor importance as there is only a negligible presence of carbonates in the Duiwe and Touw River catchments and both

rivers are acid. Due to the high infiltration capacity of the dune cordons and the resulting rarity of surface runoff (Parsons, 2014), erosion and transport of carbonates from the dunes and their deposition in the coastal lakes likely plays only a minor role; this was demonstrated at Groenvlei (~20 km east of Eilandvlei; Fig. 1B), where the vast majority of lacustrine carbonates formed within the lake (Wündsche et al., 2016). Contributions of old carbon to Eilandvlei that stem from the dissolution of dune carbonates are therefore negligible. Moreover, the dissolution rates of sedimentary carbonates are generally low in alkaline waters (Morse and Arvidson, 2002). The amount of dissolved inorganic carbon (DIC) originating from exchanges of atmospheric CO₂ with the lake water is also presumed to be minor, as the uptake and solution of CO₂ is limited in alkaline waters (Morrill et al., 2006; Talling, 1976). Hence, it can be hypothesized that the major proportion of inorganic carbon reaching the lake is provided as DIC by entering seawater via the Touw River estuary and the Serpentine Channel. The lake water DIC, in turn, provides a source for the chemical and biogenic precipitation of carbonates or it is assimilated as bicarbonate by the abundant aquatic plants and algae for photosynthesis (Lucas et al., 1978; Van den Berg et al., 2002) (Fig. 2). These aquatic plants/algae provide a large portion of the biomass within the lake and metabolize the bicarbonate into organic compounds which are eventually deposited as part of the organic sediment fraction. A minor part of this fraction is possibly provided by the deposition of particulate organic matter (POM) which originates from the semi-aquatic, emergent plants of the littoral zone as well as from the terrestrial vegetation and soils within the river catchments. The fact that our coring position is at the central part of the lake, supports the assumption that the main part of the organic sediment fraction of EV13 originated from detritus of aquatic plants/algae rather than from semi-aquatic or terrestrial vegetation (Fig. 2).

During the past 'marine embayment' and 'lagoon system' phases, more pronounced connections between the Wilderness embayment and the ocean allowed greater incursions of seawater

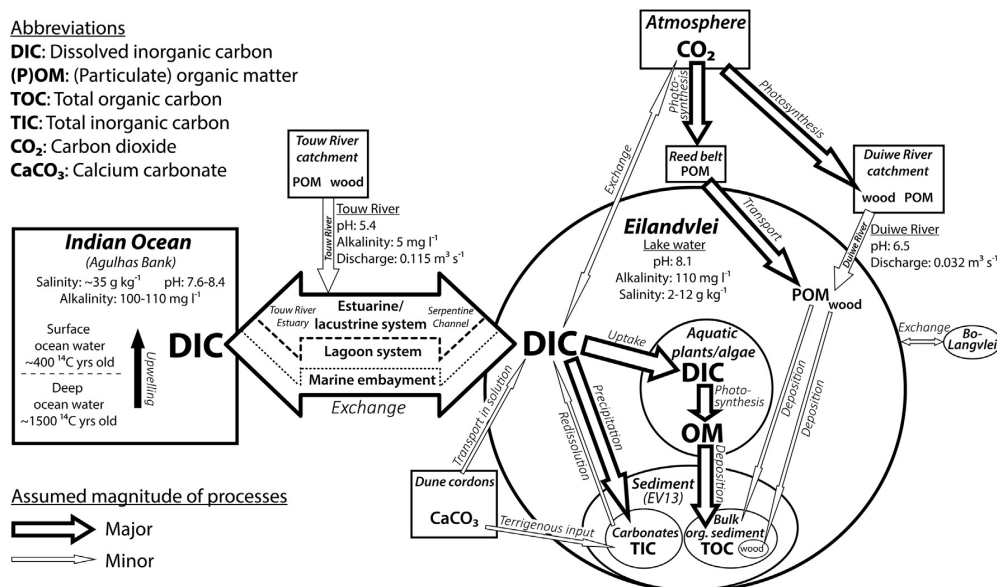


Fig. 2. Conceptual schematic showing distinct carbon reservoirs and carbon-bearing compounds within and around Eilandvlei. Arrows indicate the directions of processes/interactions between individual elements of the system; the width of the arrows depicts the assumed magnitude of processes. The subdivisions of the main arrow represent the variations in past connectivity between the Indian Ocean and Eilandvlei.

(Kirsten, 2014; Martin, 1959, 1968). Hence, the lake water salinities and DIC concentrations were probably higher during the lagoon phase, even higher during the marine phase and substantially lower during the 'estuarine/lacustrine system' phase, particularly during periods of enhanced freshwater inflow from the rivers (Kirsten, 2014).

2. Material and methods

2.1. Sample recovery

2.1.1. Pre-bomb shells

Two marine pre-bomb shells were obtained from the Iziko South African Museum collection in Cape Town. The shells were collected alive and the year of collection is known from the documentation at the museum. One shell belonging to the species *Ocenebra fenestrata* (Gastropoda; Gould, 1860) was collected in 1898 at Mossel Bay (34° 9.48483' S, 22° 6.67817' E) to the west of our core site. The other shell is an individual of the species *Drillia caffra* (Gastropoda; E. A. Smith, 1882) and was collected at Jeffreys Bay (34° 2.57567' S, 24° 55.8665' E) in 1939 (Fig. 1A).

2.1.2. Sediment cores

In October 2013, several sediment cores (diameter: 90 mm) were recovered from the profundal zone of Eilandvlei (33° 59.719' S, 22° 38.403' E; water depth: 6 m) (Fig. 1B). One short core (EV13-2: 156 cm length; UWITEC gravity corer) and two overlapping long cores (EV13-3: 30.22 m, EV13-4: 9.86 m; UWITEC piston coring system; www.uwitec.at) were retrieved. All cores were split, photographed and described lithologically. Based on the correlation of distinct marker layers, a final composite profile (EV13) with a length of 30.47 m was established.

2.2. Sediment contents of total inorganic carbon, organic carbon and nitrogen

For the determination of sediment total inorganic carbon (TIC), organic carbon (TOC) and nitrogen (TN) concentrations, EV13 was subsampled at 16 cm intervals. The subsamples were freeze-dried, ground (<40 μm) and homogenized. Measurements of the total carbon (TC) and TN contents were conducted using a CNS elemental analyser (EuroEA, Eurovector). After which, carbonates were eliminated by treating the samples with HCl (3% and 20% at 80 °C) and measured with the CNS analyser again to obtain the TOC contents. TIC concentrations were calculated as the difference between TC and TOC. Finally, the molar TOC/TN ratios were calculated. Based on marked shifts in the TIC data distinct core units (I-V) were defined (Fig. 3).

2.3. Palaeomagnetic measurements

The natural remanent magnetization (NRM) was studied using stepwise (17 steps) alternating field (AF) demagnetization with peak AFs from 0 to 100 mT on a u-channel collected from the EV13-2 core. AFs were incremented at 5 mT steps from 0 to 70 mT, and 10 mT steps from 70 to 100 mT. NRM was acquired continuously at 1 cm intervals using a 2G Enterprises liquid helium-free magnetometer at the Oregon State University, USA. Inclination and declination of the characteristic remanent magnetization (ChRM) and maximum angular deviation (MAD) values were determined using principle component analyses (Kirschvink, 1980) implemented in the UPmag software (Xuan and Channell, 2009). An Excel macro allowing the calculation of the Median Destructive Field (MDF) was used (Mazaud, 2005). Declination data are relative and centred to zero since the azimuth could not be controlled during

coring. Owing to the width of the response function of the SQUID sensors some smoothing occurs in the data (Weeks et al., 1993). In order to account for edge effects, the data for the top and basal 5 cm are shown in grey for each u-channel. The obtained data were subsequently compared to the CALS3k.4 (Korte and Constable, 2011) predictions for the coordinates of the coring location from GEOMAGIA50.v3 (Brown et al., 2015), to the gufm1 magnetic field model derived from historical records (Jackson et al., 2000) as well as to measured archaeomagnetic data from the Limpopo region, South Africa (Neukirch et al., 2012; Tarduno et al., 2015).

2.4. ¹⁴C dating and ΔR calculations

2.4.1. Pre-bomb shells

For AMS ¹⁴C dating, the two marine pre-bomb shells were sent entirely intact to Beta Analytic Inc. (Miami, Florida, USA) who conducted the 'acid etch' method for pretreatment of the specimens. In order to determine the ΔR values, at first the calendar ages (cal BP) of the years of the shell collection were converted into the corresponding ¹⁴C ages (BP) of the Marine13 calibration curve (¹⁴C age_{Marine13}) (Reimer et al., 2013). In case the year of the shell collection fell between available values of the Marine13 curve, the corresponding ¹⁴C ages were linearly interpolated. The ΔR values were finally calculated by subtracting these corresponding ¹⁴C ages from the conventional ¹⁴C ages obtained from the shell measurements (¹⁴C age_{shell}):

$$\Delta R = {}^{14}\text{C age}_{\text{shell}} - {}^{14}\text{C age}_{\text{Marine13}} \quad (1)$$

The errors of the ΔR values (σ_{ΔR}) were determined by considering the 1σ uncertainties of the conventional ages of the shell measurements (σ_{shell}) as well as those of the corresponding ¹⁴C ages derived from the Marine13 curve (σ_{Marine13}) by applying the formula (Stuiver et al., 1986):

$$\sigma_{\Delta R} = \sqrt{\sigma_{\text{shell}}^2 + \sigma_{\text{Marine13}}^2} \quad (2)$$

after which, the weighted average of both ΔR values (ΔR_{mean}) was calculated and the uncertainty of this average (σ_{ΔR(mean)}) was propagated as follows (Bevington and Robinson, 2003):

$$\Delta R_{\text{mean}} = \frac{\sum_i \frac{\Delta R_i}{\sigma_{\Delta R_i}^2}}{\sum_i \frac{1}{\sigma_{\Delta R_i}^2}} \quad (3)$$

$$\sigma_{\Delta R(\text{mean})} = \sqrt{\frac{1}{\sum_i \frac{1}{\sigma_{\Delta R_i}^2}}} \quad (4)$$

2.4.2. Sediment core samples

Where present in the cores, wood fragments (particularly bark or twigs) were sampled preferentially, since it can be assumed that these macrofossils are of terrestrial origin and therefore, the plants assimilated mainly carbon from the atmospheric CO₂ pool during their lifetime (Hutchinson et al., 2004; Kim et al., 2012; Watanabe et al., 2010). However, due to the paucity of wood fragments, bulk material was sampled additionally to provide ages for all different facies of the record. For the bulk samples, the organic sediment fraction was used for ¹⁴C dating. In order to examine and correct expected offsets in the dating results of these different materials (Hutchinson et al., 2004; Kim et al., 2012), three pairs each consisting of one wood and one bulk sample from the same core depth, were taken from the upper, middle and lower part of the record (at

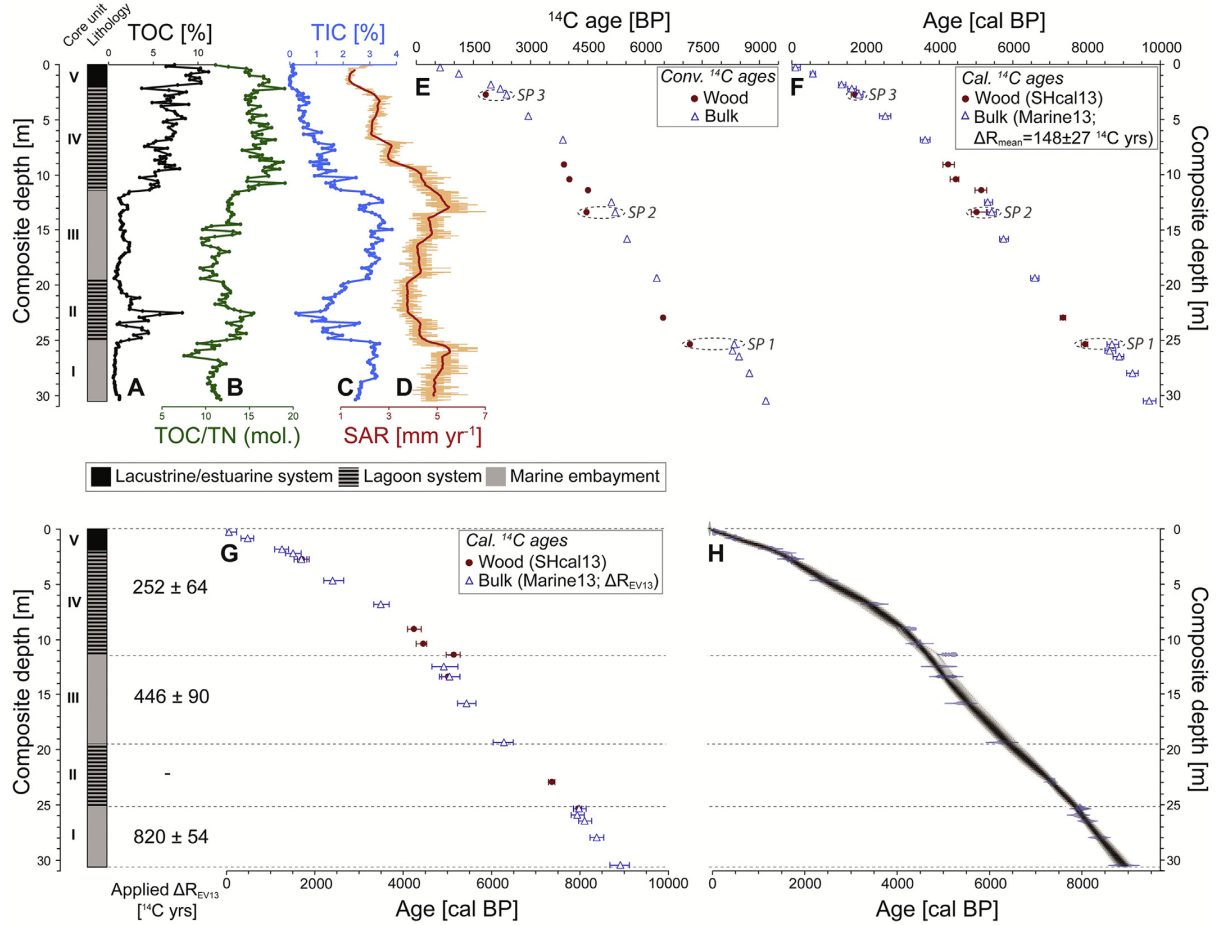


Fig. 3. Lithology and inferred core units of the EV13 record are shown on the left; **A)** Total organic carbon (TOC); **B)** Molar TOC/total nitrogen (TN) ratio; **C)** Total inorganic carbon (TIC); **D)** Sediment accumulation rate (SAR, orange line) derived from **H)** with a 100-point running mean (red line); **E)** Conventional radiocarbon ages of measured bulk and wood samples plotted against composite depth (note that the 1σ error bars are smaller than the symbols); **F)** Calibrated ages with 2σ uncertainties based on the application of the SHcal13 calibration curve (Hogg et al., 2013) for the wood samples and the Marine13 data (Reimer et al., 2013) using $\Delta R_{\text{mean}} = 148 \pm 27$ ¹⁴C yrs for all bulk samples. **G)** Bulk samples were calibrated using the Marine13 curve applying different ΔR_{EV13} values for the respective core units (note that no bulk sample was taken from unit II); **H)** Final chronology based on the calibrated ages shown in **G)** calculated using the R software package Bacon 2.2 (Blaauw and Christen, 2011). (For interpretation of the references to colour in this figure legend, the reader is referred to the web version of this article.)

2.75, 13.39 and 25.35 m composite depth). Unfortunately, no comparative macroscopic shell fragments were present at the core depths in which wood occurred. In total, 24 samples were taken, thereof 17 bulk and seven wood samples. The sediment surface bulk sample from EV13-2 (0–1 cm) was dated at the Radiochronology Laboratory, Centre for Northern Studies, Laval University (Québec, Canada). The remaining 23 samples were sent to Beta Analytic Inc. (Miami, Florida, USA).

The obtained ¹⁴C ages of the wood samples were calibrated using the SHcal13 data set (Hogg et al., 2013). Two approaches were tested to determine the most robust method for the calibration of the bulk samples. Firstly, bulk samples were calibrated using the Marine13 curve (Reimer et al., 2013) applying $\Delta R_{\text{mean}} \pm \sigma \Delta R_{\text{(mean)}}$ derived from the shell ages. Secondly, three ΔR values were estimated based on the three bulk/wood sample pairs. Due to the following reasons these ΔR values derived from the bulk/wood sample pairs are indexed as ΔR_{EV13} : the Marine13 curve with associated ΔR values is usually applied to samples from the marine

environment only taking into account the reservoir effect that is caused by old marine carbon (Reimer et al., 2013; Stuiver and Braziunas, 1993; Stuiver et al., 1986). Even if it seems likely that the ¹⁴C ages obtained from the bulk samples are for the most part a result of old marine carbon which was assimilated by aquatic plants and algae (Fig. 2), it cannot be ruled out that also minor amounts of terrestrial (old) carbon were contained in the measured samples. Thus, there is a degree of uncertainty with regards to the validity of the calculated ΔR_{EV13} values reflecting only a marine reservoir effect. However, it is important to emphasise that the main goal of the ΔR_{EV13} values based on bulk/wood sample pairs is to correct the reservoir effects that emerge due to the dating of different material and finally to establish a reliable chronology for the EV13 record.

The calculation of ΔR_{EV13} was carried out as outlined in previous studies using marine/terrestrial sample pairs (Russell et al., 2011; Southon et al., 1995). Applied to our approach, the wood samples represent the terrestrial component and the bulk samples act as the marine counterpart. At first, the 1σ calibrated calendar age range of

the wood samples (SHcal13) (Hogg et al., 2013) was transferred to the Marine13 curve (Reimer et al., 2013) providing an equivalent marine ^{14}C age range for the terrestrial counterpart of the sample pairs (Southon et al., 1995). In case the intersections of the calibrated calendar age range fell between available values of the Marine13 curve, the equivalent marine ^{14}C ages were linearly interpolated. For the calculation of ΔR_{EV13} , the arithmetic mean of the equivalent marine ^{14}C age range ($^{14}\text{C age}_{\text{equ.mar.}} \pm \sigma_{\text{equ.mar.}}$) was finally subtracted from the conventional ^{14}C age of the bulk counterpart ($^{14}\text{C age}_{\text{bulk}}$):

$$\Delta R_{\text{EV13}} = ^{14}\text{C age}_{\text{bulk}} - ^{14}\text{C age}_{\text{equ.mar.}} \quad (5)$$

The errors of the ΔR_{EV13} values ($\sigma_{\Delta R(\text{EV13})}$) were calculated using the 1σ uncertainties of the conventional bulk ^{14}C ages (σ_{bulk}) and the half of the equivalent marine ^{14}C age range ($\sigma_{\text{equ.mar.}}$) (Russell et al., 2011; Southon et al., 1995):

$$\sigma_{\Delta R(\text{EV13})} = \sqrt{\sigma_{\text{bulk}}^2 + \sigma_{\text{equ.mar.}}^2} \quad (6)$$

The Marine13 curve (Reimer et al., 2013) and the three different ΔR_{EV13} values obtained from this approach were then used to correct all bulk ^{14}C ages of the respective core units where the sample pairs were taken (Fig. 3G, H). For the uppermost unit, where no bulk/wood sample pair is available, the Marine13 curve (including the nearest ΔR_{EV13} from the unit below) was used to calibrate the bulk ^{14}C ages.

For each sample the calibrated 2σ age ranges, the relative likelihoods of the individual ranges and the median calibrated ages (each rounded to the closest ten) were calculated using the OxCal 4.2 software (Bronk Ramsey, 2009). The final age-depth relation was modelled using the R software package Bacon 2.2 (Blaauw and Christen, 2011). Finally, the sediment accumulation rate was calculated based on this age-depth relation.

3. Results and discussion

3.1. Core lithology, TIC, TOC and TOC/TN data

The sediments of EV13 are characterized by several distinct facies which are clearly distinguishable in terms of colour, sediment structure and carbonate contents. The latter is represented by changes in the TIC data which is strongly inversely correlated with concentrations of TOC ($r = -0.90$) (Fig. 3A, C). TOC values reveal a strong correlation with the molar TOC/TN ratios ($r = 0.80$) (Fig. 3A, B). TIC values range between 0 and 3.9 wt% across the record, TOC values between 0.5 and 11.2 wt%. The molar TOC/TN ratios vary between 7.5 and 19.1 (Fig. 3B).

It is very likely that the TIC data represents the (bio)geochemically formed carbonates, which reflect the degree of marine influence at our coring position. This is corroborated by other proxy data from ongoing micropalaeontological investigations (e.g., diatoms and ostracods) on this sediment core which show a good correlation in the abundance of marine species to our TIC data (Kirsten, unpubl. data; Frenzel, pers. comm.).

Based on this, the EV13 record was divided in five units I to V (Fig. 3). Units I (30.47–25.19 m) and III (19.55–11.44 m) mainly consist of light grey, homogeneous sediments showing the highest TIC (lowest TOC) values and are therefore designated as 'marine embayment' facies. The units II (25.19–19.55 m) and IV (11.44–1.86 m) are characterized by grey to blackish, layered sediments with moderate TIC and TOC contents and are provisionally defined as 'lagoon system' facies. The topmost unit V (1.86–0 m) exhibits a dark grey to black colour with undefined layers and very low TIC (high TOC) concentrations (Fig. 3). Unit V is thus designated

as 'estuarine/lacustrine' facies.

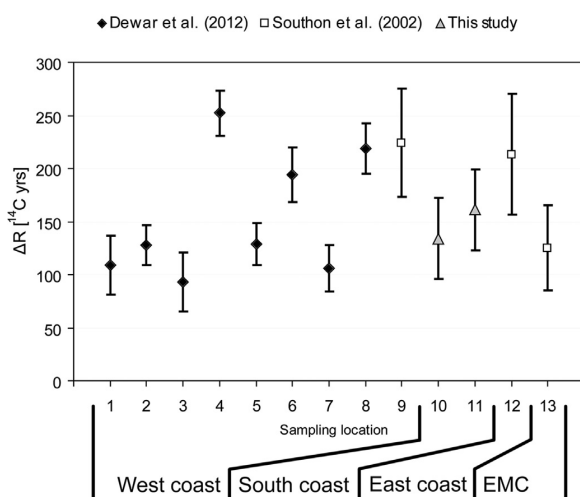
TOC/TN ratios are widely used to give information about the origin of organic matter. Generally, molar values between 4 and 10 are typical for algae, whilst vascular land plants are mostly characterized by ratios greater than 20 (Meyers, 1994). By comparison, Müller and Mathesius (1999) measured TOC/TN (mass) ratios of various species from coastal lagoons in the southern Baltic Sea and found that terrestrial plants show TOC/TN ratios between 10 and 85, aquatic macrophytes range from 6 to 44 and plankton reveals ratios around 6. Mean TOC/TN ratios are 16.2 for *Potamogeton pectinatus* and 12.0 for *Ruppia cirrhosa* in these systems (Müller and Mathesius, 1999) (molar: ~18.9 and 14.0, respectively), which are aquatic macrophyte species also occurring in Eilandvlei. Molar TOC/TN ratios of 20.1 ± 0.2 for *Potamogeton pectinatus* (syn.: *Stuckenia pectinata*) were additionally determined by Hobbs et al. (2012) at Lake Christina (Minnesota, USA). The algae *Chara globularis* has a molar ratio of about 24.7 (Lake Constance, Germany) (Richter and Gross, 2013). Molar TOC/TN ratios of the semi-aquatic species *Phragmites australis* can vary between -9 and 31 mainly depending on which part of the plant is measured (Treboň basin, Czech Republic) (Tylová et al., 2008). Moreover, several other factors have to be considered for the interpretation of sediment TOC/TN ratios, such as variations in the rate of decomposition of the organic litter before it enters the anaerobic sediment layer, for example due to changes in temperature or oxygen concentrations (Asaeda et al., 2002). Furthermore, sediment TOC/TN ratios rise with an increasing age of the sediment (Galman et al., 2008). The elevated TOC/TN ratios in the EV13 units II, IV and V (between 10.5 and 19.5) are therefore not necessarily reflecting an increased contribution of terrestrial organic matter to the lake sediment, but may rather be a result of a changing species composition of the aquatic macrophytes/algae, possibly caused by changes in salinity.

3.2. ΔR and ΔR_{EV13} values

The ΔR values derived from the pre-bomb marine shells (Table 1, Fig. 4) represent the first ones for the south coast of South Africa. The sample collected near Mossel Bay (Beta - 392092) yields a $\Delta R = 134 \pm 38$ ^{14}C yrs and the one collected at Jeffreys Bay (Beta - 392093) a $\Delta R = 161 \pm 38$ ^{14}C yrs. Together the samples provide the $\Delta R_{\text{mean}} = 148 \pm 27$ ^{14}C yrs. These new ΔR values from the south coast are in a similar range as available ΔR data from the west and east coast of South Africa (Fig. 4). Eight pre-bomb shell samples from the west coast provide ΔR values ranging from 93 ± 28 to 252 ± 21 ^{14}C yrs (Dewar et al., 2012). Furthermore, Dewar and Pfeiffer (2010) estimated a ΔR of ~350 ^{14}C yrs for the southwest coast of South Africa. An additional $\Delta R = 224 \pm 51$ ^{14}C yrs was obtained from the Cape of Good Hope (Southon et al., 2002). Considering all available data from the west coast, a pooled mean $\Delta R = 146 \pm 85$ ^{14}C yrs was calculated by Dewar et al. (2012) which is very close to the value of $\Delta R_{\text{mean}} = 148 \pm 27$ ^{14}C yrs calculated in this study for the south coast. Moreover, ΔR decreased at the west coast from AD 1820–1940 and based thereon, it was hypothesized that the recent past represents a period of decreased upwelling in the Benguela system (Dewar et al., 2012). For the east coast of South Africa, hitherto, only a single $\Delta R = 213 \pm 57$ ^{14}C yrs is available (Southon et al., 2002), which is slightly higher than the $\Delta R_{\text{mean}} = 148 \pm 27$ ^{14}C yrs calculated in this study, but still within a similar range. From the East Madagascar Current, which represents the major source current of the Agulhas Current (Stramma and Lutjeharms, 1997), a $\Delta R = 125 \pm 40$ ^{14}C yrs was obtained (Southon et al., 2002). In general, our new ΔR values from the south coast are well in the range of those from both sources, the Benguela and Agulhas current systems each affecting the Agulhas Bank (Figs. 1, 4).

Table 1
 Calculated ΔR values derived from pre-bomb shells.

Lab ID	Species (Class)	Locality, Province	Coordinates	Year of shell collection [AD]	Corresponding ^{14}C year of shell collection (Marine13) [BP]	1 σ conv. ^{14}C age [BP]	$\Delta R \pm \sigma_{\Delta R}$ [^{14}C yrs]
Beta - 392092	<i>Ocenebra fenestrata</i> (Gastropoda)	Mossel Bay, Western Cape	34° 9.48483' S 22° 6.67817' E	1898	456 \pm 23	590 \pm 30	134 \pm 38
Beta - 392093	<i>Drillia caffra</i> (Gastropoda)	Jeffreys Bay, Eastern Cape	34° 2.57567' S 24° 55.8665' E	1939	459 \pm 23	620 \pm 30	161 \pm 38
$\Delta R_{\text{mean}} \pm \sigma_{\Delta R(\text{mean})}$:							148 \pm 27


Fig. 4. ΔR values with 1 σ errors obtained within this study in comparison to available values from Dewar et al. (2012) and Southon et al. (2002) from the east, west and south coast of South Africa as well as from the East Madagascar Current (EMC). The different sampling locations displayed as numbers on the x-axis can be found in Fig. 1A. Note that the ΔR values reported in Southon et al. (2002) and Dewar et al. (2012) were originally calculated using previous calibration curves (Marine98 and Marine09, respectively) and therefore slightly differ from the updated ΔR values presented here (based on the current Marine13 calibration curve).

The calculated ΔR_{EV13} values are 820 ± 54 ^{14}C yrs for sample pair (SP) 1 (lowermost one), 446 ± 90 ^{14}C yrs for SP 2 (middle) and 252 ± 64 ^{14}C yrs for SP 3 (uppermost one; Table 2, Fig. 3). SP 1 and SP 2 were sampled from core units I and III, respectively, representing the ‘marine embayment’ phase with TIC concentrations of about 3.1 and 3.2% and TOC concentrations around 1.4 and 1.0%. In contrast, SP 3 was taken from unit IV representing the ‘lagoon system’ phase with a TIC content of ~0.3% and a TOC content of ~6.3%. The fact that SP 3 despite its much higher TOC percentage reveals a distinctively lower ΔR_{EV13} value than SP 1 and SP 2 suggests that the amount of old terrestrial carbon influencing the

measured bulk sample is negligible. The $\Delta R_{\text{EV13}} = 252 \pm 64$ ^{14}C yrs may substantiate that the bulk organic sediment fraction is mainly composed of deposited detritus of aquatic plants/algae that probably assimilated old marine carbon. If the bulk organic sediment would be mainly composed of material originating from terrestrial plants (which were in equilibrium with atmospheric CO_2 during their lifetime), no or at least not such a high offset between the wood and bulk samples would be expected. The ΔR_{EV13} value of SP 3 (252 ± 64 ^{14}C yrs) is also in a similar range as $\Delta R_{\text{mean}} = 148 \pm 27$ ^{14}C yrs from the dated shells in this study, for which an influence of terrestrial carbon can be excluded. The two ΔR_{EV13} values derived from SP 1 and SP 2 show a difference of ~370 ^{14}C yrs. As both SPs are from ‘marine embayment’ facies and have similar TIC and TOC concentrations, their difference may be related to the DIC containing variable concentrations of ^{14}C during these periods rather than different DIC concentrations of the water at our coring position. This, in turn, may reflect changes in the intensity and/or frequency of upwelling of old carbon along the southern Cape coast between the early (SP 1, $7960^{+80}/_{-110}$ cal BP) and the mid-Holocene (SP 2, $5020^{+260}/_{-150}$ cal BP) (ages from the final calibrated age range of the respective wood sample; Fig. 3G–H; Table 3).

The validity of our ΔR_{EV13} values is supported by comparisons with other studies, particularly referring to changes in the intensity/frequency of upwelling between the early and mid-Holocene. For example, a transition from high ΔR values off the Chilean-Peruvian coast during the early Holocene (10400–6840 cal BP) to lower ΔR values at the mid-Holocene (5180–1160 cal BP) were related not only to major oceanographic changes in the Humboldt Current, but also in the Southern Ocean and hence the ACC (Ortlieb et al., 2011). Sea surface temperature anomalies possibly caused by increased upwelling between 11000 and 8000 yrs ago were proposed for the southern Benguela region by Cohen et al. (1992). This was corroborated by a marine record recovered off the Namibian coast (Farmer et al., 2005); shell Mg/Ca data of the foraminifer species *Globigerina bulloides* were used as a proxy for sea surface temperatures which were related to the intensity of upwelling in the Benguela system. These data suggest an intensification of upwelling in the area from 8400 to 5800 cal BP (Farmer et al., 2005) that also may have affected the seawater ^{14}C concentrations off the southern Cape coast.

Table 2
 Calculated ΔR_{EV13} values using bulk/wood sample pairs from the same depth of sediment core EV13.

Sample pair (SP)	Composite depth [m]	Wood			Bulk		$\Delta R_{\text{EV13}} \pm \sigma_{\Delta R(\text{EV13})}$ [^{14}C yrs]	
		Lab ID	1 σ conventional ^{14}C age [BP]	1 σ calibrated age range (SHcal13) [cal BP]	Equivalent 1 σ ^{14}C age range (Marine13) [BP]	Lab ID		1 σ conventional ^{14}C age [BP]
SP 3	2.75	Beta - 386526	1830 \pm 30	1620–1778	2118 \pm 56	Beta - 415642	2370 \pm 30	252 \pm 64
SP 2	13.39	Beta - 377597	4470 \pm 30	4882–5214	4774 \pm 85	Beta - 394839	5220 \pm 30	446 \pm 90
SP 1	25.35	Beta - 377257	7180 \pm 40	7935–8005	7520 \pm 45	Beta - 394840	8340 \pm 30	820 \pm 54

Table 3

Conventional radiocarbon ages as well as 2σ calibrated age ranges with their relative likelihoods and median calibrated ages (OxCal 4.2) (Bronk Ramsey, 2009) of dated bulk and wood samples from the EV13 record.

Lab ID	Composite depth [m]	1σ conventional ¹⁴ C age [BP]	Dated material	Applied calibration curve	Applied ΔR _{EV13} [¹⁴ C yrs]	2σ cal age range(s) [cal BP] (rel. likelihood [%])	Median cal age [cal BP]
ULA-5059	0–0.005	(101.6 ± 0.21 pMC)	bulk (org. sediment)	-	-	-	-
Beta - 400619	0.29	630 ± 30	bulk (org. sediment)	Marine13	252 ± 64	0 ^a - 150 (86.9) 160 - 230 (8.5)	60
Beta - 400620	0.85	1120 ± 30	bulk (org. sediment)	Marine13	252 ± 64	330 - 620 (95.4)	490
Beta - 394838	1.84	1960 ± 30	bulk (org. sediment)	Marine13	252 ± 64	1090 - 1410 (95.4)	1260
Beta - 394837	2.21	2210 ± 30	bulk (org. sediment)	Marine13	252 ± 64	1340 - 1690 (95.4)	1510
Beta - 386526	2.75	1830 ± 30	wood (bark and twigs)	SHcal13	-	1610 - 1820 (95.4)	1710
Beta - 415642	2.75	2370 ± 30	bulk (org. sediment)	Marine13	252 ± 64	1530 - 1870 (95.4)	1700
Beta - 388028	4.68	2940 ± 30	bulk (org. sediment)	Marine13	252 ± 64	2200 - 2660 (95.4)	2400
Beta - 388029	6.83	3850 ± 30	bulk (org. sediment)	Marine13	252 ± 64	3330 - 3680 (95.4)	3500
Beta - 377595	9.08	3880 ± 30	wood fragments	SHcal13	-	4100 - 4110 (0.5) 4140 - 4410 (94.9)	4250
Beta - 373397	10.41	4020 ± 30	wood fragments	SHcal13	-	4290 - 4530 (95.4)	4460
Beta - 377596	11.40	4510 ± 30	wood (bark)	SHcal13	-	4970 - 5290 (95.4)	5140
Beta - 391036	12.48	5120 ± 30	bulk (org. sediment)	Marine13	446 ± 90	4650 - 5240 (95.4)	4920
Beta - 377597	13.39	4470 ± 30	wood (bark)	SHcal13	-	4870 - 5080 (69.1) 5100 - 5130 (3.1) 5160 - 5280 (23.2)	5020
Beta - 394839	13.39	5220 ± 30	bulk (org. sediment)	Marine13	446 ± 90	4820 - 5290 (95.4)	5050
Beta - 388030	15.81	5530 ± 30	bulk (org. sediment)	Marine13	446 ± 90	5230 - 5650 (95.4)	5440
Beta - 388031	19.35	6310 ± 30	bulk (org. sediment)	Marine13	446 ± 90	6030 - 6490 (95.4)	6280
Beta - 376842	22.94	6480 ± 30	wood (bark)	SHcal13	-	7280 - 7430 (95.4)	7360
Beta - 377257	25.35	7180 ± 40	wood fragments	SHcal13	-	7850 - 8040 (95.4)	7960
Beta - 394840	25.35	8340 ± 30	bulk (org. sediment)	Marine13	820 ± 54	7850 - 8140 (95.4)	7980
Beta - 391035	25.93	8300 ± 30	bulk (org. sediment)	Marine13	820 ± 54	7800 - 8100 (95.4)	7940
Beta - 388032	26.46	8470 ± 30	bulk (org. sediment)	Marine13	820 ± 54	7970 - 8270 (95.4)	8110
Beta - 377258	27.96	8740 ± 40	bulk (org. sediment)	Marine13	820 ± 54	8220 - 8540 (95.4)	8380
Beta - 364765	30.47	9170 ± 40	bulk (org. sediment)	Marine13	820 ± 54	8670 - 9120 (95.4)	8920

^a 0 cal BP represents the end of the Marine13 calibration curve.

3.3. Core chronology

3.3.1. ¹⁴C chronology

As expected, the conventional ¹⁴C ages obtained for the EV13 core samples show an offset between the bulk and wood material which is particularly evident regarding the three sample pairs from the same core depth: for SP 1 from 25.35 m composite depth, the bulk sample reveals a 1σ conventional age range which is 1160 ± 42 ¹⁴C yrs older than the associated wood sample. This offset decreases upwards with 750 ± 42 ¹⁴C yrs for SP 2 (13.39 m) and 540 ± 42 ¹⁴C yrs for SP 3 (2.75 m) (differences of the conventional ¹⁴C ages ± 1σ ranges added in quadrature; Taylor, 1997; Fig. 3E).

In order to conduct a reservoir correction of the marine-influenced bulk samples, initially the Marine13 calibration curve was tested applying the ΔR_{mean} = 148 ± 27 ¹⁴C yrs (derived from the two pre-bomb shells) on all bulk samples (Fig. 3F). Regarding

the three SPs, the resulting offsets between the bulk and wood counterparts decrease as follows (differences of the median calibrated ages ± added/subtracted 2σ ranges): SP 1: 730 ⁺²⁹⁰/₋₂₂₀ cal yrs, SP 2: 410 ⁺²⁷⁰/₋₃₈₀ cal yrs, SP 3: 110 ⁺²¹⁰/₋₂₈₀ cal yrs. For the upper part of the core, the 2σ ranges of the SPs indeed move much closer together (SP 2) or even overlap (SP 3). However, for SP 1 there still remains a marked offset between the wood and the bulk sample (Fig. 3F). Thus, this approach provides ineffective results for the calibration of the entire record. For that reason, the three estimated ΔR_{EV13} values were employed in relation to their respective core units as a reservoir correction for the bulk samples equalizing the offsets for all SPs (Tables 2 and 3, Fig. 3G). The topmost unit V, where no bulk/wood SP was available, was also calibrated using the ΔR_{EV13} = 252 ± 64 ¹⁴C yrs obtained from SP 3 in unit IV, except for the surface sample which contains 101.6 ± 0.21% modern carbon. The sediment surface was therefore set to -63 cal

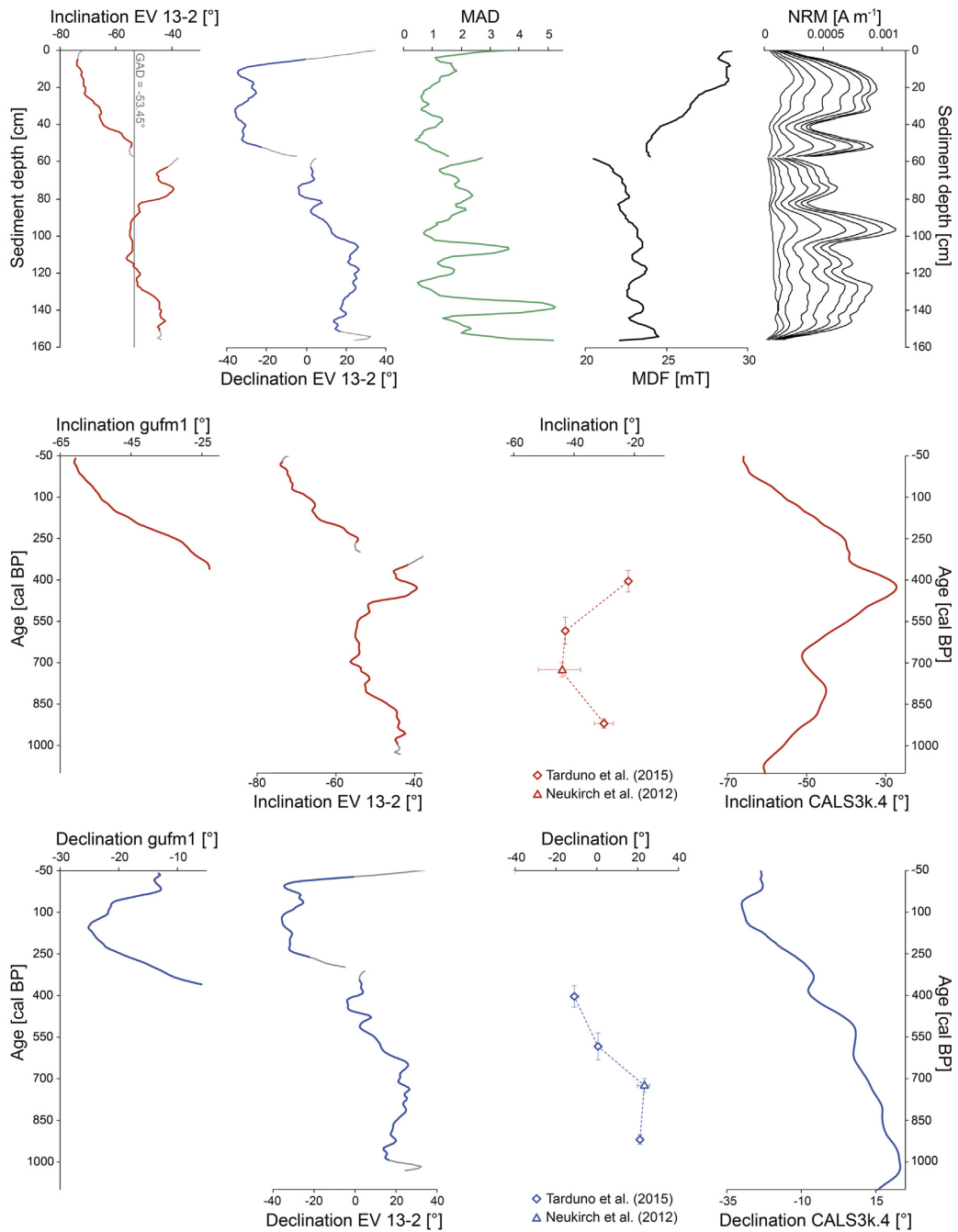


Fig. 5. Inclination, declination, maximum angular deviation (MAD), median destructive field (MDF) and natural remanent magnetization (NRM) data measured on the EV 13-2 gravity core forming the uppermost part of the composite profile EV13 plotted against sediment depth (top); the grey line in the top left graph represents the geocentric axial dipole (GAD) value for the site latitude ($GAD = -53.45^\circ$). Comparison of the inclination (middle) and declination (bottom) of EV 13-2 plotted against age (derived from the established ^{14}C chronology), with the model predictions of CAL3k.4 (Korte and Constable, 2011) and gufm1 (Jackson et al., 2000) for the coring location as well as archaeomagnetic data from the Limpopo region, South Africa. The inclination and declination values from EV13-2 plotted in grey are affected by edge effects caused by the applied u-channel method. The archaeomagnetic data (means) and errors were compiled from tables given in Neukirch et al. (2012) and Tarduno et al. (2015). The uppermost declination point from Tarduno et al. (2015) was corrected by -360° .

BP representing the year of the core recovery. This approach applying distinct ΔR_{EV13} values provides more plausible results than that using ΔR_{mean} for the calibration of all bulk samples. Hence, the distinct ΔR_{EV13} values were used to calculate the final chronology which reveals a basal median age of 8920^{+200}_{-250} cal BP (Table 3; Fig. 3H). By comparison, the rejected approach would have resulted in a basal median age of 9700^{+180}_{-160} cal BP overestimating the basal age of the record by 780^{+430}_{-360} cal yrs.

The fact that the surface sample reveals a modern age, on the one hand supports the assumption that the amount of old terrestrial carbon entering Eilandvlei is negligible, but on the other hand this seems to contradict the application of a reservoir correction on the remaining bulk samples from unit V. However, a freshening of the lake system is apparent for the last 120 yrs possibly related to human activities in the catchment (Kirsten, 2014). Additionally, Russell (2013) indicated a decreased connectivity to the ocean as well as a decline in submerged plant biomass within Eilandvlei and ultimately a decrease in pH during the last few decades. This may explain why the bulk organic sediment at the surface is not influenced by a reservoir effect as the aquatic plants do not assimilate as much marine bicarbonate as they probably did before.

The calculated sediment accumulation rates (SAR) for this record show a pattern which is similar to the TIC data (Fig. 3C, D). Slightly higher rates appear for the 'marine embayment' units I and III, intermediate values for the 'lagoon system' facies (units II and IV) and low values for the 'lacustrine/estuarine' facies at unit V (Fig. 3D). The averaged SAR for the entire record is about 3.9 mm yr^{-1} .

3.3.2. Palaeomagnetic secular variation stratigraphy

In order to confirm the applied reservoir correction in unit V, the respective part of the record (gravity core EV 13-2) is evaluated using palaeomagnetic secular variation stratigraphy: NRM intensities are in the range of $5 \cdot 10^{-4}$ and $1.1 \cdot 10^{-3} \text{ A m}^{-1}$ (Fig. 5). A ChRM was isolated between 10 and 40 mT. MAD values of the ChRM are mostly below 5, indicating a sufficiently well preserved magnetization (Stoner and St-Onge, 2007). Despite the presence of the South Atlantic (geomagnetic) Anomaly (SAA; Hartmann and Pacca, 2009; Heirtzler, 2002; Shah et al., 2016), the inclination values vary around the ones expected, based on the geocentric axial dipole (GAD) value (Tauxe, 2005) for the site latitude ($\text{GAD} = -53.45^\circ$). Especially between 1.5 and 0.6 m ($990\text{--}350$ cal BP), the inclination data oscillate around the GAD value and tend to steeper values towards the top of the core (260 cal BP-present) (Fig. 5), which might be related to variations in the position and magnitude of the SAA during the last centuries (Hartmann and Pacca, 2009).

The final age-depth relation for the upper part of the EV13 record was used to plot the inclination and declination data on an age axis which was then compared with the CALS3k.4 (Korte and Constable, 2011) and the gufm1 predictions (Jackson et al., 2000) for the coring location as well as with four measured archaeomagnetic data points obtained from Neukirch et al. (2012) and Tarduno et al. (2015) about 1500 km northeast of Eilandvlei (Limpopo region, South Africa) (Fig. 5). Although Eilandvlei is relatively far away from any direct palaeomagnetic record, strong similarities are apparent in both the inclination and declination of EV 13-2 and the compared data. For the period from 990 to 400 cal BP our record shows a good agreement of the inclination and declination pattern and range with the archaeomagnetic data (Neukirch et al., 2012; Tarduno et al., 2015). The EV13 declination data for this period is also in good accordance with the CALS3k.4 model predictions (Korte and Constable, 2011). Although highs and lows in inclination show a similar pattern in the EV13 record and in the archaeomagnetic data, they appear to be less pronounced in the CALS3k.4

model predictions before 550 cal BP.

For the time from 400 cal BP to the present patterns in the inclination data of our EV13 record, the gufm1 (Jackson et al., 2000) and the CALS3k.4 (Korte and Constable, 2011) model predictions are very similar, all showing a trend towards steeper inclination (Fig. 5). For this period, the declination pattern from our record especially resembles the gufm1 predictions in which declination is more robust than inclination in this area (Jackson et al., 2000).

Summarising, the good agreement of the compared data suggests that palaeomagnetic secular variation stratigraphy represents a powerful tool to validate our established ^{14}C chronology for the upper part of the EV13 record. In particular, the application of a reservoir correction for the bulk samples (using $\Delta R_{\text{EV13}} = 252 \pm 64^{14}\text{C}$ yrs) from the topmost unit V is hence confirmed. Moreover, the data presented here are the first measured ones for Holocene sediments from this area.

4. Conclusions

Considering the paucity of available Holocene sediment records from southern Africa, the recovery of the 30.5 m core from coastal lake Eilandvlei (EV13) represents an exceptional discovery particularly in terms of its temporal resolution, continuity and preservation. The two new presented ΔR values of 134 ± 38 and $161 \pm 38^{14}\text{C}$ yrs are the first data available for the south coast of South Africa. For the establishment of a robust chronology for the EV13 record, the testing of two different approaches showed that it is insufficient to apply a constant $\Delta R_{\text{mean}} = 148 \pm 27^{14}\text{C}$ yrs (average ΔR derived from the two pre-bomb shells) for the reservoir correction of all bulk ages of the record. A reliable ^{14}C chronology was obtained by the determination of variable reservoir effects (ΔR_{EV13}) affecting Eilandvlei during the Holocene. Comparisons with other studies suggest that an intensified/more frequent upwelling was particularly apparent in the early-Holocene possibly causing the highest reservoir offsets for this record. The final established chronology reveals a median basal age of 8920^{+200}_{-250} cal BP.

The palaeomagnetic secular variation data corroborate the topmost part of the final chronology agreeing with model predictions and archaeomagnetic data. Furthermore, they represent the first of its kind from southern Africa for Holocene sediments. Palaeomagnetic secular variation stratigraphy seems to be a key for future investigations to assess synchronicities in palaeoenvironmental reconstructions in southern Africa.

The presented chronology for the EV13 record provides a solid basis for prospective palaeoenvironmental studies on this unique geoarchive. A multi-proxy approach will give detailed insights into sea level and climatic changes in southern Africa during the past 8920^{+200}_{-250} cal BP. The chronological control of this ultra-high-resolution record allows its use as a master profile for southern Africa in comparison with other regional and global studies.

Acknowledgements

This study was funded by the German Federal Ministry of Education and Research (BMBF). The investigations were conducted within the collaborative project "Regional Archives for Integrated Investigations" (RAIN), which is embedded in the international research programme SPACES (Science Partnership for the Assessment of Complex Earth System Processes).

We are deeply grateful to South African National Parks (Rondevlei Scientific Services Sedgefield) for the permission to conduct our fieldwork on Eilandvlei which is part of the protected Garden Route National Park. We thank Elizabeth Hoenson from the Iziko South African Museum in Cape Town for providing the two pre-bomb shells. Sabine Stahl is acknowledged for her help during

the laboratory work as well as Bastian Reinwarth, Matthias Zabel, Peter Frenzel and Paula J. Reimer for discussion. Finally we thank Sayed Hess, Bastian Reinwarth, Lynne J. Quick and Richard Niederreiter for their help during the fieldwork as well as Andrew Jackson for providing gufm1 predictions for the EV13 coring location.

References

- Ahlborn, M., Haberzettl, T., Wang, J., Alivernini, M., Schlütz, F., Schwarz, A., Su, Y., Frenzel, P., Daut, G., Zhu, L., Mäusbacher, R., 2015. Sediment dynamics and hydrologic events affecting small lacustrine systems on the southern-central Tibetan Plateau – the example of IT Lake. *Holocene* 25, 508–522.
- Allanson, B.R., Whitfield, A.K., 1983. The Limnology of the Touw River Floodplain. South African Scientific Programmes. Report No 79, Pretoria.
- Asaeda, T., Hietz, P., Tanaka, N., Karunaratne, S., 2002. Seasonal fluctuations in live and dead biomass of *Phragmites australis* as described by a growth and decomposition model: implications of duration of aerobic conditions for litter mineralization and sedimentation. *Aquat. Bot.* 73, 223–239.
- Ascough, P.L., Cook, G.T., Dugmore, A.J., 2005. Methodological approaches to determining the marine radiocarbon reservoir effect. *Prog. Phys. Geogr.* 29, 532–547.
- Ascough, P.L., Cook, G.T., Dugmore, A.J., Barber, J., Higney, E., Scott, E.M., 2004. Holocene variations in the Scottish marine radiocarbon reservoir effect. *Radiocarbon* 46, 611–620.
- Balfour, D., Bond, W., 1993. Factors limiting climber distribution and abundance in a southern African forest. *J. Ecol.* 93–100.
- Bateman, M.D., Carr, A.S., Dunajko, A.C., Holmes, P.J., Roberts, D.L., McLaren, S.J., Bryant, R.G., Marker, M.E., Murray-Wallace, C.V., 2011. The evolution of coastal barrier systems: a case study of the Middle-Late Pleistocene Wilderness barriers, South Africa. *Quat. Sci. Rev.* 30, 63–81.
- Baxter, A.J., Meadows, M.E., 1999. Evidence for Holocene sea level change at verlorenvlei, Western Cape, South Africa. *Quat. Int.* 56, 65–79.
- Bevington, P.R., Robinson, D.K., 2003. *Data Reduction and Error Analysis for the Physical Sciences*. McGraw-Hill, New York.
- Birch, G., Du Plessis, A., Willis, J., 1978. Offshore and onland geological and geophysical investigations in the Wilderness Lakes region. *Trans. Geol. Soc. S. Afr.* 81, 339–352.
- Blaauw, M., Christen, J.A., 2011. Flexible paleoclimate age-depth models using an autoregressive gamma process. *Bayesian Anal.* 6, 457–474.
- Booth, P., 2011. Stratigraphic, structural and tectonic enigmas associated with the Cape Fold Belt: challenges for future research. *South Afr. J. Geol.* 114, 235–248.
- Bronk Ramsey, C., 2009. Bayesian analysis of radiocarbon dates. *Radiocarbon* 51, 337–360.
- Brown, M.C., Donadini, F., Korte, M., Nilsson, A., Korhonen, K., Lodge, A., Lengyel, S.N., Constable, C.G., 2015. GEOMAGIA50. v3: 1. general structure and modifications to the archeological and volcanic database. *Earth Planets Space* 67, 1–31.
- Browning, C., Macey, P., 2015. Lithostratigraphy of the george pluton units (Cape granite suite), South Africa. *South Afr. J. Geol.* 118, 323–330.
- Carr, A.S., Boom, A., Chase, B.M., Meadows, M.E., Grimes, H.L., 2015. Holocene sea level and environmental change on the west coast of South Africa: evidence from plant biomarkers, stable isotopes and pollen. *J. Paleolimnol.* 53, 415–432.
- Chase, B.M., Meadows, M.E., 2007. Late Quaternary dynamics of southern Africa's winter rainfall zone. *Earth-Science Rev.* 84, 103–138.
- Cohen, A.L., Parkington, J.E., Brundrit, G.B., van der Merwe, N.J., 1992. A Holocene marine climate record in mollusc shells from the southwest African coast. *Quat. Res.* 38, 379–385.
- Compton, J.S., 2001. Holocene sea-level fluctuations inferred from the evolution of depositional environments of the southern Langebaan Lagoon salt marsh, South Africa. *Holocene* 11, 395–405.
- Dewar, G., Pfeiffer, S., 2010. Approaches to estimating marine protein in human collagen for radiocarbon date calibration. *Radiocarbon* 52, 1611.
- Dewar, G., Reimer, P.J., Sealy, J., Woodborne, S., 2012. Late-Holocene marine radiocarbon reservoir correction (ΔR) for the west coast of South Africa. *Holocene* 22, 1481–1489.
- DWS, 2015. Resource Water Quality Data for Gouritz WMA. Department of Water and Sanitation, Republic of South Africa. https://www.dwa.gov.za/jwqs/wms/data/WMA16_reg_WMS_nobor.htm.
- Enkin, R.J., Dallimore, A., Baker, J., Southon, J.R., Ivanochko, T., Lian, O., 2013. A new high-resolution radiocarbon Bayesian age model of the Holocene and Late Pleistocene from core MD02-2494 and others, Effingham Inlet, British Columbia, Canada; with an application to the paleoseismic event chronology of the Cascadia Subduction Zone 1. *Can. J. Earth Sci.* 50, 746–760.
- Farmer, E.C., Demenocal, P.B., Marchitto, T.M., 2005. Holocene and deglacial ocean temperature variability in the Benguela upwelling region: implications for low-latitude atmospheric circulation. *Paleoceanography* 20, PA2018.
- Feng, G., Jin, S., Reales, J.M.S., 2013. Antarctic circumpolar current from satellite gravimetric models ITC-GRACE2010, GOCE-TIM3 and satellite altimetry. *J. Geodyn.* 72, 72–80.
- Ferré, E., Améglio, L., 2000. Preserved magnetic fabrics vs. annealed microstructures in the syntectonic recrystallised George granite, South Africa. *J. Struct. Geol.* 22, 1199–1219.
- Finch, J.M., Hill, T.R., 2008. A late quaternary pollen sequence from Mfabeni Peatland, South Africa: reconstructing forest history in Maputaland. *Quat. Res.* 70, 442–450.
- Frimmel, H., Van Achterbergh, E., 1995. Metamorphism of calc-silicate and associated rocks in the Pan-African Kaaimans Group, Saldania Belt, South Africa. *Mineralogy Petrology* 53, 75–102.
- Galman, V., Rydberg, J., de-Luna, S.S., Bindler, R., Renberg, I., 2008. Carbon and nitrogen loss rates during aging of lake sediment: Changes over 27 years studied in varved lake sediment. *Limnol. Oceanogr.* 53, 1076.
- Haberzettl, T., 2015. *Advances in Limnogeology and Paleolimnology with a Special Focus on Corroborated Chronologies Using Paleomagnetic Secular Variations*. Habilitation Thesis. Friedrich Schiller University Jena, Jena.
- Haberzettl, T., Baade, J., Compton, J., Daut, G., Dupont, L., Finch, J., Frenzel, P., Green, A., Hahn, A., Hebbeln, D., 2014. Paleoenvironmental investigations using a combination of terrestrial and marine sediments from South Africa-The RAIN (Regional Archives for Integrated iNvestigations) approach. *Zentralblatt für Geol. Paläontologie*, Teil 55–73.
- Haberzettl, T., Henkel, K., Kasper, T., Ahlborn, M., Su, Y., Wang, J., Appel, E., Stoner, J., Daut, G., Zhu, L., Mäusbacher, R., 2015. Independently dated paleomagnetic secular variation records from the Tibetan Plateau. *Earth Planet. Sci. Lett.* 416, 98–108.
- Hart, R., 1995. South African coastal lakes. *Wetl. S. Afr.* 103–130.
- Hartmann, G.A., Pacca, I.G., 2009. Time evolution of the South Atlantic magnetic anomaly. *An. Acad. Bras. Ciências* 81, 243–255.
- Heirtzler, J., 2002. The future of the South Atlantic anomaly and implications for radiation damage in space. *J. Atmos. Solar-Terrestrial Phys.* 64, 1701–1708.
- Hobbs, W.O., Hobbs, J.M.R., LaFrançois, T., Zimmer, K.D., Theissen, K.M., Edlund, M.B., Michelutti, N., Butler, M.G., Hanson, M.A., Carlson, T.J., 2012. A 200-year perspective on alternative stable state theory and lake management from a biomaniipulated shallow lake. *Ecol. Appl.* 22, 1483–1496.
- Hogg, A.G., Hua, Q., Blackwell, P.G., Niu, M., Buck, C.E., Guilderson, T.P., Heaton, T.J., Palmer, J.G., Reimer, P.J., Reimer, R.W., Turney, C.S.M., Zimmermann, S.R.H., 2013. SHCal13 Southern Hemisphere calibration, 0–50,000 years cal BP. *Radiocarbon* 55, 1889–1903.
- Howard-Williams, C., 1980. Aquatic macrophyte communities of the Wilderness lakes: community structure and associated environmental conditions. *J. Limnological Soc. South Afr.* 6, 85–92.
- Hughes, K.A., Baillie, M.G., Bard, E., Beck, J.W., Bertrand, C.J., Blackwell, P.G., Buck, C.E., Burr, G.S., Cutler, K.B., Damon, P.E., Edwards, R.L., Fairbanks, R.G., Friedrich, M., Guilderson, T.P., Kromer, B., McCormac, G., Manning, S., Bronk Ramsey, C., Reimer, P.J., Reimer, R.W., Remmele, S., Southon, J.R., Stuiver, M., Talamo, S., Taylor, F.W., van der Plicht, J., Weyhenmeyer, C.E., 2004. Marine04 marine radiocarbon age calibration, 0–26 cal kyr BP. *Radiocarbon* 46, 1059–1086.
- Hutchinson, I., James, T.S., Reimer, P.J., Bornhold, B.D., Clague, J.J., 2004. Marine and limnic radiocarbon reservoir corrections for studies of late-and postglacial environments in Georgia Basin and Puget Lowland, British Columbia, Canada and Washington, USA. *Quat. Res.* 61, 193–203.
- Illenberger, W.K., 1996. The geomorphologic evolution of the Wilderness dune cordons, South Africa. *Quat. Int.* 33, 11–20.
- Jackson, A., Jonkers, A.R., Walker, M.R., 2000. Four centuries of geomagnetic secular variation from historical records. *Philosophical Transactions of the Royal Society of London A: Mathematical. Phys. Eng. Sci.* 358, 957–990.
- Jury, M., Brundrit, G., 1992. Temporal organization of upwelling in the southern Benguela ecosystem by resonant coastal trapped waves in the ocean and atmosphere. *South Afr. J. Mar. Sci.* 12, 219–224.
- Jury, M., MacArthur, C., Brundrit, G., 1990. Pulsing of the Benguela upwelling region: large-scale atmospheric controls. *South Afr. J. Mar. Sci.* 9, 27–41.
- Kasper, T., Haberzettl, T., Doberschütz, S., Daut, G., Wang, J., Zhu, L., Nowaczyk, N., Mäusbacher, R., 2012. Indian Ocean summer monsoon (IOSM)-dynamics within the past 4 ka recorded in the sediments of lake Nam Co, central Tibetan plateau (China). *Quat. Sci. Rev.* 39, 73–85.
- Kim, J.C., Eum, C.H., Yi, S., Kim, J.Y., Hong, S.S., Lee, J.-Y., 2012. Optically stimulated luminescence dating of coastal sediments from southwestern Korea. *Quat. Geochronol.* 10, 218–223.
- Kirschvink, J., 1980. The least-squares line and plane and the analysis of palaeomagnetic data. *Geophys. J. Int.* 62, 699–718.
- Kirsten, K., 2014. *Late Holocene Diatom Community Responses to Climate Variability along the Southern Cape Coastal Plain*. South Africa. PhD Thesis. University of Cape Town, Cape Town, South Africa.
- Korte, M., Constable, C., 2011. Improving geomagnetic field reconstructions for 0–3ka. *Phys. Earth Planet. Interiors* 188, 247–259.
- Little, E.A., 1993. Radiocarbon age calibration at archaeological sites of coastal Massachusetts and vicinity. *J. Archaeol. Sci.* 20, 457–471.
- Lucas, W., Tyree, M., Petrov, A., 1978. Characterization of photosynthetic ¹⁴C assimilation by *Potamogeton lucens* L. *J. Exp. Bot.* 29, 1409–1421.
- Lutjeharms, J., Monteiro, P., Tyson, P., Obura, D., 2001. The oceans around southern Africa and regional effects of global change: START Regional Syntheses. *South Afr. J. Sci.* 97, 119–130.
- Marker, M.E., Holmes, P.J., 2002. The distribution and environmental implications of coversand deposits in the Southern Cape, South Africa. *South Afr. J. Geol.* 105, 135–146.
- Martin, A.R.H., 1959. The stratigraphy and history of Groenvlei, a South African coastal fen. *Aust. J. Bot.* 7, 142–167.

- Martin, A.R.H., 1962. Evidence relating to the Quaternary history of the Wilderness lakes. *Trans. Geol. Soc. South Afr.* 65, 19–42.
- Martin, A.R.H., 1968. Pollen analysis of Groenvlei lake sediments, Knysna (South Africa). *Rev. Palaeobot. Palynology* 7, 107–144.
- Mazaud, A., 2005. User-friendly software for vector analysis of the magnetization of long sediment cores. *Geochem. Geophys. Geosystems* 6. <http://dx.doi.org/10.1029/2005GC001036>.
- Meadows, M.E., Baxter, A.J., 2001. Holocene vegetation history and palaeoenvironments at Klaarfontein springs, Western Cape, South Africa. *Holocene* 11, 699–706.
- Meyers, P.A., 1994. Preservation of elemental and isotopic source identification of sedimentary organic matter. *Chem. Geol.* 114, 289–302.
- Morrill, C., Overpeck, J.T., Cole, J.E., Liu, K.-b., Shen, C., Tang, L., 2006. Holocene variations in the Asian monsoon inferred from the geochemistry of lake sediments in central Tibet. *Quat. Res.* 65, 232–243.
- Morse, J.W., Arvidson, R.S., 2002. The dissolution kinetics of major sedimentary carbonate minerals. *Earth-Science Rev.* 58, 51–84.
- Mucina, L., Rutherford, M.C., 2006. The Vegetation of South Africa, Lesotho and Swaziland. South African National Biodiversity Institute, Pretoria.
- Müller, A., Mathesius, U., 1999. The palaeoenvironments of coastal lagoons in the southern Baltic Sea, I. The application of sedimentary C org/N ratios as source indicators of organic matter. *Palaeogeogr. Palaeoclimatol. Palaeoecol.* 145, 1–16.
- Neukirch, L.P., Tarduno, J.A., Huffman, T.N., Watkeys, M.K., Scribner, C.A., Cottrell, R.D., 2012. An archeomagnetic analysis of burnt grain bin floors from ca. 1200 to 1250 AD Iron-Age South Africa. *Phys. Earth Planet. Interiors* 190, 71–79.
- Neumann, F.H., Scott, L., Bousman, C., Van As, L., 2010. A Holocene sequence of vegetation change at Lake Eteza, coastal KwaZulu-Natal, South Africa. *Rev. Palaeobot. Palynology* 162, 39–53.
- Oeschger, H., Siegenthaler, U., Schotterer, U., Gugelmann, A., 1975. A box diffusion model to study the carbon dioxide exchange in nature. *Tellus* 27, 168–192.
- Oikawa, K., Yongsiri, C., Takeda, K., Harimoto, T., 2003. Seawater flue gas desulfurization: its technical implications and performance results. *Environ. Prog.* 22, 67–73.
- Ortlieb, L., Vargas, G., Saliège, J.-F., 2011. Marine radiocarbon reservoir effect along the northern Chile–southern Peru coast (14–24 S) throughout the Holocene. *Quat. Res.* 75, 91–103.
- Parsons, R.P., 2014. Quantifying the Role of Groundwater in Sustaining Groenvlei, a Shallow Lake in the Southern Cape Region of South Africa. PhD Thesis. University of the Free State, Bloemfontein, South Africa.
- Petchev, F., Anderson, A., Zondervan, A., Ulm, S., Hogg, A., 2008. New marine ΔR values for the South Pacific subtropical gyre region. *Radiocarbon* 50, 373–397.
- Philippson, B., Olsen, J., Lewis, J.P., Rasmussen, P., Ryves, D.B., Knudsen, K.L., 2013. Mid-to late-Holocene reservoir-age variability and isotope-based palaeoenvironmental reconstruction in the Limfjord, Denmark. *Holocene* 23, 1017–1027.
- Quick, L.J., Meadows, M.E., Bateman, M.D., Kirsten, K.L., Mäusbacher, R., Haberzettl, T., Chase, B.M., 2016. Vegetation and climate dynamics during the last glacial period in the fynbos-afrotemperate forest ecotone, southern Cape, South Africa. *Quat. Int.* 404 (Part B), 136–149.
- Reimer, P.J., Bard, E., Bayliss, A., Beck, J.W., Blackwell, P.G., Bronk Ramsey, C., Buck, C.E., Cheng, H., Edwards, R.L., Friedrich, M., Grootes, P.M., Guilderson, T.P., Haffidason, H., Hajdas, I., Hatté, C., Heaton, T.J., Hoffmann, D.L., Hogg, A.G., Hughen, K.A., Kaiser, K.F., Kromer, B., Manning, S.W., Niu, M., Reimer, R.W., Richards, D.A., Scott, E.M., Southon, J.R., Staff, R.A., Turney, C.S.M., van der Plicht, J., 2013. IntCal13 and Marine13 radiocarbon age calibration curves 0–50,000 years cal BP. *Radiocarbon* 55, 1869–1887.
- Reimer, P.J., McCormac, F.G., Moore, J., McCormick, F., Murray, E.V., 2002. Marine radiocarbon reservoir corrections for the mid to late Holocene in the eastern subpolar North Atlantic. *Holocene* 12, 129–135.
- Reinwarth, B., Franz, S., Baade, J., Haberzettl, T., Kasper, T., Daut, G., Helmschrot, J., Kirsten, K.L., Quick, L.J., Meadows, M.E., 2013. A 700-year record on the effects of climate and human impact on the southern Cape coast inferred from lake sediments of Eilandvlei, Wilderness Embayment, South Africa. *Geogr. Ann. Ser. A, Phys. Geogr.* 95, 345–360.
- Richter, D., Gross, E.M., 2013. Chara can outcompete Myriophyllum under low phosphorus supply. *Aquat. Sci.* 75, 457–467.
- Roberts, S.J., Hodgson, D.A., Sterken, M., Whitehouse, P.L., Verleyen, E., Vyverman, W., Sabbe, K., Balbo, A., Bentley, M.J., Moreton, S.G., 2011. Geological constraints on glacio-isostatic adjustment models of relative sea-level change during deglaciation of Prince Gustav Channel, Antarctic Peninsula. *Quat. Sci. Rev.* 30, 3603–3617.
- Russell, I., 1999. Changes in the water quality of the wilderness and Swartvlei lake systems, South Africa. *Koedoe* 42, 57–72.
- Russell, I., 2003. Changes in the distribution of emergent aquatic plants in a brackish South African estuarine-lake system. *Afr. J. Aquatic Sci.* 28, 103–122.
- Russell, I., 2013. Spatio-temporal variability of surface water quality parameters in a South African estuarine lake system. *Afr. J. Aquatic Sci.* 38, 53–66.
- Russell, N., Cook, G., Ascough, P., Scott, E., Dugmore, A., 2011. Examining the inherent variability in ΔR : new methods of presenting ΔR values and implications for MRE studies. *Radiocarbon* 53, 277–288.
- Sabatier, P., Dezileau, L., Blanchemanche, P., Siant, G., Condomines, M., Bentaleb, I., Piquès, G., 2010. Holocene variations of radiocarbon reservoir ages in a Mediterranean lagoonal system. *Radiocarbon* 52, 91.
- Sarnthein, M., Balmer, S., Grootes, P.M., Mudelsee, M., 2015. Planktic and benthic ¹⁴C reservoir ages for three ocean basins, calibrated by a suite of ¹⁴C plateaus in the glacial-to-deglacial Suigetsu atmospheric ¹⁴C record. *Radiocarbon* 57, 129–151.
- Schalke, H.J.W.G., 1973. The upper quaternary of the Cape flats area (Cape Province, South Africa). *Scr. Geol.* 15, 1–67.
- Schimmelmann, A., Lange, C.B., Roark, E.B., Ingram, B.L., 2006. Resources for Paleooceanographic and Paleoclimatic analysis: a 6,700-Year stratigraphy and regional radiocarbon reservoir-age (ΔR) record based on varve Counting and ¹⁴C-AMS dating for the Santa Barbara basin, offshore California, USA. *J. Sediment. Res.* 76, 74–80.
- Schumann, E., Perrins, L., Hunter, I., 1982. Upwelling along the South coast of the Cape Province, South Africa. *South Afr. J. Sci.* 78, 238–242.
- Scott, L., Lee-Thorp, J.A., 2004. Holocene climatic trends and rhythms in southern Africa. In: Battarbee, R.W., Gasse, F., Stickley, C.E. (Eds.), *Past Climate Variability through Europe and Africa*. Springer, Dordrecht, pp. 69–91.
- Shah, J., Koppers, A.A., Leitner, M., Leonhardt, R., Muxworthy, A.R., Heunemann, C., Bachtadse, V., Ashley, J.A., Matzka, J., 2016. Palaeomagnetic evidence for the persistence or recurrence of geomagnetic main field anomalies in the South Atlantic. *Earth Planet. Sci. Lett.* 441, 113–124.
- Southon, J.R., Kashgarian, M., Fontugne, M., Metivier, B., Yim, W.W., 2002. Marine reservoir corrections for the Indian Ocean and Southeast Asia. *Radiocarbon* 44, 167–180.
- Southon, J.R., Rodman, A.O., True, D., 1995. A comparison of marine and terrestrial radiocarbon ages from northern Chile. *Radiocarbon* 37, 389–393.
- Stager, J.C., Mayewski, P.A., White, J., Chase, B.M., Neumann, F.H., Meadows, M.E., King, C.D., Dixon, D.A., 2012. Precipitation variability in the winter rainfall zone of South Africa during the last 1400 yr linked to the austral westerlies. *Clim. Past* 8, 877–887.
- Stager, J.C., Ryves, D.B., King, C., Madson, J., Hazzard, M., Neumann, F.H., Maud, R., 2013. Late Holocene precipitation variability in the summer rainfall region of South Africa. *Quat. Sci. Rev.* 67, 105–120.
- Stoner, J., St-Onge, G., 2007. Magnetic stratigraphy in paleoceanography: reversals, excursions, paleointensity and secular variation. In: Hillaire-Marcel, C., de Vernal, A. (Eds.), *Proxies in Late Cenozoic Paleooceanography*, (Developments in Marine Geology), vol. 1. Elsevier, pp. 99–138.
- Stramma, L., Lutjeharms, J.R.E., 1997. The flow field of the subtropical gyre of the South Indian Ocean. *J. Geophys. Res.* 102, 5513–5530.
- Stuiver, M., Braziunas, T.F., 1993. Modeling atmospheric ¹⁴C influences and ¹⁴C ages of marine samples to 10,000 BC. *Radiocarbon* 35, 137–189.
- Stuiver, M., Pearson, G.W., Braziunas, T., 1986. Radiocarbon age calibration of marine samples back to 9000 cal yr BP. *Radiocarbon* 28, 980–1021.
- Talling, J., 1976. The depletion of carbon dioxide from lake water by phytoplankton. *J. Ecol.* 79–121.
- Tarduno, J.A., Watkeys, M.K., Huffman, T.N., Cottrell, R.D., Blackman, E.G., Wendt, A., Scribner, C.A., Wagner, C.L., 2015. Antiquity of the South Atlantic Anomaly and evidence for top-down control on the geodynamo. *Nat. Commun.* 6 <http://dx.doi.org/10.1038/ncomms8865>.
- Tauxe, L., 2005. Inclination flattening and the geocentric axial dipole hypothesis. *Earth Planet. Sci. Lett.* 233, 247–261.
- Taylor, J.R., 1997. An Introduction to Error Analysis: the Study of Uncertainties in Physical Measurements. University Science Books, Sausalito.
- Tylová, E., Steinbachová, L., Votrubová, O., Lorenzen, B., Brix, H., 2008. Different sensitivity of Phragmites australis and Glyceria maxima to high availability of ammonium-N. *Aquat. Bot.* 88, 93–98.
- Van den Berg, M.S., Coops, H., Simons, J., Pilon, J., 2002. A comparative study of the use of inorganic carbon resources by Chara aspera and Potamogeton pectinatus. *Aquat. Bot.* 72, 219–233.
- Walker, N.D., 1986. Satellite observations of the Agulhas Current and episodic upwelling south of Africa. *Deep Sea Res.* 33, 1083–1106.
- Watanabe, T., Matsunaka, T., Nakamura, T., Nishimura, M., Izutsu, Y., Minami, M., Nara, F.W., Kakegawa, T., Wang, J., Zhu, L., 2010. Last glacial–Holocene geochronology of sediment cores from a high-altitude Tibetan lake based on AMS ¹⁴C dating of plant fossils: implications for paleoenvironmental reconstructions. *Chem. Geol.* 277, 21–29.
- Weeks, R., Laj, C., Endignoux, L., Fuller, M., Roberts, A., Manganne, R., Blanchard, E., Goree, W., 1993. Improvements in long-core measurement techniques: applications in palaeomagnetism and paleoceanography. *Geophys. J. Int.* 114, 651–662.
- Wüdsch, M., Haberzettl, T., Kirsten, K.L., Kasper, T., Zabel, M., Dietze, E., Baade, J., Daut, G., Meschner, S., Meadows, M.E., 2016. Sea level and climate change at the southern cape coast, South Africa, during the past 4.2 kyr. *Palaeogeogr. Palaeoclimatol. Palaeoecol.* 446, 295–307.
- Xuan, C., Channell, J.E., 2009. UPmag: MATLAB software for viewing and processing u channel or other pass-through paleomagnetic data. *Geochem. Geophys. Geosystems* 10. <http://dx.doi.org/10.1029/2009GC002584>.

Chapter 4

Holocene environmental change along the southern Cape coast of South Africa – Insights from the Eilandvlei sediment record spanning the last 8.9 kyr

Authors: Michael Wündsch, Torsten Haberzettl, Hayley C. Cawthra,
Kelly L. Kirsten, Lynne J. Quick, Matthias Zabel, Peter Frenzel,
Jussi Baade, Gerhard Daut, Thomas Kasper,
Michael E. Meadows, Roland Mäusbacher

Submitted to:
Quaternary Science Reviews

Keywords: Coastal lake sediments, Sedimentary geochemistry, Palaeoclimate, Sea level change,
Southern Annular Mode, El Niño-Southern Oscillation

Holocene environmental change along the southern Cape coast of South Africa – Insights from the Eilandvlei sediment record spanning the last 8.9 kyr

Michael Wündsch^{1,*}, Torsten Haberzettl¹, Hayley C. Cawthra^{2,3}, Kelly L. Kirsten⁴,
Lynne J. Quick⁴, Matthias Zabel⁵, Peter Frenzel⁶, Jussi Baade¹, Gerhard Daut¹,
Thomas Kasper¹, Michael E. Meadows⁴, Roland Mäusbacher¹

¹Physical Geography, Institute of Geography, Friedrich Schiller University Jena, Löbdergraben 32, 07743 Jena, Germany

²Marine Geoscience Unit, Council for Geoscience, PO Box 572, 7535 Bellville, South Africa

³Centre for Coastal Palaeoscience, Nelson Mandela Metropolitan University, PO Box 77000, 6031 Port Elizabeth, South Africa

⁴Department of Environmental and Geographical Science, University of Cape Town, South Lane, Upper Campus, 7701 Rondebosch, South Africa

⁵MARUM – Center for Marine Environmental Sciences, University of Bremen, Leobener Str., 28359 Bremen, Germany

⁶Institute of Geosciences, Friedrich Schiller University Jena, Burgweg 11, 07749 Jena, Germany

*corresponding author: E-mail: michael.wuendsch@uni-jena.de

Abstract

This study explores the potential of sediments deposited in the coastal lake Eilandvlei, located within the Wilderness embayment at the southern Cape coast of South Africa, for Holocene palaeoenvironmental reconstructions. The specific aim is to trace back the long-term rainfall variability for the region as well as the evolution of the present coastal lake via distinct phases of connectivity to the ocean due to sea level changes. For this purpose, a seismic survey was conducted as well as a multi-proxy approach (including geochemical, mineralogical, micropalaeontological and granulometric data) on a 30.5 m sediment core spanning the last ~8.9 kyr, which was recovered from the central part of the lake. The acquired data are compared to available sea level and climate reconstructions. The interpreted data indicate that marine conditions prevailed at the core site from 8920 to 4670 cal BP. The rapid sea level rise during the early Holocene probably caused the inundation of a palaeovalley that most likely had formed at lower sea levels during the Pleistocene. Towards the mid-Holocene the sea level exceeded its present height and created a marine embayment. Between 4670 and 1240 cal BP, the embayment became distinctly more disconnected from the ocean forming a lagoon system. During the last ~1.2 kyr, the present estuarine/coastal lake system established.

The palaeoclimatic interpretation indicates reduced rainfall from 8920 to 7870 cal BP and 6440 to 3000 cal BP. In contrast, our proxies suggest that the region received more rainfall between 7870-6440 cal BP and 3000 cal BP-present. Additionally, three extreme rainfall events were reconstructed between 2070 and 1250 cal BP. The reconstructed rainfall variations are discussed within the context of e.g., shifts in the position of the Antarctic sea ice extent and the mid-latitude westerly wind belt as well as changes in the El Niño-Southern Oscillation (ENSO). The study provides an exceptional record giving insights into Holocene palaeoenvironmental changes in an area of extremely complex environmental dynamics.

41 **Keywords**

42 Coastal lake sediments, Sedimentary geochemistry, Palaeoclimate, Sea level change, El Niño-
43 Southern Oscillation, Southern Annular Mode

44

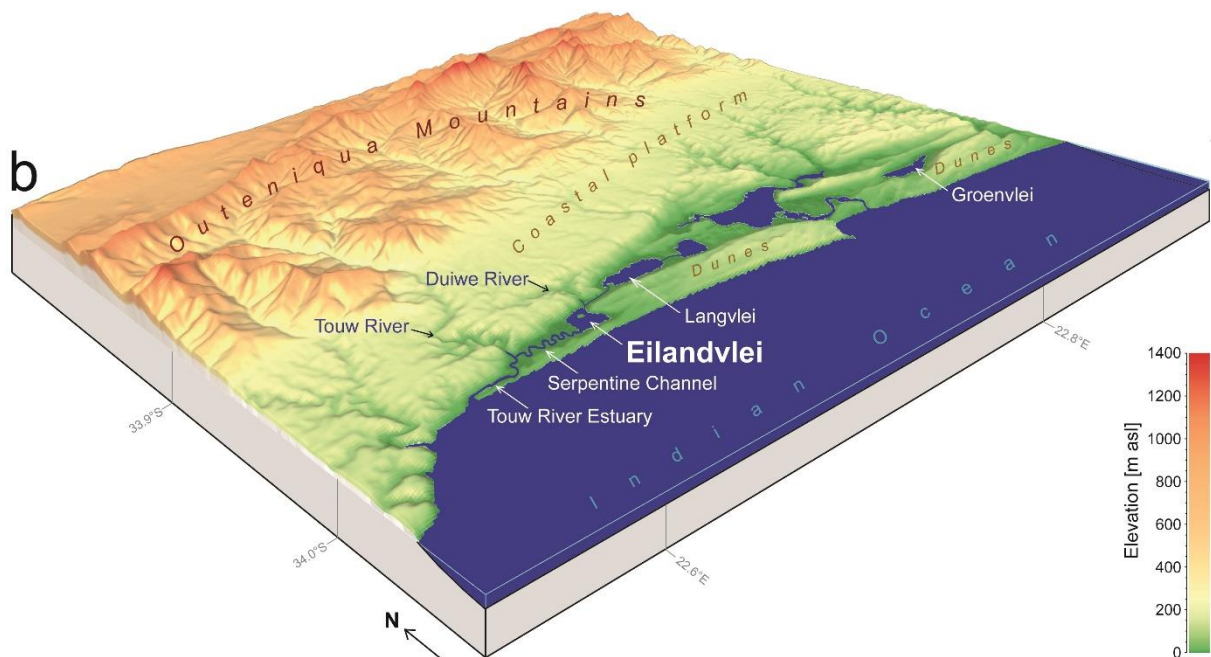
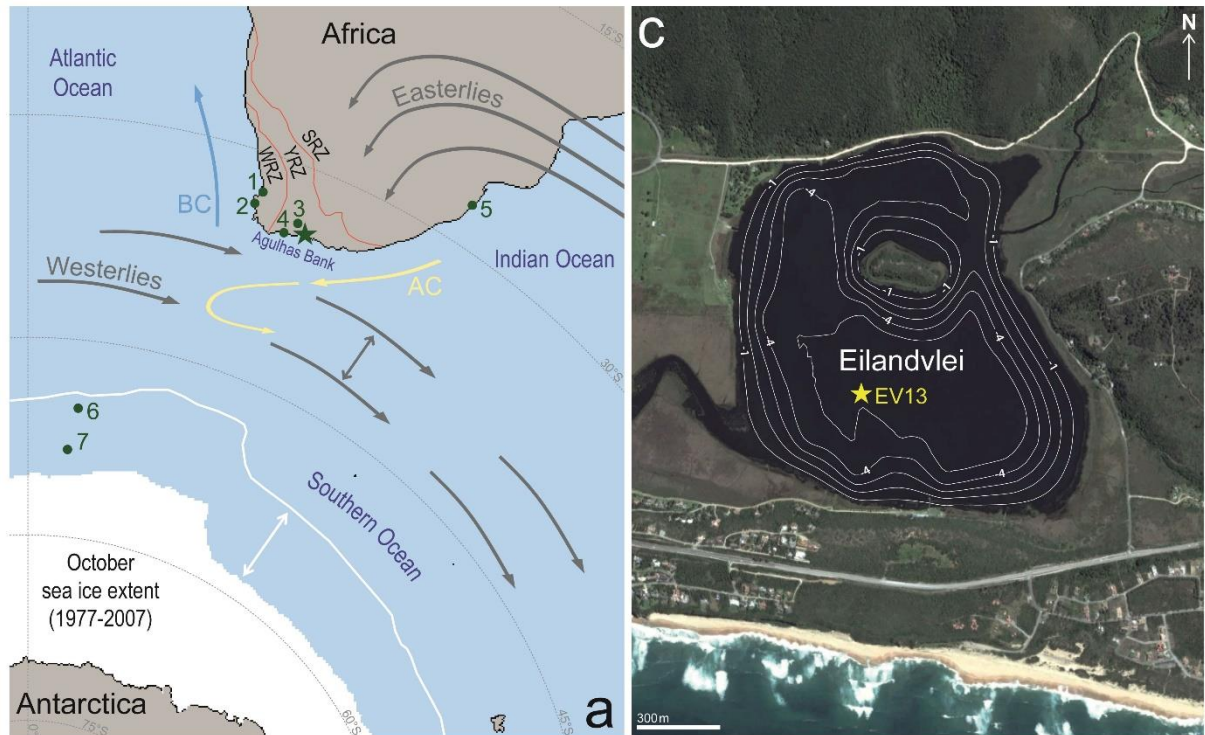
45 **1 Introduction**

46 The southern Cape coast represents an exceptional region within South Africa in terms of its rainfall
47 regime and seasonality. While large parts of the country (eastern and central part) receive the majority
48 of rainfall from tropical moisture-bearing systems during austral summer (SRZ: summer rainfall zone;
49 Fig. 1a) and a narrow belt along the west coast is supplied with rainfall by the mid-latitude westerlies
50 during austral winter (WRZ: winter rainfall zone), the southern Cape coast is part of an intermediary
51 area between the SRZ and WRZ where rainfall occurs throughout the year (YRZ: year-round rainfall
52 zone) (Chase and Meadows, 2007; Engelbrecht et al., 2015; Scott and Lee-Thorp, 2004). Despite the
53 agricultural importance of the southern Cape coast, its modern rainfall variability is not fully understood
54 (Weldon and Reason, 2014) and even more challenging is the generation and evaluation of
55 palaeoclimatic proxy data.

56 Although Holocene geoarchives are generally rare in South Africa (Chase and Meadows, 2007;
57 Haberzettl et al., 2014; Scott and Lee-Thorp, 2004), some palaeoenvironmental records are available
58 from the YRZ (Chase et al., 2013; Cohen and Tyson, 1995; Hahn et al., 2016; Kirsten, 2014; Martin,
59 1959, 1968; Quick, 2013; Quick et al., 2015; Reinwarth et al., 2013; Talma and Vogel, 1992; Wündsch
60 et al., 2016a). However, the existing data is still too sparse to develop a coherent understanding of
61 environmental dynamics and changing interactions between tropical and temperate climate systems
62 affecting the southern Cape coast during the Holocene (Chase et al., 2013).

63 Coastal geoarchives, such as lagoons or coastal lakes, provide an advantageous opportunity for
64 palaeoenvironmental reconstructions, as they can contain well-preserved and continuous Holocene
65 sediment sequences. However, a dominant signal reflected in these systems is often due to sea level
66 changes and associated alterations of their geomorphological configuration (e.g., Baxter and Meadows,
67 1999; Carr et al., 2015; Compton, 2001; Meadows and Baxter, 2001).

68 This study explores sediments deposited in the coastal lake Eilandvlei located in the Wilderness
69 embayment at the southern Cape coast of South Africa (Fig. 1). In addition to a seismic survey, this
70 paper focuses on the investigation of a 30.5 m sediment core (EV13) that was retrieved from the central
71 part of the lake. As a solid basis for palaeoenvironmental reconstructions, an age-depth model was
72 established indicating a continuous sedimentation during the last ~8.9 kyr (Wündsch et al., 2016b). Here
73 we apply a multi-proxy approach in order to pursue the following two research aims: 1) the
74 reconstruction of the evolution towards the present coastal lake system via distinct phases of
75 connectivity to the ocean due to Holocene sea level and geomorphological changes; 2) a
76 palaeoclimatological reconstruction of the long-term rainfall variability at the southern Cape coast
77 during the last ~8.9 kyr.



78
79
80
81
82
83
84
85
86
87
88
89
90
91
92
93

Fig. 1: a) Location of the study area (b; star) and the three rainfall zones of southern Africa (WRZ: winter rainfall zone, SRZ: summer rainfall zone, YRZ: year-round rainfall zone); also shown are atmospheric (circumpolar westerlies, tropical easterlies) and oceanic circulation systems (AC: Agulhas Current, BC: Benguela Current) as well as other study sites mentioned in the text (1: Verlorenvlei (Baxter and Meadows, 1999), 2: Langebaan Lagoon (Compton, 2001), 3: Cango Caves (Talma and Vogel, 1992), 4: Still Bay (Quick et al., 2015), 5: several South African east coast sites (Ramsay, 1995) as well as 6 and 7: marine sediment cores from the East Atlantic sector of the Southern Ocean: TN057-17 (Nielsen et al., 2004) (6) and TTN057-13PC4 (Hodell et al., 2001) (7). The mean October sea ice extent around Antarctica between 1977 and 2007 is depicted based on data from the National Snow and Ice Data Center (nsidc.org). The double arrows indicate in a simplified form past latitudinal migrations of the Antarctic sea ice extent and the westerlies. The map was created using GeoMapApp 3.6.3 (www.geomapapp.org). b) 3D digital terrain model (twofold vertical exaggeration) of the southern Cape coast section including the Wilderness embayment with coastal lake Eilandvlei. The 3D model was created by means of the software QGIS 2.16.3 using 90 m SRTM DEM data from Jarvis et al. (2008). c) Map of lake Eilandvlei (google Earth image) showing the coring position of the EV13 sediment core (yellow star) and bathymetric data (given in metres relative to the lake surface) according to Reinwarth et al. (2013).

94 2 Study area

95 Eilandvlei is one of several coastal lakes located within the Wilderness embayment at the southern Cape
96 coast of South Africa (Fig. 1). The embayment probably started to form during the Pleistocene and
97 evolved into its present configuration after multiple transgressive-regressive cycles (Bateman et al.,
98 2011; Birch et al., 1978; Cawthra et al., 2014; Martin, 1962). The lake is separated from the Indian
99 Ocean by lithified dunes (aeolianites) of Pleistocene age that mainly consist of quartz sand and bioclasts
100 cemented by calcium carbonate. These aeolianites are partly covered by unconsolidated Holocene sands
101 (Bateman et al., 2011; Illenberger, 1996). North of the embayment, there is an up to 200 m high coastal
102 platform with bedrocks composed of granites (Browning and Macey, 2015; Ferré and Améglio, 2000)
103 and metasedimentary rocks (Frimmel and Van Achterbergh, 1995), which are partly covered by
104 Pleistocene sands (Marker and Holmes, 2002). The coastal platform had been incised by the Duiwe and
105 Touw River (Fig. 1b) forming steep valleys. The upper catchments of these rivers are part of the up to
106 1500 m high Outeniqua Mountains which are mainly built of quartzites, quartzitic sandstones and shales
107 (Balfour and Bond, 1993; Booth, 2011).

108 At present, Eilandvlei is connected to the Indian Ocean via the Serpentine Channel and the Touw
109 River estuary (Fig. 1b). At the Touw River estuary mouth, a sandbar sometimes forms temporarily,
110 blocking the surface connection to the ocean. When the estuary mouth is open, seawater enters the Touw
111 River estuary increasing its salinity. When the estuary mouth is closed, freshwater runoff from the Touw
112 River mixes with saline water in the estuary and leads to a rising water level that may cause the backflow
113 of brackish water from the Touw River estuary via the Serpentine Channel into Eilandvlei. Moreover,
114 evaporation increases the lake water salinity, which ranges between 2 and 12 g kg⁻¹ (1991-2010)
115 (Russell, 2013). The Duiwe River represents another source of freshwater entering Eilandvlei from the
116 northeast. To the east, the lake is connected via a narrow channel to the adjacent coastal lake Langvlei.

117 The terrestrial vegetation around Eilandvlei is characterised by various species of the Fynbos
118 Biome which predominantly occur on the surrounding dunes. Moreover, different species of the
119 Southern Afrotemperate Forest are distributed especially in the river valleys (Mucina and Rutherford,
120 2006; Quick et al., 2016). The littoral zone around the lake as well as the floodplains of the channels,
121 are dominated by semi-aquatic, emergent plants (Howard-Williams, 1980; Russell, 2003). Aquatic,
122 submerged plants and algae represent a major proportion of the biomass within the lake (Allanson and
123 Whitfield, 1983; Howard-Williams, 1980).

124 The southern Cape coast receives rainfall almost uniformly distributed throughout the year with
125 11 to 12 months each contributing at least 5 % to the annual rainfall (1979-2011) (Engelbrecht et al.,
126 2015). The area is relatively humid, but annual rainfall totals can be very variable, ranging between 375
127 and 1474 mm (mean: 800 mm), as recorded by the three closest weather stations in the area between
128 1993 and 2016 (Knysna: 40 km east of EV13, George: 25 km west, George Witfontein: 20 km
129 northwest) (SAWS, 2017). Rainfall at the southern Cape is caused by complex interactions of the mid-
130 latitude westerlies with tropical moisture-bearing systems (Tyson, 1986). The main synoptic-scale

131 weather systems bringing rainfall from the mid-latitude westerlies are ridging anticyclones (contributing
132 46 % to the mean total annual rainfall at the southern Cape coast) and cut-off lows (16 %); rainfall of
133 tropical origin is mainly brought by tropical-temperate trough cloud bands (28 %) (Engelbrecht et al.,
134 2015). Ridging anticyclones produce onshore flow that leads to orographic rainfall at the coast-parallel
135 running Outeniqua Mountains (Fig. 1b) (Weldon and Reason, 2014). According to Favre et al. (2013),
136 cut-off lows can contribute 15 to more than 35 % of annual precipitation. Cut-off lows are likely
137 responsible for most of the extreme heavy rainfall events producing hazardous floods in the area that
138 can destroy infrastructure and threaten lives (Engelbrecht et al., 2015; Rouault et al., 2002; Weldon and
139 Reason, 2014). The occurrence of cut-off lows was linked to the El Niño-Southern Oscillation (ENSO)
140 indicating an increased number of cut-off lows during the mature phases of La Niña (Engelbrecht and
141 Landman, 2016; Favre et al., 2013; Weldon and Reason, 2014).

142 Further, it was found that rainfall variability in South Africa is probably related to another
143 principal climate mode of the southern hemisphere, the Antarctic Oscillation, also referred to as the
144 Southern Annular Mode (SAM) which can be defined as the atmospheric zonal mean pressure gradient
145 between the mid-latitudes ($\sim 40^{\circ}\text{S}$) and Antarctica ($\sim 65^{\circ}\text{S}$) (Marshall, 2003; Thompson and Wallace,
146 2000). When the SAM is in its positive phase, the pressure gradient is enhanced resulting in a
147 strengthening and poleward contraction of the westerly jet favouring the equatorward propagation of
148 evolving eddies. When the SAM is negative, the pressure gradient is low and the weaker westerly jet
149 shifts equatorwards (Abram et al., 2014; Hartmann and Lo, 1998; Marshall, 2003). While a positive
150 (negative) phase of the SAM was linked to less (more) rainfall in the WRZ, the reversed relationship
151 was found for the southern Cape coast and the SRZ with more (less) rainfall when the SAM is positive
152 (negative) (Engelbrecht and Landman, 2016; Reason and Rouault, 2005). Rainfall along the southern
153 Cape coast is further related to meso-scale circulations which are influenced by the local topography as
154 well as the sea surface temperatures (SST) of the Agulhas Current affecting the onshore flowing
155 moisture-laden air (Engelbrecht and Landman, 2016; Engelbrecht et al., 2015; Rouault et al., 2002;
156 Singleton and Reason, 2006). High SSTs facilitate evaporation and thus may increase the amount of
157 moisture brought by onshore flowing air.

158 **3 Materials and methods**

159 **3.1 Seismics**

160 A sub-bottom profiling survey was conducted in Eilandvlei in February 2014. A total of 20 lines of data
161 were collected, equating to a coverage of 16 line km. A Design Projects boomer was used to collect
162 medium-penetration seismic profiling data. An Applied Acoustic Engineering CSP1000 power supply
163 that produces a maximum energy output of 1000 J s^{-1} was used to power the boomer plate and a Design
164 Projects 8 element hydrophone array was used in conjunction with an Octopus 760 seismic processor to
165 acquire and store the seismic data in SEG-Y format. The boomer system was triggered every 600 ms at
166 an energy level of 500 J and the reflected seismic data were acquired using a sampling rate of 24 kHz
167 and a sweep period of 75 ms. The Octopus 760 was used for real-time processing, digital recording and

168 as a post-processing workstation. The geodetic parameters applied to the boomer data presented were
169 produced in the Universal Transverse Mercator (UTM) projection of zone 34 south (World Geodetic
170 System (WGS) 1984 ellipsoid). The boomer seismic data were processed using inhouse software of the
171 Council for Geoscience. Stacking, filters and time-varied gain were applied to enhance the seismic
172 records. Post-processing of the reflection seismic data involved the application of time-varied gain, a
173 bandpass filter generally optimised between 450 and 1800 Hz, swell filter and seafloor tracking.

174

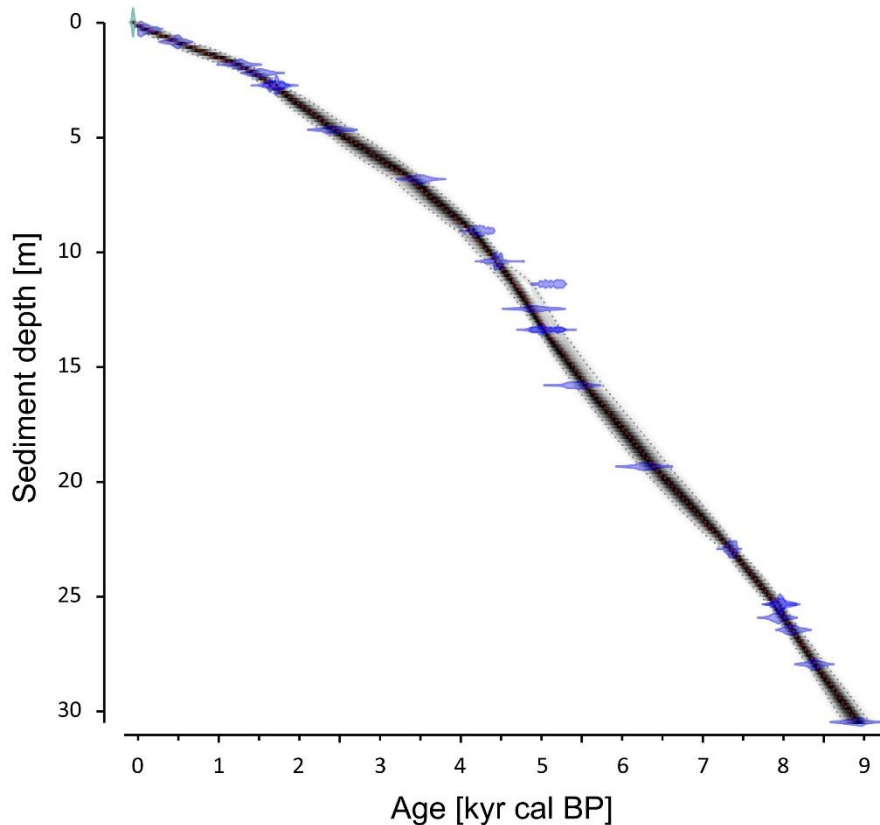
175 ***3.2 Sample recovery and height measurement***

176 Based on an initial hydroacoustic survey using a 12 kHz echosounder (Innomar SES-96 light), multiple
177 sediment cores were retrieved from the profundal zone of Eilandvlei (33°59.719'S, 22°38.403'E;
178 Fig. 1c) in October 2013. A short core of 156 cm length (EV 13-2) was recovered using a UWITEC
179 gravity corer. Two overlapping long cores (EV13-3: 30.22 m, EV13-4: 9.86 m) were retrieved by a
180 UWITEC piston coring system (www.uwitec.at). After the cores were split, photographed and described
181 lithologically, a final composite profile (EV13: 30.47 m) was compiled based on the correlation of
182 prominent marker layers (Wündsche et al., 2016b). The measured water depth at the core site was 6.0 m
183 on the 18.10.2013, with an assumed uncertainty of ± 0.2 m (gauge reading Eilandvlei = 0.48 m). The
184 height of the water surface at the coring location was measured on 24.10.2013 (gauge reading Eilandvlei
185 = 0.53 m) using differential GNSS (LEICA GS10 and GS15 receivers) with reference to the South
186 African network of permanent GNSS stations (TrigNet). The measured height of the water surface of
187 Eilandvlei was 32.205 m HAE ± 0.01 m = 1.465 m ALT ± 0.1 m based on the latest hybrid geoid model
188 of South Africa (SAGEOID10) (Chandler and Merry, 2010). The sediment/water interface at the coring
189 position was hence located at about 4.5 m below the present mean sea level (PSL).

190

191 ***3.3 Sediment core chronology***

192 An age-depth model for the EV13 core was established based on 24 radiocarbon ages (Wündsche et al.,
193 2016b). The chronology, revealing a basal age of 8920 $^{+200}_{-250}$ cal BP (Fig. 2) and an average sediment
194 accumulation rate of 3.9 mm yr⁻¹, considers temporal variations in the regional marine reservoir effect
195 (ΔR) affecting the EV13 core site throughout the Holocene (Wündsche et al., 2016b).



196

197
198
199
200

Fig. 2: ^{14}C based age-depth model for the EV13 sediment core as established by Wüdsch et al. (2016b). The blue areas represent the 2σ probability distributions of the calibrated ^{14}C ages; the blackish-grey area shows the 2σ age-depth relation as modelled by the R software package Bacon 2.2 (Blaauw and Christen, 2011).

201 **3.4 Sediment core subsampling and determination of the water content**

202 The EV13 core sections were subsampled with plastic syringes at 16 cm intervals and subsequently in
203 a finer resolution in core sections where major changes are indicated by additional investigations. In
204 order to determine the sediment water content (W in wt%), the wet mass (m_w) was weighed before and
205 the dry mass (m_d) after freeze-drying of the subsamples. W was then calculated as follows (Håkanson
206 and Jansson, 2002):

207

$$W = \frac{m_w - m_d}{m_w} \cdot 100 \quad (1)$$

208

209 **3.5 Grain size analyses**

210 For the sediment grain size analyses, subsamples (at 16 cm intervals) were initially treated with H_2O_2
211 (30%) and HCl (10%) to eliminate organic matter and carbonates, respectively. After which, a solution
212 of $\text{Na}_4\text{P}_2\text{O}_7 \cdot 10 \text{H}_2\text{O}$ (0.1 M) was added as a dispersion medium and the samples were shaken for 2 h.
213 Samples were then measured with a Laser Diffraction Particle Size Analyser (Beckman Coulter LS
214 13320) using the Aqueous Liquid Module. The optical light scattering was modelled based on the
215 Fraunhofer diffraction theory (de Boer et al., 1987). Samples were measured in several runs until a
216 reproducible signal was obtained; the first reproducible run was used for further statistical processing.
217 Subsequently, the grain size data were evaluated by means of a modified version of Gradistat 4.2 (Blott

218 and Pye, 2001) which provides sediment percentages for all grain size fractions as defined by Friedman
 219 and Sanders (1978). In order to reduce the number of fractions and to condense fractions that show
 220 similar trends, the obtained grain size data of these individual fractions were tested for correlations and
 221 subsequently grouped accordingly.

222

223 **3.6 Geochemical analyses**

224 The dried subsamples were ground (<40 µm) and homogenized. Aliquots were used for geochemical
 225 and mineralogical investigations. Sediment contents of total organic carbon (TOC) and total inorganic
 226 carbon (TIC) were determined at 16 cm intervals (Wüdsch et al., 2016b). For the preparation of the
 227 ICP-OES measurements, the ground subsamples were brought into solution using a microwave-
 228 supported, modified aqua regia digestion (1 ml deionised H₂O, 2 ml HCl 30 %, 4 ml HNO₃ 30 %). After
 229 which, element concentrations of Al, Ca, Fe, K, Na, and S were measured at 16 cm intervals (and
 230 additionally in a finer resolution in core sections where major changes occurred in the already measured
 231 and evaluated data) using a Varian 725-ES instrument. Concentrations of the elements Al, Br and Si
 232 were determined on the freeze-dried and ground samples at 32 cm intervals using a conventional XRF
 233 analyser (PANalytical Epsilon3-XL XRF spectrometer) (e.g., Häggi et al. 2016; Zhang et al. 2015).
 234 Additionally, the split cores were measured with an Avaatech XRF core scanner (Richter et al., 2006)
 235 at the University of Bremen. Preparation and measurements of the split cores were conducted as
 236 described in Tjallingii et al. (2007). Measurements were carried out in two runs with generator settings
 237 of 10 kV and 30 kV, respectively, to obtain a wide range of element intensities. However, the reliability
 238 of XRF scanning data can be reduced due to matrix effects or varying water contents (Tjallingii et al.,
 239 2007). Hence, in this work only the XRF scanning data for Br and Si/Al are shown, as for these data
 240 good correlations between the quantitative XRF and the XRF scanning data were obtained ($r(\text{Br})=0.95$;
 241 $r(\text{Si/Al})=0.68$).

242

243 *3.6.1 Calculation of the chemical index of alteration (CIA)*

244 The determined element concentrations of Al, Ca, K and Na were used to calculate the chemical index
 245 of alteration (CIA) representing an indicator for the degree of chemical weathering (Nesbitt and Young,
 246 1982):

$$247 \quad \text{CIA} = \frac{\text{Al}_2\text{O}_3}{\text{Al}_2\text{O}_3 + \text{CaO}^* + \text{Na}_2\text{O}^{**} + \text{K}_2\text{O}} \cdot 100 \quad (2)$$

248 The CaO* value represents the amount of CaO which is incorporated in silicates only and was therefore
 249 corrected for the Ca content that is bound in carbonates (Fedo et al., 1995; Nesbitt and Young, 1982).
 250 Similarly, the Na₂O** value solely represents the amount of Na₂O being contained in silicates. However,
 251 sediments at Eilandvlei interact with sea water from the Indian Ocean introducing considerable amounts
 252 of Na⁺ into the lake and eventually into the sediment pore water. During sample drying, the pore water
 253 was removed and the dissolved sea salts remained as solid phase in the sample. For the calculation of

254 the CIA, Na contents were corrected for sea salt-Na as it was suggested by other studies from marine-
 255 influenced environments (McLennan et al., 1990; Monien et al., 2011). It was found that corrections for
 256 sea salt-Na can be calculated considering the sediment water contents as well as the salinity of the pore
 257 waters (Monien et al., 2011). Hence, for the dried samples we corrected the measured total Na contents
 258 (Na_{total} in wt%) according to the following formula to obtain sea salt-corrected Na ($\text{Na}_{\text{corr.}}$ in wt%):

$$259 \quad \text{Na}_{\text{corr.}} = \text{Na}_{\text{total}} - \frac{W \cdot \text{Na}_w}{(100 - W) \cdot (100 - \text{Na}_w)} \cdot 100 \quad (3)$$

260 where W is the water content of the sample (in wt%) and Na_w (in wt%) represents the Na concentration
 261 sourced from sea salt in the pore waters. The median Na^+ concentration of the lake water in Eilandvlei
 262 was $1910 \mu\text{g ml}^{-1}$ for the period between 1977 and 2015 (DWS, 2015). Under the simplifying
 263 assumptions that the salinity (and thus the Na^+ concentration) at the core site was constant throughout
 264 time and the density of the pore water was 1 g ml^{-1} , the value of $1910 \mu\text{g ml}^{-1}$ was converted to
 265 0.191 wt% and plugged in for Na_w in equation (3).

266

267 *3.6.2 Correction of the total Br contents*

268 For the calculation of Br/TOC ratios, total Br contents were corrected by the amount of inorganic Br
 269 arising from dissolved Br^- ions in the marine-influenced pore water after sample drying. For that
 270 purpose, the mean inorganic Br concentration of 1 wt% interstitial water was estimated according to
 271 Ziegler et al. (2008) and dependent on the varying water contents, the inorganic Br contents were then
 272 calculated for each sample and eventually subtracted from the total Br concentrations to obtain an
 273 estimate for organic Br contents.

274

275 *3.7 Marine foraminifera*

276 In total, 60 subsamples, thereof 51 samples from the core and nine core catcher samples, were analysed
 277 for the micropalaeontological composition. The damp sediment samples were washed over a $200 \mu\text{m}$
 278 sieve with tap water after 1-2 h treatment with a weak H_2O_2 solution (~5%). Sieve residues were oven-
 279 dried at 60°C . All foraminifer tests were picked from the residues under a low-power stereo-microscope,
 280 or very rich samples were split before using a micro-splitter for obtaining a minimum of 300 individuals.
 281 The identification of picked foraminifera relies on Murray (1979), Lowry (1988), Scott et al. (2001) and
 282 Schmidt-Sinns (2008). All well-preserved tests were counted, disregarding strongly abraded,
 283 fragmented and such tests with sediment infill or heavy incrustations.

284 Ecological classification used here relies mainly on Murray (2006) and distinguishes between
 285 stenohaline benthic Foraminifera living (almost) exclusively within the marine salinity range (30-40‰),
 286 other benthics intruding or living in brackish waters and planktic taxa. This classification is used for
 287 identification of marine influence and salinity range at the coring site over time.

288

289

290 **3.8 Diatoms**

291 Fossil diatom frustules were extracted from the sediment matrix at a 16 cm resolution generating 174
292 samples, then treated with 30% H₂O₂ and 10% HCl to remove organics and carbonates, respectively.
293 Thereafter, coarse grained particulates and clay were removed from the resultant residue by a series of
294 sieving, swirling and settling (Battarbee, 1986). The concentrated solution of diatom frustules was dried
295 on a coverslip, mounted on a slide in Pleurax and counted under a light microscope at a magnification
296 of up to X1000. Identification of diatom species were based on available diatom manuals and online
297 reference systems (e.g., Kelly et al., 2005; Taylor et al., 2007). A minimum count of 300 frustules had
298 to be achieved for the sample to be included in the analysis. To summarise the variability in the diatom
299 assemblage principal component analysis (PCA) was conducted on the raw percentage diatom data. The
300 analysis excluded species deemed as rare, in this case all species that occur less than 5% throughout the
301 record. The PCA was performed using the package VEGAN v2.0-5 in the open-source statistical
302 software R (Oksanen et al., 2013).

303

304 **4 Results and interpretations**

305 **4.1 Seismics**

306 A total of five seismic units (A-E) are identified from the sub-bottom profiling survey. The basal unit A
307 is acoustically impenetrable geological bedrock, which is intercepted 100-150 m below the lakefloor
308 and is inferred to represent well-consolidated Mesozoic sedimentary rocks of the Uitenhage Group
309 (Fig. 3). Unit A is overlain by stacked, high-relief, deposits (unit B) which are suggested to represent
310 aeolianite based on correlations to locally exposed geological outcrops (e.g., Bateman et al., 2004, 2011;
311 Illenberger, 1996) and submerged units in the adjacent Wilderness embayment lakes (Cawthra et al.,
312 2014). The seismic character of aeolianite is dominated by chaotic internal reflectors and calcretised
313 surfaces which generate acoustic impedance. A massive, acoustically-transparent, package of
314 unconsolidated sediment drapes the bedrock and aeolianite which lacks discernible or clear reflectors
315 and reaches a maximum thickness of 12 m. Evidence of draping within the swales of aeolianite
316 topography suggests that these deposits infilled the existing basin at relatively high rates of
317 sedimentation. This unit was not sampled, but might be composed of mixed terrestrial and marine
318 sediment (unit C). Core EV13 penetrates the uppermost two seismic units D and E (Fig. 3). Unit D
319 attains a thickness of up to 20 m and this wedge is bounded by upper and lower reflectors which mark
320 changes in density and depositional style. The geometry of the reflectors within unit D is sub-parallel
321 with evidence for subtle retrogradation indicating transgressive conditions. Unit E is masked by source
322 ringing of the seismic system in the uppermost part of the deposit and reflectors are obscured by shallow
323 multiples. However, the high organic content of the sediments (Wündsche et al., 2016b) renders the
324 deposits acoustically impenetrable to resolve structures. The maximum thickness reached of unit E is
325 11 m.

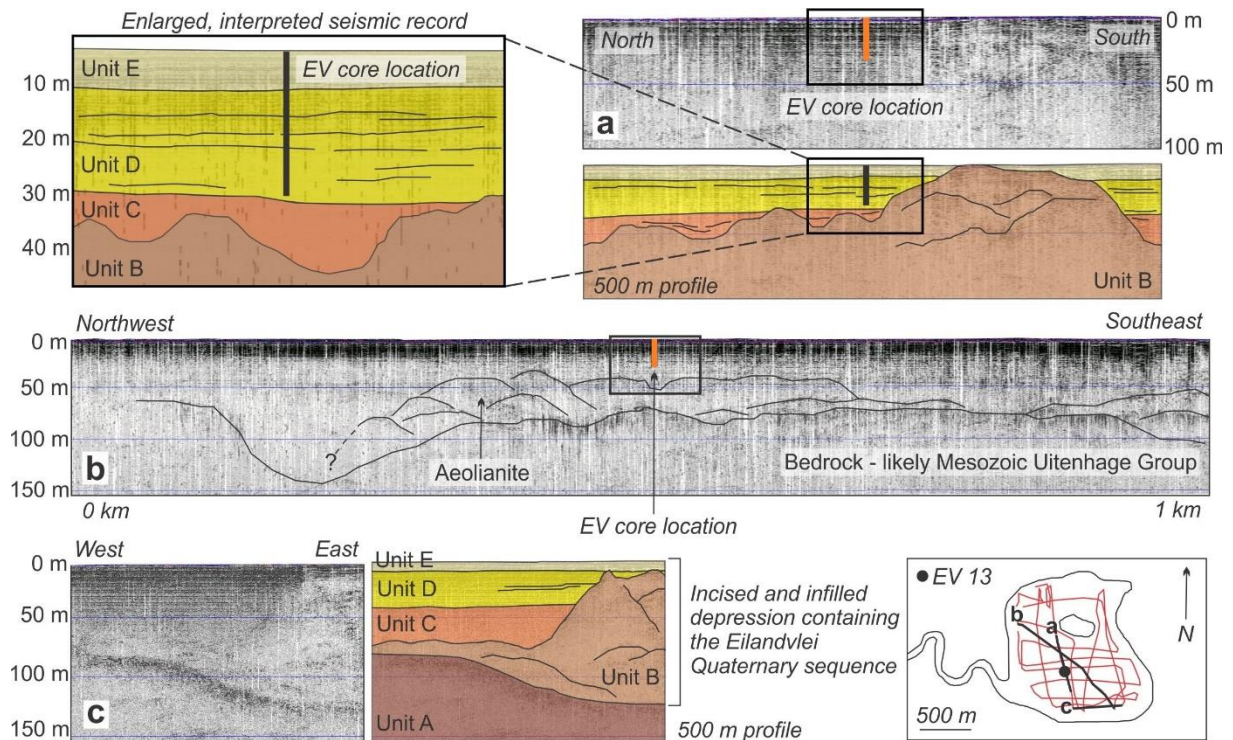


Fig. 3: Boomer seismic profiles in Eilandvlei and annotated interpreted units. Five packages dominate the sequence across all profiles gathered, and these are composed of bedrock (unit A), aeolianite (unit B), acoustically transparent sediments (unit C), and the packages intercepted and sampled by core EV13 (Units D and E). The maximum penetration of the boomer sub-bottom profiler was 150 m in Eilandvlei.

4.2 Geochemical, grain size and micropalaeontological data

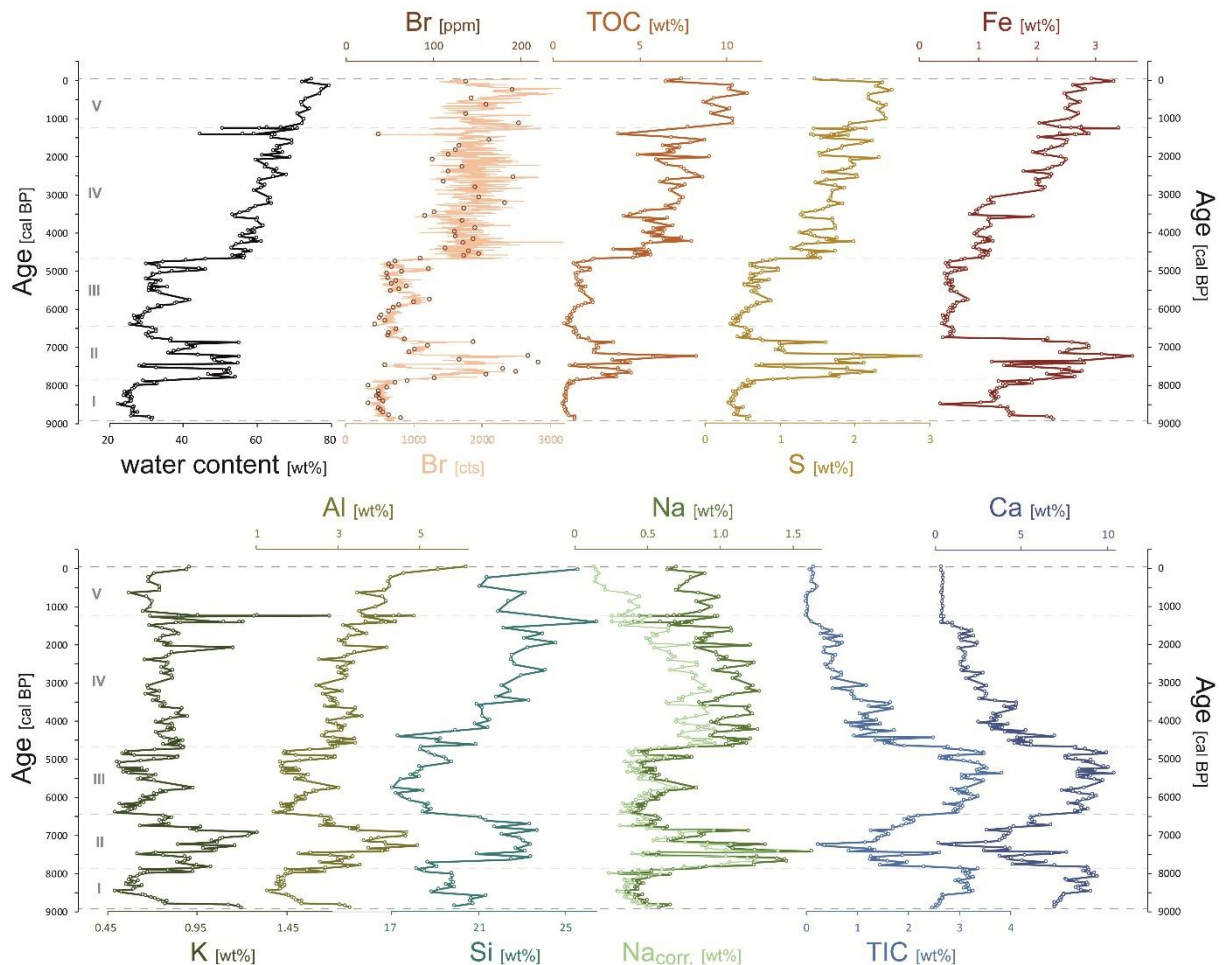
Based on marked shifts in the lithology and TIC data, the EV13 sediment core was subdivided in five units (Wündsche et al., 2016b): unit I (8920-7870 cal BP), II (7870-6440 cal BP), III (6440-4670 cal BP), IV (4670-1240 cal BP) and V (1240 cal BP-present). The core units I-III correspond to the seismic unit D and core units IV-V coincide with seismic unit E.

4.2.1 Proxies for changes in marine influence

TIC and Ca

The Ca and TIC data reveal a strong correlation ($r=0.99$; Fig. 4) indicating that nearly all Ca and TIC are bound as calcium carbonate. TIC and Ca contents are high in units I and III. In contrast, units II and IV are characterized by distinctly lower values and unit V contains only negligible concentrations of TIC and Ca.

High (low) Ca and TIC values reflect high (low) proportions of carbonates which were probably deposited as biogenic remains or precipitated chemically from the water column due to an increased (decreased) marine influence on the EV13 core site. The interpretation of Ca and TIC as marine indicators is consistent with other studies from marine environments (e.g., Govin et al., 2012; Peterson et al., 2000).



352

353

354

355

356

357 *Br/TOC*358 Total Br and TOC concentrations are well-correlated ($r=0.85$; Fig. 4) indicating that the main part of Br

359 is bound in or adsorbed to organic matter. Br and TOC contents are low in units I and III and high in

360 units II, IV and V (Fig. 4). The Br/TOC ratios show a distinct shift between the units III and IV. While

361 units I-III are characterized by high Br/TOC ratios with slightly lower ratios in parts of unit II, in

362 contrast, units IV-V reveal lower ratios (Fig. 5).

363

364

365

366

367

368

369

370

371

372

Fig. 4: Water content and geochemical element concentrations of the EV13 record: ICP-OES data: Al, Ca, Fe, K, Na and S as well as sea salt-corrected Na ($Na_{corr.}$); conventional XRF analyser data: Br and Si; and XRF scanning data: Br, TIC and TOC data were obtained by Wündsche et al. (2016b). The core units are given on the left and indicated as grey dashed lines.

373 *TOC/S*

374 S contents are strongly correlated with the TOC data ($r=0.92$; Fig. 4). TOC/S ratios reveal a marked
 375 shift at the transition from unit III to IV. TOC/S ratios are low in units I-III and distinctly higher in units
 376 IV-V (Fig. 5). This distinct shift in the TOC/S ratios is also visible in a cross plot of TOC versus S
 377 (Fig. 6) revealing that the data of the units I-III plot close along the line representing a ratio of
 378 $TOC/S=2.8$, which is typical for Holocene “normal” marine sediments (Berner, 1982; Berner and
 379 Raiswell, 1983; Lyons and Berner, 1992; Morse and Berner, 1995). In contrast, data points of units IV-V
 380 plot along a regression line with a distinct non-zero intercept on the S-axis, which might reflect that
 381 these sediments were deposited under euxinic or semi-euxinic conditions during which the water
 382 column was intermittently stratified with oxygen-depleted bottom waters (Raiswell and Berner, 1985).

383

384 *Diatoms*

385 The full diatom assemblage of the investigated EV13 core is given in Kirsten et al. (subm.). The PCA
 386 identified two axes of significance, which explained 36% of the total variance. The first axis indicates a
 387 strong relationship between the structure of the diatom community and marine inputs, thus the primary
 388 factor influencing the system is marine waters. The second axis is linked to changes in freshwater inputs
 389 into the system promoting a community more tolerant of a dilute-brackish environment. Principal
 390 component (PC) 1 has large positive loadings on marine diatoms such as *Dimeregramma minor var.*
 391 *minor*, *Dimeregramma minor var. nanum* and *Delphineis minutissima* and large negative loadings on
 392 transitional and dilute taxa, which are able to tolerate a variable degree of freshwater inputs. This
 393 includes *Cyclotella caspia*, *Cocconeis placentula* and *Navicula cryptocephala*. The PC 1 data shows a
 394 similar pattern across the record as the Ca contents with increased values in units I and III, slightly lower
 395 values in unit II as well as a decreasing trend in unit IV and low values in unit V (Fig. 5).

396

397 *Marine foraminifera*

398 Foraminifer taxa classified as marine comprise, in order of abundance, *Challengerella*, large and heavily
 399 ornamented *Ammonia*, *Spiroloculina*, Textulariinae, *Quinqueloculina*, *Elphidium* (with acute
 400 periphery), *Pararotalia*, *Triloculina* and *Cibicides/Lobatula*; very rare are *Bulimina*, *Glabratella*,
 401 *Planorbulina*, *Rosalina bradyi*, *Spirillina* and unilocular lagenids. High proportions of marine
 402 foraminifera occur within unit I, the top of unit II and the base of unit III. The base of unit II and large
 403 parts of unit IV reveal lower percentages, whereas marine foraminifera are absent at the top of unit IV
 404 and throughout unit V (Fig. 5).

405 The marine foraminifera document the impact of marine waters in a coastal setting as well as
 406 normal marine salinity if they are autochthonous. Such a marine impact could be strong and regular
 407 water exchange in an embayment or estuary. Continuous dominance of marine foraminifers is typical
 408 for a normal marine habitat, i.e., an embayment, outer estuary or lagoon prone to strong water exchange
 409 with the open sea. High proportions of marine foraminifers in the EV13 record hence reflect an open

410 bay or outer estuary under marine salinity, whereas decreased marine foraminifer proportions are
411 indicative of a deteriorating water exchange.

412

413 *4.2.2 Proxies for changes in terrestrial sediment deposition*

414

415 *Terrigenous element (Al, Fe, K, Na, Si) concentrations, Si/Al ratios and grain size data*

416 Compared to the Ca and TIC data, generally inverse patterns can be observed for most of the terrigenous
417 elements like Al, Fe, K, Na, and Si (Fig. 4). These element concentrations are low in unit I and moderate
418 to high in unit II. Similar to unit I, unit III reveals low Al, Fe, K, Na, and Si contents. An abrupt shift in
419 the data is conspicuous at the transition from unit III to IV. Al, Fe, K, Na, and Si concentrations are
420 enriched in unit IV relative to unit III. Whilst Al, Fe and Si data show an increasing trend throughout
421 units IV and V, K contents oscillate around a relatively constant level and Na concentrations decrease.

422 The terrigenous sediments were deposited probably after both fluvial and aeolian transport.
423 Similar to other studies (Haug et al., 2001; Peterson et al., 2000), high Fe values in the EV13 record are
424 interpreted to reflect a high proportion of terrigenous sediments that were deposited during periods of
425 generally increased regional precipitation amounts and river discharge in the Eilandvlei watershed.

426 Especially remarkable are three distinct peaks in the K data (and less pronounced in Al and Fe)
427 at 2070 ⁺¹⁹⁰/₋₁₆₀, 1410 ⁺¹²⁰/₋₁₂₀ and 1250 ⁺¹³⁰/₋₁₆₀ cal BP (Fig. 4) which are related to three sediment layers
428 with a clearly different colour compared to the sediments above and below. It is hypothesized that these
429 layers were deposited after short extreme rainfall events, possibly supplying high amounts of K-rich
430 shales from the upper catchment in the Outeniqua Mountains.

431 Si/Al ratios are low at the base and at the top of unit I and distinctly increased in between. They
432 remain low in unit II and fluctuate around intermediate values in the units III and IV. At the top of unit
433 IV, Si/Al ratios decrease and remain low in unit V (Fig. 5). Si/Al ratios most likely reflect variations in
434 the proportion of quartz to feldspars and other aluminosilicates (Jones and Bowser, 1978). Accordingly,
435 Si/Al ratios are well-correlated with the 31-250 µm grain size fraction (very coarse silt to fine sand) and
436 inversely correlated with the <16 µm grain size data (clay to medium silt) (Fig. 5). High Si/Al ratios are
437 possibly related to greater contributions of sand from the surrounding dune cordons. The unconsolidated
438 Holocene cover sands on top of the cemented Pleistocene aeolianites are mainly composed of quartz
439 sand with 58 % fine, 40 % medium, and 1 % coarse sands (Bateman et al., 2011). Higher amounts of
440 these dune sands possibly reached the EV13 core site by aeolian transport during drier periods with less
441 vegetation cover on the dunes following the interpretations of Martin (1968) and Wündsche et al. (2016a).

442

443 *Chemical index of alteration (CIA)*

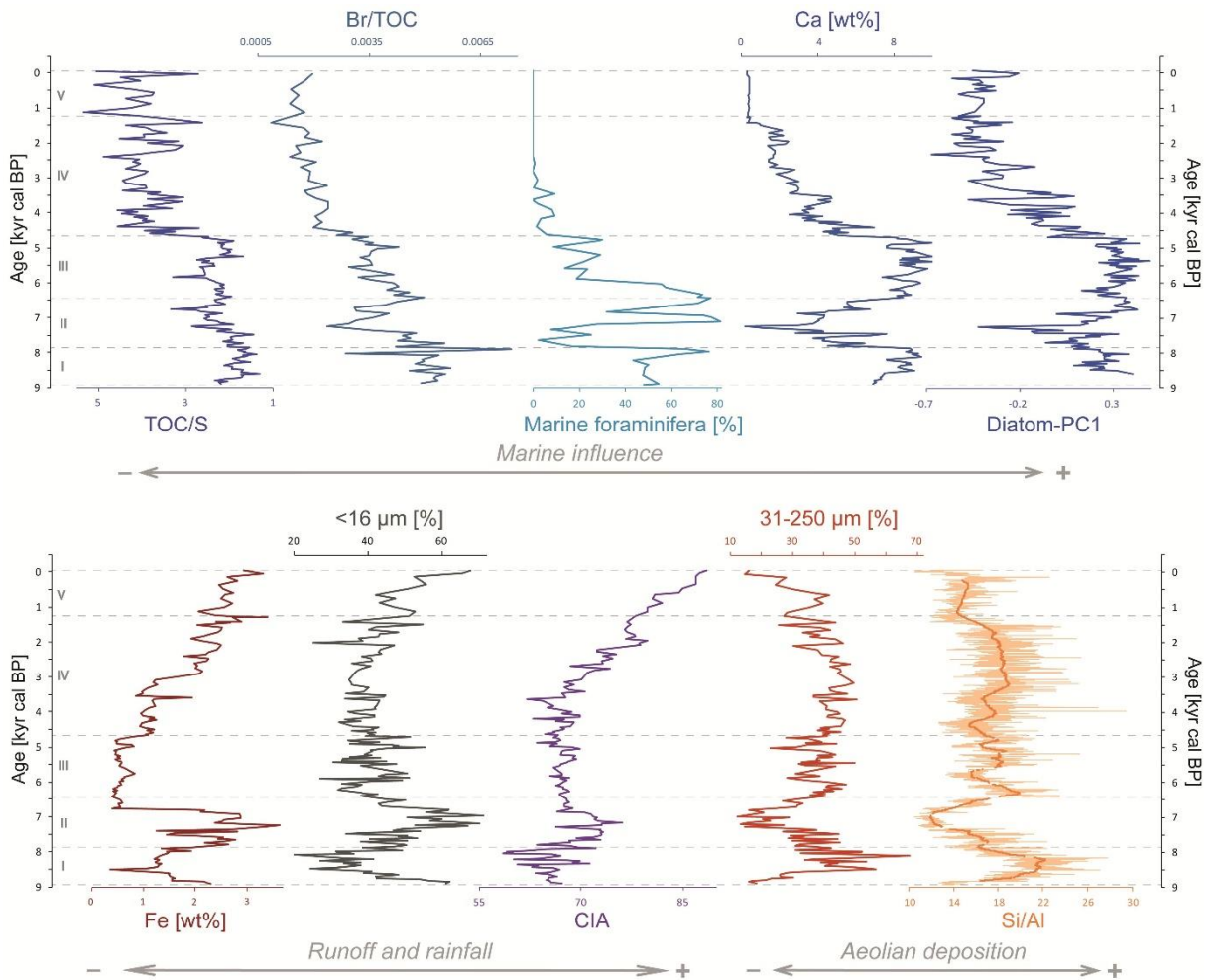
444 For the calculation of the CIA, CaO* was set to zero in equation (2) as nearly all Ca is bound in
445 carbonates. The CIA values in unit I are varying between 58 and 72 (Fig. 5). Within unit II, the CIA
446 ranges from 63 to 76. In unit III and the lower part of unit IV (6440-3000 cal BP), CIA values are lying

447 between 62 and 70. Throughout the upper part of unit IV as well as unit V (3000 cal BP-present), the
448 CIA values (between 68 and 89) show an increasing trend reaching the highest CIA=89 of the entire
449 record at the topmost sample.

450 The CIA was established as an indicator for the degree of chemical (silicate) weathering of rocks
451 and sediments, a process whose intensity strengthens with increasing humidity (Nesbitt and Young,
452 1982). While unweathered feldspars typically show CIA values around 50, the leaching of alkali and
453 alkaline earth elements during chemical weathering produces CIA values close to 100 for kaolinite
454 (Nesbitt and Young, 1982). Although some studies demonstrated the restrictions for the use of the CIA
455 as palaeoclimatic proxy (Goldberg and Humayun, 2010; Li and Yang, 2010; Shao et al., 2012; Xiao et
456 al., 2010), others plausibly linked variations in the CIA of lake sediment records to palaeohydrological
457 changes in the watersheds (Brisset et al., 2013; Minyuk et al., 2007; Nath et al., 2000; Roy et al., 2008,
458 2012). Our CIA data include a degree of uncertainty as the applied constant past salinity for the sea salt-
459 Na correction in equation (3) is most likely not true for the entire period covered by the EV13 record.
460 Nevertheless, the CIA and the <16 μm grain size data are significantly correlated supporting the
461 reliability of at least the major trends in the data (Fig. 5), since a progressing weathering is usually
462 associated with decreasing grain sizes (Shao et al., 2012). Whether the CIA data truly reflect variations
463 in catchment weathering rates or if fine-grained material (with higher CIA values) is preferentially
464 transported during periods of increased rainfall remains unclear, but in both cases high CIA values could
465 indicate wetter conditions. The CIA and <16 μm grain size data moreover show a similar pattern as the
466 Fe record (Fig. 5). It is hence concluded that they reveal the similar palaeoenvironmental signal, namely
467 that the deposition of fine-grained, more weathered, and iron-rich material is linked to increased regional
468 precipitation and river discharge in the watershed of Eilandvlei.

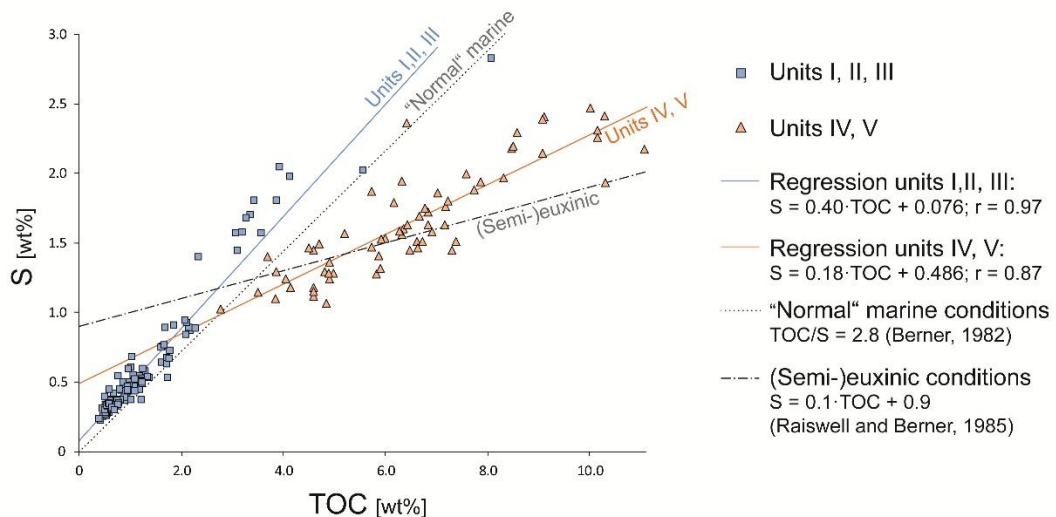
469 Summarizing, these proxies suggest that the periods between 8920-7870 cal BP and 6440-
470 3000 cal BP were characterized by a low to moderate terrestrial sediment supply to Eilandvlei and hence
471 relatively low rainfall and river runoff. Moreover, it is indicated that the (aeolian) deposition of dune
472 sands was increased, possibly due to a less dense vegetation cover on the dunes and/or increased wind
473 strengths. By contrast, high terrigenous sediment inputs due to increased rainfall and runoff are indicated
474 for the periods between 7870-6440 cal BP and 3000 cal BP-present.

475



476
477
478
479
480
481

Fig. 5: Top: Proxies interpreted as reflecting the degree of marine influence at the EV13 core site during sediment deposition: TOC/S, Br/TOC, marine foraminifera, Ca and the diatom principal component (PC) 1. Bottom: Interpreted palaeoclimatic proxies reflecting river runoff and rainfall in the Eilandvlei catchment (Fe, grain size fraction <16 μm, chemical index of alteration (CIA)) as well as the deposition of sand (Si/Al XRF scanning data with a 100-point running mean and grain size fractions 31-250 μm).



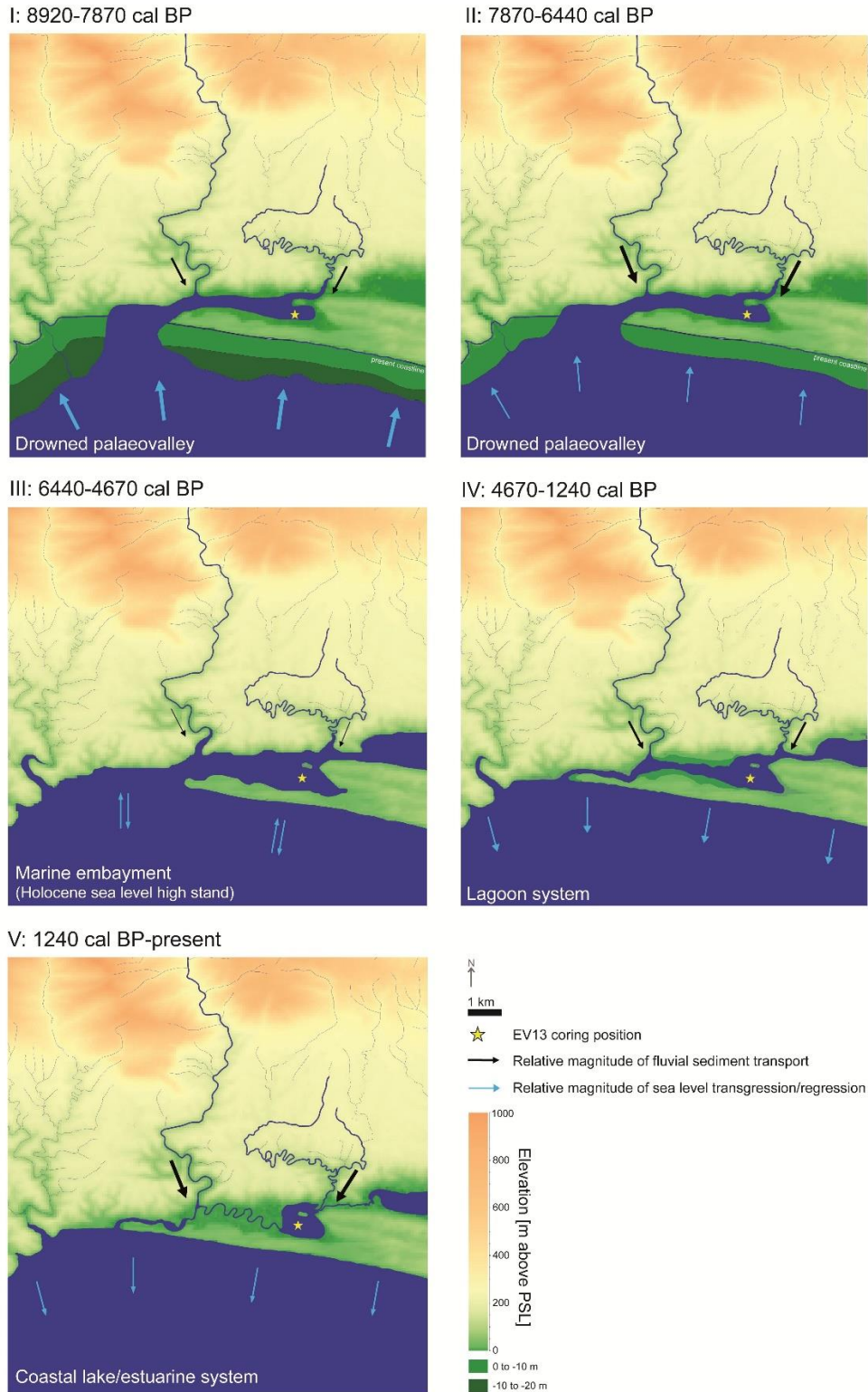
482
483
484
485
486
487
488
489
490
491

Fig. 6: Cross plot of TOC versus S: data from the core units I, II and III plot along the regression line $S = 0.4 \cdot \text{TOC} + 0.076$, which is similar to that typical for sediments deposited under "normal" marine conditions ($\text{TOC}/\text{S} = 2.8$; Berner, 1982). Data from the units IV and V reveal a regression line of $S = 0.18 \cdot \text{TOC} + 0.486$ possibly indicating (semi-)euxinic conditions ($S = 0.1 \cdot \text{TOC} + 0.9$; Raiswell and Berner, 1985) during deposition. TOC and S data in the cross plot are presented on a CaCO_3 -free basis in order to avoid spurious correlations which may arise due to dilution effects (Raiswell and Berner, 1985).

492 **5 Discussion**

493 **5.1 Coastal lake development in consequence of Holocene sea level and climate change**

494 Building on the approach of Bateman et al. (2011), who reconstructed the Pleistocene evolution of the
 495 Wilderness embayment, Fig. 7 provides a sketch of its possible Holocene development based on the
 496 results obtained in this study.



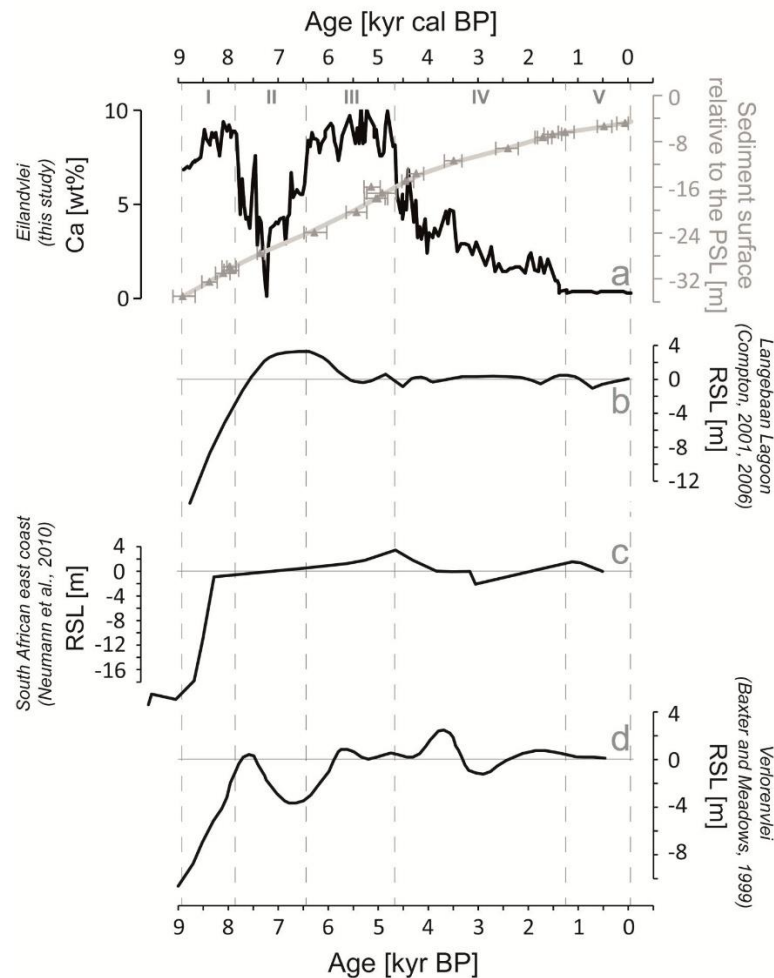
497

498 Fig. 7: Sketch of the Holocene evolution of the Wilderness embayment towards the present coastal lake/estuarine system. The
 499 maps were created by means of the software QGIS 2.16.3 using 90 m SRTM DEM data from Jarvis et al. (2008); the offshore -10
 500 and -20 m isobaths according to Birch et al. (1978) were used to indicate the possible palaeo-coastlines in the two topmost figures.

501 *Unit I: 8920-7870 cal BP (~35-30 m below PSL)*

502 The proxies reflecting the degree of marine impact (Ca, TOC/S, Br/TOC, diatom PC 1, marine
503 foraminifera; Fig. 5, 6) indicate that marine conditions prevailed at the EV13 position between 8920 and
504 7870 cal BP. Comparisons with sea level reconstructions reveal that the post-glacial transgression
505 caused a rapid sea level rise from more than 10 m below PSL at 8920 cal BP to nearly the height of the
506 PSL at 7870 cal BP (Fig. 8) (Baxter and Meadows, 1999; Camoin et al., 1997; Clark and Lingle, 1979;
507 Compton, 2001, 2006; Fleming et al., 1998; Neumann et al., 2010; Ramsay, 1995). Hence, the shore
508 line at the southern Cape coast must have been located generally further offshore at 8920 cal BP than at
509 present, but the EV13 core site was already flooded with sea water (Fig. 7). The Wilderness embayment
510 was probably connected to one or more palaeovalleys which had formed at lower sea levels during the
511 Pleistocene by fluvial erosion of the Duiwe and Touw rivers (Bateman et al., 2011; Cawthra et al., 2014).
512 During the post-glacial sea level rise these palaeovalleys and the Wilderness embayment were flooded
513 (Fig. 7, 8) creating drowned valleys similar to other coastal areas in New Zealand (Abraham et al., 2008),
514 the United States (Zaremba et al., 2016) and France (Traini et al., 2013). Our seismic data show that the
515 Holocene sediments with more than 30 m thickness (in some parts >100 m) were deposited over nearly
516 the whole north-south extension of modern Eilandvlei (Fig. 3). This indicates that not only a relatively
517 narrow river valley was drowned, but that a wider, low-lying depression must have been located within
518 the embayment, which possibly formed due to previous sea level changes and the associated evolution
519 of an initial back-barrier lagoon system during the Pleistocene (Bateman et al., 2011). Additionally, the
520 system was probably modified repeatedly by the through-flowing Duiwe and Touw rivers.

521 The proxies reflecting the deposition of terrigenous sediments that were brought by the
522 inflowing rivers (e.g., Fe, CIA) point to relatively low to moderate inputs of weakly weathered sediments
523 during this time (Fig. 5). High proportions of deposited coarse-grained quartz (Si/Al, 31-250 μm
524 fraction) may reflect the increased (aeolian) input of dune sands. It is concluded that regional rainfall
525 and river discharge was relatively low and movement of sands was possibly favoured by a less dense
526 vegetation cover on the dunes.



527

528 Fig. 8: Comparison of a) Ca data as well as the calibrated ¹⁴C ages (grey triangles) and the modelled age-depth relation for the
 529 EV13 record (grey line; representing the past sediment surface relative to the present mean sea level (PSL)) with relative sea
 530 level (RSL) reconstructions from b) Langebaan Lagoon (Compton, 2001) revised by Compton (2006); c) several sites at the South
 531 African east coast (Ramsay, 1995; Ramsay and Cooper, 2002), the sea level curve is shown as revised by Neumann et al. (2010);
 532 d) Verlorenvlei (Baxter and Meadows, 1999). Note that curves a, b and c refer to calibrated and d to conventional ¹⁴C years BP.
 533

534 *Unit II: 7870-6440 cal BP (~30-24 m below PSL)*

535 Holocene sea level reconstructions suggest a reduction of the speed of the sea level rise during this time
 536 (Fig. 8). The sea level likely reached and exceeded the height of the PSL. The water level in the drowned
 537 palaeovalley probably rose, progressively flooding more parts of the Wilderness embayment and
 538 widening the submerged area (Fig. 7).

539 The high proportion of terrestrial sediments (high Fe, Al, K, Na) deposited during this time point
 540 to generally increased river discharge and rainfall. This is supported by the high values of the <16 μm
 541 fraction and the CIA reflecting the deposition of more weathered material. Some of the marine proxies
 542 (Ca, marine foraminifera, diatom PC1) show lower values which might reflect dilution effects by
 543 increased river discharge and freshwater inputs. Nevertheless, the TOC/S data still point to “normal”
 544 marine conditions (Fig. 5, 6) and the core site was probably still dominated by sea water due to the
 545 strong connection between the embayment and the ocean during this time. Some of the marine (Ca,
 546 diatom PC1) and terrestrial (Fe, Al, K) proxy data reveal distinct and inversed variations (Fig. 4, 5)
 547 suggesting that the Wilderness embayment passed through a highly dynamic period which was

548 characterized by both advancing marine inundations as well as increased fluvial sediment and freshwater
549 supply.

550

551 *Unit III: 6440-4670 cal BP (24-16 m below PSL)*

552 Most of the marine proxies (Ca, TOC/S, Br/TOC, diatom PC 1) indicate fully marine conditions at the
553 core site between 6440 and 4670 cal BP. Although differing in the exact timing of the maximum high
554 stand, various studies agree that higher sea levels prevailed during the mid-Holocene than at present
555 (Baxter and Meadows, 1999; Clark and Lingle, 1979; Compton, 2001, 2006; Marker and Miller, 1993;
556 Ramsay, 1995) (Fig. 8). Thus, the Wilderness embayment was probably submerged entirely with a
557 relatively wide and well pronounced connection to the ocean (Fig. 7). The Holocene maximum sea level
558 at Eilandvlei likely occurred at the latest between 6440 and 4670 cal BP as the EV13 proxies point to a
559 strong marine impact during this time (Fig. 5). This is supported by evidence from an exposed shell bed
560 near Knysna (ca. 40 km east of Eilandvlei) indicating a maximum high stand of approximately 3 m
561 above PSL at 6300 cal BP (Compton, 2001; Marker and Miller, 1993).

562 Terrigenous proxies (Fe, CIA) suggest reduced fluvial sediment supply from the catchment as
563 well as low to moderate weathering of the sediments (Fig. 5), which might reflect generally decreased
564 regional rainfall and river discharge. However, the deposition of fluvial sediments at the EV13 core site
565 might be reduced due to the high sea level causing a strong marine impact as well as greater distances
566 between the core site and the mouths of the Touw and Duiwe rivers. The increased deposition of coarse-
567 grained quartz (high values for Si/Al, 31-250 μm fraction) might reflect enhanced aeolian transport in
568 the catchment due to a less dense vegetation cover on the dunes, higher mean wind strengths and/or
569 more frequent storm events.

570

571 *Unit IV: 4670-1240 cal BP (16-6.4 m below PSL)*

572 At 4670 cal BP, all marine proxies show a marked and relatively abrupt shift towards a reduced marine
573 impact at the core site (Fig. 5). This significant change reflects the increasing separation of the marine
574 embayment from the ocean due to a dropping sea level after the Holocene maximum high stand (Fig. 8).

575 As in unit III, terrigenous proxies (Fe, CIA) indicate prolonged low rainfall and river discharge
576 between 4670 and 3000 cal BP as well as increased aeolian deposition of dune sands (Si/Al, 31-250 μm
577 fraction). At Groenvlei, a lake ~20 km east of Eilandvlei (Fig. 1b), the increased deposition of sand
578 between 4200 and 2700 cal BP was also interpreted as enhanced aeolian transport due to drier conditions
579 and a less dense vegetation cover on the dunes (Martin, 1968; Wündsche et al., 2016a). Furthermore,
580 Bateman et al. (2011) identified a major phase of unconsolidated sand movement at the Wilderness
581 dunes between 3700 and 2400 cal BP. Together with a dropping sea level, the sand movement may have
582 contributed to a narrowing of the connection between the ocean and the Wilderness embayment that
583 probably developed into a lagoon system (Fig. 7). The transition from a marine embayment to a lagoon
584 stage is in agreement with previous sediment studies from Eilandvlei (Kirsten, 2014) and Groenvlei

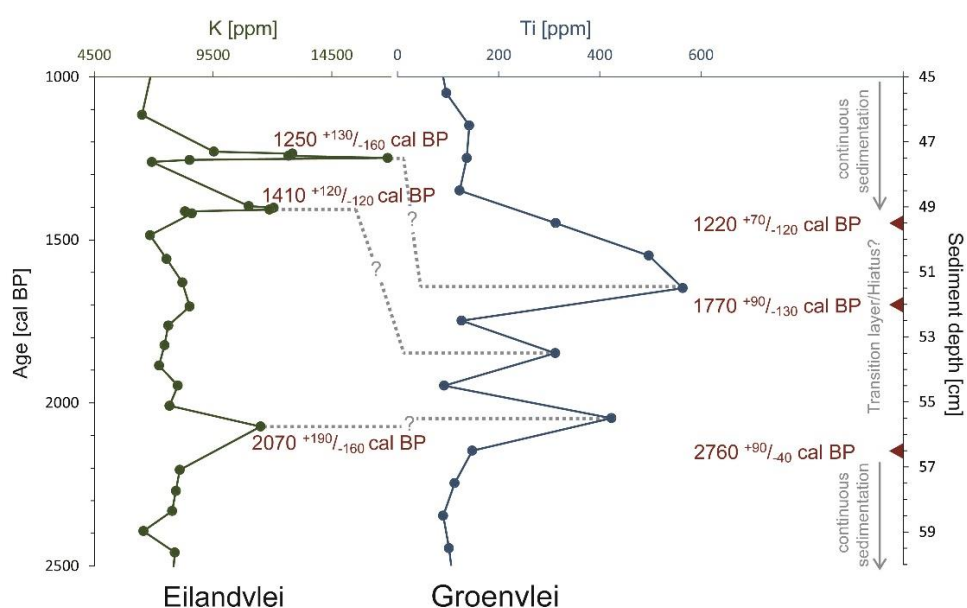
585 (Martin, 1959, 1968). The increased TOC/S ratios possibly reflect a transition of the water composition
 586 within the Wilderness embayment to (semi-)euxinic conditions (Raiswell and Berner, 1985) (Fig. 5, 6).
 587 The progressing separation of the embayment led to reduced exchanges between the water masses of
 588 the lagoon with those of the ocean, which would have increased the influence of freshwater inputs from
 589 the rivers on the total water composition at the core site. During times of decreased wind stress, this
 590 possibly resulted in the intermittent formation of an oxygen-depleted bottom water layer.

591 Between 3000 and 1240 cal BP, terrigenous proxies (Fe, CIA) suggest progressively increasing
 592 rainfall and river discharge in the area (Fig. 5). At 2070 $^{+190}_{-160}$, 1410 $^{+120}_{-120}$ and 1250 $^{+130}_{-160}$ cal BP,
 593 marked peaks in the K data indicate that three extreme rainfall and runoff events occurred within a short
 594 period. Similarly, the occurrence of heavy rainfall events has been reconstructed at Groenvlei, where
 595 the timing of these events could only be roughly estimated for the period between 2710 and 1210 cal BP
 596 BP (Wündsich et al., 2016a). It is suggested that the event layers recorded at Eilandvlei and Groenvlei
 597 can be correlated to each other (Fig. 9) reflecting the regional occurrence of heavy rainfall events.

598

599 *Unit V: 1240 cal BP-present (6.4-4.5 m below PSL)*

600 The marine proxies indicate a reduced marine impact on the core site. A clear shift in the Ca and TIC
 601 data towards lower values reveals that negligible amounts of carbonates were deposited since
 602 1240 cal BP. The sea level probably reached its present height (Fig. 8) and the present-day
 603 lacustrine/estuarine coastal lake system developed (Fig. 7). This coincides with previous studies from
 604 Groenvlei which turned into a freshwater system with decreased marine influence since 1210 cal BP
 605 (Wündsich et al., 2016a). Terrigenous proxies (Fe, CIA) indicate increased precipitation and runoff,
 606 although the climatic signal might be superimposed by human impact in the lake catchment since the
 607 late 19th century (Reinwarth et al., 2013).



608
 609
 610
 611
 612

Fig. 9: Comparison of K data from the EV13 record (plotted on age scale for the period from 2500 to 1000 cal BP) with Ti data from the Groenvlei sediment core between 60 and 45 cm sediment depth (Wündsich et al., 2016a). On the right, three calibrated ^{14}C ages from the Groenvlei core are shown (triangles). A possible linkage between three peaks in both data sets - each interpreted as heavy rainfall events - is indicated by grey dotted lines.

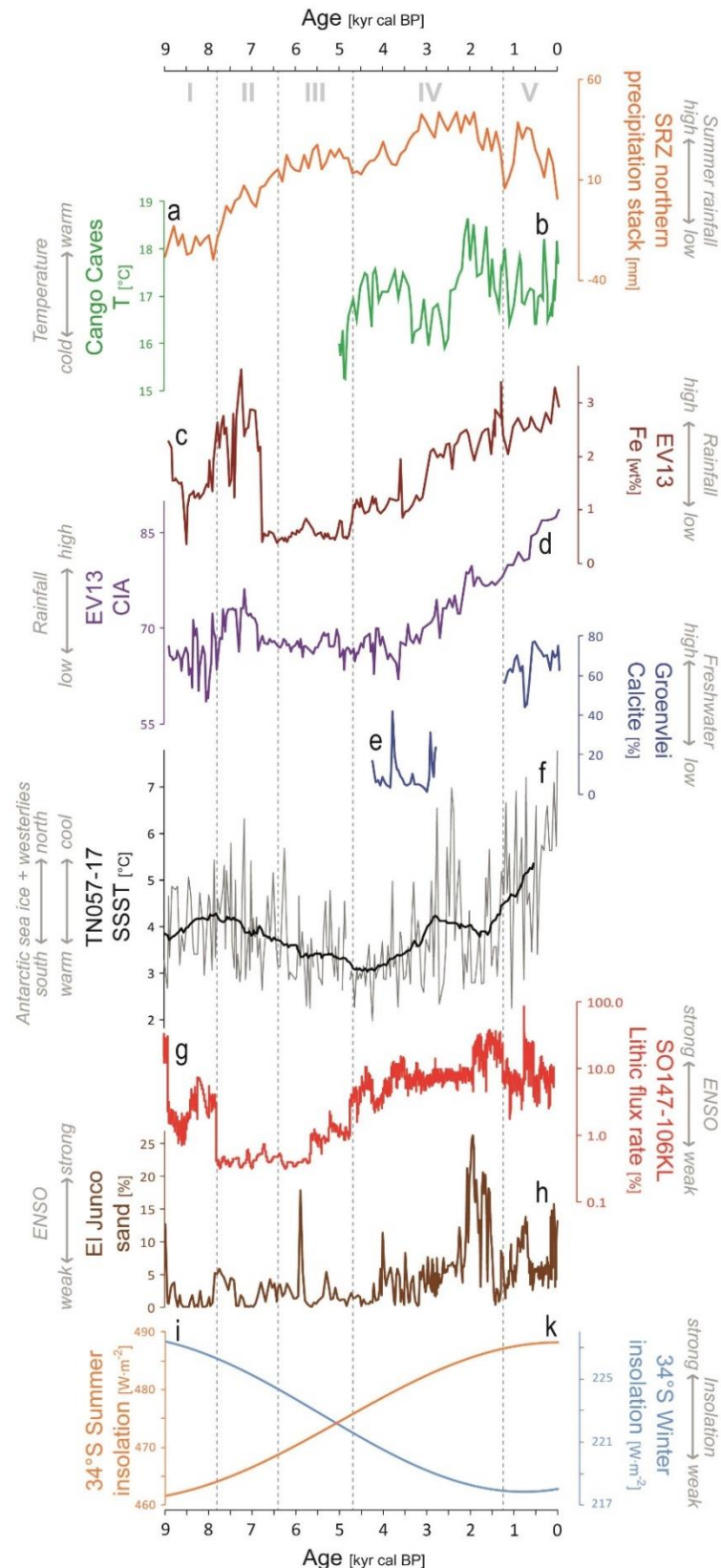
613 **5.2 (Trans)regional palaeoclimatic correlations and implications**

614 The presented EV13 data bear resemblances to trends found in other palaeoenvironmental
615 reconstructions from the Wilderness region. Previous investigations were conducted on sediment cores
616 from Groenvlei (Martin, 1959, 1968; Wündsche et al., 2016a), suggesting relatively drier climates than
617 at present between 4210 and 2710 cal BP and more humid conditions comparable to the present from
618 1210 cal BP onwards possibly interrupted by slightly drier conditions during the time period of the Little
619 Ice Age (LIA; 610-140 cal BP) (Wündsche et al., 2016a). The general trend from drier to wetter
620 conditions at Groenvlei since 4210 cal BP was inferred from distinct shifts in the sedimentary calcite
621 contents which were interpreted as freshwater proxies and which are in good agreement with the data
622 from Eilandvlei presented in this study (Fig. 10c, d, e). The terrigenous proxies from the EV13 record
623 (Fe, CIA) also suggest reduced rainfall prior to ~3000 cal BP and an increasingly wetter climate
624 thereafter, however no expression of a drier phase during the LIA is visible in this data.

625 The local mean summer (winter) insolation at Eilandvlei (~34°S) rose (diminished) throughout
626 the Holocene (Fig. 10i, k; Berger and Loutre, 1991), which may have influenced temperatures and
627 evaporation especially at the Agulhas Bank off the Wilderness embayment. During the late Holocene, a
628 distinct temperature rise was inferred from a speleothem record from the Cango Caves (~75 km
629 northwest of Eilandvlei; Talma and Vogel, 1992) at 2500 cal BP (Fig. 10b). A higher solar insolation,
630 higher air and sea surface temperatures probably increased evaporation which possibly contributed to
631 an enhanced uptake of moisture by onshore flowing air and increased rainfall amounts at the southern
632 Cape coast during the late Holocene as recorded by the EV13 data.

633 A multi-proxy record of Holocene environmental change in the YRZ is available from a wetland
634 near Still Bay (~110 km southwest of Eilandvlei) (Quick et al., 2015). The record spans the last ~16 kyr
635 and was interpreted to reflect relatively humid conditions during the early (11000-7000 cal BP) and late
636 Holocene (2200 cal BP-present) as well as a more arid period during the mid-Holocene (7000-
637 3300 cal BP) (Quick et al., 2015). This pattern is broadly in agreement with the rainfall cycles
638 reconstructed for Eilandvlei in this study, although the timing of the environmental changes reveals
639 offsets of up to ~800 yr and in contrast to Eilandvlei, no dry spell was recorded at Still Bay during the
640 early Holocene. These offsets may be due to dating uncertainties or actual local differences in the
641 palaeoclimatic conditions.

642



643

644 Fig. 10: Comparison of palaeoclimatic proxy data: **a**: northern precipitation stack of South Africa's summer rainfall zone (SRZ) (Chevalier and Chase, 2015); **b**: reconstructed temperature data from the Congo Caves speleothem record (Talma and Vogel, 2015); **c**: Fe concentrations and **d**: chemical index of alteration (CIA) from the EV13 record (this study); **e**: calcite contents from Groenvlei lake sediments (Wüdsch et al., 2016a); **f**: reconstructed summer sea surface temperatures (SSST) from marine sediment core TN057-17 from the East Atlantic sector of the Southern Ocean (grey line) (Nielsen et al., 2004) with a 25-point running mean (black line); **g**: lithic flux rate in marine sediment core SO147-106KL from Peru reflecting ENSO events (Rein et al., 2005); **h**: sand contents reflecting ENSO frequency from El Junco lake sediments (Conroy et al., 2008); **i**: winter and **k**: summer insolation for the 34°S latitude (Berger and Loutre, 1991).

652 Various palaeoclimatic studies from the SRZ and WRZ were conducted for the Holocene,
653 revealing distinct similarities but also many discrepancies which remain matters for debate. For further
654 details, the reader is referred to studies giving an overview and discussing the available evidence from
655 SRZ and WRZ sites (e.g., Chase and Meadows, 2007; Chevalier and Chase, 2015; Scott et al., 2012;
656 Zhao et al., 2016). As summarized by Zhao et al. (2016), the early Holocene (9900-7800 cal BP) was
657 probably characterized by humid conditions in the WRZ and dry conditions in the SRZ (Neumann et
658 al., 2010; Scott et al., 2012; Zhao et al., 2016). In the northeast of South Africa representing that part of
659 the SRZ which is not influenced by the southern westerlies, summer rainfall distinctly increased after
660 7800 cal BP as a result of increasing southern hemisphere summer insolation (Fig. 10a) (Chevalier and
661 Chase, 2015). In contrast, the WRZ was getting drier during the mid-Holocene showing an inverse trend
662 to the increasing summer insolation (Zhao et al., 2016). The increasing humidity in the SRZ during the
663 Holocene may have contributed to more rainfall at the EV13 core site (YRZ) by enhanced interactions
664 of tropical moisture-bearing systems with the mid-latitude westerlies. The onset of the wet period at
665 EV13 between 7870 to 6440 cal BP coincides with an increase in precipitation in the SRZ from
666 7800 cal BP onwards (Fig. 10a, c). The period of increased rainfall at Eilandvlei during the late
667 Holocene (3000 cal BP-present) might have been also influenced by high contributions of summer
668 rainfall. However, between 6440 and 3000 cal BP the EV13 proxies for terrigenous input (Fe, CIA)
669 suggest reduced rainfall at the southern Cape coast in contrast to the increased summer precipitation
670 reconstructed for the SRZ during that time.

671 Similarities are apparent between the EV13 palaeoclimatic proxies, like for example the CIA,
672 with reconstructed summer sea surface temperatures (SSST) from the TN057-17 core site in the
673 Southeast Atlantic sector of the Southern Ocean (Nielsen et al., 2004) during the last 8920 years
674 (Fig. 10d, f). High (low) SSSTs are related to a decreased (increased) number of months per year during
675 which this site was covered by Antarctic sea ice (Fig. 1a). This interpretation is supported by results
676 from another sediment core from the Southern Ocean (TTN057-13PC4; ~360 km south of the TN057-
677 17 site; Fig. 1a) which led to similar conclusions, namely the termination of the Holocene hypsithermal
678 at ~5500 cal BP followed by the onset of the Neoglacial cooling with an emerging sea ice cover in the
679 area (Hodell et al., 2001) (Fig. 1a). Hence, the Antarctic sea ice probably expanded equatorwards during
680 this time which is consistent with the onset of the Neoglacial period as suggested by other studies
681 (Clapperton, 1990; Magny and Haas, 2004; Porter, 2000). Towards the late Holocene, the sea ice
682 presence at core site TTN057-13PC4 declined (Hodell et al., 2001) and SSSTs at site TN057-17
683 increased (Nielsen et al., 2004) which corresponds to a poleward contraction of the Antarctic sea ice.
684 Wet (dry) conditions at the southern Cape coast broadly coincide with warm (cool) SSSTs at site TN057-
685 17 and a poleward contraction (equatorward expansion) of Antarctic sea ice (Fig. 10c-f).

686 Although there is a great disagreement in the scientific community about the position and
687 migrations of the southern hemisphere westerlies during the late Quaternary (Fletcher and Moreno,
688 2012), various studies suggest that equatorward (poleward) shifts of the westerlies are associated with

689 equatorward expansions (poleward contractions) of the Antarctic sea ice extent (Chase and Meadows,
690 2007; Kastner et al., 2010; Mayr et al., 2007; Stuut et al., 2004; Stuut and Lamy, 2004). Based on this
691 assumption, the proxies reflecting the Antarctic sea ice presence in the Southern Ocean (Hodell et al.,
692 2001; Nielsen et al., 2004) could be regarded as indirect indicators for latitudinal shifts of the westerlies.
693 Following this, the westerlies were possibly shifted polewards during the early and late Holocene,
694 whereas during the Neoglacial cooling in the mid-Holocene, the westerlies were displaced
695 equatorwards. This would be broadly in agreement with model results from Varma et al. (2012)
696 suggesting a clear trend towards a poleward movement of the southern westerlies during the last
697 7000 years. Wet (dry) conditions at the southern Cape coast would be therefore related to a poleward
698 contraction (equatorward expansion) of the mid-latitude westerlies.

699 Such a mechanistic link between past changes in the Antarctic sea ice extent and the position of
700 the westerlies would be in line with modern climate observations of rainfall variability at the southern
701 Cape coast. A poleward displacement of the westerlies during the early and late Holocene would
702 correspond to a positive phase of the SAM (Abram et al., 2014; Marshall, 2003) which is known to
703 cause more rainfall at the southern Cape coast and less rainfall in the WRZ in modern times (Engelbrecht
704 and Landman, 2016). Hence, the relatively wet conditions indicated by the EV13 record for the early
705 and late Holocene, might have been caused by poleward migrations of the westerly jet favouring the
706 equatorward expansion of emerging eddies creating an enhanced trough-ridge pattern in the westerlies
707 (Hartmann and Lo, 1998; Lindsay and Jury, 1991). Such a trough-ridge pattern may have produced
708 more ridging anticyclones and cut-off lows which are responsible for substantial amounts of rainfall
709 within our area of investigation at present (Engelbrecht et al., 2015). In contrast, the equatorward
710 expansion of sea ice during the mid-Holocene Neoglacial period and the drier conditions recorded at
711 EV13 would be related to an equatorward displacement of the westerlies and hence, a negative phase of
712 the SAM.

713 Another large-scale climate mode that probably influences the modern southern Cape coast
714 rainfall variability is ENSO, creating more rainfall from cut-off lows during La Niña events (Engelbrecht
715 and Landman, 2016; Favre et al., 2013; Weldon and Reason, 2014). Holocene ENSO reconstructions
716 are available from Lake El Junco (Conroy et al., 2008) (Fig. 10h) and Laguna Pallcacocha (Moy et al.,
717 2002) (both in Ecuador). Both suggest that ENSO was mitigated during the early and enhanced during
718 the late Holocene from ~4000 cal BP onwards. Another ENSO reconstruction is available from a marine
719 sediment core recovered at site SO147-106KL off Peru (Rein et al., 2005; Fig. 10g). By contrast, this
720 record not only suggests a prevailing ENSO climate mode during the late Holocene, but also during the
721 early Holocene until 7800 cal BP. Between 7800 and 4700 cal BP, the record coincides with the other
722 ENSO reconstructions suggesting less ENSO events during this time. The ENSO proxy data established
723 by Rein et al. (2005) show a similar pattern as the Fe concentrations from the EV13 record (Fig. 10c,
724 g), although the major changes are temporally shifted by more than 1000 years, which might be due to
725 dating uncertainties. Summarizing, wetter (drier) conditions recorded at Eilandvlei were possibly also

726 related to an enhanced (diminished) ENSO climate mode causing more frequent/intense La Niña events
727 with its teleconnections affecting the southern Cape coast of South Africa. The impact of ENSO on
728 migrations of the circumpolar southern hemisphere westerlies during the late Quaternary was discussed
729 by Fletcher and Moreno (2012). The authors concluded that the westerlies migrated in a zonally
730 symmetric manner prior to ~5000 cal BP. Thereafter, the zonal symmetry collapsed with the onset of
731 ENSO which was possibly due to an insolation-driven increase of the thermal gradient between the
732 equator and the South Pole which in turn amplified the westerlies and the atmospheric circulation in
733 general (Fletcher and Moreno, 2012). During the late Holocene, the amplified and asymmetric westerly
734 jet possibly caused a strengthened ridging of anticyclones (Mason and Jury, 1997) that brought more
735 rainfall to the southern Cape coast. Changing SSTs and SST gradients in the Southern Ocean probably
736 also played an important role for the (anti)cyclogenesis in that area and eventually for the amount of
737 rainfall reaching the southern Cape coast (Mason and Jury, 1997). The three heavy rainfall events
738 reconstructed from the EV13 and Groenvlei data (at 2070 ⁺¹⁹⁰/₋₁₆₀, 1410 ⁺¹²⁰/₋₁₂₀ and 1250 ⁺¹³⁰/₋₁₆₀ cal BP;
739 Fig. 9) might have been caused by cut-off lows, which have been suggested in recent studies to cause
740 extreme floods at the southern Cape coast and to be related to La Niña events (Engelbrecht and
741 Landman, 2016; Weldon and Reason, 2014). Hence, both ENSO and SAM might have played a
742 substantial role among various factors causing rainfall at the EV13 core site throughout the Holocene.

743

744 **6 Conclusions**

745 The 30.5 m sediment record from the coastal lake Eilandvlei represents a unique geoarchive giving
746 insights into Holocene environmental change at the southern Cape coast of South Africa. According to
747 the multi-proxy data, Eilandvlei passed through distinct phases of connectivity to the ocean resulting in
748 variable exchanges with sea water. Between 8920 and 4670 cal BP marine conditions prevailed at the
749 core site which was most likely located within a palaeovalley that formed at lower sea levels during the
750 Pleistocene. This palaeovalley was drowned by the rapidly rising sea during the early Holocene. After
751 its mid-Holocene high stand the sea level dropped and the embayment became distinctly more
752 disconnected from the ocean turning into a lagoon system from 4670 to 1240 cal BP. After 1240 cal BP,
753 the lagoon system became even more disconnected from the sea and the present estuarine/coastal lake
754 system developed.

755 The record further suggests marked changes in the long-term rainfall variability since
756 8920 cal BP. During the early to mid-Holocene, rainfall was low from 8920 to 7870 cal BP and high
757 from 7870 to 6440 cal BP. For the period between 6440 and 3000 cal BP, reduced rainfall is indicated.
758 Increasing rainfall is inferred for the late Holocene (3000 cal BP-present). The comparison of
759 palaeorainfall proxies derived from the Eilandvlei record with other Holocene proxy data indicates a
760 relationship to ENSO, SAM and the Antarctic sea ice extent. High (low) rainfall at the southern Cape
761 coast seem to be related to a poleward contraction (equatorward expansion) of the Antarctic sea ice
762 extent and the mid-latitude westerlies, which corresponds to a positive (negative) phase of SAM.

763 Moreover, an enhanced (diminished) ENSO climate mode possibly contributes to more (less) rainfall
764 along the southern Cape coast. Indeed, these hypotheses need to be tested by future research.

765

766 **Acknowledgements**

767 This study was funded by the German Federal Ministry of Education and Research (BMBF). The
768 investigations were conducted within the collaborative project “Regional Archives for Integrated
769 Investigations” (RAIN), which is embedded in the international research programme SPACES (Science
770 Partnership for the Assessment of Complex Earth System Processes).

771 We are deeply grateful to South African National Parks (Garden Route National Park Scientific
772 Services, Sedgefield) for the permission to conduct our fieldwork on Eilandvlei. We thank Sayed Hess,
773 Richard Niederreiter and Bastian Reinwarth for their helping hands during the fieldwork as well as
774 Stephanie Meschner, Sascha Fürstenberg, Nico Blaubach and Carmen Kirchner for their help during the
775 data acquisition. Jacques Labrie is acknowledged for providing the modified version of the Gradistat
776 4.2 software. Finally, we thank Brian M. Chase for his comments on an earlier version of the manuscript.

777

778 **References**

- 779 Abraham, G.M., Nichol, S.L., Parker, R.J., Gregory, M.R., 2008. Facies depositional setting, mineral maturity and
780 sequence stratigraphy of a Holocene drowned valley, Tamaki Estuary, New Zealand. *Estuarine, Coastal
781 and Shelf Science* 79, 133-142.
- 782 Abram, N.J., Mulvaney, R., Vimeux, F., Phipps, S.J., Turner, J., England, M.H., 2014. Evolution of the Southern
783 Annular Mode during the past millennium. *Nature Climate Change* 4, 564-569.
- 784 Allanson, B.R., Whitfield, A.K., 1983. The Limnology of the Touw River floodplain. South African Scientific
785 Programmes, Report No 79, Pretoria.
- 786 Balfour, D., Bond, W., 1993. Factors limiting climber distribution and abundance in a southern African forest.
787 *Journal of Ecology*, 93-100.
- 788 Bateman, M.D., Carr, A.S., Dunajko, A.C., Holmes, P.J., Roberts, D.L., McLaren, S.J., Bryant, R.G., Marker,
789 M.E., Murray-Wallace, C.V., 2011. The evolution of coastal barrier systems: a case study of the Middle-
790 Late Pleistocene Wilderness barriers, South Africa. *Quaternary Science Reviews* 30, 63-81.
- 791 Bateman, M.D., Holmes, P.J., Carr, A.S., Horton, B.P., Jaiswal, M.K., 2004. Aeolianite and barrier dune
792 construction spanning the last two glacial–interglacial cycles from the southern Cape coast, South Africa.
793 *Quaternary Science Reviews* 23, 1681-1698.
- 794 Battarbee, R., 1986. Diatom analysis. *Handbook of Holocene Palaeoecology and Palaeohydrology*. Wiley, New
795 York, USA.
- 796 Baxter, A.J., Meadows, M.E., 1999. Evidence for Holocene sea level change at Verlorenvlei, Western Cape, South
797 Africa. *Quaternary International* 56, 65-79.
- 798 Berger, A., Loutre, M.-F., 1991. Insolation values for the climate of the last 10 million years. *Quaternary Science
799 Reviews* 10, 297-317.
- 800 Berner, R.A., 1982. Burial of organic carbon and pyrite sulfur in the modern ocean: its geochemical and
801 environmental significance. *American Journal of Science* 282, 451-473.
- 802 Berner, R.A., Raiswell, R., 1983. Burial of organic carbon and pyrite sulfur in sediments over Phanerozoic time:
803 a new theory. *Geochimica et Cosmochimica Acta* 47, 855-862.
- 804 Birch, G., Du Plessis, A., Willis, J., 1978. Offshore and onland geological and geophysical investigations in the
805 Wilderness Lakes region. *Transactions of the Geological Society of South Africa* 81, 339-352.
- 806 Blaauw, M., Christen, J.A., 2011. Flexible paleoclimate age–depth models using an autoregressive gamma process.
807 *Bayesian Analysis* 6, 457-474.
- 808 Blott, S.J., Pye, K., 2001. GRADISTAT: a grain size distribution and statistics package for the analysis of
809 unconsolidated sediments. *Earth Surface Processes and Landforms* 26, 1237-1248.
- 810 Booth, P., 2011. Stratigraphic, structural and tectonic enigmas associated with the Cape Fold Belt: challenges for
811 future research. *South African Journal of Geology* 114, 235-248.
- 812 Brisset, E., Miramont, C., Guiter, F., Anthony, E.J., Tachikawa, K., Poulenard, J., Arnaud, F., Delhon, C., Meunier,
813 J.-D., Bard, E., 2013. Non-reversible geosystem destabilisation at 4200 cal. BP: Sedimentological,

- 814 geochemical and botanical markers of soil erosion recorded in a Mediterranean alpine lake. *The Holocene*
815 23, 1863-1874.
- 816 Browning, C., Macey, P., 2015. Lithostratigraphy of the George Pluton Units (Cape Granite Suite), South Africa.
817 *South African Journal of Geology* 118, 323-330.
- 818 Camoin, G., Colonna, M., Montaggioni, L., Casanova, J., Faure, G., Thomassin, B., 1997. Holocene sea level
819 changes and reef development in the southwestern Indian Ocean. *Coral Reefs* 16, 247-259.
- 820 Carr, A.S., Boom, A., Chase, B.M., Meadows, M.E., Grimes, H.L., 2015. Holocene sea level and environmental
821 change on the west coast of South Africa: evidence from plant biomarkers, stable isotopes and pollen.
822 *Journal of Paleolimnology* 53, 415-432.
- 823 Cawthra, H.C., Bateman, M.D., Carr, A.S., Compton, J.S., Holmes, P.J., 2014. Understanding Late Quaternary
824 change at the land–ocean interface: a synthesis of the evolution of the Wilderness coastline, South Africa.
825 *Quaternary Science Reviews* 99, 210-223.
- 826 Chandler, G., Merry, C., 2010. The South African geoid 2010: SAGEOID10. Position IT, 29-33.
- 827 Chase, B.M., Boom, A., Carr, A.S., Meadows, M.E., Reimer, P.J., 2013. Holocene climate change in southernmost
828 South Africa: rock hyrax middens record shifts in the southern westerlies. *Quaternary Science Reviews*
829 82, 199-205.
- 830 Chase, B.M., Meadows, M.E., 2007. Late Quaternary dynamics of southern Africa's winter rainfall zone. *Earth-*
831 *Science Reviews* 84, 103-138.
- 832 Chevalier, M., Chase, B.M., 2015. Southeast African records reveal a coherent shift from high-to low-latitude
833 forcing mechanisms along the east African margin across last glacial–interglacial transition. *Quaternary*
834 *Science Reviews* 125, 117-130.
- 835 Clapperton, C.M., 1990. Quaternary glaciations in the Southern Hemisphere: an overview. *Quaternary Science*
836 *Reviews* 9, 299-304.
- 837 Clark, J.A., Lingle, C.S., 1979. Predicted relative sea-level changes (18,000 years BP to present) caused by late-
838 glacial retreat of the Antarctic ice sheet. *Quaternary Research* 11, 279-298.
- 839 Cohen, A., Tyson, P.D., 1995. Sea-surface temperature fluctuations during the Holocene off the south coast of
840 Africa: implications for terrestrial climate and rainfall. *The Holocene* 5, 304-312.
- 841 Compton, J.S., 2001. Holocene sea-level fluctuations inferred from the evolution of depositional environments of
842 the southern Langebaan Lagoon salt marsh, South Africa. *The Holocene* 11, 395-405.
- 843 Compton, J.S., 2006. The mid-Holocene sea-level highstand at Bogenfels Pan on the southwest coast of Namibia.
844 *Quaternary Research* 66, 303-310.
- 845 Conroy, J.L., Overpeck, J.T., Cole, J.E., Shanahan, T.M., Steinitz-Kannan, M., 2008. Holocene changes in eastern
846 tropical Pacific climate inferred from a Galápagos lake sediment record. *Quaternary Science Reviews* 27,
847 1166-1180.
- 848 de Boer, G.B., de Weerd, C., Thoenes, D., Goossens, H.W., 1987. Laser diffraction spectrometry: Fraunhofer
849 diffraction versus Mie scattering. *Particle & Particle Systems Characterization* 4, 14-19.
- 850 DWS (Department of Water and Sanitation), 2015. Resource water quality data for Gouritz WMA., Department
851 of Water and Sanitation, Republic of South Africa,
852 https://www.dwa.gov.za/iwqs/wms/data/WMA16_reg_WMS_nobor.htm.
- 853 Engelbrecht, C.J., Landman, W.A., 2016. Interannual variability of seasonal rainfall over the Cape south coast of
854 South Africa and synoptic type association. *Climate Dynamics* 47, 295-313.
- 855 Engelbrecht, C.J., Landman, W.A., Engelbrecht, F.A., Malherbe, J., 2015. A synoptic decomposition of rainfall
856 over the Cape south coast of South Africa. *Climate Dynamics* 44, 2589-2607.
- 857 Favre, A., Hewitson, B., Lennard, C., Cerezo-Mota, R., Tadross, M., 2013. Cut-off lows in the South Africa region
858 and their contribution to precipitation. *Climate Dynamics* 41, 2331-2351.
- 859 Fedo, C.M., Nesbitt, H.W., Young, G.M., 1995. Unraveling the effects of potassium metasomatism in sedimentary
860 rocks and paleosols, with implications for paleoweathering conditions and provenance. *Geology* 23, 921-
861 924.
- 862 Ferré, E., Améglio, L., 2000. Preserved magnetic fabrics vs. annealed microstructures in the syntectonic
863 recrystallised George granite, South Africa. *Journal of Structural Geology* 22, 1199-1219.
- 864 Fleming, K., Johnston, P., Zwart, D., Yokoyama, Y., Lambeck, K., Chappell, J., 1998. Refining the eustatic sea-
865 level curve since the Last Glacial Maximum using far-and intermediate-field sites. *Earth and Planetary*
866 *Science Letters* 163, 327-342.
- 867 Fletcher, M.-S., Moreno, P.I., 2012. Have the Southern Westerlies changed in a zonally symmetric manner over
868 the last 14,000 years? A hemisphere-wide take on a controversial problem. *Quaternary International* 253,
869 32-46.
- 870 Friedman, G.M., Sanders, J.E., 1978. *Principles of sedimentology*. Wiley, New York, USA.
- 871 Frimmel, H., Van Achterbergh, E., 1995. Metamorphism of calc-silicate and associated rocks in the Pan-African
872 Kaaimans Group, Saldania Belt, South Africa. *Mineralogy and Petrology* 53, 75-102.
- 873 Goldberg, K., Humayun, M., 2010. The applicability of the Chemical Index of Alteration as a paleoclimatic
874 indicator: An example from the Permian of the Paraná Basin, Brazil. *Palaeogeography,*
875 *Palaeoclimatology, Palaeoecology* 293, 175-183.

- 876 Govin, A., Holzwarth, U., Heslop, D., Ford Keeling, L., Zabel, M., Mulitza, S., Collins, J.A., Chiessi, C.M., 2012.
877 Distribution of major elements in Atlantic surface sediments (36 N–49 S): Imprint of terrigenous input
878 and continental weathering. *Geochemistry, Geophysics, Geosystems* 13, 1, doi:10.1029/2011GC003785.
879 Gribble, G.W., 2000. The natural production of organobromine compounds. *Environmental Science and Pollution*
880 *Research* 7, 37-49.
- 881 Haberzettl, T., Baade, J., Compton, J., Daut, G., Dupont, L., Finch, J., Frenzel, P., Green, A., Hahn, A., Hebbeln,
882 D., Helmschrot, J., Humphries, M., Kasper, T., Kirsten, K.L., Mäusbacher, R., Meadows, M.E.,
883 Meschner, S., Quick, L.J., Schefuß, E., Wüdsch, M., Zabel, M., 2014. Paleoenvironmental investigations
884 using a combination of terrestrial and marine sediments from South Africa - The RAIN (Regional
885 Archives for Integrated iNvestigations) approach. *Zentralblatt für Geologie und Paläontologie, Teil I,*
886 *Heft 1, 55-73.*
- 887 Häggi, C., Sawakuchi, A.O., Chiessi, C.M., Mulitza, S., Mollenhauer, G., Sawakuchi, H.O., Baker, P.A., Zabel,
888 M., Schefuß, E., 2016. Origin, transport and deposition of leaf-wax biomarkers in the Amazon Basin and
889 the adjacent Atlantic. *Geochimica et Cosmochimica Acta* 192, 149-165.
- 890 Hahn, A., Schefuß, E., Andò, S., Cawthra, H.C., Frenzel, P., Kugel, M., Meschner, S., Mollenhauer, G., Zabel,
891 M., 2016. Linking catchment hydrology and ocean circulation in Late Holocene southernmost Africa.
892 *Climate of the Past Discussions.* doi:10.5194/cp-2016-100.
- 893 Håkanson, L., Jansson, M., 2002. Principles of lake sedimentology. Blackburn Press, Caldwell, New Jersey, USA.
- 894 Hartmann, D.L., Lo, F., 1998. Wave-driven zonal flow vacillation in the Southern Hemisphere. *Journal of the*
895 *Atmospheric Sciences* 55, 1303-1315.
- 896 Haug, G.H., Hughen, K.A., Sigman, D.M., Peterson, L.C., Röhl, U., 2001. Southward migration of the intertropical
897 convergence zone through the Holocene. *Science* 293, 1304-1308.
- 898 Hetzel, A., Brumsack, H.-J., Schnetger, B., Böttcher, M., 2006. Inorganic geochemical characterization of
899 lithologic units recovered during ODP Leg 207 (Demerara Rise). *Proceedings of the Ocean Drilling*
900 *Program, Scientific Results* 207, 1-37.
- 901 Hodell, D.A., Kanfoush, S.L., Shemesh, A., Crosta, X., Charles, C.D., Guilderson, T.P., 2001. Abrupt cooling of
902 Antarctic surface waters and sea ice expansion in the South Atlantic sector of the Southern Ocean at
903 5000 cal yr BP. *Quaternary Research* 56, 191-198.
- 904 Howard-Williams, C., 1980. Aquatic macrophyte communities of the Wilderness lakes: community structure and
905 associated environmental conditions. *Journal of the Limnological Society of Southern Africa* 6, 85-92.
- 906 Illenberger, W.K., 1996. The geomorphologic evolution of the Wilderness dune cordons, South Africa. *Quaternary*
907 *International* 33, 11-20.
- 908 Jarvis, A., Reuter, H.I., Nelson, A., Guevara, E., 2008. Hole-filled SRTM for the globe Version 4. available from
909 the CGIAR-CSI SRTM 90m Database (<http://srtm.csi.cgiar.org>).
- 910 Jones, B.F., Bowser, C.J., 1978. The mineralogy and related chemistry of lake sediments, In: Lerman, A. (Ed.),
911 *Lakes: Chemistry, Geology, Physics.* Springer, New York, pp. 179-235.
- 912 Kastner, S., Enters, D., Ohlendorf, C., Haberzettl, T., Kuhn, G., Lücke, A., Mayr, C., Reyss, J.-L., Wastegård, S.,
913 Zolitschka, B., 2010. Reconstructing 2000 years of hydrological variation derived from laminated
914 proglacial sediments of Lago del Desierto at the eastern margin of the South Patagonian Ice Field,
915 Argentina. *Global and Planetary Change* 72, 201-214.
- 916 Kelly, M., Bennion, H., Cox, E.J., Goldsmith, B., Jamieson, J., Juggins, S., Mann, D., Telford, R., 2005. Common
917 freshwater diatoms of Britain and Ireland: an interactive key. Environment Agency, Bristol, UK.
- 918 Kirsten, K., 2014. Late Holocene diatom community responses to climate variability along the southern Cape
919 coastal plain, South Africa. PhD Thesis. University of Cape Town, Cape Town, South Africa.
- 920 Kirsten, K., Haberzettl, T., Wüdsch, M., Frenzel, P., Meschner, S., Smit, A.J., Quick, L.J., Mäusbacher, R.,
921 Meadows, M.E., subm. The impact of sea level changes on the southern Cape coast, South Africa and
922 the variability of the Agulhas Bank environment during the Holocene. *Continental Shelf Research.*
- 923 Leri, A.C., Hakala, J.A., Marcus, M.A., Lanzirotti, A., Reddy, C.M., Myneni, S.C., 2010. Natural organobromine
924 in marine sediments: New evidence of biogeochemical Br cycling. *Global Biogeochemical Cycles* 24,
925 doi:10.1029/2010GB003794.
- 926 Li, C., Yang, S., 2010. Is chemical index of alteration (CIA) a reliable proxy for chemical weathering in global
927 drainage basins?. *American Journal of Science* 310, 111-127.
- 928 Lindsay, J., Jury, M., 1991. Atmospheric circulation controls and characteristics of a flood event in central South
929 Africa. *International Journal of Climatology* 11, 609-627.
- 930 Lowry, F.M.D., 1988. Foraminiferal Thanatocoenoses from the continental shelf of southern Africa. University
931 College, London, UK.
- 932 Lyons, T.W., Berner, R.A., 1992. Carbon-sulfur-iron systematics of the uppermost deep-water sediments of the
933 Black Sea. *Chemical Geology* 99, 1-27.
- 934 Magny, M., Haas, J.N., 2004. A major widespread climatic change around 5300 cal. yr BP at the time of the Alpine
935 Ice-man. *Journal of Quaternary Science* 19, 423-430.
- 936 Marker, M.E., Holmes, P.J., 2002. The distribution and environmental implications of coversand deposits in the
937 Southern Cape, South Africa. *South African Journal of Geology* 105, 135-146.

- 938 Marker, M.E., Miller, D.E., 1993. A Mid-Holocene high stand of the sea at Knysna. *South African Journal of*
939 *Science* 89, 100-101.
- 940 Marshall, G.J., 2003. Trends in the Southern Annular Mode from observations and reanalyses. *Journal of Climate*
941 16, 4134-4143.
- 942 Martin, A.R.H., 1959. The stratigraphy and history of Groenvlei, a South African coastal fen. *Australian Journal*
943 *of Botany* 7, 142-167.
- 944 Martin, A.R.H., 1962. Evidence relating to the Quarternary history of the Wilderness lakes. *Transactions of the*
945 *Geological Society of South Africa* 65, 19-42.
- 946 Martin, A.R.H., 1968. Pollen analysis of Groenvlei lake sediments, Knysna (South Africa). *Review of*
947 *Palaeobotany and Palynology* 7, 107-144.
- 948 Mason, S., Jury, M., 1997. Climatic variability and change over southern Africa: a reflection on underlying
949 processes. *Progress in Physical Geography* 21, 23-50.
- 950 Mayer, L.M., Macko, S.A., Mook, W.H., Murray, S., 1981. The distribution of bromine in coastal sediments and
951 its use as a source indicator for organic matter. *Organic Geochemistry* 3, 37-42.
- 952 Mayer, L.M., Schick, L.L., Allison, M.A., Ruttenger, K.C., Bentley, S.J., 2007. Marine vs. terrigenous organic
953 matter in Louisiana coastal sediments: The uses of bromine: organic carbon ratios. *Marine Chemistry*
954 107, 244-254.
- 955 Mayr, C., Wille, M., Haberzettl, T., Fey, M., Janssen, S., Lücke, A., Ohlendorf, C., Oliva, G., Schäbitz, F.,
956 Schleser, G.H., Zolitschka, B., 2007. Holocene variability of the Southern Hemisphere westerlies in
957 Argentinean Patagonia (52 S). *Quaternary Science Reviews* 26, 579-584.
- 958 McLennan, S., Taylor, S., McCulloch, M., Maynard, J., 1990. Geochemical and Nd-Sr isotopic composition of
959 deep-sea turbidites: crustal evolution and plate tectonic associations. *Geochimica et Cosmochimica Acta*
960 54, 2015-2050.
- 961 Meadows, M.E., Baxter, A.J., 2001. Holocene vegetation history and palaeoenvironments at Klaarfontein Springs,
962 Western Cape, South Africa. *The Holocene* 11, 699-706.
- 963 Minyuk, P.S., Brigham-Grette, J., Melles, M., Borkhodoev, V.Y., Glushkova, O.Y., 2007. Inorganic geochemistry
964 of El'gygytgyn Lake sediments (northeastern Russia) as an indicator of paleoclimatic change for the last
965 250 kyr. *Journal of Paleolimnology* 37, 123-133.
- 966 Monien, P., Schnetger, B., Brumsack, H.-J., Hass, H.C., Kuhn, G., 2011. A geochemical record of late Holocene
967 palaeoenvironmental changes at King George Island (maritime Antarctica). *Antarctic Science* 23, 255-
968 267.
- 969 Moore, P.D., Webb, J.A., Collison, M.E., 1991. *Pollen analysis*. Blackwell scientific publications, Oxford, UK.
- 970 Morse, J.W., Berner, R.A., 1995. What determines sedimentary C/S ratios? *Geochimica et Cosmochimica Acta*
971 59, 1073-1077.
- 972 Moy, C.M., Seltzer, G.O., Rodbell, D.T., Anderson, D.M., 2002. Variability of El Niño/Southern Oscillation
973 activity at millennial timescales during the Holocene epoch. *Nature* 420, 162-165.
- 974 Mucina, L., Rutherford, M.C., 2006. *The vegetation of South Africa, Lesotho and Swaziland*. South African
975 National Biodiversity Institute, Pretoria.
- 976 Murray, J.W., 1979. *British Nearshore Foraminiferids: Keys and Notes for the Identification of the Species*.
977 Academic Press, London, UK.
- 978 Murray, J.W., 2006. *Ecology and applications of benthic foraminifera*. Cambridge University Press, Cambridge,
979 UK.
- 980 Nakagawa, T., Brugiapaglia, E., Digerfeldt, G., Reille, M., Beaulieu, J.L.d., Yasuda, Y., 1998. Dense-media
981 separation as a more efficient pollen extraction method for use with organic sediment/deposit samples:
982 comparison with the conventional method. *Boreas* 27, 15-24.
- 983 Nath, B.N., Kunzendorf, H., Plüger, W., 2000. Influence of provenance, weathering, and sedimentary processes
984 on the elemental ratios of the fine-grained fraction of the bedload sediments from the Vembanad Lake
985 and the adjoining continental shelf, southwest coast of India. *Journal of Sedimentary Research* 70, 1081-
986 1094.
- 987 Nesbitt, H.W., Young, G.M., 1982. Early Proterozoic climates and plate motions inferred from major element
988 chemistry of lutites. *Nature* 299, 715-717.
- 989 Neumann, F.H., Scott, L., Bousman, C., Van As, L., 2010. A Holocene sequence of vegetation change at Lake
990 Eteza, coastal KwaZulu-Natal, South Africa. *Review of Palaeobotany and Palynology* 162, 39-53.
- 991 Nielsen, S.H., Koç, N., Crosta, X., 2004. Holocene climate in the Atlantic sector of the Southern Ocean: Controlled
992 by insolation or oceanic circulation?. *Geology* 32, 317-320.
- 993 Oksanen, J., Blanchet, F.G., Kindt, R., Legendre, P., Minchin, P.R., O'Hara, R., Simpson, G.L., Solymos, P.,
994 Stevens, M.H.H., Wagner, H., 2013. Package 'vegan'. [http://cran.r-](http://cran.r-project.org/web/packages/vegan/index.html)
995 [project.org/web/packages/vegan/index.html](http://cran.r-project.org/web/packages/vegan/index.html).
- 996 Olsen, J., Kjær, K.H., Funder, S., Larsen, N.K., Ludikova, A., 2012. High-Arctic climate conditions for the last
997 7000 years inferred from multi-proxy analysis of the Bliss Lake record, North Greenland. *Journal of*
998 *Quaternary Science* 27, 318-327.

- 999 Peterson, L.C., Haug, G.H., Hughen, K.A., Röhl, U., 2000. Rapid changes in the hydrologic cycle of the tropical
1000 Atlantic during the last glacial. *Science* 290, 1947-1951.
- 1001 Porter, S.C., 2000. Onset of neoglaciation in the Southern Hemisphere. *Journal of Quaternary Science* 15, 395-
1002 408.
- 1003 Price, N., Calvert, S., 1977. The contrasting geochemical behaviours of iodine and bromine in recent sediments
1004 from the Namibian shelf. *Geochimica et Cosmochimica Acta* 41, 1769-1775.
- 1005 Quick, L.J., 2013. Late Quaternary palaeoenvironments of the southern Cape, South Africa: palynological
1006 evidence from three coastal wetlands. PhD Thesis. University of Cape Town, Cape Town, South Africa.
- 1007 Quick, L.J., Carr, A.S., Meadows, M.E., Boom, A., Bateman, M.D., Roberts, D.L., Reimer, P.J., Chase, B.M.,
1008 2015. A late Pleistocene–Holocene multi-proxy record of palaeoenvironmental change from Still Bay,
1009 southern Cape Coast, South Africa. *Journal of Quaternary Science* 30, 870-885.
- 1010 Quick, L.J., Meadows, M.E., Bateman, M.D., Kirsten, K.L., Mäusbacher, R., Haberzettl, T., Chase, B.M., 2016.
1011 Vegetation and climate dynamics during the last glacial period in the fynbos-afrotemperate forest ecotone,
1012 southern Cape, South Africa. *Quaternary International* 404, Part B, 136-149.
- 1013 Raiswell, R., Berner, R.A., 1985. Pyrite formation in euxinic and semi-euxinic sediments. *American Journal of*
1014 *Science* 285, 710-724.
- 1015 Ramsay, P.J., 1995. 9000 years of sea-level change along the southern African coastline. *Quaternary International*
1016 31, 71-75.
- 1017 Ramsay, P.J., Cooper, J.A.G., 2002. Late Quaternary sea-level change in South Africa. *Quaternary Research* 57,
1018 82-90.
- 1019 Reason, C., Rouault, M., 2005. Links between the Antarctic Oscillation and winter rainfall over western South
1020 Africa. *Geophysical Research Letters* 32, L07705, doi:10.1029/2005GL022419.
- 1021 Rein, B., Lückge, A., Reinhardt, L., Sirocko, F., Wolf, A., Dullo, W.C., 2005. El Niño variability off Peru during
1022 the last 20,000 years. *Paleoceanography* 20.
- 1023 Reinwarth, B., Franz, S., Baade, J., Haberzettl, T., Kasper, T., Daut, G., Helmschrot, J., Kirsten, K.L., Quick, L.J.,
1024 Meadows, M.E., 2013. A 700-year record on the effects of climate and human impact on the southern
1025 Cape coast inferred from lake sediments of Eilandvlei, Wilderness Embayment, South Africa. *Geografiska Annaler: Series A, Physical Geography* 95, 345-360.
- 1027 Richter, T.O., Van der Gaast, S., Koster, B., Vaars, A., Gieles, R., de Stigter, H.C., De Haas, H., van Weering,
1028 T.C., 2006. The Avaatech XRF Core Scanner: technical description and applications to NE Atlantic
1029 sediments. Geological Society, London, Special Publications 267, 39-50.
- 1030 Rouault, M., White, S., Reason, C., Lutjeharms, J., Jobard, I., 2002. Ocean–atmosphere interaction in the Agulhas
1031 Current region and a South African extreme weather event. *Weather and Forecasting* 17, 655-669.
- 1032 Roy, P., Caballero, M., Lozano, R., Smykatz-Kloss, W., 2008. Geochemistry of late quaternary sediments from
1033 Tecocomulco lake, central Mexico: Implication to chemical weathering and provenance. *Chemie der*
1034 *erde-Geochemistry* 68, 383-393.
- 1035 Roy, P., Jonathan, M.P., Pérez-Cruz, L.L., Sánchez-Córdova, M.M., Quiroz-Jiménez, J.D., Romero, F.M., 2012.
1036 A millennial-scale Late Pleistocene–Holocene palaeoclimatic record from the western Chihuahua Desert,
1037 Mexico. *Boreas* 41, 707-718.
- 1038 Russell, I., 2003. Changes in the distribution of emergent aquatic plants in a brackish South African estuarine-lake
1039 system. *African Journal of Aquatic Science* 28, 103-122.
- 1040 Russell, I., 2013. Spatio-temporal variability of surface water quality parameters in a South African estuarine lake
1041 system. *African Journal of Aquatic Science* 38, 53-66.
- 1042 SAWS (South African Weather Service), 2017. Rainfall data from the weather stations 0012661 7 (George WO),
1043 0014123 3 (Knysna), and 0028776 9 (George Witfontein). South African Weather Service, Pretoria.
- 1044 Schmidt-Sinns, J., 2008. Rezente benthische Foraminiferen im Bereich des Benguelastroms, Südwestafrika –
1045 Verbreitungsmuster und ihre steuernden Faktoren. PhD thesis. University of Bonn, Bonn, Germany.
- 1046 Scott, D.B., Medioli, F.S., Schafer, C.T., 2001. Monitoring in coastal environments using foraminifera and
1047 thecamoebian indicators. Cambridge University Press, Cambridge, UK.
- 1048 Scott, L., Lee-Thorp, J.A., 2004. Holocene climatic trends and rhythms in southern Africa. In: Battarbee, R.W.,
1049 Gasse, F., Stickley, C.E. (Eds.). *Past Climate variability through Europe and Africa*. Springer, Dordrecht,
1050 69-91.
- 1051 Scott, L., Neumann, F.H., Brook, G.A., Bousman, C.B., Norström, E., Metwally, A., 2012. Terrestrial fossil-pollen
1052 evidence of climate change during the last 26 thousand years in Southern Africa. *Quaternary Science*
1053 *Reviews* 32, 100-118.
- 1054 Shao, J., Yang, S., Li, C., 2012. Chemical indices (CIA and WIP) as proxies for integrated chemical weathering
1055 in China: inferences from analysis of fluvial sediments. *Sedimentary Geology* 265, 110-120.
- 1056 Singleton, A., Reason, C., 2006. Numerical simulations of a severe rainfall event over the Eastern Cape coast of
1057 South Africa: sensitivity to sea surface temperature and topography. *Tellus* 58A, 355-367.
- 1058 Song, Y., Müller, G., 1993. Freshwater sediments: sinks and sources of bromine. *Naturwissenschaften* 80, 558-
1059 560.

- 1060 Stuu, J.-B.W., Crosta, X., Van der Borg, K., Schneider, R., 2004. Relationship between Antarctic sea ice and
1061 southwest African climate during the late Quaternary. *Geology* 32, 909-912.
- 1062 Stuu, J.-B.W., Lamy, F., 2004. Climate variability at the southern boundaries of the Namib (southwestern Africa)
1063 and Atacama (northern Chile) coastal deserts during the last 120,000 yr. *Quaternary Research* 62, 301-
1064 309.
- 1065 Talma, A., Vogel, J.C., 1992. Late Quaternary paleotemperatures derived from a speleothem from Cango caves,
1066 Cape province, South Africa. *Quaternary Research* 37, 203-213.
- 1067 Taylor, J.C., Harding, W.R., Archibald, C., 2007. An illustrated guide to some common diatom species from South
1068 Africa. Water Research Commission Report TT 282/07, Pretoria, South Africa.
- 1069 Thompson, D.W., Wallace, J.M., 2000. Annular modes in the extratropical circulation. Part I: Month-to-month
1070 variability. *Journal of Climate* 13, 1000-1016.
- 1071 Tjallingii, R., Röhl, U., Kölling, M., Bickert, T., 2007. Influence of the water content on X-ray fluorescence core-
1072 scanning measurements in soft marine sediments. *Geochemistry, Geophysics, Geosystems* 8, 2,
1073 doi:10.1029/2006GC001393.
- 1074 Traini, C., Ménier, D., Proust, J.-N., Sorrel, P., 2013. Transgressive systems tract of a ria-type estuary: The Late
1075 Holocene Vilaine River drowned valley (France). *Marine Geology* 337, 140-155.
- 1076 Tyson, P.D., 1986. Climatic change and variability in southern Africa. Oxford University Press, Cape Town, South
1077 Africa.
- 1078 Varma, V., Prange, M., Merkel, U., Kleinen, T., Lohmann, G., Pfeiffer, M., Renssen, H., Wagner, A., Wagner, S.,
1079 Schulz, M., 2012. Holocene evolution of the Southern Hemisphere westerly winds in transient simulations
1080 with global climate models. *Climate of the Past* 8, 391-402.
- 1081 Weldon, D., Reason, C., 2014. Variability of rainfall characteristics over the South Coast region of South Africa.
1082 *Theoretical and applied climatology* 115, 177-185.
- 1083 Wüdsch, M., Haberzettl, T., Kirsten, K.L., Kasper, T., Zabel, M., Dietze, E., Baade, J., Daut, G., Meschner, S.,
1084 Meadows, M.E., 2016a. Sea level and climate change at the southern cape coast, South Africa, during the
1085 past 4.2 kyr. *Palaeogeography, Palaeoclimatology, Palaeoecology* 446, 295-307.
- 1086 Wüdsch, M., Haberzettl, T., Meadows, M.E., Kirsten, K.L., Kasper, T., Baade, J., Daut, G., Stoner, J.S.,
1087 Mäusbacher, R., 2016b. The impact of changing reservoir effects on a 14C chronology for a Holocene
1088 sediment record from South Africa. *Quaternary Geochronology* 36, 148-160.
- 1089 Xiao, S., Liu, W., Li, A., Yang, S., Lai, Z., 2010. Pervasive autocorrelation of the chemical index of alteration in
1090 sedimentary profiles and its palaeoenvironmental implications. *Sedimentology* 57, 670-676.
- 1091 Zaremba, N., Mallinson, D.J., Leorri, E., Culver, S., Riggs, S., Mulligan, R., Horsman, E., Mitra, S., 2016. Controls
1092 on the stratigraphic framework and paleoenvironmental change within a Holocene estuarine system:
1093 Pamlico Sound, North Carolina, USA. *Marine Geology* 379, 109-123.
- 1094 Zhang, Y., Chiessi, C.M., Mulitza, S., Zabel, M., Trindade, R.I.F., Hollanda, M.H.B.M., Dantas, E.L., Govin, A.,
1095 Tiedemann, R., Wefer, G., 2015. Origin of increased terrigenous supply to the NE South American
1096 continental margin during Heinrich Stadial 1 and the Younger Dryas. *Earth and Planetary Science Letters*
1097 432, 493-500.
- 1098 Zhao, X., Dupont, L., Schefuß, E., Meadows, M.E., Hahn, A., Wefer, G., 2016. Holocene vegetation and climate
1099 variability in the winter and summer rainfall zones of South Africa. *The Holocene* 26, 843-857.
- 1100 Ziegler, M., Jilbert, T., de Lange, G.J., Lourens, L.J., Reichert, G.J., 2008. Bromine counts from XRF scanning as
1101 an estimate of the marine organic carbon content of sediment cores. *Geochemistry, Geophysics,
1102 Geosystems* 9, 5, doi:10.1029/2007GC001932.

Author: Michael Wündsch

5.1 Synthesis and discussion

The presented thesis builds on previous studies from the YRZ (chapter 1.2) and significantly contributes to drawing a clearer picture of Holocene environmental change along the southern Cape coast of South Africa. There is considerable evidence that distinct climatic variations occurred throughout the Holocene as well as sea level changes impacting coastal regions. The early Holocene was probably characterized by relatively moderate (8920 to 7870 cal BP) to high rainfall (7870 to 6440 cal BP) at Eilandvlei ([Wündsich et al., *subm.*](#)). A similar shift from dry (~8000-7200 BP) to wet conditions (~7200-6800 BP) was concluded for Groenvlei ([Martin, 1968](#)). This partly coincides with reconstructions from Still Bay (Fig. 1-2), where relatively humid conditions were suggested for the period between 11000 and 7000 cal BP ([Quick et al., 2015](#)), although at this site no moderate/dry phase was recorded during this time (Fig. 5-1).

The sea level was rapidly rising during the early Holocene, reaching and exceeding its present height between about 7500 and 5500 cal BP ([Compton, 2001, 2006](#)). This probably led to the establishment of marine conditions prevailing at Eilandvlei between 8920 and 4670 cal BP ([Wündsich et al., *subm.*](#)). Similar conclusions were drawn by [Martin \(1959, 1968\)](#) who inferred that Groenvlei passed through a marine stage from ~7000 to 4000 BP (Fig. 5-1).

During the mid-Holocene, the proxy data from Eilandvlei indicate reduced rainfall between 6440 and 3000 cal BP ([Wündsich et al., *subm.*](#)). This is broadly in agreement with generally more arid conditions as recorded at Groenvlei ([Martin, 1968](#): ~6800-2000 BP; [Wündsich et al., 2016a](#): 4210-2710 cal BP), at Still Bay ([Quick et al., 2015](#): 7000-3300 cal BP) and at the marine core site GeoB18308-1 off the Gouritz River mouth ([Hahn et al., 2016](#): 4880-1150 cal BP) (Fig. 1-2, 5-1). Moreover, this dry period was possibly associated with lower temperatures as indicated by the Cango Cave stalagmite record for the period between 5000 and 2500 cal BP ([Talma and Vogel, 1992](#)).

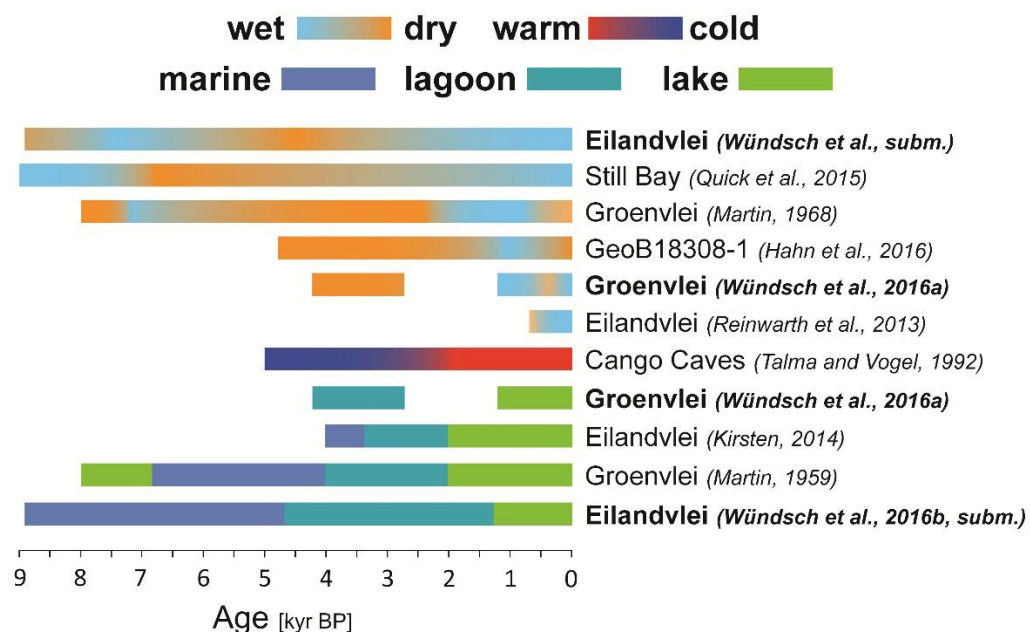


Fig. 5-1: Comparison of generalized Holocene palaeoenvironmental trends inferred from available proxy data sets from the year-round rainfall zone (YRZ). The studies included in this thesis are highlighted in bold. Note that the data presented from Martin (1959, 1968) refer to conventional ^{14}C ages whereas the remaining data are based on calibrated ^{14}C ages.

After the mid-Holocene sea level high stand, which occurred around 6300 cal BP at the southern Cape coast (Compton, 2001; Marker and Miller, 1993), the marine influence on the coastal areas was declining. Consequently, Eilandvlei likely turned into a lagoon system (Wündsche et al., 2016b, *subm.*: at 4670 cal BP; Kirsten, 2014: at 3450 cal BP) as well as Groenvlei (Martin, 1959, 1968: at ~4000 BP; Wündsche et al., 2016a: 4210-2710 cal BP) (Fig. 5-1).

During the late Holocene, high rainfall is indicated for Eilandvlei from 3000 cal BP until present (Wündsche et al., *subm.*) (Fig. 5-1). Additionally, an increase in runoff and rainfall was reconstructed for the Eilandvlei catchment from the Little Ice Age onwards (after 550 cal BP; Reinwarth et al., 2013). Similarly, Still Bay was likely characterized by humid conditions from 2200 cal BP to the present (Quick et al., 2015). The generally more humid climate was possibly associated with increased temperatures between ~2500 cal BP and the present (Talma and Vogel, 1992). The onset of wetter climatic conditions during the late Holocene was also inferred from records recovered off the Gouritz River mouth (Hahn et al., 2016: at 1150 cal BP) and from Groenvlei (Martin, 1968: at ~2000 BP; Wündsche et al., 2016a: at 2710 cal BP), however, these studies also provide indications of intercalated dry periods. At Groenvlei, slightly drier conditions were inferred during the Little Ice Age from 610 to 140 cal BP (Wündsche et al., 2016a). A forest decline around Groenvlei was reconstructed between ~250 BP and the present, which was attributed to the arrival of European colonists and possibly to drier conditions as well (Martin, 1968). The proxy data obtained from the GeoB18308-1 site suggest that the wet spell during the Medieval Climate Anomaly (1150-650 cal BP) was followed by drier conditions with the onset of the Little Ice Age (600 cal BP-the present; Hahn et al., 2016) (Fig. 5-1). Furthermore, at least three extreme rainfall events (at 2070 ⁺¹⁹⁰/₋₁₆₀, 1410 ⁺¹²⁰/₋₁₂₀ and 1250 ⁺¹³⁰/₋₁₆₀ cal BP) were reconstructed at Eilandvlei (Wündsche et al., *subm.*) and Groenvlei (between 2710 and 1210 cal BP; Wündsche et al., 2016a) suggesting a regional occurrence of these short-term events during that time.

The sea level was only slightly varying during the late Holocene and eventually reached its present height (Compton, 2001, 2006). As a result, the marine influence on the lagoons decreased and the present coastal lakes established (Kirsten, 2014; Martin, 1959; Wündsche et al., 2016a, *subm.*). The timing of the transition from the lagoon stage towards the present coastal lake system slightly differs between the reconstructions from Groenvlei (Martin, 1959: at ~2000 BP; Wündsche et al., 2016a: at 1210 cal BP) and Eilandvlei (Kirsten, 2014: at 2000 cal BP; Wündsche et al., 2016b, *subm.*: at 1240 cal BP).

Summarizing, the palaeoenvironmental reconstructions from the YRZ are generally in good agreement (Fig. 5-1). The records suggest a relatively high marine influence during the rapid sea level rise in the early Holocene as well as during the sea level high stand in the mid-Holocene. Within the late Holocene, the sea level was dropping and reaching its present elevation. Thus, the coastal lagoons became progressively isolated from the ocean and evolved into their present coastal lake configuration as demonstrated for Eilandvlei (Kirsten, 2014; Wündsche et al., *subm.*) and Groenvlei (Martin, 1959; Wündsche et al., 2016a). The palaeoclimatic data indicates a moderate to humid early Holocene, followed by a marked dry period during the mid-Holocene (Fig. 5-1). During the late Holocene, generally more humid

conditions established which are comparable to the present. Moreover, several extreme rainfall events probably occurred during that time. However, there are also contrary palaeoenvironmental interpretations for certain periods and locations (e.g., for the period of the Little Ice Age between ~500 cal BP and the present; Fig. 5-1). These differences might be either due to dating uncertainties and/or inadequate proxy interpretations or they may reflect actual local differences in the palaeoclimatic evolution.

5.2 Driving forces of Holocene climate change at the southern Cape coast

For the development of a profound understanding of Holocene climate dynamics and its driving mechanisms at the southern Cape coast, the reliable reconstruction of environmental changes and its timing is essential. This thesis provides a valuable contribution, as particularly the Eilandvlei record represents a unique, continuous sediment sequence that is reliably dated (Wündsche et al., 2016b) and reflects significant environmental changes (Wündsche et al., *subm.*). Moreover, the palaeoclimatic interpretation inferred from the Groenvlei record (Wündsche et al., 2016a) is broadly in line with that from Eilandvlei for the period covered by both records.

Another key component for comprehending past climate variability is the understanding of recent climate factors and dynamics. However, Weldon and Reason (2014) noted that despite the agricultural and touristic importance of the southern Cape coast region, its modern rainfall variability is not well understood yet. Therefore, several climatological studies focussing on the southern Cape coast were published within the last few years (Engelbrecht and Landman, 2016; Engelbrecht et al., 2015, 2016; Favre et al., 2013; Weldon and Reason, 2014). Some of these works aimed to quantify the relative contributions of different synoptic-scale weather systems to the total annual rainfall in the area. It was found that ridging anticyclones and cut-off lows are the main weather systems bringing rainfall from the mid-latitude westerlies and that tropical-temperate trough cloud bands represent the major systems supplying rainfall of tropical origin (Engelbrecht et al., 2015; Favre et al., 2013). The occurrence of some of these weather systems was linked to the principal climate modes of the El Niño-Southern Oscillation (ENSO) and the Southern Annular Mode (SAM). An increased frequency of cut-off lows affecting the southern Cape coast was observed during La Niña years (Engelbrecht and Landman, 2016; Favre et al., 2013; Weldon and Reason, 2014). Moreover, increased rainfall along the southern Cape coast occurs when the SAM is in its positive phase (Engelbrecht and Landman, 2016), which means that the atmospheric zonal mean pressure gradient between the mid-latitudes and Antarctica is enhanced resulting in a strengthening and poleward contraction of the mid-latitude westerly wind jet (Abram et al., 2014; Marshall, 2003). This poleward displacement of the westerlies promotes the equatorward expansion of arising eddies (Hartmann and Lo, 1998), such as cut-off lows and ridging anticyclones. The poleward shift (positive SAM) is moreover associated with an increased asymmetry and an enhanced trough-ridge pattern within the westerlies (Lindesay and Jury, 1991; Mason and Jury, 1997). This favours the occurrence of ridging anticyclones affecting the southern Cape coast. Moreover, high SSTs in the South Atlantic and South Indian Ocean sectors of the

Southern Ocean play an important role for an increased (anti)cyclogenesis in that area (Mason and Jury, 1997).

In order to identify possible triggers for Holocene palaeorainfall changes at the southern Cape coast, the proxy data recorded in the cores from Groenvlei and Eilandvlei were compared to Holocene data sets from other studies (Wündsche et al., *subm.*). Holocene ENSO reconstructions are available from Ecuador suggesting the onset of an ENSO-dominated climate between 5000 and 3000 cal BP resulting in an increased frequency of ENSO events throughout the late Holocene (Conroy et al., 2008; Moy et al., 2002). An increased occurrence of La Niña events might therefore have contributed to the wetter conditions recorded at Groenvlei and Eilandvlei during the late Holocene. A SAM reconstruction is thus far available only for the last millennium suggesting that SAM is in its most positive state at present (Abram et al., 2014), which is in agreement with increasingly wetter conditions recorded at Eilandvlei and Groenvlei. There is a controversial debate among scientists about the position and migrations of the southern hemisphere westerlies during the late Quaternary (Fletcher and Moreno, 2012), but various studies suggest that a poleward (equatorward) displacement of the westerly wind belt is accompanied by a poleward contraction (equatorward expansion) of the Antarctic sea ice extent (Chase and Meadows, 2007; Stuut et al., 2004; Stuut and Lamy, 2004). Based on this assumption, available reconstructions of SSTs and sea ice coverage from the Southeast Atlantic section of the Southern Ocean (Hodell et al., 2001; Nielsen et al., 2004) can be regarded as indirect indicators for migrations of the westerlies (and hence SAM) during the Holocene. These records indicate a mid-Holocene readvance of Antarctic sea ice during the Neoglacial period, whereas sea ice retreated during the early and late Holocene (Hodell et al., 2001; Nielsen et al., 2004). Following the line of argument above, the moderate to humid conditions recorded at Eilandvlei during the early and late Holocene, might have been associated with a poleward contraction of Antarctic sea ice and the westerlies, whereas the dry conditions during the mid-Holocene would be related to an equatorward expansion of sea ice and the westerlies. Relationships between ENSO and the southern hemisphere westerlies during the late Quaternary were discussed by Fletcher and Moreno (2012). The authors concluded that zonal migrations of the westerlies were symmetric around Antarctica prior to the mid-Holocene whereas the symmetry collapsed thereafter due to the onset of an ENSO-dominated climate that was probably related to an insolation-driven increase in the thermal gradient between the equator and Antarctica (Fletcher and Moreno, 2012). Such an increased asymmetry would have favoured an enhanced trough-ridge pattern within the westerlies which in turn would have increased the occurrence of ridging anticyclones and cut-off lows affecting the southern Cape coast.

The humid conditions inferred from the Eilandvlei and Groenvlei records for the late Holocene were thus possibly caused by the interplay of the principal climate modes of ENSO and SAM during the Holocene. Moreover, increased precipitation at the southern Cape coast was possibly related to a greater contribution of rainfall of tropical origin. Palaeohydrological reconstructions from the SRZ suggest a relatively dry early Holocene and increasing rainfall thereafter which was linked to an increasing local summer insolation (Chevalier and Chase,

2015). This might have led to an increased formation of tropical-temperate cloud bands over southern Africa that produced more rainfall reaching the southern Cape coast. The rainfall variability at the Wilderness lakes was possibly also related to regional temperature changes as the distinctly higher temperatures recorded at the Cango Caves after 2500 cal BP (Talma and Vogel, 1992) coincide with high rainfall at the southern Cape coast during the late Holocene. Similarly, the local mean summer insolation (at 34°S) was continuously rising throughout the Holocene (Berger and Loutre, 1991), which might have caused a warming of the Agulhas Bank possibly promoting an increased evaporation and uptake of moisture by the onshore flowing air.

5.3 Conclusions

This thesis contains a compilation of studies reconstructing the nature and timing of palaeoenvironmental changes at the southern Cape coast of South Africa during the past ~8.9 kyr. The investigated sediment sequences from Eilandvlei and Groenvlei provide new and unique geoarchives for this region, particularly in terms of its preservation and temporal resolution. As shown particularly for the sediment record from Eilandvlei, this thesis highlights the importance of the application of temporally variable marine reservoir corrections to establish reliable ¹⁴C chronologies for marine-influenced geoarchives. Moreover, the potential of palaeomagnetic stratigraphy as an independent age control tool was demonstrated. The combination of these methods helped to avoid drawing erroneous conclusions from single data sets and allowed a reliable palaeoenvironmental reconstruction for different time periods.

The reconstruction suggests that sea level variations were the dominant trigger steering the evolution from a drowned palaeovalley in the early Holocene via a marine embayment and a lagoon phase to an estuarine/coastal lake system during the late Holocene and at present. The palaeoclimatic data suggest a moderate to humid early Holocene, followed by a prolonged dry period throughout the mid-Holocene and wetter conditions during the late Holocene until present. Comparison with other Holocene palaeoclimatic studies indicates that the long-term rainfall variability at the southern Cape coast is related to migrations of the Antarctic sea ice extent and the mid-latitude westerlies as well as to variations in ENSO. Increased (decreased) rainfall at the southern Cape seems to be associated with a poleward contraction (equatorward expansion) of the Antarctic sea ice extent and the westerlies as well as an enhanced (diminished) ENSO climate mode.

5.4 Implications for future climate change at the southern Cape coast

Future climate change scenarios published in the 5th IPCC Assessment Report predict a general warming as well as mean decreases in evaporation and rainfall for southern Africa (Collins et al., 2013). Smaller-scale predictions differentiate between arid regions that will presumably be subjected to amplified droughts and shorter rainfall seasons and more humid regions of South Africa, for which more extreme rainfall events and a greater weather unpredictability are prognosticated (DEA, 2013; Thomas et al., 2007; Ziervogel et al., 2014). For the humid southern

Cape coast, hence, more extreme rainfall events can be expected in the future. Such events occurred several times within the last decades and were often caused by cut-off lows whose frequency, in turn, was linked to ENSO (Engelbrecht and Landman, 2016; Weldon and Reason, 2014). The three reconstructed extreme rainfall events between 2070 and 1250 cal BP (Wündsche et al., 2016a, *subm.*) occurred during a period for which an enhanced magnitude and frequency of ENSO events is suggested by available reconstructions (Conroy et al., 2008; Moy et al., 2002; Rein et al., 2005). A better understanding and monitoring of ENSO and its teleconnections affecting the southern Cape coast is thus crucial for improving predictions of such extreme weather phenomena.

The future predictions of the IPCC further suggest substantial reductions in the Antarctic sea ice extent as well as a strengthening and poleward migration of the mid-latitude westerlies until the end of the 21st century (Collins et al., 2013). In this thesis, it is hypothesized that poleward contractions of the Antarctic sea ice extent and the circumpolar westerlies are associated with more humid conditions along the southern Cape coast of South Africa (Wündsche et al., *subm.*). If both the hypotheses of this thesis as well as the IPCC predictions are true, the southern Cape coast will become even more humid at the end of this century than it is today and possibly more humid than it ever was during the last ~8.9 kyr.

As a result of the prognosticated global warming, the IPCC moreover predicts a global mean sea level rise of up to 1 m relative to the present for the end of the 21st century (Church et al., 2013). Such a scenario would probably cause a higher marine impact on low-lying coastal areas, such as the Wilderness embayment, by inundating sea water. This might create a lagoon system or a marine embayment with an increased submerged area around Eilandvlei as it was reconstructed for the past in this thesis (Wündsche et al., *subm.*).

5.5 Outlook

The sediment cores from Groenvlei and Eilandvlei regarded in this thesis, were retrieved in October 2013. The publications presented here, established chronologies for these records and provide first palaeoenvironmental reconstructions for the southern Cape coast. Future research needs to show if the presented transregional palaeoclimatic hypotheses will withdraw scientific verification. Collaborators of the RAIN project conducted further work especially on the exceptional EV13 core and several data sets are waiting for publication. Detailed palynological records were established by Quick et al. (*in prep.*). Additionally, diatom assemblages were extensively explored (Kirsten et al., *subm.*) as well as ostracods and foraminifera (Frenzel and Meschner, *pers. comm.*). A sediment core from Vankervelsvlei, a fen about 3 km northeast of Groenvlei, is currently investigated enabling a palaeoenvironmental reconstruction further back in time.

The seismic survey of Eilandvlei revealed that the deposited sediment sequence reaches distinctly greater thicknesses (in parts >100 m) than the recovered EV13 core of 30.5 m length (Wündsche et al., *subm.*). A new coring campaign may bring an even longer sediment core potentially allowing palaeoenvironmental reconstructions for the Pleistocene.

Although the presented thesis provides novel and valuable information about Holocene environmental dynamics at the southern Cape coast, some questions remain unanswered which may be addressed by future research. For example, this work provides information on the qualitative trends and changes in rainfall. However, quantitative rainfall data might be reconstructed by applying a probability density function-based climate reconstruction method using palynological data (Chevalier et al., 2014) or by physically-based models using stable isotope data (Nichols et al., 2010; Steinman et al., 2012). Palynological and stable isotope analyses might further provide more detailed information about rainfall sources (Feakins et al., 2014) and seasonality (Chase et al., 2015).

This thesis reconstructs the evolution of the Wilderness embayment via distinct phases of connectivity to the ocean due to Holocene sea level changes. Although precise height measurements were conducted at the EV13 site and ^{14}C -dated samples of the sediment core can be regarded as indicators for the position of the palaeo-sediment/water interface, the establishment of a local relative sea level curve was not possible as no information about the palaeo-water depths at the coring position is available. Such palaeo-water depth reconstructions may be possible by investigating suitable foraminifera assemblages (Cann et al., 1988; Van Hinsbergen et al., 2005).

The data presented in this thesis provide information on the Holocene rainfall variability along the southern Cape coast located in the YRZ. Within the framework of the RAIN project, further terrestrial and marine geoarchives from the WRZ and SRZ are investigated. Together, these archives from the three rainfall zones represent an east-west transect across the southern African sub-continent. An integration of all results from the different rainfall zones may give insights into temporal and spatial shifts in the extent of each rainfall zone. Furthermore, a comparison of results obtained from terrestrial and marine geoarchives might lead to a better understanding of interactions between atmospheric and oceanic circulation systems affecting Holocene climate dynamics in southern Africa.

5.6 References

- Abram, N.J., Mulvaney, R., Vimeux, F., Phipps, S.J., Turner, J., England, M.H., 2014. Evolution of the Southern Annular Mode during the past millennium. *Nature Climate Change* 4, 564-569.
- Berger, A., Loutre, M.-F., 1991. Insolation values for the climate of the last 10 million years. *Quaternary Science Reviews* 10, 297-317.
- Cann, J.H., Belperio, A.P., Gostin, V.A., Murray-Wallace, C.V., 1988. Sea-level history, 45,000 to 30,000 yr BP, inferred from benthic foraminifera, Gulf St. Vincent, South Australia. *Quaternary Research* 29, 153-175.
- Chase, B.M., Lim, S., Chevalier, M., Boom, A., Carr, A.S., Meadows, M.E., Reimer, P.J., 2015. Influence of tropical easterlies in southern Africa's winter rainfall zone during the Holocene. *Quaternary Science Reviews* 107, 138-148.
- Chase, B.M., Meadows, M.E., 2007. Late Quaternary dynamics of southern Africa's winter rainfall zone. *Earth-Science Reviews* 84, 103-138.
- Chevalier, M., Chase, B.M., 2015. Southeast African records reveal a coherent shift from high-to low-latitude forcing mechanisms along the east African margin across last glacial-interglacial transition. *Quaternary Science Reviews* 125, 117-130.
- Chevalier, M., Cheddadi, R., Chase, B.M., 2014. CREST (Climate REconstruction SofTware): a probability density function (PDF)-based quantitative climate reconstruction method. *Climate of the Past* 10, 2081-2098.

- Church, J.A., Clark, P.U., Cazenave, A., Gregory, J.M., Jevrejeva, S., Levermann, A., Merrifield, M.A., Milne, G.A., Nerem, R.S., Nunn, P.D., Payne, A.J., Pfeffer, W.T., Stammer, D., Unnikrishnan, A.S., 2013: Sea Level Change. In: Stocker, T.F., Qin, D., Plattner, G.-K., Tignor, M., Allen, S.K., Boschung, J., Nauels, A., Xia, Y., Bex, V., Midgley, P.M. (Eds.). *Climate Change 2013: The Physical Science Basis. Contribution of Working Group I to the Fifth Assessment Report of the Intergovernmental Panel on Climate Change*. Cambridge University Press, Cambridge, United Kingdom and New York, NY, USA.
- Collins, M., Knutti, R., Arblaster, J., Dufresne, J.-L., Fichefet, T., Friedlingstein, P., Gao, X., Gutowski, W.J., Johns, T., Krinner, G., Shongwe, M., Tebaldi, C., Weaver, A.J., Wehner, M., 2013. Long-term Climate Change: Projections, Commitments and Irreversibility. In: Stocker, T.F., Qin, D., Plattner, G.-K., Tignor, M., Allen, S.K., Boschung, J., Nauels, A., Xia, Y., Bex, V., Midgley, P.M. (Eds.). *Climate Change 2013: The Physical Science Basis. Contribution of Working Group I to the Fifth Assessment Report of the Intergovernmental Panel on Climate Change*. Cambridge University Press, Cambridge, United Kingdom and New York, NY, USA.
- Compton, J.S., 2001. Holocene sea-level fluctuations inferred from the evolution of depositional environments of the southern Langebaan Lagoon salt marsh, South Africa. *The Holocene* 11, 395-405.
- Compton, J.S., 2006. The mid-Holocene sea-level highstand at Bogenfels Pan on the southwest coast of Namibia. *Quaternary Research* 66, 303-310.
- Conroy, J.L., Overpeck, J.T., Cole, J.E., Shanahan, T.M., Steinitz-Kannan, M., 2008. Holocene changes in eastern tropical Pacific climate inferred from a Galápagos lake sediment record. *Quaternary Science Reviews* 27, 1166-1180.
- DEA (Department of Environmental Affairs), 2013. Long-Term Adaptation Scenarios for South Africa. Report No. 7 for the long-term adaptation scenarios flagship research program (LTAS). Department of Environmental Affairs, Pretoria, South Africa.
- Engelbrecht, C.J., Landman, W.A., 2016. Interannual variability of seasonal rainfall over the Cape south coast of South Africa and synoptic type association. *Climate Dynamics* 47, 295-313.
- Engelbrecht, C.J., Landman, W.A., Engelbrecht, F.A., Malherbe, J., 2015. A synoptic decomposition of rainfall over the Cape south coast of South Africa. *Climate Dynamics* 44, 2589-2607.
- Engelbrecht, C.J., Landman, W.A., Graham, R., McLean, P., 2016. Seasonal predictive skill of intraseasonal synoptic type variability over the Cape south coast of South Africa by making use of the Met Office Global Seasonal Forecast System 5. *International Journal of Climatology*.
- Favre, A., Hewitson, B., Lennard, C., Cerezo-Mota, R., Tadross, M., 2013. Cut-off lows in the South Africa region and their contribution to precipitation. *Climate Dynamics* 41, 2331-2351.
- Feakins, S.J., Kirby, M.E., Cheetham, M.I., Ibarra, Y., Zimmerman, S.R., 2014. Fluctuation in leaf wax D/H ratio from a southern California lake records significant variability in isotopes in precipitation during the late Holocene. *Organic Geochemistry* 66, 48-59.
- Fletcher, M.-S., Moreno, P.I., 2012. Have the Southern Westerlies changed in a zonally symmetric manner over the last 14,000 years? A hemisphere-wide take on a controversial problem. *Quaternary International* 253, 32-46.
- Hahn, A., Schefuß, E., Andò, S., Cawthra, H.C., Frenzel, P., Kugel, M., Meschner, S., Mollenhauer, G., Zabel, M., 2016. Linking catchment hydrology and ocean circulation in Late Holocene southernmost Africa. *Climate of the Past Discussions*. doi:10.5194/cp-2016-100.
- Hartmann, D.L., Lo, F., 1998. Wave-driven zonal flow vacillation in the Southern Hemisphere. *Journal of the Atmospheric Sciences* 55, 1303-1315.
- Hodell, D.A., Kanfoush, S.L., Shemesh, A., Crosta, X., Charles, C.D., Guilderson, T.P., 2001. Abrupt cooling of Antarctic surface waters and sea ice expansion in the South Atlantic sector of the Southern Ocean at 5000 cal yr BP. *Quaternary Research* 56, 191-198.
- Kirsten, K., 2014. Late Holocene diatom community responses to climate variability along the southern Cape coastal plain, South Africa. PhD Thesis. University of Cape Town, Cape Town, South Africa.
- Kirsten, K., Haberzettl, T., Wündsche, M., Frenzel, P., Meschner, S., Smit, A.J., Quick, L.J., Mäusbacher, R., Meadows, M.E., subm. The impact of sea level changes on the southern Cape coast, South Africa and the variability of the Agulhas Bank environment during the Holocene. *Continental Shelf Research*.
- Lindesay, J., Jury, M., 1991. Atmospheric circulation controls and characteristics of a flood event in central South Africa. *International Journal of Climatology* 11, 609-627.

- Marker, M.E., Miller, D.E., 1993. A Mid-Holocene high stand of the sea at Knysna. *South African Journal of Science* 89, 100-101.
- Marshall, G.J., 2003. Trends in the Southern Annular Mode from observations and reanalyses. *Journal of Climate* 16, 4134-4143.
- Martin, A.R.H., 1959. The stratigraphy and history of Groenvlei, a South African coastal fen. *Australian Journal of Botany* 7, 142-167.
- Martin, A.R.H., 1968. Pollen analysis of Groenvlei lake sediments, Knysna (South Africa). *Review of Palaeobotany and Palynology* 7, 107-144.
- Mason, S., Jury, M., 1997. Climatic variability and change over southern Africa: a reflection on underlying processes. *Progress in Physical Geography* 21, 23-50.
- Moy, C.M., Seltzer, G.O., Rodbell, D.T., Anderson, D.M., 2002. Variability of El Niño/Southern Oscillation activity at millennial timescales during the Holocene epoch. *Nature* 420, 162-165.
- Nichols, J., Booth, R.K., Jackson, S.T., Pendall, E.G., Huang, Y., 2010. Differential hydrogen isotopic ratios of Sphagnum and vascular plant biomarkers in ombrotrophic peatlands as a quantitative proxy for precipitation—evaporation balance. *Geochimica et Cosmochimica Acta* 74, 1407-1416.
- Nielsen, S.H., Koç, N., Crosta, X., 2004. Holocene climate in the Atlantic sector of the Southern Ocean: Controlled by insolation or oceanic circulation?. *Geology* 32, 317-320.
- Quick, L.J., Carr, A.S., Meadows, M.E., Boom, A., Bateman, M.D., Roberts, D.L., Reimer, P.J., Chase, B.M., 2015. A late Pleistocene–Holocene multi-proxy record of palaeoenvironmental change from Still Bay, southern Cape Coast, South Africa. *Journal of Quaternary Science* 30, 870-885.
- Quick, L.J., Wüdsch, M., Kirsten, K.L., Chevalier, M., Chase, B.M., Mäusbacher, R., Meadows, M.E., Haberzettl, T., in prep. High resolution record of Holocene climate and vegetation dynamics along the southern Cape coast of South Africa.
- Rein, B., Lückge, A., Reinhardt, L., Sirocko, F., Wolf, A., Dullo, W.C., 2005. El Niño variability off Peru during the last 20,000 years. *Paleoceanography* 20.
- Reinwarth, B., Franz, S., Baade, J., Haberzettl, T., Kasper, T., Daut, G., Helmschrot, J., Kirsten, K.L., Quick, L.J., Meadows, M.E., 2013. A 700-year record on the effects of climate and human impact on the southern Cape coast inferred from lake sediments of Eilandvlei, Wilderness Embayment, South Africa. *Geografiska Annaler: Series A, Physical Geography* 95, 345-360.
- Steinman, B.A., Abbott, M.B., Mann, M.E., Stansell, N.D., Finney, B.P., 2012. 1,500 year quantitative reconstruction of winter precipitation in the Pacific Northwest. *Proceedings of the National Academy of Sciences* 109, 11619-11623.
- Stuut, J.-B.W., Crosta, X., Van der Borg, K., Schneider, R., 2004. Relationship between Antarctic sea ice and southwest African climate during the late Quaternary. *Geology* 32, 909-912.
- Stuut, J.-B.W., Lamy, F., 2004. Climate variability at the southern boundaries of the Namib (southwestern Africa) and Atacama (northern Chile) coastal deserts during the last 120,000 yr. *Quaternary Research* 62, 301-309.
- Talma, A., Vogel, J.C., 1992. Late Quaternary paleotemperatures derived from a speleothem from Cango caves, Cape province, South Africa. *Quaternary Research* 37, 203-213.
- Thomas, D.S., Twyman, C., Osbahr, H., Hewitson, B., 2007. Adaptation to climate change and variability: farmer responses to intra-seasonal precipitation trends in South Africa. *Climatic Change* 83, 301-322.
- Van Hinsbergen, D., Kouwenhoven, T., Van der Zwaan, G., 2005. Paleobathymetry in the backstripping procedure: Correction for oxygenation effects on depth estimates. *Palaeogeography, Palaeoclimatology, Palaeoecology* 221, 245-265.
- Weldon, D., Reason, C., 2014. Variability of rainfall characteristics over the South Coast region of South Africa. *Theoretical and applied climatology* 115, 177-185.
- Wüdsch, M., Haberzettl, T., Cawthra, H.C., Kirsten, K.L., Quick, L.J., Zabel, M., Frenzel, P., Baade, J., Daut, G., Kasper, T., Meadows, M.E., Mäusbacher, R., subm. Holocene environmental change along the southern Cape coast of South Africa – Insights from the Eilandvlei sediment record spanning the last 8.9 kyr. *Quaternary Science Reviews*.

- Wündsch, M., Haberzettl, T., Kirsten, K.L., Kasper, T., Zabel, M., Dietze, E., Baade, J., Daut, G., Meschner, S., Meadows, M.E., Mäusbacher, R., 2016a. Sea level and climate change at the southern Cape coast, South Africa, during the past 4.2 kyr. *Palaeogeography, Palaeoclimatology, Palaeoecology* 446, 295-307.
- Wündsch, M., Haberzettl, T., Meadows, M.E., Kirsten, K.L., Kasper, T., Baade, J., Daut, G., Stoner, J.S., Mäusbacher, R., 2016b. The impact of changing reservoir effects on the ¹⁴C chronology of a Holocene sediment record from South Africa. *Quaternary Geochronology* 36, 148-160.
- Ziervogel, G., New, M., Archer van Garderen, E., Midgley, G., Taylor, A., Hamann, R., Stuart-Hill, S., Myers, J., Warburton, M., 2014. Climate change impacts and adaptation in South Africa. *WIREs Climate Change* 5, 605-620.

Statement of authorship (Selbstständigkeitserklärung)

I declare that I prepared this thesis independently and using the specified tools, personal messages and sources.

(Ich erkläre, dass ich die vorliegende Arbeit selbstständig und unter Verwendung der angegebenen Hilfsmittel, persönlichen Mitteilungen und Quellen angefertigt habe.)

Jena, 22. Mai 2017

Michael Wündsch